AN ISOTOPICALLY AND THERMOCHRONOLOGICALLY CONSTRAINED MODEL FOR LEAD-ZINC AND BARIUM MINERALIZATION RELATED TO CARBONIFEROUS BASIN EVOLUTION IN NOVA SCOTIA, CANADA

by

CASEY EDWARD RAVENHURST

Submitted in partial fulfillment
of the requirements for the degree of
Doctor of Philosophy
at
Dalhousie University
Halifax, Nova Scotia, Canada
June 20th, 1987

DALHOUSIE UNIVERSITY

FACULTY OF GRADUATE STUDIES

The undersigned hereby certify that they have read and recommend to the Faculty of Graduate Studies for acceptance a thesis entitled " An Isotopically and Thermochronologically Constrained Model for Lead-Zinc and Barium Mineralization Related to Carboniferous Basin Evolution in Nova Scotia, Canada"

by Casey Edward Ravenhurst

in partial fulfillment of the requirements for the degree of Doctor of Philosophy.

Dated March 26, 1987

External Examiner RICHARD KYLE

Research Supervisor MARCO ZENTILLI

Examining Committee P.H REYNOLDS

N.CULSHAW

P.D.HACQUEBARD

P.J.C. RYAN

DALHOUSIE UNIVERSITY

Date June 19, 1987

Author Casey Edward Ravenhurst

Title AN ISOTOPICALLY AND THERMOCHRONOLOGICALLY CONSTRAINED MODEL FOR LEAD-ZINC AND BARIUM MINERALIZATION RELATED TO CARBONIFEROUS BASIN EVOLUTION IN NOVA SCOTIA, CANADA

Department or School: Geology

Degree: Ph.D. Convocation October Year 1987

Permission is herewith granted to Dalhousie University to circulate and to have copied for non-commercial purposes, at its discretion, the above title upon the request of individuals or institutions.

TABLE OF CONTENTS

LIST OF FIGURES

LIST OF TABLES

ABSTRACT

Mississippi Valley-type lead-zinc and barium deposits in central Nova Scotia generally occur at the Tournaisian-Visean clastic-carbonate/evaporite disconformity overlying Cambrian to Devonian metasedimentary and granitic rocks. The deposits are located at the southern margin of the (~10 km deep) Carboniferous Fundy/Magdalen Basin.

Fluid inclusion homogenization temperatures of ore-stage to post-ore minerals range from 250° to 140°C and fluid salinity is ~24 eq. wt% NaCl. Zircon fission track dates are 313±44(2σ) Ma for the Gays River Zn-Pb deposit and 250±34(2σ) Ma for the Smithfield Pb-Zn-Cu-Ba deposit (both open-space fill). An Rb-Sr isochron of illite samples from a 10 metre section of Tournaisian clastic rocks (away from mineralization) gives an age of 300±6 Ma for a strontium homogenization event. Lead and strontium isotope data indicate that Tournaisian rock could have been a source (at 300 Ma) for galena mineralization and for radiogenic strontium ($^{87}Sr/^{86}Sr$=0.712) in ore-stage minerals at the larger deposits. Visean carbonate carbon and sulfate were the dominant sources of carbon and sulfur. Non-biogenic sulfate reduction at the deposits is the likely sulfide precipitation mechanism. Hydrogen and oxygen isotopic data support a basinal brine source. A genetic model of compaction-driven, episodic basinal brine expulsion is favoured.

Mathematical modelling using the TWODEPEP finite element program indicate that the fluids could have originated at >5 km depth under Visean evaporites in the Magdalen Basin. Tournaisian clastic rocks and immediately overlying Pembroke breccia are likely aquifers. A pulse of regional tectonism could have set off at least one massive, hydrofracturing, fluid expulsion event by about 300 Ma.

ACKNOWLEDGEMENTS

I thank my advisor Marcos Zentilli for constant enthusiasm, support and encouragement throughout the duration of this project. I thank Peter Reynolds for giving much of his time and energy to this project and for the long discussions of the data and constructive criticism of the thesis drafts. Harold Krueger through Geochron Laboratories and his Research Awards Program made possible the isotopic work on the fluid inclusion fluids and some of the strontium isotope work. I thank J. Blenkinsop, Carleton University for allowing us use of his strontium isotope laboratory and for providing excellent rubidium and strontium analyses. Dr. C. C. McMullen of McMaster University did the sulfur isotope analyses. Many thanks to Mike Avery of AGC for the excellent vitrinite reflectance results and to Lloyd Snowdon of ISPG for the pyrolysis and CHN analyses.

Keith Taylor provided advice on numerous aspects of sample preparation and laboratory techniques as well as helping with the interpretation of the X-ray diffraction patterns and the handling of radioactive material. Gordon Brown prepared the doubly-polished thin sections used for the fluid inclusion work. Doug Meggison did excellent drafting work on some of the thesis figures and put in some extra time when it was needed most. Access to the Gays River core was provided by Esso Minerals Canada Ltd. The Ph.D. thesis work of Samuel Akande and the B.Sc. thesis work of Mark Ponsford contributed samples to this study. Dr. Peter von Bitter at the Royal Ontario Museum contributed some samples to this study. John Dickie provided an excellent summary of the geology of the Pembroke Breccia as part of a course project.

Chris Beaumont provided the TWODEPEP program and Jean Braun assisted with its implementation.

Financial contributions to this research were made through operating grants to Marcos Zentilli and Peter Reynolds from the Natural Sciences and Engineering Research Council of Canada (NSERC), and graduate scholarships to the author from NSERC and Petro-Canada Ltd. Some of the strontium isotope work was funded by the Geological Survey of Canada Economic Geology Division (contract #OST85-00052) under the Canada-Nova Scotia Mineral Development Agreement.

CHAPTER 1

INTRODUCTION

1.1 General Statement

The occurrence of lead-zinc and barium deposits marginal to many sedimentary basins suggests a genetic link between the deposits and hydrothermal fluids evolved from these basins. A hypothesis to explain this link must address the problem of timing, fluid paths, metal source(s) and temperature of the mineralizing event with respect to basin evolution. The purpose of this project is to develop and test a quantitative model relating the thermal, structural, and fluid-flow history of Carboniferous basins in Nova Scotia, to the formation of mineral deposits around their margins.

A wide range of isotopic, geologic and thermochronologic data have been used in this study to constrain a mathematical model of fluid-flow. Field work and sampling of drillcore and outcrop was done over two summers, followed by extensive laboratory time preparing samples for isotopic analysis, fluid inclusion microthermometry and fission track dating. The fluid inclusion, fission track and most of the isotopic work was done at Dalhousie University. Some isotopic work was done at Carleton University and some was done commercially at Geochron Laboratories and at McMaster University. As part of this project, a fission track dating facility was established at Dalhousie University.

The mineral deposits studied are all located at the southern margin of the major Fundy/Magdalen Basin and south of the Cobequid-Chedabucto

Fault System/Minas Geofracture (Figure 1.1). They range from the formerly producing Zn-Pb mine at Gays River and the presently producing Ba quarry at Brookfield, to the small barite vein occurrences at Hilden and Southvale (Figure 1.2). Almost all the deposits occur near the base of the Carboniferous Windsor Group (Figure 1.3) and many are associated with faults. The small Pb deposit at Pembroke was mined over 100 years ago and the Smithfield Pb-Zn-Cu-Ba deposit was recently the focus of a diamond drilling project by Granges Exploration. I spent very little time on the large Walton/Magnet Cove Ba-Zn-Cu-Pb-Ag deposit, a former producer.

This project was successful in documenting the relationship between the mineral deposits and the fluids evolved from the Carboniferous basins, and in dating the mineralizing event. The fluid-flow model developed probably has worldwide applications to similar deep basins with evaporites and mineral deposits around their margins.

1.2 Current thinking on models of formation

The Nova Scotia deposits have affinities with Mississippi Valley-type (similar geologic setting and mineralization) and Irish-type deposits (similar mineralization and temperatures of formation). Work to date on the Mississippi Valley-type (MVT) Pb-Zn deposits (Anderson and Macqueen, 1982) indicates that these deposits show a strong spatial relationship to sedimentary basins; they occur on the margins of basins and in arches and domes separating basins (Figure 1.4). The deposits probably formed epigenetically as a normal consequence of the evolution of nearby sedimentary basins. Mineralizing fluids were thought to have originated

in the relatively shallow (<5 km) intracratonic basins nearby. However, new theories have the fluids originating in the major Appalachiian and Arkoma Basins and migrating long distances (~800 km)(Oliver, 1986).

The processes that may link the deposits with brines generated within the basins remain controversial (e.g. Jackson and Beales, 1967; Garven and Freeze, 1984a, 1984b; Bethke, 1985; Oliver,1986). Work on fluid inclusions in ore-stage and post-ore minerals has yielded the average salinity (>20 equivalent wt % NaCl), temperature (80-150^{o}C), and density (1.1 g/cc) of the mineralizing brines. Stable isotope work has provided information on the source of the fluids and of some of the minerals. Nevertheless, there are still many unanswered questions about MVT deposits concerning the source of the metals, the character and source of the mineralizing fluids, the paths that the mineralizing fluids take, and the timing of mineralization. Even the reasons for deposition are still being debated (Anderson, 1983). Genetic models for these carbonate-hosted deposits (Mississippi Valley-type and Irish-type) throughout the world, range from early hydrothermal fluid circulation (Russell, 1978), to diagenetic compaction-driven (Jackson and Beales, 1967) or tectonically-driven (Oliver, 1986) fluid flow, to very late gravity-driven fluid flow (Garven and Freeze, 1984a, 1984b).

The Nova Scotian deposits studied, formed in a tectonic environment very different from the intracratonic setting of the major MVT deposits of the mid-continent of North America (e.g. Anderson and Macqueen, 1982; Bradley, 1982). They occur along the south margin of the major (~10 km deep) Fundy/Magdalen "pull-apart" Basin (Bradley, 1982), which contains significant thicknesses of evaporites. Genetic hypotheses that can be

applied to the Nova Scotian deposits studied include near-syngenetic sabkha-type deposition (MacLeod, 1975; 1984), early diagenetic deposition from convecting hydrothermal fluids (Russell, 1976), formation from late diagenetic compaction-driven mineralizing fluids that migrated laterally from the adjacent sedimentary basins (Lydon, 1978), formation from gravity-driven fluids present after uplift of part of the basin (as suggested by Garven and Freeze (1984a, 1984b) for the Pine Point deposit), or deposition from fluids from a "deep source" (as suggested by Krebs and Macqueen (1984) for the Pine Point deposit). A genetic model for the Nova Scotian deposits must be constrained by the thermal history of the basin/deposit system, the timing of fluid movement, and by the isotopic composition of ores and host rocks. All the Nova Scotian deposits show strong epigenetic characteristics, with some having a well-defined paragenetic sequence composed of pre-ore, ore, and post-ore stages (Akande and Zentilli, 1984, Figure 10). Fluid inclusion homogenization temperatures and salinity estimates in calcite, fluorite and barite at Gays River (Akande, 1982), have made the sabkha model untenable for that deposit. The age of the mineralizing event at Gays River could be as old as the host Gays River formation (Visean, 348 Ma; Harland et al. (1982)), and must be at least 113 Ma, the Middle Cretaceous age of unconsolidated sediments that truncate the orebody (Davies et al., 1983). Circumstantial evidence led Akande and Zentilli (1984) to postulate an age of $\sim$300 Ma for the ores, roughly coinciding with a widespread tectonic (Keppie, 1982; Mann et al., 1983) and thermal event in Nova Scotia (Reynolds et al., 1981; Zentilli and Reynolds, 1985). This thermal event coincides with the timing of the Alleghenian

orogeny in the central Appalachians and the Hercynian orogeny of Europe.

What follows is a review of the methods available to constrain age, depositional temperatures, and sources of fluids, metals and gangue minerals at MVT and Irish-type deposits. These parameters must be known in order to constrain quantitative genetic models.

1.3 Timing of the mineralizing event

Age of mineralization is a key parameter that must be known in order to narrow possible genetic hypotheses. Efforts have been made by others to date ores using:

a) Paleomagnetics. This is a method that relies on the assumption that no post-mineralization rotation of faulted blocks has occurred (Beales et al., 1980; Wu and Beales, 1981). The Gays River deposit shows extensive faulting and attempts to date it using paleomagnetics were not successful (E.C. Jowett, oral comm., 1984). A Permian age has been determined by this method for the Pine Point deposit (see Sangster, 1983), which does not agree with the mid-Carboniferous lead isotope model age determined by Kyle (1981).

b) K-Ar dating. Dating of pyrite and micaceous minerals occurring with ore has been shown to be possible by the $^{40}Ar/^{39}Ar$ method (York et al., 1980), but the concentration of K (and Ar) in sulfides is very low and the blocking (or closure) temperature for mica is quite high (>300°C). Fluid inclusion

homogenization temperatures indicate that mineralizing fluid temperatures in the Nova Scotian deposits were probably <300°C and thus the K-Ar clock would not have been completely reset during the mineralizing event.

Work by Halliday and Mitchell (1983, 1984) has shown that it is possible to date low temperature (200°C) hydrothermal events by the K-Ar method on hypogene clays. It is necessary to separate illite or 2M-muscovite from recrystallized wallrock material, although K-feldspar was often included in the sample without a significant effect on the determined age.

Microcline or other K-rich feldspars preserve a record of thermal evolution in the temperature range 100° - 200°C, which can be revealed by $^{40}Ar/^{39}Ar$ spectrum analysis. This information, in conjunction with the observation of fission track annealing in coexisting apatites, allows the estimation of the temperature-time conditions of the last thermal event in sedimentary basins (Harrison and Bé, 1983). No attempt has yet been made to date ore deposits using this method.

c) Lead isotope methods. When applied to galena this method depends on the accuracy of the model used to interpret the data. If a two-stage model is used, an accurate knowledge of the age of the source rock is needed (Faure, 1977). This is usually not readily determinable. Kyle (1981) uses a single-stage model to determine the age of the Pine Point deposit. Krebs and Macqueen (1984) use this age to constrain their genetic model for the

deposit.

d) Rb-Sr dating. Dating of sulfides and authigenic glauconite has been tried and shows some promise (Medford et al., 1983; Lange et al., 1983; Posey et al., 1983). Sulfides contain very low concentrations of Rb and Sr, and dating is tenuous. Glauconite and 2M-illite, however, have much higher Rb and Sr concentrations, with Rb>Sr (Stein and Kish, 1985; Clauer, 1982). Meaningful dates can only be obtained from these minerals if they are directly associated with the sulfide mineralization or with the assumed aquifer for the mineralizing fluids (Stein and Kish, 1985).

e) Fission track dating. Fission tracks in apatite, zircon and sphene record the time when the rock cooled through the 100°C, 175°C and 225°C isotherms respectively. The method has been used to give the date of crystallization, the date of later heating or metamorphism, and the uplift history of basins. Dating of low temperature ore deposits is just starting to be done (e.g. Naeser and Cunningham, 1984). The method has been used mainly to determine the amount and duration of uplift events (Naeser, 1979; Parrish, 1983) and even the paleogeothermal gradient at the time of uplift (Parrish, 1983).

f) Vitrinite reflectance. This technique is a maximum reading thermometer dependent on both time and temperature. It is used mainly in basin evaluation to determine the level of organic

maturation of the oil-forming components in sedimentary rocks. But, vitrinite reflectance of bitumen associated with an ore deposit host rock can give the length of time of the mineralizing event, if the temperature of the fluids is independently known, for example from fluid inclusions (e.g. Cathles and Smith, 1983).

1.4 Temperatures of mineralizing fluids

a) Fluid inclusion microthermometry. Fluid inclusion studies can yield a wealth of information about the temperature, salinity, density, and possibly also about the chemical composition of the mineralizing fluids (Roedder, 1976, 1984). A minimal amount of equipment is needed. Some restrictions on the pressure conditions (depth of formation) that existed during deposition can be determined under certain conditions in some cases.

Fluid inclusions from quartz overgrowths, quartz veins and carbonate cements, formed during diagenesis of sandstone-filled sedimentary basins represent good tools for studying the evolution of composition, temperature and pressure of diagenetic fluids over time and space (Pagel and Poty, 1983). Such studies have been done on the Athabasca and Francevillian basins and on a petroleum source rock from Venezuela (Visser, 1982). The results from Venezuela indicate that quartz vein fillings were formed at the onset of liquid hydrocarbon expulsion from the source rocks. At the present time, few comparisons and

correlations between coal rank (vitrinite reflectance) and fluid inclusions are available in the published literature. This is probably because quartz overgrowths are often not useable for fluid inclusion studies.

b) Vitrinite reflectance. Although this method is a time-temperature thermometer, it is mainly dependent on temperature; the rank (or reflectance) of the organic material doubles for each 10°C rise in temperature (Lopatin, 1971). Vitrinite reflectance data represents the temperature-time integral of the thermal history and as such can be used to check the thermal history determined by other methods. Some drillhole results (Utting, 1980) and a regional study of surface samples (Hacquebard and Donaldson, 1970) are already available for the study area.

c) Conodont colouration is a method similar to vitrinite reflectance. A conodont study is being carried out on 890 metres of drillcore (DDH# SB-1) from the center of the Shubenacadie basin, by Dr. Peter von Bitter at the Royal Ontario Museum in Toronto (oral comm., 1984).

d) Isomerization and aromatization. The extent of isomerization and aromatization of hydrocarbons has been used to determine the thermal maturation of petroleum source beds in sedimentary basins. This method may be much more useful than other thermal maturation methods for the separation of the effects of

temperature and time (Mackenzie et al., 1983). However, the kinetics of this organic process have not been completely worked out, the analysis is costly and the facilities are not readily available (C. Beaumont, oral comm., 1984).

1.5 Source and paths of the mineralizing fluids

The origin of the mineralizing fluids can be determined by hydrogen and oxygen isotopic analyses of fluid inclusion fluids (in non-oxygen bearing minerals), or by isotopic analysis of gangue minerals such as gypsum and clays (for δD), carbonates and quartz (for $\delta^{18}O$), associated with the mineralizing event. The latter method requires a calculation using fractionation factors and the temperature of the mineralizing event, and may be less reliable due to the possibility of isotopic fractionation by later fluids (Taylor, 1974). The evidence for late dedolomitization of the host carbonates at Gays River (Akande, 1982) indicates that this does occur. The $\delta^{18}O$ of the mineralizing fluids at Gays River has been calculated from the $\delta^{18}O$ of ore-stage calcite, assuming that the temperature of ore deposition is correctly known from fluid inclusions (Akande, 1982).

The paths that the mineralizing fluids took out of the basin can probably be traced isotopically, and by mapping the basin/basement faults and other structural features. It has been shown that the passage of mineralizing fluids through carbonate host rocks was recorded by the alteration of the carbon and oxygen isotopic composition of the carbonates (Hall and Friedman, 1969; Pinckney and Rye, 1972; Sverjensky, 1981a; Akande and Zentilli, 1984).

1.6 Source of metals and gangue minerals

The source of metals and gangue minerals can be determined by using stable isotopes of C, S, Pb and Sr as tracers. The use of rare earth elements (REEs) is handicapped by the insufficient knowledge of partition coefficients and solubilities in aqueous systems (Grant and Bliss, 1983). Isotopes of C and S are not simple tracers; the isotopic composition of the precipitated minerals is controlled by the chemistry and temperature of the ore solutions and the degree to which equilibrium is attained, as well as by the source (Rye and Ohmoto, 1974).

Pb and Sr can be very useful and consistent tracers in minerals with low U/Pb or low Rb/Sr ratios (e.g. Kessen et al., 1981; Kesler et al., 1983; Lange et al., 1983). The isotopic composition of galena lead measured today is expected to be the same as when the galena formed. This isotopic composition was determined by the U/Pb ratio(s) of the system(s) from which it was derived. Strontium isotopes are useful for tracing the Ca and Ba component of such minerals as calcite, barite and fluorite, and for tracing the fluid in fluid inclusions (Medford et al., 1983). To determine the isotopic composition to which the rocks were homogenized, a Rb-Sr isochron must be constructed for mineral separates that may have been leached and reset by the hot mineralizing fluids (e.g. feldspars and clays). The initial $^{87}Sr/^{86}Sr$ ratio may then indicate the source or paths of the mineralizing fluids.

No Sr isotopic determinations had been made, before this study, on any of the carbonate-hosted deposits in Nova Scotia, either for age dating or for tracing the origin of the mineralization.

1.7 Mathematical modelling

One of the final steps is to represent the temperature, pressure, and resulting fluid velocities by a mathematical model. When the geothermal gradient is known or can be estimated, and the pressure-temperature boundary conditions can be set, then the coupled momentum transport and energy transport equations can be solved (Sharp, 1978). These equations contain a number of hydraulic and thermal parameters which are estimated and then refined by comparing model results to known pressure-temperature values. In theory, this method should give a pressure-temperature-time-space model for the basin.

1.8 Summary of model constraints for this study

The thesis problem is to test the various genetic models by determining mineralization temperatures, isotopic compositions, and age of mineralization for a number of Pb-Zn and Ba deposits located on the southern margin of the Fundy/Magdalen Basin. Mineralization temperatures and fluid salinity are determined using fluid inclusions. Vitrinite reflectance measurements of organic material are used to constrain estimates of the duration of the mineralizing event. The timing of the mineralizing event is determined using tectonic information, Rb-Sr dating of clays in the likely aquifer for the fluids, $^{40}Ar/^{39}Ar$ dating of muscovite from altered basement wallrock, and fission track dating of detrital apatite and zircon from host rock at the deposits. Lead isotopic determinations of galena and a whole rock sample constrain the possible sources of the metals as well as the

timing of the mineralizing event. Strontium isotopic determinations of calcite, barite, fluorite and host rocks constrain the sources of some minerals. Oxygen and hydrogen isotopic determinations of ore-stage calcite and fluid inclusion fluids in the minerals constrain the possible sources of the fluids. Sulfur isotopic determinations of sulfides and sulfates, and carbon isotopic determinations of carbonates, constrain the possible precipitation mechanisms at the depositional sites. Mathematical modelling of fluid pressures under the evaporite seal is done using the TWODEPEP finite element program.

My objective in this thesis is to develop a model that explains the observed features of the basin/deposit system, and that may predict the location of unknown deposits and hydrocarbon occurrences, both in Nova Scotia and in similar geologic settings worldwide.

Figure 1.1 The late Paleozoic Fundy/Magdalen basin system. This pull-apart basin is thought to have formed between dextral shears in New Brunswick and Newfoundland. The figure shows selected sub-basins, faults and uplifted blocks (after Bradley, 1982). Abbreviations used are as follows: SSB, Stellarton Sub-basin; MSB, Mabou Sub-basin; CM, Caledonia Massif; CH, Cobequid Highlands; AH, Antigonish Highlands; CBH, Cape Breton Highlands.

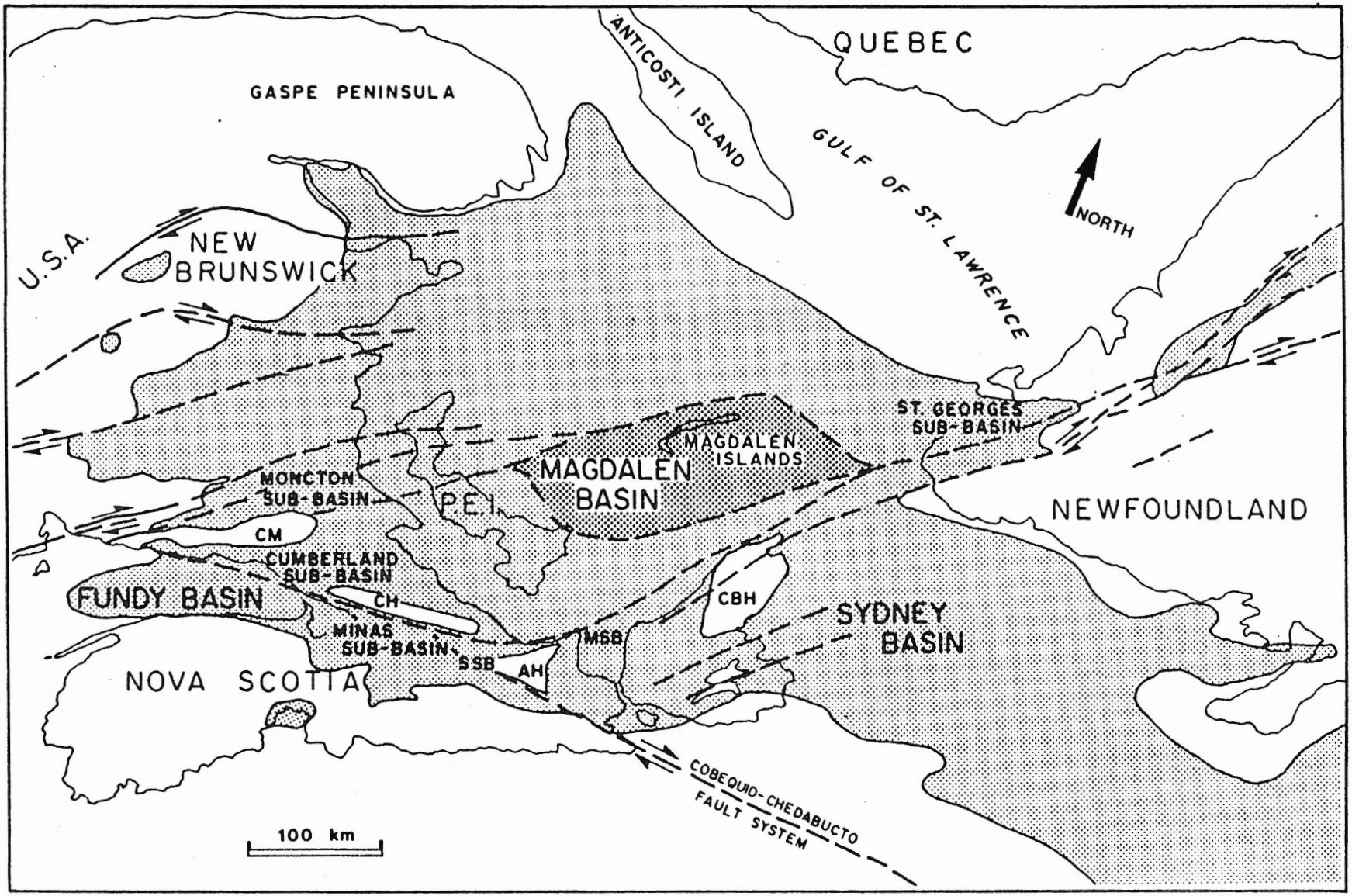
GASPE PENINSULA
ANTICOSTI ISLAND
QUEBEC
GULF OF ST. LAWRENCE
NORTH
U.S.A.
NEW BRUNSWICK
ST. GEORGES SUB-BASIN
S. MAGDALEN ISLANDS
MAGDALEN BASIN
MONCTON SUB-BASIN
P.E.I.
NEWFOUNDLAND
CM
CUMBERLAND SUB-BASIN
FUNDY BASIN
CH
CBH
SYDNEY BASIN
MINAS SUB-BASIN
MSB
SSB
AH
NOVA SCOTIA
COBEQUID-CHEDABUCTO FAULT SYSTEM
100 km

Figure 1.1

Figure 1.2 Location map of mineral occurrences and sampling sites in the Minas Sub-basin. 1=Gays River, 2=Southvale, 3=Selco survey, 4=Pembroke, 5=Smithfield, 6=Middle Stewiacke, 7=Brookfield, 8=Hilden, 9=Black Rocks, 10=Walton/Magnet Cove, 11=Nine Mile River, 12A=Upper Brookside (isochron site), 13=Lake Fletcher, 14=Glen Brook, 15=DDH# 84-1, 16&17=Hacquebard and Donaldson (1970) sampling sites, 18=Quarry, 19=DDH# BP-6 & BP-7, 20=DDH# SB-1.

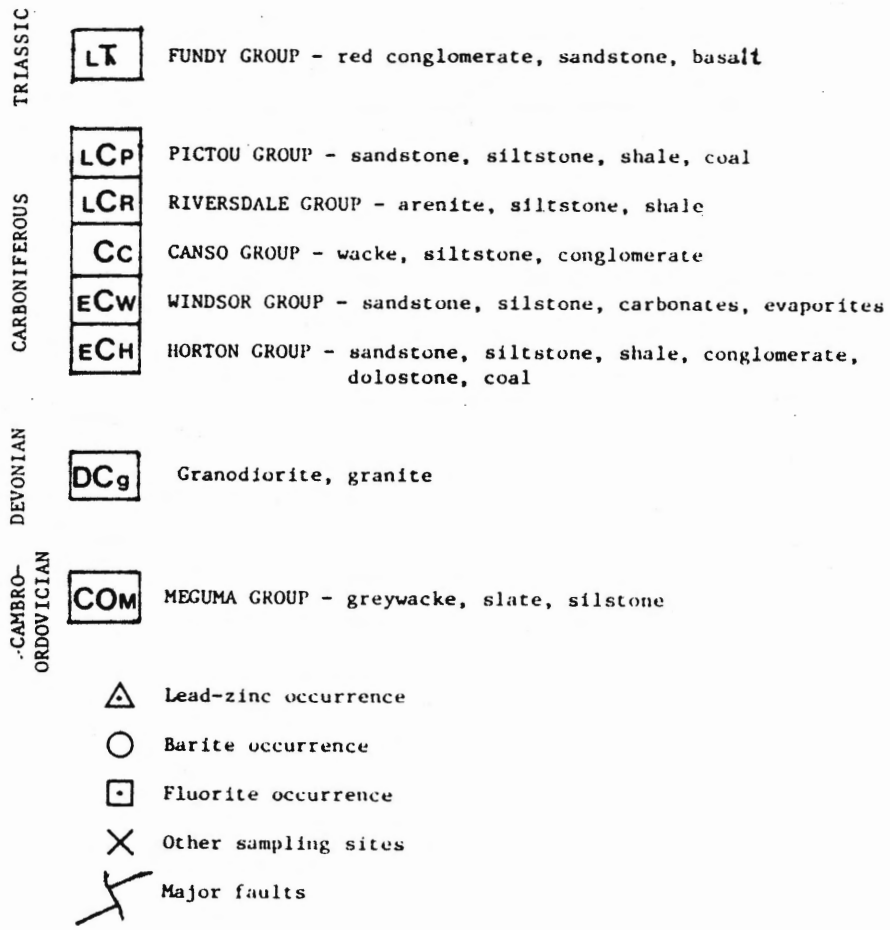

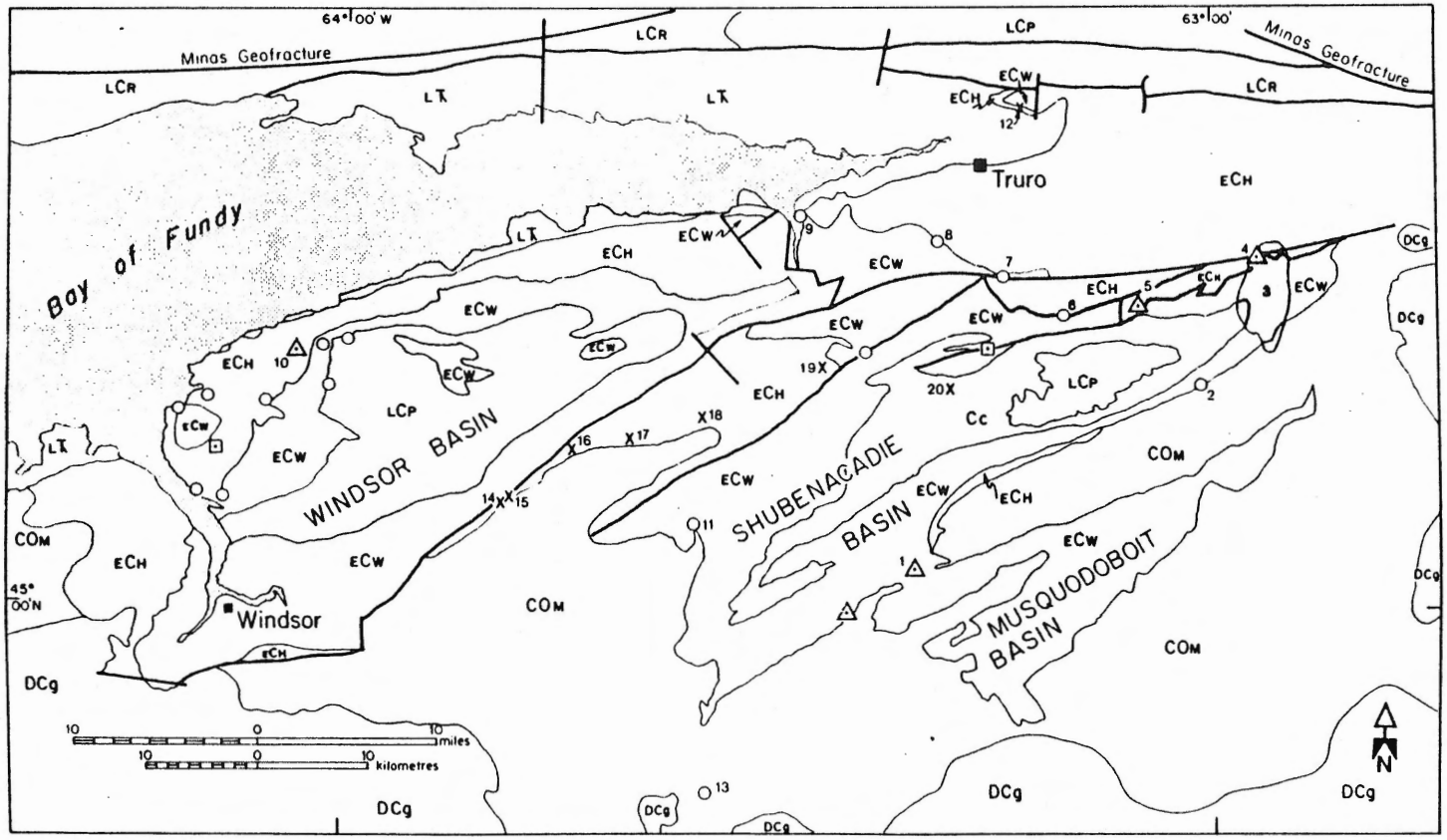
64°100' W
63°100'
Minas Geofracture
Minas Geofracture
LCR
LCR
LCP
LT
LT
ECW
ECH
12
Truro
ECH
Bay of Fundy
LT
ECH
ECW
9
8
7
4
5
6
3
DCg
ECW
ECW
ECW
ECW
ECW
ECH
10
19X
20X
LCP
2
LT
ECW
LCP
WINDSOR BASIN
X16
X17
X18
14
15
ECH
Cc
COM
ECW
SHUBENACADIE
BASIN
ECW
ECH
11
1
COM
ECH
ECW
45°
00'N
Windsor
ECH
COM
MUSQUODOBOIT
BASIN
DCg
10 0 10 miles
10 0 10 kilometres
13
DCg
DCg
DCg
DCg
N

Figure 1.2

Figure 1.3 Stratigraphy of the Mississippian Windsor Group. Shubenacadie and Musquodoboit basins (simplified from Giles and Boehner, 1979).

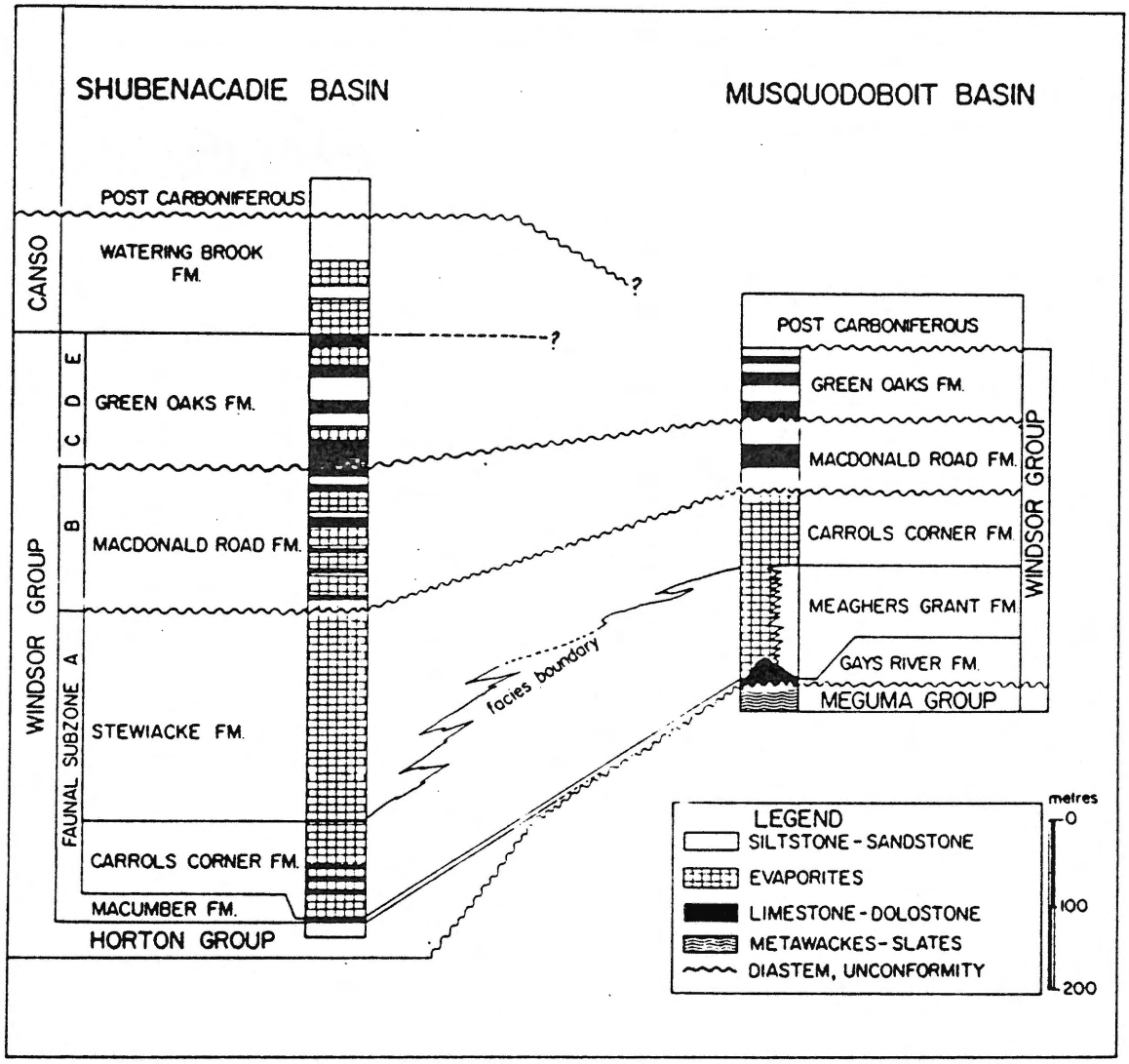
SHUBENACADIE BASIN
MUSQUODOBOIT BASIN
CANSO
POST CARBONIFEROUS
WATERING BROOK FM.
WINDSOR GROUP
FAUNAL SUBZONE E
FAUNAL SUBZONE D
FAUNAL SUBZONE C
FAUNAL SUBZONE B
FAUNAL SUBZONE A
GREEN OAKS FM.
MACDONALD ROAD FM.
STEWIACKE FM.
CARROLS CORNER FM.
MACUMBER FM.
HORTON GROUP
facies boundary
POST CARBONIFEROUS
GREEN OAKS FM.
MACDONALD ROAD FM.
CARROLS CORNER FM.
MEAGHERS GRANT FM.
GAYS RIVER FM.
MEGUMA GROUP
WINDSOR GROUP
LEGEND
SILTSTONE - SANDSTONE
EVAPORITES
LIMESTONE - DOLOSTONE
METAWACKES - SLATES
DIASTEM, UNCONFORMITY
metres
0
100
200

Figure 1.3

Figure 1.4 Location map of lead-zinc districts and basins of the Mississippi Valley (modified after Anderson, 1978). The major districts (in stipple pattern) are concentrated in the archs and domes separating the sedimentary basins. 1=Upper Mississippi Valley district, 2=Southeast Missouri district (Viburnum Trend and Old Lead Belt), 3=Tri-state district, 4=Central Missouri district, 5=Illinois-Kentucky fluorspar district (Cave-in-Rock and Salem), 6=Central Kentucky district (Gratz-Lockport), 7=Central Tennessee district (Elmwood), 8=East Tennessee district (Mascot, Copper Ridge, Sweetwater). An area with minor economic mineralization is 9=Northwest Ohio (Auglaize, Lima, White Rock).

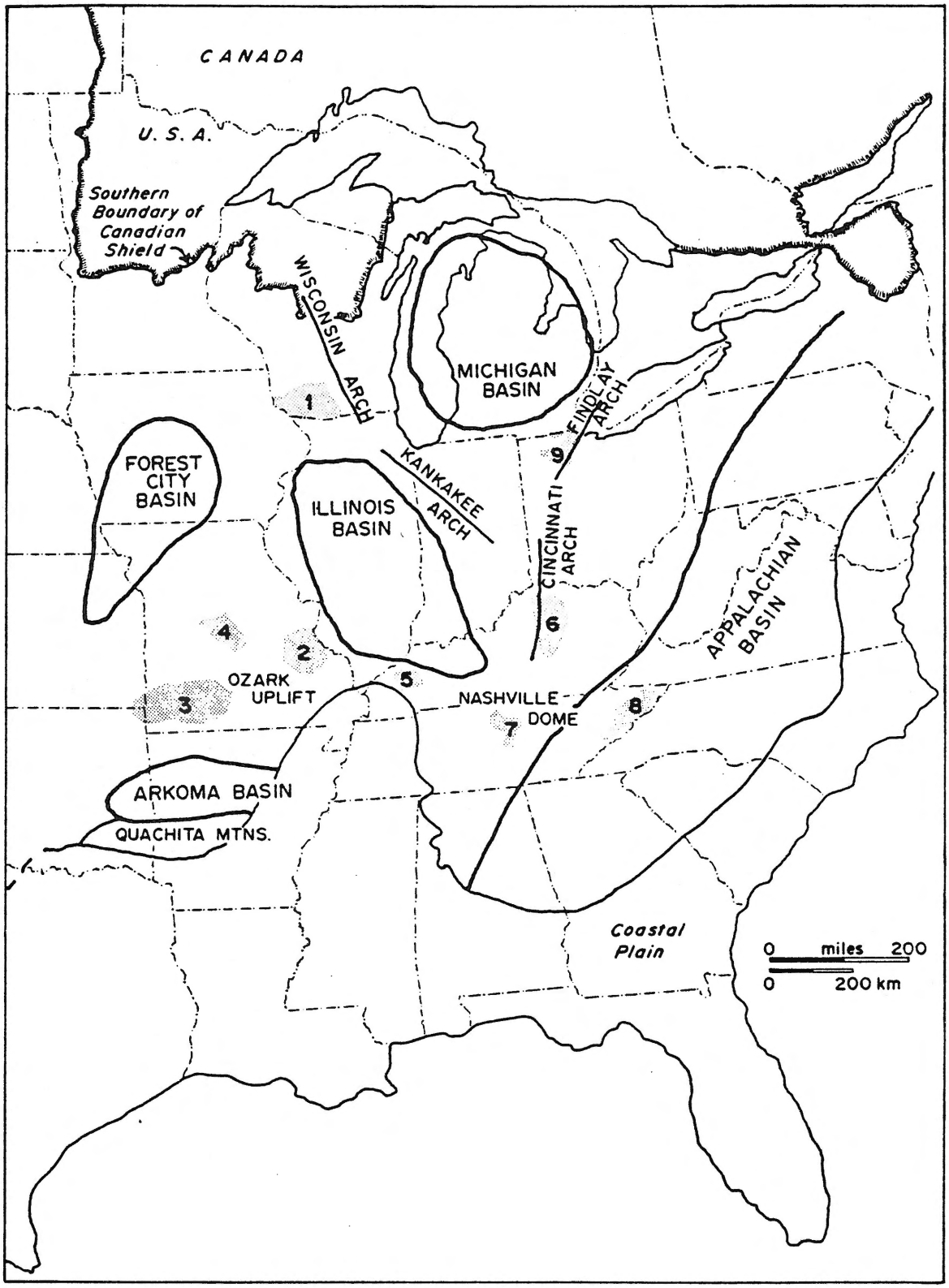
CANADA
U. S. A.
Southern Boundary of Canadian Shield
WISCONSIN ARCH
MICHIGAN BASIN
FINDLAY ARCH
1
FOREST CITY BASIN
KANKAKEE ARCH
ILLINOIS BASIN
9
CINCINNATI ARCH
APPALACHIAN BASIN
4
2
6
OZARK UPLIFT
3
5
NASHVILLE DOME
7
8
ARKOMA BASIN
QUACHITA MTNS.
Coastal Plain
0 miles 200
0 200 km

Figure 1.4

CHAPTER 2

REGIONAL STRATIGRAPHIC SETTING OF THE DEPOSITS

2.1 Sedimentary history of the Fundy/Magdalen Basin

The Late Paleozoic Fundy/Magdalen Basin (Figure 1.1) is an excellent example of a sedimentary basin with thick evaporites and Pb-Zn and/or Ba deposits located near its margins. The basin is large (>250,000 km^2) and deep (>8 km) and its tectonic and sedimentary evolution are reasonably well known.

After the Devonian Acadian Orogeny, the Maritime region of Canada was dominated by dextral wrench faulting (Figure 1.1) on east-west and northeast-southwest trending fault systems (Webb, 1969). Upper Paleozoic successor basins were formed in a complex series of grabens which are now interpreted as pull-apart basins related to wrenching (Fralick and Schenk, 1981; Bradley, 1982). Despite individual differences, there is a common overall pattern in the evolution of the successor basins, and all the sub-basins can be considered to form part of a major basin system - the Fundy/Magdalen Basin - formed between dextral fault systems in Newfoundland and New Brunswick (e.g. Bradley, 1982). Onshore exposure is limited, and erosion has removed a considerable proportion of its younger strata, but the Fundy/Magdalen Basin is by far the largest of Upper Paleozoic basins in the entire Appalachians (Bradley, 1982). These post-Acadian successor basins contained thick accumulations (up to 12 km before erosion) of terrestrial and shallow marine sediments (Belt, 1968; Sheridan and

Drake, 1968; Howie and Barss, 1975; Fralick and Schenk, 1981; Bradley, 1982) and could therefore have provided substantial volumes of basinal fluids.

Upper Paleozoic strata in the northern Appalachians lie unconformably on rocks that were deformed, metamorphosed, and intruded as a result of continental collision during the Devonian Acadian Orogeny (Schenk, 1969; Bird and Dewey, 1970; Rodgers, 1970). The late Devonian landscape was probably dominated by imposing mountains, and from the end of the Devonian to early Permian, sedimentation was widespread and probably continuous on a regional scale (Bradley, 1982), although the section is nowhere complete (Kelley, 1967).

In Atlantic Canada, geologists have traditionally divided the sequence, in ascending stratigraphic order, into the Horton, Windsor, Canso, Riversdale, Cumberland, and Pictou groups (Bell, 1929). However, many of these units are time-transgressive, (Hacquebard et al., 1960; Belt, 1964; Howie and Barss, 1975), and are better referred to as stages, which have been defined on the basis of spores from reference sections (Belt, 1964). The geologic time scale of Harland et al. (1982) was adopted here for the approximate time equivalents of each group.

The Horton Group (360-350 Ma)

Horton Group strata (Figure 1.3) were mainly deposited in fault-bounded continental basins and typically vary rapidly through fanglomerate, fluvial, and lacustrine facies (including non-marine limestone and evaporite; Howie and Barss, 1975). Basalt-rhyolite suites of tholeiitic to alkaline affinity were erupted during the deposition of

these post-Acadian, pre-Visean sediments. The tectonic environment of this sedimentation and volcanism is generally interpreted to reflect wrench faulting resulting from regional shear (Eisbacher, 1969, 1970; Fralick and Schenk, 1981; Bradley, 1982; Blanchard et al., 1984). Analogies can be drawn with the basins associated with the San Andreas fault system in California (McLaughlin and Nilson, 1982; Crowell, 1974), Anatolia, New Zealand, and elsewhere (Mann et al., 1983). Intracontinental transforms are characterized by contemporaneous subsidence, deformation, high heat flow, and volcanism. Bradley (1982) suggests that the Horton strata are the result of the initial crustal thinning and rapid subsidence phase of the basin. A thickness of at least 3 to 4 km of Horton and related strata accumulated (Figure 2.1) (Howie and Barss, 1975).

The Windsor Group (348-336 Ma)

The Windsor Group is composed of a thick (>600 m), laterally-extensive sequence of carbonates, evaporites, and siltstones unconformably overlying pre-Carboniferous basement or Horton red-beds (Figures 2.2 and 2.3). These strata represent the only major marine deposits in the Carboniferous sequence, and are preceded and followed by continental sedimentation. The Windsor Group strata were deposited after a significant erosional and depositional hiatus in the early Visean (Geldsetzer, 1978; Smith and Collins, 1984). They progressively onlapped basement and were probably laterally continuous over an enlarged basin area. The hypothesized thermal subsidence basin in which the Windsor Group strata formed is the predicted result of

crustal/lithospheric stretching beneath the Fundy/Magdalen Basin (Bradley, 1982).

i) The Macumber Formation

The Macumber Formation is the lowermost representative of the Windsor Group. It generally consists of a 1 m to 25 m unit of well-laminated, fine-grained, black, fetid (bituminous), dolostone (Schenk, 1984). Dessication cracks and sun-crack polygons, as well as anhydrite pseudomorphs after gypsum (Schenk, 1984) suggest that the Macumber was subjected to very early subaerial dessication, and that at least part of the sulphate precipitated as gypsum. Most workers (Schenk, 1967; Geldsetzer, 1978, for example), agree that the initial marine transgression was very rapid. Evidence for rapid subsidence of sedimentary basins in early Carboniferous times is found in the formation of the (Waulsortian) carbonate mud banks that host Pb-Zn mineralization in Ireland and Britain (Boyce et al., 1983). A tectonic setting that led to the formation of depressions, such as those of the Afar and the Dead Sea, could have resulted in sudden flooding due to breaching of a sill. Hallam (1977) noted a long-term fall in sea level that began in Visean time, and this effect could have led to dessication of the Windsorian basin, as suggested for the Mediterranean Messinian (Miocene) evaporite by Hsu (1972).

ii) The Gays River Formation

The fossiliferous Gays River Formation (Giles and Boehner, 1979) and its lateral equivalents provide evidence for normal marine conditions in the basin. Several of these thick (25 to 110 m) carbonate banks

developed exclusively on basement highs where the Windsor Group oversteps the Horton Group and rests on basement rocks of the Meguma Group (Giles et al., 1979).

Schenk and Hatt (1984) suggest that the Gays River reef (one of the largest in the region) formed during rapid marine transgression, then became an island and was subjected to dolomitization, subaerial exposure, karstic dissolution and enhancement of porosity. The control exerted by porosity on the lead-zinc mineralization at Gays River has been discussed by Akande and Zentilli (1984). Both the Macumber Formation, and the Gays River Formation, which may (Giles, 1981) or may not (Schenk, 1984) be time equivalents, were covered by a thick sheet of evaporitic strata in the Shubenacadie Basin. In the Musquodoboit Basin, carbonate banks of the Gays River Formation are overlain and flanked by terrigenous rocks of the Meaghers Grant Formation (Figure 1.3). The degree of dolomitization af the Gays River Formation appears to be unrelated to the lateral or vertical proximity of evaporitic strata (Giles et al., 1979).

iii) The Pembroke Breccia

Between the Macumber Formation and the overlying evaporites an irregular layer of breccia occurs in many areas of the basin, known as the Pembroke breccia, or (later dismissed because of precedence) "Pembroke Formation" (Weeks, 1948). Many different units appear to have been called Pembroke breccia, but here I refer mainly to the breccias that occur immediately underneath the evaporites in various locations throughout the Minas Sub-Basin. The breccia is a chaotic, unsorted mass

of angular fragments or slabs of extremely variable sizes, (from a few mm up to several m) mainly of Macumber laminated limestone, in a matrix of fine grained, impure to pure, and sparry calcite. Scattered exotic pebbles of granite and other Horton clasts occur in pipes and masses of cavity fill. The breccia unit is extremely variable in thickness. It varies from a few centimetres, or non-existent, to 30 metres in thickness, or may occur in lenses 5 m wide and 2 m deep. At the Walton barite deposit, the Pembroke breccia attains its greatest thicknesses near major orebodies (Weeks, 1948; Boyle et al., 1976).

The origin of the Pembroke breccia has been controversial. Early workers interpreted the breccia simply as a sedimentary breccia formed during an erosional episode immediately following the deposition of the basal Windsor limestone. Clifton (1967) proposed that the breccia formed only near an erosion surface by collapse and disintegration long after the deposition of the Windsor Group, perhaps in Triassic or post-Triassic times. Schenk (1984) interpreted the breccia as part of the evaporitic environment resulting from pre-anhydrite exposure and karstification, and thus an integral part of the shallow depositional environment. Boyle et al. (1976) suggested that hydrothermal dissolution may have been responsible for the breccias observed near the Walton barite deposit. During my field work, I have observed intraformational breccias within the Macumber which are undoubtedly of tectonic origin. My work leads me to offer a new hypothesis for the origin of the Pembroke breccia. I suggest that this breccia is the result of (or locally has been strongly modified by) hydrofracturing by circulating, hot, overpressured hydrothermal brines under an impervious

evaporite seal, in Pennsylvanian times.

iv) The Evaporite Seal

Between 30 (Hacquebard, 1972) and 50 (Boehner, 1986) percent of the sedimentary rocks of the Windsor Group consist of evaporites, primarily anhydrite, gypsum, and halite, with lesser amounts of potash. Boehner (1986) showed that at least the lower part of the Windsor Group (a major carbonate unit followed by anhydrite and salt), can be correlated throughout the basin (Figure 2.1). Approximately 100 m of anhydrite, followed upward by 150 to 300 m of halite, form almost a continuous layer, or in terms of permeability, an aquatard or nearly impervious seal.

Because much of the evaporitic strata is now anhydrite, most authors imply that the anhydrite was the primary phase, and that gypsum is a product of secondary hydration. It is well known that anhydrite can crystallize directly, or form extremely early in the diagenetic history of evaporite sequences (Kendall, 1984; Schenk, 1984). Schenk (1984) described many occurrences of pseudomorphs of anhydrite after gypsum in the Windsor Group, and gypsum is probably more abundant than anhydrite as a primary phase in most evaporite depositional environments (e.g. Shearman, 1971; Schreiber et al., 1976; Kendall, 1984), although it is often difficult to establish how soon after deposition a transformation into anhydrite took place. It is clear that the Windsor Group strata have been subjected to temperatures higher than the field of stability of gypsum; therefore none of the original gypsum present in the rocks would have survived. If any gypsum dehydrated during the

accumulation of sediments in the basin, large volumes of water would have been released (Fyfe et al., 1978), and would have had very significant effects on the hydraulic behaviour of the Fundy/Magdalen Basin.

Canso, Riversdale and Cumberland Groups (336-300 Ma)

The Windsor marine transgression represented a considerable widening of the basin, and this trend continued to the end of the Paleozoic. Thus, the age of post-Acadian strata lying directly on basement decreases toward the basin margins (van de Poll, 1972; Bradley, 1982; Mann et al., 1983). This fits the model of McKenzie (1978), which would attribute the accumulation of these onlapping strata to thermal subsidence due mainly to stretching in the Magdalen Basin, with possible minor local effects of stretching in smaller pull-aparts.

During Namurian and Early Westphalian times, rocks of the Canso, Riversdale and Cumberland Groups were deposited, with maximum accumulation taking place in the Cumberland Sub-basin and the southern part of the Magdalen Basin. The isopachs indicate accumulations of over 1.8 km of Canso-Riversdale lithologies there, and the same area continued to be active during deposition of the late Pennsylvanian to Permian Pictou Group. A thickness of over 3.6 km of Cumberland-Pictou strata is recorded in that area. Outside that region, subsidence appears to have followed the thermal pattern (Bradley, 1982), and thicknesses of strata are an order of magnitude lower.

The Pictou Group (300-280 Ma)

During Late Westphalian to Early Permian, deformation was concentrated along the southern border of the Magdalen Basin, such as the Stellarton Sub-basin. Fluvial coal measures of the Westphalian C to Lower Permian Pictou Group blanket all earlier Carboniferous units, and overstep basement. Thicknesses of the Pictou Group range from less than 100 m to about 2.7 km, southeast of Prince Edward Island (Hacquebard, 1972, 1986).

2.2 The Nova Scotian Pb-Zn and Ba deposits

The Shubenacadie Basin of Nova Scotia is a small (65 x 16 km) Carboniferous basin in the southeastern portion of the Minas Sub-basin, which comprises part of the evaporite/carbonate platform of the main Fundy/Magdalen Basin (Figure 1.1). Around its margin and near major faults, there are numerous carbonate- and clastic-hosted mineral deposits (Figure 1.2) including the Gays River Zn-Pb and Walton Ba-Zn-Cu-Pb-Ag deposits, both former producers. The Pb-Zn-Ba mineralization occurs in Windsor carbonates (Gays River Zn-Pb and Southvale Ba deposits), at the Horton/Windsor contact (Walton Ba-Zn-Cu-Pb-Ag and Smithfield Pb deposits), or in the upper Horton Group clastic rocks (Brookfield Ba deposit). The Pembroke Pb deposit occurs in carbonates higher up in the Windsor succession.

The following numbers refer to deposit locations on Figure 1.2. A number of the smaller deposits have been described in a regional study by Felderhof (1978).

(1) The Gays River Zn-Pb deposit contains about 12 million tonnes of 7% combined lead and zinc hosted in a dolomitized carbonate bank of the Gays River Formation (MacEachern and Hannon, 1974a; 1974b; Akande and Zentilli, 1983; 1984).

(2) The Southvale Ba occurrence is a small bed of fine-grained to cryptocrystalline barite showing replacement characteristics, and underlain by the basal dolomitic limestone of the Windsor Group (Felderhof, 1978).

(4) The lead at Pembroke occurs as galena in calcite veins and with vug-filling calcite, in a limestone of the Windsor Group (Ponsford, 1983).

(5) The Smithfield Pb-Zn-Cu-Ba occurrence contains a half million tonne of 6% combined lead and zinc and occurs in a brecciated basal Windsor limestone, disconformably overlying highly pyritized Horton clastic rocks (Felderhof, 1978; Walker, 1978).

(6) Barite mineralization at the Middle Stewiacke occurrence is structurally controlled and is hosted in massive limestone and limestone breccia of the upper Windsor Group, where it is in fault contact with Horton clastic rocks (Felderhof, 1978).

(7) The Brookfield Ba deposit contains at least 56,000 tonnes of 50% barite and is a "replacement" deposit hosted entirely in fractured Horton clastic rocks (Felderhof, 1978), but is in direct contact with the overlying Windsor limestone. Barite is intergrown with siderite. Secondary quartz is also present (Stevenson, 1951).

(8) The barite at Hilden occurs as a vein in basal limestone and limestone breccia of the Windsor Group (Felderhof, 1978).

(10) At Walton/Magnet Cove the barite and sulfide orebodies occur in a limestone conglomerate (Pembroke breccia), fissile limestone, and anhydrite directly overlying the Horton clastics (Boyle, 1972; Boyle et al., 1976).

(13) The barite at Lake Fletcher occurs as a vein in Meguma slates (Felderhof, 1978).

The Gays River Zn-Pb deposit, which was the main deposit studied, occurs in a dolomitized carbonate bank of the lower Carboniferous Windsor Group which unconformably overlies the lower Paleozoic basement rocks of the Meguma Group at this location and in the Musquodoboit basin (Figure 1.3). The deposit shows many similarities to MVT deposits, but gives fluid inclusion homogenization temperatures (>200^{o}C) (Akande, 1982; Akande and Zentilli, 1984) which are more characteristic of the Irish Carboniferous carbonate-hosted deposits (Roedder, 1976). The latter are generally excluded from compilations of MVT deposits.

Figure 2.1 Restored stratigraphic sections NE-SW across the Magdalen Basin (from Howie and Barss, 1975). The geologic time scale of Harland et al. (1982) was adopted for the following time equivalents (although some of these units are time-transgressive):

Horton Group = 360-350 Ma

Windsor Group = 348-336 Ma

Canso Group = 336-325 Ma

Riversdale Group = 325-305 Ma

Cumberland Group = 305-300 Ma

Pictou Group = 300-280 Ma

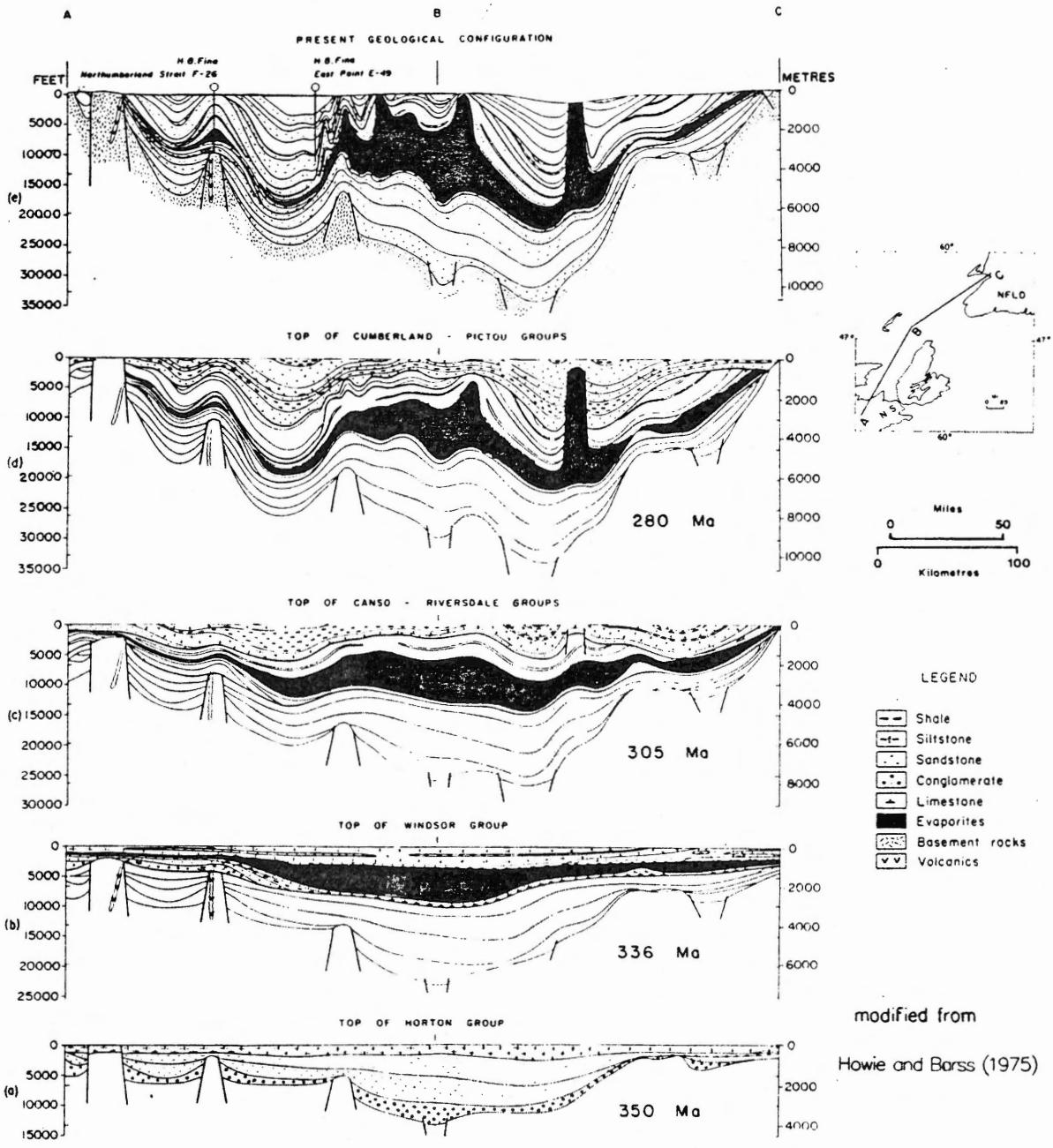
A
B
C
PRESENT GEOLOGICAL CONFIGURATION
H.B.Fina
Northumberland Strait F-26
H.B.Fina
East Point E-49
FEET
METRES
(e)
TOP OF CUMBERLAND - PICTOU GROUPS
(d)
280 Ma
TOP OF CANSO - RIVERSDALE GROUPS
(c)
305 Ma
TOP OF WINDSOR GROUP
(b)
336 Ma
TOP OF HORTON GROUP
(a)
350 Ma
NFLD
N.S.
Miles
Kilometres
LEGEND
Shale
Siltstone
Sandstone
Conglomerate
Limestone
Evaporites
Basement rocks
Volcanics
modified from
Howie and Barss (1975)

Figure 2.1

CHAPTER 3

THERMAL HISTORY OF THE DEPOSITS/BASIN SYSTEM

The Nova Scotian deposits, and MVT deposits in general, occur at or near the margins of large sedimentary basins. If there is a link between the mineralizing fluids and basinal brines, then this should be recorded in the rocks through which the fluids passed. The thermal history of the rocks can be determined by a number of techniques. I have used homogenization temperatures of primary fluid inclusions in ore minerals at the deposits and vitrinite reflectance of organics at the depositional sites and in sedimentary strata of the basin.

3.1 Fluid inclusion microthermometry

Hot metal-bearing brines move from source beds to chemical traps (depositional sites) in an analogous manner to primary migration of petroleum into physical traps (Anderson and Macqueen, 1982). Brines from deep sedimentary basins are enriched in Ca, Sr, Ba, and F and depleted in Mg and SO_4 compared to seawater. The concentrations of Pb and Zn are close to average crustal values and salinities in brines range from 10 to 40 wt%, many times seawater values (3.5 wt%) but similar to those measured in fluid inclusion fluids in ore minerals (Hanor, 1979; Roedder, 1979; Ohmoto, 1986).

Components of ore-forming fluids trapped in fluid inclusions in Mississippi Valley-type and related deposits fall within the concentration range measured in basinal brines. The lower Mg/K and Na/K ratios in fluid inclusion fluids (Roedder, 1979) are the only major

difference, possibly due to exchange between the hot fluids and the aquifer. Many deposits formed at perhaps 100 m to 1 km depth (Anderson and Macqueen, 1982). Fluid inclusions in ore minerals in MVT deposits record minimum temperatures of 80° to 200°C (not pressure corrected). This means that given normal geothermal gradients of 25° to 80°C in the earth's crust, the depositional sites and possibly a large area nearby, had anomalously high temperatures at the time of formation. Leach and Rowan (1986) argued that the mineralizing fluids in the Ozark region of Missouri were in thermal equilibrium with an enormous volume of rock.

Primary fluid inclusions are the remnants of the ore-forming fluids trapped by irregularities in crystal growth. Only these inclusions (and possibly some pseudosecondary inclusions) are likely to give good estimates of mineralization temperatures. Pseudosecondary inclusions appear to be secondary because they occur along healed fractures, but may instead be formed by fracturing and rehealing during growth of the host crystal (Roedder, 1976). Data from these inclusions may be identical to those from primary inclusions and are often used to give mineralization temperatures. Once the mineral begins to cool, the pressure-temperature conditions in the inclusion follow an isochore until a vapour bubble comes out of solution. Therefore, the homogenization temperature determined is a minimum entrapment/mineralization temperature that can only be corrected to the true entrapment temperature if an independent estimate of the fluid pressure at the time of formation can be made.

A regional approach similar to that of Leach and Rowan (1986) is attempted here. These authors showed that fluid inclusions in both mineralized and barren rock record the passage of hot, saline fluids

regionally throughout most of the Paleozoic section in the Ozarks. They argued that fluids probably originated in the Ouachita mountains to the south. There is a regional trend of decreasing fluid inclusion homogenization temperatures to the north, and a southward increase in the rank of Pennsylvanian coals (Leach and Rowan, 1986).

Sample preparation and measurement procedures

Fluid inclusion homogenization temperatures on selected samples from the various deposits were determined following the methods described in Akande and Zentilli (1984) and Akande (1982). Some measurements were made on small chips of the mineral, whereas most were done on the more than 20 doubly polished plates (50 to 80 μm thick). These were prepared by cutting 1 to 2 mm slices on a small, continuous rim diamond saw and then polishing one surface (to 1 μm finish) and mounting that on a glass slide with Lakeside cement. Further hand polishing of the other surface to 1 μm finish was then done on a glass plate. The mineral sections were then slid off the glass by heating the thin section to about 100°C and then they were soaked in acetone overnight.

Fluid inclusions studied were selected following the criteria of Roedder (1976) for primary inclusions. However, applying these criteria does not guarantee that only primary inclusions were measured. All inclusions measured were oval or roundish in shape and at least 5 μm in diameter.

A gas-flow heating and freezing stage manufactured by Fluid Inc. was used to run the new samples and to verify some previous results from Akande (1982). The stage was calibrated using the two inclusion standards provided with the system. After some adjustments, the H_2O

standard was found to melt at +0.3°C rather than 0.0°C and the pure CO_2 of the H_2O-CO_2 inclusion melted at -55.6°C rather than the true value of -56.6°C. The possiblity of a 1° or 2°C error in the temperature measurements was deemed acceptable. More than 100 new fluid inclusion homogenization temperatures were measured; 14 of these inclusions were also subjected to freezing runs to determine fluid salinity (Table 3.1).

Homogenization temperatures were measured by raising the temperature quite quickly at first and then much more slowly within 10 to 20 degrees of the homogenization temperature (2 or 3 degrees/minute). The exact moment of disappearance of the vapour bubble was often not visible, but I adopted a technique that is often used in fluid inclusion work. Once an inclusion is homogenized, the vapour bubble does not immediately reappear upon cooling; it suddenly pops out of solution at a temperature 30° or 40°C below the homogenization temperature. By repeatedly raising and lowering the temperature (each time to a slightly higher temperature), to the point at which the vapour bubble did not immediately reappear upon cooling, I was able to determine the homogenization temperature (Th).

Freezing experiments were run on some of the more clearly visible inclusions. The temperature was first lowered to about -100°C to achieve freezing, and then slowly raised. When the inclusion became quite grainy, this was recorded as the eutectic or first melting temperature (Te) (Crawford, 1981). Final melting temperature was recorded as Tm. Salinity in equivalent weight percent NaCl was calculated from Tm using formulae in Potter et al. (1978) and in Roedder (1984). These formula only apply for Tm > -20.8°C (salinity = 23.3 equivalent wt% NaCl). I assumed that many of the fluid inclusions

measured were exhibiting metastable behaviour which is common in the range Tm = -20.8° to -28° (salinity to 26.3 equivalent wt% NaCl)(Roedder, 1984). A simple linear relationship between these two points was used to calculate the salinities. Inclusions containing daughter NaCl crystals were assumed to have salinities greater than 26.5 wt% (Roedder, 1984).

Crushing tests were made on some fluid inclusions from the Gays River and Pembroke deposits. The crushing stage used was a simple hinge device manufactured by Chaixmeca, France. The small samples were mounted in oil between two glass slides, placed between metal plates and centred under the viewing hole. The clamp was then tightened slowly while observing the fluid inclusions through the microscope.

Results and interpretation

Fluid inclusion homogenization temperatures measured in ore-stage minerals from deposits around the Minas Sub-basin (Figure 3.1) are all in the 140° to 250°C range (Table 3.1). Oil-like droplets are present in fluid inclusions in fluorite at the Gays River Zn-Pb deposit, and pockets of hydrocarbons plus brines have been found during mining at the Walton Ba-Pb-Zn deposit, Nova Scotia (M. Zentilli, oral comm., 1986). Small crystals (probably NaCl daughter crystals) were noticeable in some inclusions at all the deposits studied. The relative size of these crystals indicates a fluid salinity of < 30 wt% equivalent NaCl (see Roedder, 1984).

No pressure corrections were made to homogenization temperature data. Depths of formation are poorly known with estimates ranging from < 1 km (Akande, 1982) on the basis of stratigraphic information, to > 3 km

estimated by Mahony (1986) using Hacquebard's coalification curve for the Maritimes (Hacquebard, 1974)(see section 3.2). A depth of formation of 3.6 km would require a pressure correction of 90°C be added to the tabulated homogenization temperatures (Akande, 1982). Akande (1982) argued that these pressure corrected temperatues would be too high at Gays River given the simple mineralogy of the deposit. I have evidence from $^{40}Ar/^{39}Ar$ dating of muscovite (see section 5.3) that temperatures must have approached 300°C in order to cause the amount of partial argon loss that is evident in the age spectrum. The determination of the magnitude of the pressure correction at all the deposits is a problem that needs further work.

Homogenization temperature (Th) of mineralized calcite at and near Gays River (Figure 3.1; Table 3.1) are less than those measured by Akande (1982) in ore-stage calcite from the main orebody. Mineralized calcite is calcite closely associated with sphalerite and galena but paragenetic sequence is unclear; ore-stage calcite is a subset of mineralized calcite. Errors quoted in these data are one standard error of the mean calculated from all the "primary" inclusions in a paragenetic mineral stage from a deposit. The mean homogenization temperature of all mineralized calcite (including Akande's ore-stage calcite) is 165 ± 3 °C (32 inclusions). Sphalerite temperatures plotted (mean = 214 ± 4 °C; 9 inclusions) are from Akande (1982). The homogenization temperatures of calcite associated with mineralization at Smithfield (mean = 158 ± 2 °C; 7 inclusions) are very similar to those measured at Gays River. However, homogenization temperatures of inclusions in sphalerite at Smithfield are much lower (mean = 156 ± 3 °C; 8 inclusions) than those at Gays River. Values at Pembroke are some

of the highest measured in mineralized calcite (mean = 204 ± 5 °C; 28 inclusions). Homogenization temperatures in barite cover quite a large range; at Walton/Magnet Cove they range from 155° to 233°C (mean = 187 ± 7 °C; 10 inclusions) and at Brookfield the range is from 164° to 260°C (mean = 220 ± 10 °C; 10 inclusions). Inclusions in clear crystalline barite tend to have higher Th than those in more amorphous barite which has numerous small monophase inclusions. The barite samples almost always contain numerous secondary inclusions along cleavage planes.

Ulrich and Bodnar (1984) showed that barite is a poor choice for fluid inclusion studies because stretching occurs readily, thereby causing erroneously high homogenization temperatures. They found that stretching occurred in 42% of inclusions when heated only 10°C above homogenization temperatures. About 8% of inclusions stretched before homogenization temperatures were reached. Generally stretching caused the homogenization temperature to rise by an amount less than or equal to the amount of overheating (Ulrich and Bodnar, 1984). Therefore, only the lowest homogenization temperatures measured at Walton and Brookfield are likely to be valid.

The freezing experiments gave quite consistent eutectic (Te) and final melting (Tm) temperatures (Table 3.1), which were interpreted using phase diagrams for $NaCl-H_2O$ and $NaCl-CaCl_2-H_2O$ systems in Roedder (1984) and Crawford (1981). The very low eutectic melting temperatures indicate that there may be significant-amounts of $CaCl_2$ or $MgCl_2$ in the inclusion fluids. I did not observe the melting of any phase at temperatures between Te and Tm, therefore no estimation of the concentration of other salts could be made. The eutectic temperature recorded may actually be the temperature of melting of one of these

phases rather than the true Te of the system. At Pembroke a salinity of 24 and 28 weight % NaCl is indicated in two inclusions and 3 wt% NaCl in another. The much lower value in one calcite sample may indicate that it is a much later phase, although it does appear to be closely associated with mineralization. At Smithfield the average salinity of inclusions in calcite is about 24 wt% NaCl. These values for Pembroke and Smithfield mineralizing fluids agree quite closely with that of 20.4 equivalent wt% NaCl determined for post-ore minerals at Gays River (Akande, 1982).

No correlation exists between salinity and homogenization temperatures at the deposits studied (Figure 3.2). This rules out mixing of two different solutions as the primary cause of deposition, unless both fluids had identical salinities.

The crushing of fluid inclusions is a very sensitive test of the presence of noncondensable gases. If an inclusion contains only a water solution of nonvolatile salts, the bubble in it will collapse and disappear instantly when the inclusion is opened. If gases are present, they will explode outward (Roedder, 1984). If CH_4 is present, the homogenization temperatures will nevertheless give minimum temperatures of entrapment, unless there has been leakage of material or the in situ production of CH_4 (Hanor, 1980). However, if a conventional pressure correction is applied to homogenization temperature of a CH_4-bearing inclusion, then a significant overestimate of entrapment temperature will result. Hanor (1980) argued that most subsurface brines are at or near saturation with CH_4 and thus homogenization occurs on the H_2O-CH_4 liquid-vapour surface, near the subsurface pressure-temperature conditions.

Attempts were made to observe fluid inclusions in ore-stage minerals from Gays River and Pembroke during crushing, but with little success due to the small size (5 μm) of the inclusions. Further work needs to be done to determine if homogenization temperaturess in ore-stage minerals at the deposits studied are too high due to the production of methane after entrapment. The magnitude of pressure corrections applied to the homogenization temperatures also depends on whether methane is present.

3.2 Maturation of organics

The transformation of organic material in sedimentary rocks is brought about by a thermodynamic, non-biogenic process called catagenesis, organic metamorphism, eometamorphism, or simply maturation. This process is time-temperature dependent and is irreversible. The progress of the transformation can be measured by a variety of organic geochemical indicators. Only two of these indicators were used in this study: vitrinite reflectance and pyrolysis. A specific coal maceral (vitrinite) is almost exclusively used for reflectance measurements because its ability to reflect light increases with maturation level in a fairly regular manner in the "oil window" (0.5 to 1.35 %Ro). The phytoclasts are concentrated by acid leaching, then sieved to -20 mesh, mounted in epoxy resin and polished to yield a reflecting surface. At least 50 reflectance measurements of vitrinite must be made in order to have a statistically significant sample. The optical properties of the reflected light microscope and necessary accessories are outlined in Bustin et al. (1983). Problems with the method include misidentification of vitrinite, oxidation, and the presence of reworked

vitrinite in the sediments (Hacquebard, 1984).

Pyrolysis is a technique in which organic matter is subjected to a simulated maturation process in an inert helium atmosphere in the laboratory. Information derived from the analysis includes the type of source kerogen, its degree of maturation, and its petroleum potential (North, 1985).

A vitrinite reflectance study of organic material in outcrop and drillcore samples from throughout the Maritimes was done by Hacquebard and Donaldson (1970). They noted a southwestward increase in Ro values (percent reflectance in oil) within Carboniferous sedimentary rocks in New Brunswick and Nova Scotia. This could be due either to an increased geothermal gradient or simply a deeper level of erosion in that direction. Utting (1980) measured vitrinite reflectance in a suite of organic matter samples from the DDH#SB-1 drillcore in the centre of the Shubenacadie Basin (20 in Figure 1.2). This drillhole penetrates most of the Windsor strata and ends in the Horton clastic rocks (Giles and Boehner, 1979). Utting found that in the Windsor strata, reflectance values varied from 0.56 to 0.69 %Ro. At the base of the Windsor strata and into the Horton there is a rapid increase in vitrinite reflectance values (to 1.14 and 1.60 %Ro), but this is only based on 2 samples and there is a question of reworked material in one of the samples. He offered no explanation for this sudden increase.

Gize and Barnes (1982) briefly described the organic material at Gays River as markedly different from that at their previously studied Upper Mississippi Valley district. They noted the markedly lower concentrations of metallo-porphyrins and the higher maturity of the organic material at Gays River.

Sample selection and analytical procedures

The above results plus the possibility of using vitrinite reflectance to determine the duration of the thermal event for mineral deposits (Cathles and Smith, 1983) prompted me to collect organic matter from Horton strata in the Rawdon Hills (locations 14 to 19), from Horton strata in DDH#SB-1 (site 20) and from the various mineral deposits being studied (Figure 1.2). The purpose was to determine (or better define) the maturation level of strata possibly associated with the mineralizing event. Twenty-three samples of organic material probably containing vitrinite were submitted to Don McAlpine and Mike Avery at the Geological Survey of Canada/Atlantic Geoscience Centre (GSC/AGC), Bedford Institute of Oceanography, for reflectance measurements. Samples were handpicked and crushed to -20 mesh (<850 μm). At the GSC/AGC, samples were mounted (three per stub) and polished to a low relief, scratch-free surface. Vitrinite reflectance in oil (%Ro) was measured at 640X magnification using a Zeiss Photomultiplier III microscope with normal white incident light, linked to a Zonax microcomputer. The reflectance was measured by a non-rotation (random) method and then converted to %Ro max by calculation (Ro max = 1.07 * Ro random - 0.01)(Diessel, 1982).

Seventeen samples of organic material (some of them duplicates of the "vitrinite samples") were sent to Lloyd Snowdon at the Institute of Sedimentary and Petroleum Geology (ISPG), for pyrolysis, elemental CHN analysis, and for organic petrography. Some samples were crushed to -70 +130 mesh and a small >20 mg sample of carbonaceous material was submitted. If the samples contained significant organic material, they were crushed to -70 +130 mesh and 1 gram was submitted.

At the ISPG the samples were analyzed using a Rock-Eval pyrolysis system. The analysis records three peaks, the areas (S1, S2 and S3) under which represent the volumes of three components of the organic matter (North, 1985). The sample is first rapidly heated to $\sim$ 300°C and held there for 10 minutes. This produces peak S1 representing free organic compounds already generated and thus easily volatilized from the rock. The sample is then heated more slowly to 600° during which pyrolitic breakdown of kerogen occurs (Dembicki et al., 1983). The hydrocarbons produced by cracking of the kerogen up to a maximum temperature of $\sim$ 550°C give the residual petroleum potential still capable of being generated by the sample. The ratio S2:(S1+S2) should correlate directly with the H:C atomic ratio from the CHN analysis. The ratio S1:(S1+S2) is the production index. CO_2 derived from the organic matter is represented by area S3 (North, 1985). The maximum temperature, Tmax (in °C), required to volatize the organic matter is a function of the degree of maturation and can be roughly correlated with %Ro vitrinite reflectance (L. Snowdon, written comm., 1986).

Results and interpretation

All vitrinite reflectance measurements and histograms are included in Appendix A and summarized in Table 3.2. Measurement, plotting and editing of the data were carried out by M. Avery (GSC/AGC).

The vitrinite reflectance results for the Rawdon Hills (Table 3.2, locations 14 to 19) are discussed in Mahony (1986) and in GSC Report No. EPGS-DOM.1-86MPA. Included also are two results (101 and 324) from Hacquebard and Donaldson (1970)(locations 16 and 17). The samples are tabulated from west to east; the samples in the west are from the base

of the Horton strata, 10 to 90 meters above the Meguma basement, the samples in the east are approximately 250 to 450 meters below the Windsor/Horton unconformity. The maximum thickness of Horton strata in the area was estimated at 1300 m by Bell (1929) and 900 m by Stevenson (1959). In the Rawdon Hills proper, there are no continuous exposed sections where a total thickness estimate can be made (Mahony, 1986). Using the limited stratigraphic information available, I conclude that the samples in the east are from a stratigraphically higher position in the Horton section than samples in the west, and were presumably not as deeply buried as samples in the west. Yet, the eastern samples have higher vitrinite reflectance values.

Organic material from Horton strata directly underlying the Windsor/Horton contact in DDH#SB-1 has vitrinite reflectance values even higher than those in the Rawdon Hills (Utting, 1980; and Table 3.2) although there is some question of the effects of oxidation. The samples measured at the AGC (Table 3.2) give consistent reflectance measurements, although standard deviations (anisotropy) are rather high (mean %Ro max = 2.68; sample SB1-2926 was discarded because of few readings). If oxidation were prevalent, very scattered readings would be expected (Avery, oral comm., 1986). These data support a hypothesis of increased organic maturity due to the movement of hot brines through the Horton strata under the Windsor evaporite seal. Mahony (1986) used Hacquebard's (1974) coalification curve for the Maritimes to state that the vitrinite reflectance results in the Rawdon Hills require a maximum burial depth of 4 kilometers. The effect of hot fluids on the maturation process and the strong possibility of a much higher geothermal gradient in the past, makes a depth of burial of the

Windsor/Horton unconformity of 2 or 3 km most likely.

Organic material from Gays River contained some vitrinite (especially samples RGR-111 and RGR-140). The best (weighted average) estimate of the level of organic maturation at Gays River is 1.25 %Ro max. The highest organic maturation level was observed at Smithfield (RSB-122; 3.44 %Ro max). The vitrinite there was highly anisotropic. This occurs in stressed samples, which in this case may be the result of the location of the deposit in a highly faulted area. However, a sample from Middle Stewiacke which is located in the same general faulted terrane, gave quite low vitrinite reflectance values (RSB-53, 0.66 %Ro max) and low anisotropy. A similar low level of organic maturity was noted at Nine Mile River (RSB-117, 0.86 %Ro max; RSB-124, 0.41 %Ro max). These samples may represent "background" vitrinite reflectance values in areas not greatly affected by the hydrothermal fluids.

The pyrolysis and CHN analyses (Table 3.3) indicate that most of the samples contained quite high rank (high maturation level) organic material. A number of samples yielded very little pyrolyzable material and therefore little can be said about the level of organic maturation at the Brookfield, Middle Stewiacke, and Hilden barite deposits. The sample from Smithfield (RSB-122) and one from Gays River (RGR-69) have reasonable total organic carbon (TOC) values but no pyrolyzable material. This probably indicates extensive thermal alteration (high rank) although oxidation effects are also a possibility (L. Snowdon, written comm., 1986). Vitrinite reflectance data reveals that sample RSB-122 probably was of high rank.

Samples RGR-126 from Gays River and RSB-117 from Nine Mile River indicate high rank but for a different reason. The percent carbon for

these samples from CHN analysis is much higher than the TOC from pyrolysis, higher than can be accounted for by the addition of carbonate carbon. This can be explained by incomplete combustion if these samples contained highly refractory (e.g. high rank) organic matter (L. Snowdon, written comm., 1986). Sample RGR-126 has quite high vitrinite reflectance (Ro max = 1.43) and Tmax (=461), and contains a lot of semi-fusinite (Avery, oral comm., 1986)) which could explain its incomplete combustion. However, the vitrinite reflectance (Ro max = 0.86) and Tmax (=448) of sample RSB-117 do not indicate the presence of high rank material. Therefore, the high percent carbon value for this sample remains unexplained.

Sample SB1-2914 gives a very high Tmax which would normally indicate a very high level of maturation. This also indicates the presence of highly refractory organic matter but in this case it has probably been reworked and oxidized (L. Snowdon, written comm., 1986).

The samples from Gays River and Southvale give a Tmax of approximately 460 which is equivalent to a vitrinite reflectance of about 1.2 %Ro (L. Snowdon, written comm., 1986). This is in good agreement with the vitrinite reflectance data. Therefore, all the samples that cannot be explained by oxidation appear to have a maturation level above an approximately equivalent 1.2 %Ro vitrinite reflectance. The discrepancies between the geochemical data and vitrinite reflectance data may have resulted because the methods measure different components of the organic matter.

Time-temperature nomograms for vitrinite reflectance data have been constructed by Hacquebard and Donaldson (1970) and Falvey and Deighton (1982). From fluid inclusion homogenization data I know that the

minimum temperature of mineralization at the deposits fell somewhere in the range from 140° to 250°C. Using a value of %Ro >1.2 and the nomograms, the duration of the thermal anomaly associated with the mineralizing event fell somewhere in the range of 8 to 30 Ma (Hacquebard and Donaldson, 1970) or 1 to 30 Ma (Falvey and Deighton, 1982). However, if the temperature of mineralization had been higher (e.g. adding a pressure correction of approximately 90°C), the duration of the mineralizing event could have been only 3000 years (using the Falvey and Deighton (1982) nomogram).

TABLE 3.1 Fluid inclusion homogenization and freezing temperature data.

Sample Number	Location	Composition	Te(C)	Tm(C)	Wt.% NaCl	Th(C)	Th(C) (mean of)
RGR-75	Gays River	Unmin. vf. calcite					133 (2)
RGR-89	Gays River	Unmin. vf. calcite					138 (5)
RGR-93	Gays River	Min. v. calcite					142 (5)
RGR-136	Gays River	Unmin. v. calcite					138 (5)
RGR-142	Gays River	Min. vf. calcite					129 (2)
Data from Akande (1982) also plotted on Figure 3.1.							
RSB-46	Pembroke	Min. v. calcite					188 (3)
P-8	Pembroke	Min. vf. calcite	-3.0	-1.6	3	208	228(4) 181(2)
P-9	Pembroke	Unmin. vf. calcite		-31	28	156	164 (5)
P-14	Pembroke	Min. vf. calcite	-38	-22.5 NaCl Xst	24	206 165	202(5) 168(3)
Data from Ponsford (1983) also plotted on Figure 3.1.							
SV-01	Selco survey	Unmin. v. calcite					182 (4)
RSB-30a	Smithfield	Min. vf. calcite	-25 -28	-14 -24.5	18 25	157 158	158 (7)
RSB-31a	Smithfield	Unmin. v. calcite	-29 -38	-21.5 -24.4 -20.5 -21.5	23 25 23 23	187 154 162 189	174 (13)
			-42	-17.4 Xst		183	
RSB-32	Smithfield	P.O. calcite	-35	-24.5	25	159	161(5) 208(1)
RSB-121	Smithfield	Sphal.	-35 -40 -40	-22.6 -22.6 -22.2	24 24 24	165 158 159	156 (8)

RSB-35	Brookfield	Crystalline barite	228 (8)
RSB-36	Brookfield	Crystalline barite	185 (2)
EC-789	Walton	Crystalline barite	177(8) 225(2)

Unmin. = Unmineralized Min. = Mineralized
P.O. = Post-ore Sphal. = Sphalerite

TABLE 3.2 Vitrinite reflectance data.

Location	Sample Number	Description	Number of rdgs.	%Ro(mean and S.D.)	%Ro max
RGR-21	1. Gays River		22	1.29 ± .18	1.37
RGR-69	1. Gays River		11	1.03 ± .13	1.09
RGR-111	1. Gays River	Organic material in Windsor carbonates	83	1.14 ± .13	1.21
RGR-126	1. Gays River	in and near the deposit	1	1.35	1.43
RGR-140	1. Gays River		42	1.21 ± .08	1.28
RSB-122	5. Smithfield	Coaly layer in gray congl.	99	3.22 ± .65	3.44
RSB-53	6.Middle Stewiacke	Carbonaceous material in Windsor carbonate	28	0.63 ± .06	0.66
RSB-25	7. Brookfield	Carbonaceous material in Horton ss.	1	1.82	1.94
RSB-117	11. Nine Mile River	Coaly layer in Horton congl.	49	0.81 ± .04	0.86
RSB-124	11. Nine Mile River	Organic material in Macumber lmst.	30	0.39 ± .05	0.41
RSB-87	14. Glen Brook	Plant material in Horton ss.	53	0.98 ± .10	1.04
RSB-89	15. DDH# 84-1(7.0m)	Carb. material in Horton ss.	61	0.98 ± .12	1.04
RSB-90	15. DDH# 84-1(66.5m)	Plant fossil in Horton ss.	86	0.91 ± .08	0.96
RSB-91	15. DDH# 84-1(90.2m)	Coaly material in Horton sst.	88	0.87 ± .09	0.92
HD-101	16.	Coaly material	>50		0.96
HD-324	17.	Coaly material	>50		0.84
HH2-1	18. Quarry	Carb. material in Horton ss.	40	1.06 ± .10	1.12

Table 3.2 .....continued

BP6-820	19. DDH# BP-6(249.9m)		56	1.25 ± .19	1.33
BP6-797	19. DDH# BP-6(242.9m)	Carbonaceous	79	1.21 ± .17	1.28
BP6-624	19. DDH# BP-6(190.2m)	material in Horton sst.	95	1.10 ± .10	1.17
BP6-500	19. DDH# BP-6(152.4m)		63	1.23 ± .13	1.31
SB1-2914	20. DDH# SB-1(888.2m)		99	2.42 ± .38	2.58
SB1-2917	20. DDH# SB-1(889.1m)	Carbonaceous green patches	99	2.59 ± .30	2.76
SB1-2919	20. DDH# SB-1(889.7m)	in red Horton ss.	98	2.53 ± .31	2.70
SB1-2926	20. DDH# SB-1(891.8m)		16	2.41 ± .27	2.57

Table 3.3 Results of pyrolysis and CHN analyses

Location/Description	Sample Number	Tmax	S1	S2	S3	TOC	$\frac{S1}{S1+S2}$	$\frac{S2}{S1+S2}$	%C	%H	Elemental H/C
1. carbonaceous material assoc. w. sphalerite	AGR-B1	460	.06	.37	.13	.71	.139				
1. carbonaceous material in and near the deposit	RGR-5	454	.26	.85	.36	1.04	.234				
	RGR-21	460	.13	.61	.06	1.15	.176				
	RGR-69	345	0	.27	0	1.96	---				
	RGR-111	461	1.07	23.34	.40	16.90	.044	.956	18.15	.99	0.655
	RGR-117	457	.13	1.80	.34	2.81	.067				
	RGR-126	461	5.42	85.46	2.85	47.19	.060	.940	82.63	3.89	0.565
	RGR-127	306	0	.03	0	.15					
2. carbonaceous material in b.b. and shale	RSB-48	448	0	.03	.10	.28					
	RSB-72	471	0	.35	.77	1.83					
5. coaly layer in gray conglomerate	RSB-122	---	0	0	0	3.51					
6. carbonaceous material in carbonates	RSB-53	434	0	.13	.23	.30					
7. carbonaceous material in gray sandstone	RSB-25	462	0	.06	.06	.14					
8. limestone with petroliferous odor	RSB-65	408	0	.03	0	.03					
11. coaly layer in gray sandstone	RSB-117	448	.66	100.86	4.70	27.68	.0065	.993	70.83	4.31	0.731
20. green carbonaceous patches in red ss	SB1-2914	551	.71	10.00	2.50	63.85	.066	.934	49.32	1.80	0.438

Figure 3.1 Homogenization temperatures of fluid inclusions from Pb-Zn and Ba deposits. Some Gays River values are from Akande (1982) and some Pembroke results are from Ponsford (1983). Errors quoted in these data are one standard error of the mean calculated from all the primary inclusions (number in brackets) in a paragenetic mineral stage from a deposit. Blackened areas of histograms are data for sphalerite.

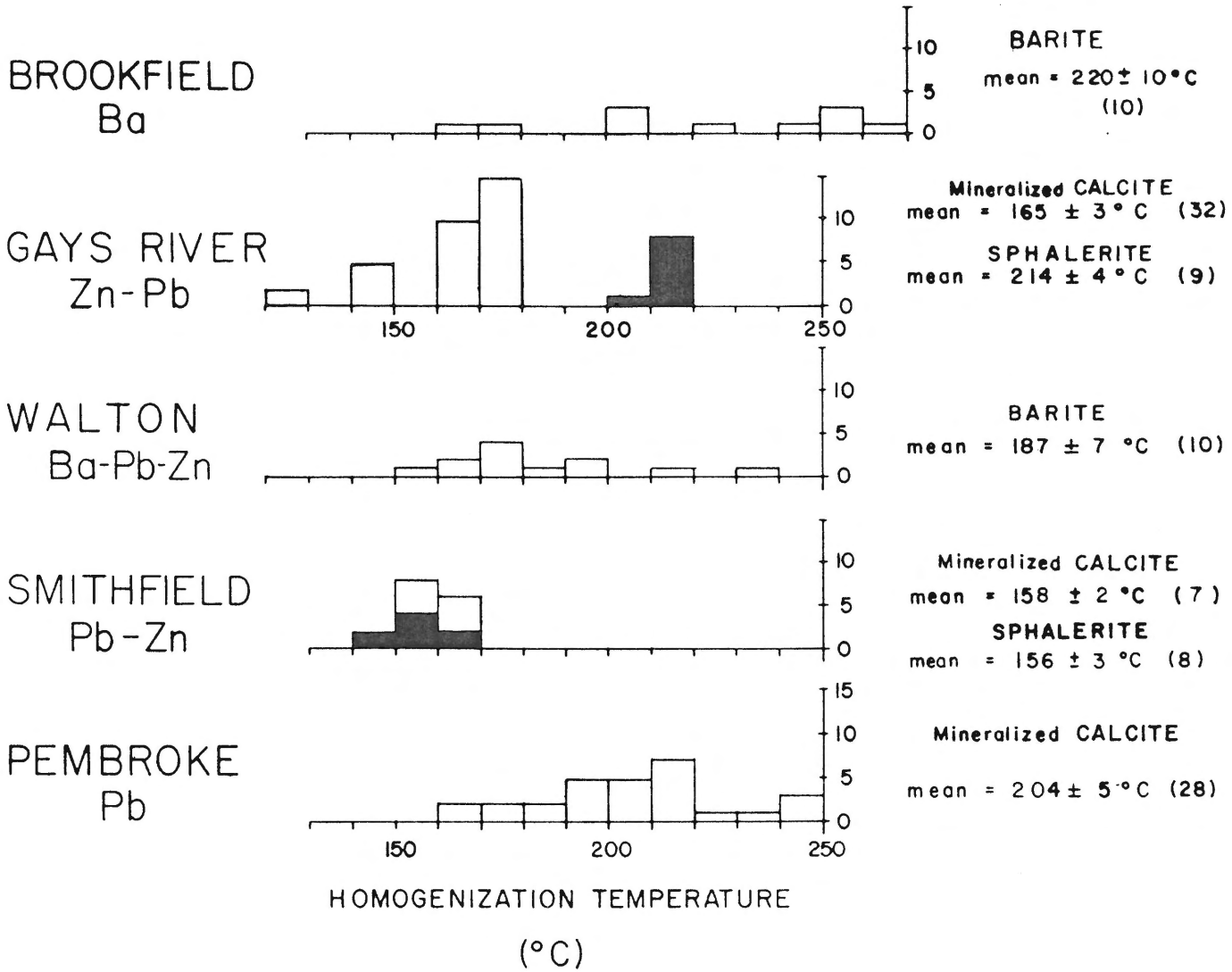
BROOKFIELD
Ba
BARITE
mean = 220 ± 10°C
(10)
GAYS RIVER
Zn-Pb
Mineralized CALCITE
mean = 165 ± 3°C (32)
SPHALERITE
mean = 214 ± 4°C (9)
WALTON
Ba-Pb-Zn
BARITE
mean = 187 ± 7 °C (10)
SMITHFIELD
Pb-Zn
Mineralized CALCITE
mean = 158 ± 2 °C (7)
SPHALERITE
mean = 156 ± 3 °C (8)
PEMBROKE
Pb
Mineralized CALCITE
mean = 204 ± 5 °C (28)
150
200
250
HOMOGENIZATION TEMPERATURE
(°C)

Figure 3.2 Salinity vs homogenization temperature for fluid inclusions. Number indicates the deposit: 1=Gays River, 4=Pembroke, 5=Smithfield. ■ = mineralized calcite, □ = unmineralized calcite, X = post-ore calcite. Arrows indicate salinities equal to or greater than values plotted. Two inclusions contained crystals at 25°C assumed to be NaCl, and are plotted with arrows at their likely minimum salinities.

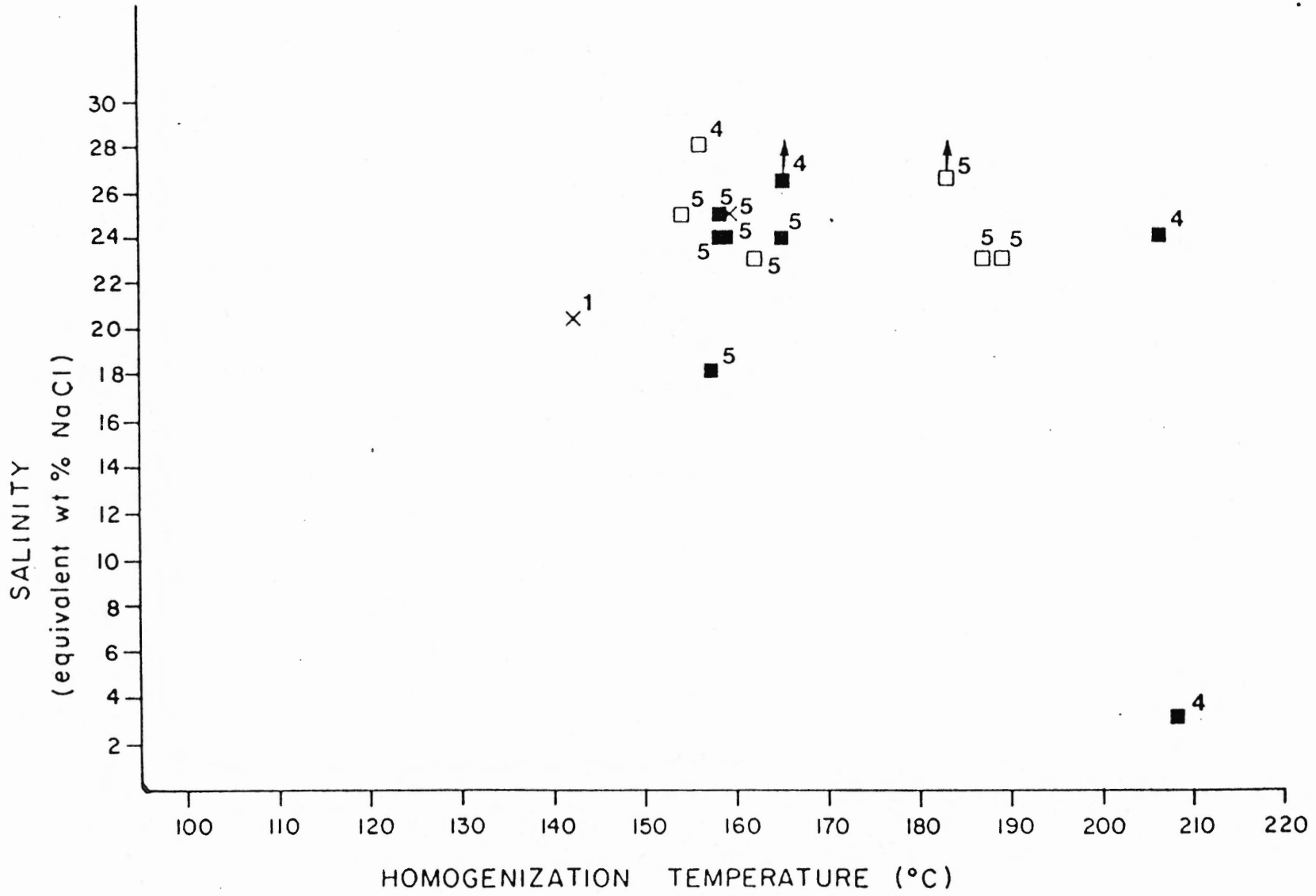
SALINITY
(equivalent wt % NaCl)
30
28
26
24
22
20
18
16
14
12
10
8
6
4
2
100
110
120
130
140
150
160
170
180
190
200
210
220
HOMOGENIZATION TEMPERATURE (°C)

Figure 3.2

CHAPTER 4

ISOTOPIC CONSTRAINTS ON FLUID PATHS AND SOURCES

Isotopic data are powerful tools for constraining genetic models for mineral deposits. Isotopic ratios of stable elements are affected differently by geological processes than are the elements themselves. Stable daughter products of radiogenic isotopes (such as ^{206}Pb, ^{207}Pb, and ^{87}Sr) and stable isotopes (such as D, ^{13}C, ^{18}O, and ^{34}S) can be used as geochemical tracers of elements and fluids. Here they have been used to determine the source of minerals and fluids, the degree of interaction between host rocks and fluids, and the precipitation mechanism.

4.1 General principles of isotopic notation

Natural fractionation of stable isotopes is of two types; equilibrium and kinetic. Equilibrium fractionation occurs between two or more phases in equilibrium, therefore it is related to the equilibrium constant (K) for the reaction, which is itself temperature dependent. Kinetic fractionations apply during non-equilibrium situations and slow reaction rates. Kinetic effects are minimized at high temperature and are only geologically important during open system behaviour at relatively low temperature (Cox et al., 1979). The possible effects of kinetic fractionation were not considered here.

Isotopic data are usually reported as δ:

$$\delta \text{ (o/oo)} = (\text{Rsample}/\text{Rstandard} - 1) \times 1000 \qquad (1)$$

$$\text{Rsample} = D/H,\ ^{18}O/^{16}O,\ ^{13}C/^{12}C,\ ^{34}S/^{32}S,\ \text{etc.}$$

Rstandard = (tables in Friedman and O'Neil, 1977;

O'Neil, 1986)

Fractionations between two phases A and B may be defined in terms of what is known as either a fractionation factor or an isotopic partition coefficient (αAB):

$$\alpha AB = RA/RB \qquad (2)$$

This is usually restricted to equilibrium fractionations only. From equation (1) it follows that;

$$\alpha AB = (1000+\delta A)/(1000+\delta B)$$

or

$$\text{Ln } \alpha AB = \text{Ln}(1+\delta A/1000) - \text{Ln}(1+\delta B/1000) \qquad (3)$$

Using the approximation:

$$\text{Ln}(1+E) \simeq E \text{ if } E<<1 \qquad (4)$$

this becomes

$$\text{Ln } \alpha AB \simeq \delta A/1000 - \delta B/1000$$

or $$1000 \text{ Ln } \alpha AB \simeq \delta A - \delta B = \text{delta AB} \qquad (5)$$

which is good for $|\delta| < 10$. This approximation is useful for quick calculation of the isotopic composition of one phase when that of the other phase and the fractionation factor are known. For large δ values, such as for δD where values are in general an order of magnitude larger than for most other isotopes, this approximation is not valid (Taylor, 1974) (see below).

4.2 Oxygen and carbon isotopes in carbonates

The oxygen isotopic compositions of minerals deposited in equilibrium with fluids, depend primarily on the isotopic composition of the fluids and the temperature-dependent fractionation factors. The fractionation factors between calcite and water over the temperature range 0° to $500^{\circ}C$ is given by:

$$1000 \ln \alpha_{\text{calcite-water}} = 2.78 * (10^6/T^2) - 3.39 \quad (6)$$

(O'Neil et al., 1969)

where T is in degrees Kelvin.

Similarly for dolomite and water at temperatures between 300 and $500^{\circ}C$:

$$1000 \ln \alpha_{\text{dolomite-water}} = 3.2 * (10^6/T^2) - 2.0 \quad (7)$$

(Northrop and Clayton, 1966)

Dolomite-water fractionations are poorly defined below $300^{\circ}C$ but there should be only 3 - 4 o/oo enrichment in heavy oxygen in dolomite relative to calcite if they are deposited in equilibrium at $100^{\circ}C$ (Fritz, 1976).

The passage of hot, mineralizing fluids through rock can initiate recrystallization and isotopic alteration especially in the vicinity of loci of ore deposition and/or in channelways for the fluids. The size of the alteration halo around the orebody or channelway and the magnitude of the oxygen isotope shift, will depend on the porosity of the host rock, its mineralogy, the temperature and chemistry of the solutions, the water/rock ratio and the degree to which isotopic equilibrium is attained. Solutions which had a long residence time in marine carbonate sediments will have little effect on the oxygen isotope

content of similar carbonates through which they pass, if no significant temperature variations occur. Therefore, only in areas where there is a significant geochemical and isotopic difference between the mineralizing fluids and certain host rocks, as well as "high" fluid temperatures, will significant isotopic halos be developed which may be useful for prospecting purposes (Fritz, 1976). Akande and Zentilli (1984) noted that dolomite host rock at the Gays River deposit was very resistant to oxygen isotopic alteration by the 200°C mineralizing fluids. However, at the Pembroke deposit Ponsford (1983) noted significant oxygen isotopic alteration of the host rock limestone by the 200°C mineralizing fluids.

Significant isotopic alteration effects have been noted by many authors, among them: Engel et al. (1958) at the Gilman mine in Colorado, Hall and Friedman (1969) at selected MVT deposits, Pinckney and Rye (1972) at the Cave-in-Rock district of Illinois, Sverjensky (1981a) at the Upper Mississippi Valley district, Sverjensky and Wasserman (1978) at the Viburnum trend, Missouri, Olson (1984) at the Nanisivik deposit, NWT, and Shelton (1983) at the Mines Gaspe copper skarn deposit. Only a small isotopic alteration effect was seen by Fritz (1969) in the carbonates at Pine Point. Hall and Friedman (1969) stated that the oxygen and carbon isotopic alteration of carbonate host rocks of MVT deposits do not seem practical as guides to ore, because the area of limestone depleted in those isotopes is small. This is refuted by some of the later work, e.g. Sverjensky and Wasserman (1978), who documented alteration extending for 1 mile away from the Buick deposit in the Viburnum Trend, and by Shelton (1983) who correlated the degree of alteration with ore grade at a skarn deposit. But, for dolomite host

rock it can be stated that significant dolomite isotopic exchange occurs only during recrystallization and not in the solid state (Fritz, 1976). In order to determine the oxygen isotopic composition of the mineralizing fluids, it is necessary to sample limestone, hydrothermal sparry dolomite or calcite, which may have attained some degree of equilibration with the mineralizing fluids.

Factors controlling carbon isotopic composition of recrystallized carbonates are considerably more variable areally and temporally than those controlling the oxygen isotopic composition. In most areas this virtually excludes the use of carbon isotopes as guides to ore (Fritz, 1976). Although the carbon isotopic content of hydrothermal carbonates is determined by the carbon isotopic content of the carbonates in solution, and temperature dependent fractionation factors (Figure 4, Fritz, 1976) similar to oxygen, changes in pH, oxygen fugacity, salinity and total concentration of carbon, at the deposition site are the controlling factors (Rye and Ohmoto, 1974). In moderate pH regions, and under moderate oxygen fugacity conditions, the predominant aqueous carbon species in an ore fluid at 200°C is H_2CO_3(apparent) = H_2CO_3 + CO_2 (Ohmoto, 1972). Hydrothermal calcite precipitates most commonly from solutions with H_2CO_3 as the dominant carbon species (Robinson, 1975). The average carbon isotopic composition ($\delta^{13}C_{\Sigma C}$) of the ore fluid is then appoximately that of H_2CO_3 (Olson, 1984). Only under these conditions, when there is no appreciable CH_4 in solution (which can be tested by examining fluid inclusions), will the carbon isotopic composition of the precipitated or recrystallized carbonates be directly related to the source. Fractionation factors between carbonate species as a function of temperature are given by Ohmoto and Rye (1979) and

Fritz (1976).

The carbon isotopic composition of total dissolved HCO_3^- (H_2CO_3, $CO_2(aq)$, HCO_3^-, $CO_3^=$, $CaHCO_3^+$, $MgHCO_3^+$, etc) in oil-field waters has been compiled by Carothers and Kharaka (1980). The carbon was found to be mainly of organic origin. At temperatures <80°C, microbial reactions produce $\delta^{13}C_{HCO3-}$ of up to +28 o/oo and, if sulfate levels are high, down to -20 o/oo. At temperatures >100°C equilibration between CO_2 and CH_4, caused by thermal degradation of organic matter, produces a range of $\delta^{13}C$ from +4.8 to -12.3 o/oo (Carothers and Kharaka, 1980).

Methane (CH_4) produced by bacteria in interstitial waters shows a range of $\delta^{13}C$ from -55 to -90 o/oo (Deines, 1980). Carbonate precipitated in equilibrium with HCO_3^- and CH_4 in solution can have a range of $\delta^{13}C$ from -64 to +21 o/oo (Deines, 1980).

Sample preparation and analytical procedures

Carbonate samples for analysis were broken off hand samples or core with a hammer and chisel. Pure calcite or dolomite were crushed to a fine powder and then reacted with 100% phosphoric acid in a vacuum line. Samples that may have been mixtures of calcite and dolomite were crushed and sieved to produce a -18 to +40 mesh (1000 to 430 μm) fraction from which clean calcite grains were carefully handpicked, crushed to -100 to +320 mesh (150 to 45 μm), and then washed repeatedly in distilled water in a sonic bath. The CO_2 gas was prepared for analysis by reacting (for 15 or 20 minutes) 5 to 20 mg of carbonate powders with 100% phosphoric acid at 50°C. This procedure effectively discriminates against CO_2 gas derived from any contaminating dolomite (Walters et al., 1972; see below). For the dolomite samples, the degree of contamination of

dolomite with calcite was checked by using the XRD technique of Hutchison (1974) and Akande (1982).

Walters et al. (1972) showed that CO_2 evolved from coexisting calcite and dolomite can be sampled separately for isotopic determination with little or no mutual interference, if the range between upper and lower limits of the particle size is no more than a factor of 10. However, a further complication is that a sufficient fraction of each carbonate must be reacted in order to avoid an additional 1-2 o/oo isotopic fractionation. For a 5-44 micron grainsize sample of calcite, the reaction has gone to >90% completion after 20 minutes at a temperature of 25°C. For a similar sample of dolomite, the reaction has only gone to 50% completion after 2.5 days. A 1 or 2 o/oo error may thus be introduced by my technique of reacting finely crushed dolomite for only 20 minutes (Table B.1). A rigorous study of the effect was not done because the main interest was in the calcite samples (see Appendix B). Walters et al. (1972) recommend collecting gas for the dolomite analysis from 3 hours after commencement, to completion of the reaction. The effect of temperature, though, is significant. By increasing the temperature to 55°C (our reactions are carried out at 50°C), the reaction rate increases by a factor of 10 (Walters et al., 1972). Therefore, at 50°C the reaction of the (5-44 micron grainsize) calcite sample with phosphoric acid should have gone to about 90% completion after only 2 minutes. For dolomite, collection should commence after 20 minutes. By using a larger grainsize (which was easier to sieve) and reacting mixed calcite/dolomite samples for about 15 minutes, I effectively discriminated against CO_2 gas derived from dolomite.

The interfering effect of organic matter on the measured isotopic

ratios of carbonate shells and fossils has been investigated by Charef and Sheppard (1984). They found that sulfur bearing (e.g. C-SH) and other organic species which are generated during the phosphoric acid attack on organic matter, are the principal sources of interfering species having the same mass as CO_2 species. This effect is especially prevalent in unmetamorphosed low-temperature karstic-type lead-zinc deposits. Charef and Sheppard (1984) showed that pretreatment of samples with 5% NaOCl, and silver phosphate treatment of the H_3PO_4 extracted gas results in a significant decrease in interference effects. The improvement is caused primarily by the pretreatment with 5% NaOCl.

Some of the Gays River samples, which gave off a petroleum odour when crushed, were pretreated with 5% NaOCl and reanalyzed, but no significant consistent effect was found.

The CO_2 gas from the samples along with a gas reference (Carrara Marble) were analyzed using a VG micromass 602D (double-collecting) mass spectrometer. Calibration of our Carrara marble laboratory standard was achieved through replicate analysis of the standard NBS-19 and also of the University of Quebec laboratory standard, UQ2; a split of the latter was provided by C. Hillaire-Marcel. A number of analyses of our Carrara marble standard were supplied by N. Shackleton (Cambridge University). Delta values for carbon are reported relative to the PDB standard; those for oxygen relative to SMOW. These were calculated according to conversion factors in Friedman and O'Neil (1977).

$$\delta^{18}O_{SMOW} = 1.03086 * \delta^{18}O_{PDB} + 30.86 \quad \text{at } 25^{\circ}C \quad (8)$$

Overall accuracy of reported analyses is ±0.3 o/oo.

The Gays River lead-zinc deposit is a site of intense isotopic alteration as shown by the work of Akande (1982). My work expanded the coverage from the mine itself over an area within about 2 km from the mine (Figure 4.1). Calcite, limestone and dolomite were sampled from drillcore and some handsamples. The drillholes used are spaced at 50 m to 300 m intervals along traverses across the area of interest (Figure 4.1).

Samples were also collected from drillcore, outcrop and mine dumps around the margin of the Minas Sub-basin, particularly at some of the other small deposits (Figure 1.2). In sampling, emphasis was placed on vein and vug-filling calcite and limestone, which are more likely to have been in isotopic equilibrium with circulating fluids. Some samples are intergrown with sphalerite and/or galena; others are not associated with sulfides. One objective was to test if the isotopic composition of calcite (either mineralized or not), could be used to map the extent of the area influenced by the mineralizing episode, as an exploration guide to highly mineralized zones. The carbon and oxygen isotopic data also constrained possible genetic models and sources of water and carbon.

Results and interpretation

i) Gays River deposit

Four distinct paragenetic stages of carbonates at the Gays River deposit were reported in Akande and Zentilli (1984). These were: (i) Gays River dolomite (the major host rock for ore); (ii) ore-stage calcite; (iii) post-ore calcite; and (iv) post-ore dedolomitized limestone (Figure 4.2). A suite of lower Windsor limestones, representing pre-dolomitization carbonates, was also analysed. The most

remarkable result from this initial study is that ore-stage calcite samples are characterized by a very narrow range in both $\delta^{18}O_{SMOW}$ and $\delta^{13}C_{PDB}$ values (13.7-14.2 o/oo, 2.2-3.1 o/oo, respectively). Gays River dolomite plots in a somewhat larger field at $\delta^{18}O_{SMOW}$ = 23.6 ± 1.0 o/oo, $\delta^{13}C_{PDB}$ = 1.2 ± 0.7 o/oo. Dedolomitized limestone was found to have essentially the same isotopic composition as the dolomite, but to be depleted in $\delta^{13}C$ by 3 o/oo relative to the latter. Post-ore calcite is characterized by relatively broad ranges in both $\delta^{18}O$ and $\delta^{13}C$ (14.3 to 23.4 o/oo and -5.7 to 1.6 o/oo respectively). The isotopic range of host rock carbonate (mostly dolomite) (Figure 4.2) was defined by my analyses from a larger area within 2 kilometers of the mine. Little isotopic exchange between the mineralizing fluids and dolomite host rock occurred, even in close proximity to highly mineralized zones.

New results from the Gays River area are tabulated in Table B.2 and plotted in Figures 4.1, 4.2 and 4.3. The fields of three of the paragenetic stages from Akande and Zentilli (1984) ((i), (ii) and (iv) above), as well as the field for Windsor limestone are shown in Figure 4.2. Analyses of post-ore calcite samples from their work are plotted together with those from the present study. Away from the mine area, few vein or vug-filling calcite samples could definitely be identified as either ore-stage or post-ore stage as defined by Akande (1982) within the main orebody. Therefore, in Figure 4.2, a distinction is made between those vein and vug-filling calcite samples associated with sulfides and those that are not. Calcite associated with mineralization (sulfides) has in general, an oxygen isotopic composition close to ore-stage calcite, but varies in $\delta^{13}C$ from the ore-stage value down to $\simeq$

-1 o/oo. Only one sample plots in the field of ore-stage calcite defined by Akande (1982). Most of the post-ore calcite analyses plot at a maximum distance from the ore-stage field (in Figure 4.2), and unmineralized calcite falls somewhere in between.

The geographical plot (Figure 4.1) shows the spatial distribution of calcite samples (excluding identifiable post-ore calcite), their isotopic compositions having been normalized to the ore-stage calcite field defined within the mine. (The absolute value of the difference in isotopic composition as plotted in Figure 4.2 was used.) Isotopic compositions of calcite similar to the ore-stage values occur, in general, close to the 2.4% Pb+Zn cutoff zone, but this calcite is not necessarily directly associated with mineralization (sulfides). The isotopic composition of calcite therefore appears to be a good exploration tool. This ore guide idea has been suggested for other carbonate systems (Pinckney and Rye, 1972; Sverjensky, 1981a; Shelton, 1981, 1983). Zones of the deposit where a high (mineralizing) fluid flow rate occurred can thus be characterized. Samples collected near the Black Brook fault (Figure 4.1), do not support the suggestion of Giles et al. (1979), that this structure was a major conduit for mineralizing fluids.

Calcite samples from Gays River for which fluid inclusion homogenization temperatures (as well as isotopic compositions) were determined are plotted in Figures 4.3a and 4.3b. These homogenization temperatures were assumed to be close to the true temperatures of trapping (Akande, 1982), although new fission track and thermal data suggest that a pressure correction of less than 90^{o}C should be applied to the data. Ore-stage and post-ore calcite from Akande and Zentilli

(1984) are shown along with results for 5 new samples. Samples for which temperatures have not been determined are represented by a histogram plotted at the side of each figure. The temperature-controlled data represent reasonably well the entire isotopic range on the histogram.

The isodelta curves on Figure 4.3a estimate (according to O'Neil et al., 1969) the oxygen isotopic composition of water in equilibrium with calcite at various temperatures (Fritz, 1976). No correction was made for the salinity of the ore fluids; no more than a 2 o/oo change would be expected (Truesdell, 1971, 1974). The ore-stage calcite analyses are tightly grouped (at 172°C) in apparent equilibrium with water which has a $\delta^{18}O$ value of +3.3 o/oo. The remaining calcite samples appear to have precipitated from a variety of waters in the range of 0 o/oo to 10 o/oo at a temperature of $\simeq$ 140°C. Following the main pulse of mineralization, hydrothermal fluids were probably variably altered in isotopic composition by dissolution of high $\delta^{18}O$ carbonate rocks and by admixture of low $\delta^{18}O$ meteoric waters. It appears (from Figure 4.2) that carbonate involvement became proportionately more important in post-ore times. Pressure-corrected fluid inclusion temperatures would result in estimated oxygen isotopic compositions for water that were higher by up to 4 o/oo.

In the carbon isotope plot (Figure 4.3b) few samples have compositions greater than the ore-stage value. The $\delta^{13}C$ values in the entire data set range from +3.8 to -8.5 o/oo, the lower values appearing at reduced frequency. The most satisfactory way to explain the data is to postulate that H_2CO_3(apparent) was the dominant carbon species in solution. Consequently, $\delta^{13}C_{\Sigma C} \simeq \delta^{13}C_{H2CO3(app.)}$. If isotopic

equilibrium is assumed, the carbon isotopic composition of the fluids can be estimated from the ore-stage data ($\delta^{13}C_{\Sigma C}$ = 2 o/oo), a value which suggests that ore-stage fluids were dominated by carbonate carbon. As temperatures fell and fluid mixing or dissolution of host carbonates occurred, carbon species remained oxidized, and therefore the isotopic composition of precipitated calcite is primarily controlled by the dependence of the isotopic fractionation factor on temperature. At 140°C, a $\delta^{13}C_{calcite}$ = +4 o/oo is predicted (see Figure 4.3b), a value close to the upper limit of observed data. The trend toward more negative $\delta^{13}C$ values is explained not by changes in oxidation state, but by localized changes in total carbon isotopic composition ($\delta^{13}C_{\Sigma C}$). Organic material which is typically depleted in ^{13}C, is relatively common in the carbonate bank at Gays River, and hydrocarbons have been noted in fluid inclusions in fluorite. Its incorporation into post-ore fluids could provide the required decrease in $\delta^{13}C_{\Sigma C}$. The decrease in $\delta^{13}C$ of successive paragenetic stages in the host rock (Figure 4.2) also suggests incorporation of oxidized organic carbon.

ii) Other deposits

Carbon and oxygen isotope data from various locations around the Minas Sub-basin obtained in the course of this study are tabulated (Table B.3) and plotted (Figure 4.4). Also plotted is data from honours theses at the Pembroke lead deposit (Ponsford, 1983) and the Smithfield lead-zinc deposit (Walker, 1978). None of the other deposits were as intensively studied as the Gays River deposit. The same sample classification and preparation methods as for the Gays River deposit were used, but few calcite samples could be definitely identified as

ore-stage or post-ore stage.

In general, the oxygen and carbon isotope data cover the same range as the data at Gays River. None of the calcite samples at any of the deposits are as much depleted in ^{18}O as the ore-stage calcite at Gays River though. Some vein calcite samples at the Pembroke Pb deposit, Southvale Ba showing and at the Walton/Magnet Cove Ba-Pb-Zn-Cu-Ag deposit are depleted in ^{18}O and could have precipitated from the same type of mineralizing fluids as at Gays River. The carbon isotope data has the same upper limit as at Gays River indicating again the predominant carbonate carbon source with a variable influence of organic carbon.

The Pembroke Pb deposit is hosted in the Macdonald Road Formation at the base of the second major cycle of marine sediments in the Windsor Group. Most of the vein calcite there has high $\delta^{13}C$ and shows a trend of increasing ^{18}O depletion with increased mineralization (sulfides). Highly mineralized vein calcite with $\delta^{18}O \simeq +19$ o/oo gives fluid inclusion homogenization temperatures of about 210°C (Table 3.1) indicating precipitation from a fluid having $\delta^{18}O \simeq +10$ o/oo. Pressure-corrected temperatures would mean that the fluid $\delta^{18}O$ was up to 4 o/oo higher.

One calcite sample (out of a total of three) from the Walton deposit gave a very low $\delta^{18}O$ (=16.8 o/oo). A much more thorough isotopic study of the deposit is needed before a definitive statement about the isotopic composition of the fluid can be made.

Vein calcite in the Macumber limestone just below the small Southvale Ba showing, gives quite low $\delta^{18}O$ values. This, together with the presence of dolomitic limestone breccia hosting the barite, may indicate

the passage of a significant amount of mineralizing fluids through the area.

At the Smithfield Pb-Zn deposit, a large range of $\delta^{13}C$ values occurs over a narrower range of $\delta^{18}O$ values in vein and vug-filling calcite. Most of the mineralized calcite plots near $\delta^{18}O \simeq 19.5$ o/oo, $\delta^{13}C \simeq -8.0$ o/oo indicating a significant influence of organic carbon. Fluid inclusion homogenization temperatures of 150° to $\simeq$ 190°C in mineralized calcite indicates precipitation from a fluid having $\delta^{18}O \simeq 8.0$ o/oo.

In only a few cases did vein calcite from other sites around the Minas Sub-basin give isotopic compositions that show the influence of hot, low $\delta^{18}O$ fluids. In general, the data plot close to the $\delta^{18}O$ field for host rock Windsor limestone. The influence of organic carbon on the $\delta^{13}C$ of vein calcite is quite variable.

4.3 Hydrogen and oxygen isotopes

Isotopes of hydrogen and oxygen of present-day formation waters (basinal brines)(Figure 4.5) indicate that they are not concentrated seawater, nor meteoric water with added salts (5 to 10x the salinity of seawater), but some complex mixture of meteoric water and seawater modified by rock-water interactions within the basins (Anderson and Macqueen, 1982). They show a general increase in both $\delta^{18}O$ and δD with increasing salinity, temperature and thus depth in the basin. Other factors such as magmatic water may be important in some cases. The hydrogen and oxygen isotopes in meteoric water follow a simple linear relationship (Figure 6.4 in Taylor 1979). The higher the latitude or elevation, the lower are δD and $\delta^{18}O$ of the meteoric water. Between basins therefore, there is a general decrease in $\delta^{18}O$ and δD as one

moves to higher latitudes, reflecting the significant contribution of meteoric water, the original connate water of deposition having been lost by compaction and subsequent flushing (Kharaka and Carothers, 1986).

The δD value measured in formation waters is mainly controlled by the source(s) of the water(s) and not by the rocks. However, it is strongly influenced by clay mineral reactions. Interlayer water in swelling clays readily reequilibrates with formation waters, and hydrogen reequilibration between formation water and structural sites in clays occurs at temperatures above 100°C (O'Neil and Kharaka, 1976). Isotopic exchange with hydrocarbons, H_2S, and hydrated minerals, and shale membrane fractionation effects (ultrafiltration), cause some change in δD of the fluids as well (Sheppard, 1983; Longstaffe, 1983).

The $\delta^{18}O$ of formation waters is dominated by oxygen in the rocks and thus reflects the isotopic composition of the rocks through which the fluids passed. Carbonate oxygen has a strong influence in shifting formation waters to heavy oxygen isotopic compositions even at low (<100°C) temperatures. But, the shift to heavy oxygen is observed in all basins, including those dominated by clastics. As temperatures rise (to >200°C), isotopic exchange between formation waters and quartz and feldspars can become significant (Kharaka and Carothers, 1986). However, the loss of interlayer water in clays and structural water during clay alteration to higher order micas probably have a significant effect on both oxygen and hydrogen isotopic compositions of formation waters.

Figure 4.5 is a plot of δD vs $\delta^{18}O$ isotopic compositions of all naturally occurring waters, including basinal brines which tend to plot

along straight lines for each basin. Sheppard (1976) concluded that these saline formation waters, which seem to have a substantial meteoric water component, are probably intimately associated with the genesis of MVT deposits. Fluid inclusion fluids from Mississippi Valley-type (MVT) deposits tend to plot inside the boxed areas on Figure 4.5 (Ohmoto, 1986). Some δD analyses of fluid inclusions in sphalerite, galena, calcite, fluorite, barite and quartz from the Cave-in-Rock district of the Mississippi Valley (Hall and Friedman, 1963) fall within the range of Illinois basin brines. This supports a genetic link between these fluids. But, it is less important to look at the present waters residing in ancient sediments than to look at processes that occurred during the active depositional and diagenesis phases of basin development (Hanor, 1979).

The Gulf of Mexico is a prime example of a basin where the formation waters are still predominantly connate in origin. Hydrogen and oxygen isotopic compositions of formation waters from overpressured and normally pressured zones in the northern Gulf of Mexico basin show a trend that passes through SMOW and away from the meteoric water of the area (Figure, 4.5). This trend of increasing $\delta^{18}O$ accompanied by decreasing δD can be explained by isotopic exchange between ocean water and clay minerals having very light original δD values of -70 o/oo (Kharaka and Carothers, 1986).

A δD vs $\delta^{18}O$ plot of the mineralizing fluid composition can reveal much about the origin and subsurface history of the hydrothermal fluids. The isotopic character of the mineralizing fluid that formed a mineral deposit can be determined in two ways: (i) by isotopic analysis of fluid inclusion fluids (in non-oxygen bearing minerals such as sulfides for

$\delta^{18}O$ and non-hydrogen-bearing minerals for δD) (ii) if it can be assumed that fluid-mineral equilibrium was attained, by isotopic analysis of minerals such as gypsum and clays (for δD), carbonates and quartz (for $\delta^{18}O$), associated with the mineralizing event. The latter method requires a calculation using experimentally determined fractionation factors (Figures 6.1 and 6.2 in Taylor, 1979), and the temperature of the mineralizing event. Temperatures can be obtained from fluid inclusion thermometry or from mineral-pair sulfur isotope geothermometry; the latter assumes cogenetic mineralization and mineral-mineral equilibrium (Rye and Ohmoto, 1974). Rye (1974) determined that in the 200° to 370°C temperature range most galena-sphalerite sulfur isotope temperatures from six ore deposits are within 20°C of fluid inclusion filling temperatures. Below 200°C, sulfur isotope disequilibrium may occur. Isotopic fractionation of the sulfides by later post-ore fluids is also always a possibility.

Sample preparation and analytical procedures

Sheppard (1976) stated that 30-40 grams of a mineral have to be crushed in a vacuum line to extract sufficient water from fluid inclusions for δD analysis. H. Krueger (oral comm., 1985) of Geochron Laboratories stated that one needs 4 milligrams of fluid for best results and 10 milligrams if both δD and $\delta^{18}O$ analyses are done. The water content by weight of the galena and barite samples were measured as 0.15% and 0.24% respectively by heating to high temperatures ($\sim$ 900°C) in an induction furnace. This means that sample size must be >3 grams.

Problems with isotopic analyses of inclusion fluids arise because

samples with both primary and secondary inclusions recording a multistage fluid history are common. It is impossible to separate these different generations of fluids but an attempt was made by heating the samples to 100°C for a few hours in an oven to drive off loosely held fluid (in secondary inclusions and fractures). The isotopic analyses were performed at Geochron Laboratories, Krueger Enterprises, Inc., Cambridge, Massachusetts. Precision of δD and $\delta^{18}O$ analyses are +2 o/oo and +1 o/oo respectively. Both are reported relative to standard mean ocean water (SMOW).

Large crystals of ore-stage calcite from Gays River (AGR-07 and AGR-91) were selected for δD analysis of fluid inclusion fluid as were mineralized vein calcite samples from Pembroke and Smithfield. Sphalerite-bearing dolomite core from DDH# GR-499 (128.5-132.5 feet depth) was crushed with hammer and mortar & pestle to $\sim$ 1 centimeter size, then dissolved in 10% acetic acid. Methylene iodide was used for heavy liquid separation of sphalerite from dolomite. Large sphalerite crystals ($\sim$ 250 um) were then handpicked from the -45 +120 mesh fraction. Gays River galena (AGR-24B) was selected from Akande's samples. All the galena and barite samples were analyzed for δD and $\delta^{18}O$ of fluid inclusion fluids. Unlike calcite, barite does not easily equilibrate oxygen isotopes between the fluid in the inclusion and the mineral as it cools (Lloyd, 1968). Chiba and Sakai (1985) showed that barite-water fractionation at <200°C is slow and the fractionation factors are strongly temperature and pH dependent. Further work analyzing the $\delta^{18}O$ of the barite itself is in progress.

A gypsum sample (DW4-405) from Akande's collection, was selected for δD analysis of the water of hydration, recovered by thermal

decomposition to anhydrite. Fractionation factors (at 25°C) from Matsubaya and Sakai (1973) were used to calculate the hydrogen isotopic composition of the original water of hydration for the gypsum.

Results and Interpretation

The water generated by thermal dehydration of gypsum sample DW4-405 gave a δD value of -100 o/oo, which corresponds to -81.6 o/oo for the original waters of hydration. Matsubaya and Sakai (1973) give a fractionation factor of $\alpha_{gyp\text{-}water} = 0.980$ between gypsum and water at 25°C. From equations (1) and (2):

$$\alpha_{gyp\text{-}water} = (1000+\delta D_{gypsum})/(1000+\delta D_{water})$$

$$0.980 = (1000-100) / (1000+\delta D_{water})$$

$$\delta D_{water} = 900/0.980 - 1000$$

$$= -81.6 \text{ o/oo}$$

Present-day meteoric waters in Nova Scotia have $\delta D \sim -50$ o/oo (Taylor, 1979).

The hydrogen and oxygen isotopic compositions of the inclusion fluids in sulfides and calcite at Gays River and the other deposits (Table 4.2 and Figure 4.5) plot outside the fields for typical MVT deposits but within the fields for formation waters and metamorphic/igneous waters. The overlap of the metamorphic water field with higher temperature and more ^{18}O-rich formation waters is to be expected because of the continuum between diagenesis and low-grade metamorphism (Sheppard, 1986). The data therefore support a basinal brine source, but due to a lack of data on nearby basins, no direct relationship with Fundy/Magdalen basinal brines or with the meteoric(?) water of gypsum

hydration can be proven at this time. The formation of brines by the interaction of metamorphic/igneous fluids with meteoric water in the deeper parts of the Fundy/Magdalen basin, cannot be ruled out. The direct involvement of marine water is not suggested by the isotopic data, although Ohmoto (1986) stated that the δD of the oceans may have fluctuated between -40 o/oo and +10 o/oo during the past 2 b.y.

The hydrogen and oxygen isotopic compositions of the inclusion fluids in barite plot to the left of the meteoric water line (Figure 4.5). These low oxygen isotopic compositions could be explained by exchange between the fluids and the host mineral as it cooled (Sheppard, 1986). Though exchange between barite and water may be slow (Chiba and Sakai, 1985) a fractionation could occur in the closed system of the fluid inclusion over the time periods involved. The large range of δD of the fluids at some of the deposits could be explained by mixing of two fluids with very different hydrogen isotopic compositions; a basinal brine and a local meteoric water similar in isotopic composition to the water of hydration of gypsum. Only the fluid that formed Lake Fletcher (δD = -27 o/oo) would not fit this model.

4.4 Sulfur isotopes

I first re-interpret here data presented in Figure 11 of Akande and Zentilli (1984), in the light of my significantly extended isotopic data base; no new data from Gays River are presented. The 5 analyses of pre-ore anhydrite yield a mean $\delta^{34}S$ = 14 ± 1 o/oo (1σ), which is in the range of that expected for Mississippian marine evaporites (Thode and Monster, 1965; Claypool et al., 1980). Because the Gays River deposit is stratigraphically overlain by this sulfate (Figure 1.3), I concur

with Akande and Zentilli (1984) that this is the dominant source of sulfur for the deposit. The range of $\delta^{34}S$ values for the Meguma basement (graywackes and shales) is -15 to +25 o/oo with an average of 7 ± 2 o/oo (Kubilius, 1983; Ohmoto, 1986). The possible role of basement sulfur in the Gays River deposit therefore remains unclear.

Note that the $\delta^{34}S$ values for galena and sphalerite are identical ($\delta^{34}S_{Gn}$ = 10.8 ± 0.2 o/oo, $\delta^{34}S_{Sp}$ = 10.8 ± 0.4 o/oo, both 1σ) based on 15 sphalerite and 16 galena analyses. If equilibrium fractionation (at 200°C) is assumed, the $\delta^{34}S$ of H_2S in the ore fluid would have been 10.4 o/oo (on the basis of Sp data) or 13.6 o/oo (from the Gn data). If temperatures were 90°C higher due to a pressure correction to the fluid inclusion temperature data, then the calculated $\delta^{34}S$ of H_2S would be about 10.5 o/oo (on the basis of the Sp data) or 12.7 o/oo (on the basis of Gn data). (H_2S can be assumed to be the dominant reduced sulfur species in hydrothermal solutions under normal pH conditions and $100^\circ < T < 350^\circ$C (Ohmoto and Rye, 1979)). Galena occurs after, or coincident with sphalerite in the paragenetic sequence. The shift in $\delta^{34}S_{H2S}$ can be explained by an increasing degree of reduction of sulfate in the fluids as mineralization progressed (see Figure 4.6).

The postulated path of the ore-forming fluid is indicated in Figure 4.6, a log fO_2 - pH diagram adapted from Ohmoto (1972) and Olson (1984). The possible range of sulfur isotopic compositions and mineral stability fields for an Fe-S-O system at T = 200°C are illustrated, given a $\delta^{34}S_{\Sigma S}$ = +14.0 o/oo and a sulfur concentration between 0.001 and 0.0001 moles/kg H_2O. The pH of the ore fluid is assumed to have been $\simeq$ 5.5 during sulfide precipitation and oxygen fugacity decreased as mineralization progressed. The postulated path corresponds to a

progressive change in $\delta^{34}S_{H2S}$ from about +10 o/oo to +14 o/oo as first sphalerite and then galena were precipitated under increasingly reduced conditions. As temperatures decreased to 170°C, pH and temperature may have fluctuated slightly resulting in alternating precipitation of ore-stage calcite and galena. As temperatures decreased to 130°C and pH increased slightly, post-ore calcite was deposited. Deposition of the latter probably resulted from the mixing of the mineralizing fluids with a less saline fluid, probably meteoric water (see discussion of oxygen isotopes). The entire depositional path falls in an oxidized carbon environment. Using higher, pressure-corrected fluid inclusion temperatures would result in a very similar path for the ore-forming fluids, however, the values of oxygen fugacity (fO_2) at which this occurred would be higher.

Post-ore sulfates which have $\delta^{34}S$ values similar to the assumed total sulfur value (gypsum, $\simeq$ 13 to 16 o/oo; barite, $\simeq$ 14 o/oo) were likely precipitated from cooler (Table 3.1), oxidized (sulfate-rich) fluids in the late stages. Very late post-ore sulfides with highly negative $\delta^{34}S$ (pyrite, $\simeq$ -46 o/oo; marcasite, $\simeq$ -10 to -46 o/oo), are best explained by biogenic reduction of sulfate at much lower temperatures.

Sample preparation

Clean samples of barite, galena and sphalerite from some of the other deposits in the Minas Sub-basin were prepared. Samples were crushed and sieved to produce a -18 to +40 mesh (1000 to 430 μm) fraction from which clean grains were handpicked. The grains were then washed with distilled water in a sonic bath. Sulfur isotopic analyses were performed on <100 mg samples at McMaster University. Analyses are

reported relative to the Canyon Diablo troilite standard (CDT). Precision of analyses is about ±0.2 o/oo.

Results and interpretation

The results (Table 4.1) show that barites from the various deposits all have $\delta^{34}S$ values quite close to the value for Mississippian marine evaporites. This is even true for the barite at Lake Fletcher, which is in a vein in the Meguma basement about 10 km from the nearest Carboniferous outcrop. The most likely explanation for Lake Fletcher is that this showing represents a vein formed in a basement fracture just below the now eroded Carboniferous basin.

The Smithfield barite is slightly elevated in $\delta^{34}S$ (=15.1 o/oo) compared to the isotopic composition of the evaporites (the assumed sulfur source). The sulfides have lower $\delta^{34}S$ (galena $\simeq$ 4.5 o/oo, sphalerite $\simeq$ 6.8 o/oo) than the sulfides at Gays River. If equilibrium fractionation (at 200°C) is assumed, the $\delta^{34}S$ of H_2S in the mineralizing fluid would have been 7.3 o/oo (on the basis of galena) and 6.4 o/oo (from the sphalerite data). Using the difference in the sulfur isotopic composition of the sphalerite and galena as a geothermometer, results in a temperature of about 287°C (formula from Ohmoto and Rye, 1979). However, more careful sulfur isotopic work on actual sphalerite-galena pairs needs to be done. In my limited set of samples sphalerite appears to have precipitated before galena. At Pembroke the galena has an even lower $\delta^{34}S$ (= -2.2 to -5.0 o/oo). The wide range of sulfur isotopic values noted at the Walton/Magnet Cove deposit by Boyle et al. (1976), with the barite having elevated $\delta^{34}S$ values (above Mississippian seawater values) and the sulfides slightly negative values, is similar

to Smithfield/Pembroke.

These data can be explained in the same way as at Gays River, using Figure 4.6. At Smithfield the barite precipitated first in a mainly oxidizing environment but with some sulfate reduction occurring, thereby causing elevated $\delta^{34}S$ of barite (>14.0 o/oo). The depositional environment then became increasingly more reducing and first sphalerite followed by galena were precipitated. A similar path may have been followed by the ore-forming fluids at Walton/Magnet Cove. At Pembroke, the depositional environment may have been even less reducing, resulting in precipitation of galena with quite low $\delta^{34}S$. A more complete data set would be needed in order to make a definitive statement, but this data does not contradict the Gays River model.

4.5 Strontium isotopes

Strontium isotopes are useful for tracing the calcium and barium component of minerals such as calcite, barite and fluorite. Because these minerals usually contain negligible quantities of rubidium, their strontium isotope ratios are a measure of the isotopic composition of the strontium in the mineralizing fluids. The strontium isotope ratios in gangue minerals from Mississippi Valley-type (MVT) deposits indicate that where mineralization is sparse, the minerals precipitated from fluids that were in local isotopic equilibrium with the host carbonates (Figure 4.7). Conversely, in districts of major economic mineralization, the ratios are anomalous and increase as mineralization progresses. In these districts, the process appears to be that of mixing of strontium-bearing fluids from the relatively rubidium-rich silicate minerals in the sedimentary succession, with locally derived

fluids (Kessen et al., 1981). Thus, within a given basin, prospects in which calcite, barite or fluorite have relatively high $^{87}Sr/^{86}Sr$ ratios may represent good exploration targets.

No strontium isotopic studies for tracing the origin of mineralization had been done on any of the lower Carboniferous carbonate-hosted deposits in Nova Scotia. However, rubidium-strontium information is available on some of the possible source rocks which may have equilibrated with the mineralizing fluids. Clarke and Halliday (1980) report that in the South Mountain batholith, granodiorite (371.8 Ma) had an initial ratio of $(^{87}Sr/^{86}Sr) = 0.7076 - 0.7090$; adamellite (364.3 Ma), $(^{87}Sr/^{86}Sr) = 0.70942$; porphyry (361.2 Ma), $(^{87}Sr/^{86}Sr) = 0.71021$. This wide range of initial strontium ratios is probably due to involvement of sediments in the formation of the peraluminous granitoids. A suite of Meguma country rock samples had $^{87}Sr/^{86}Sr = 0.7113 - 0.7177$ at the time of intrusion of the batholith. Work by Lambert et al. (1984), on the Meguma Group black slates, gives a reference line which suggests a possible age of 490 Ma with an initial ratio of 0.7130. Preliminary data on Meguma Group metagraywackes give an initial ratio $(^{87}Sr/^{86}Sr) = 0.711$ (Lambert et al., 1984). No data exist for the Horton Group clastic rocks which may have undergone equilibration of strontium (at least in glauconite or 2M-illite) (e.g. Faure, 1977; Clauer, 1982; Stein and Kish, 1985) either during burial or a low temperature regional metamorphism or during a fluid flow event.

The purpose of this part of the project was to determine:

1) if there is a genetic link between the different deposits around the margin of the Minas Sub-basin.

2) if the mineralizing fluids may have derived at least their calcium and barium components from the Horton Group clastic rocks. (Ascertaining the age of homogenization of strontium in these rocks, and thus the age of a possible hydrothermal event would be an added bonus.)
3) if strontium isotopic analysis of ore-stage minerals is a useful exploration tool.

Sample preparation and analytical procedures

At Gays River, $^{87}Sr/^{86}Sr$ ratios were determined for: (i) anhydrite from stratigraphically overlying Windsor group evaporites, (ii) host dolomite, (iii) ore-stage calcite, (iv) fluorite, (v) post-ore calcite, (vi) post-ore barite, (vii) post-ore dedolomitized limestone and (viii) post-ore gypsum (selenite). Samples of barite, calcite, and host rock carbonate were also selected from a number of mineral deposits around the margin of the Minas Sub-basin (Figure 1.2). Only clean, unweathered samples were used. Sample selection was based on position in the paragenetic sequence, location in the deposit, and colour (Table C.1).

A careful sample preparation procedure was followed. The calcite and host carbonate samples were broken up with a percussion mortar and sieved in plastic sieves to get the +20 to -45 mesh (841-355 μm) fraction. Sieves were cleaned with compressed air and super-clean ethyl alcohol between samples. This fraction was handpicked to give approximately 2 grams of very clean sample. The samples were then washed repeatedly with super-clean ethyl alcohol in a sonic bath. The dry samples were crushed using an agate mortar and pestle. The mortar and pestle were cleaned with quartz between samples. The relatively

strontium-rich barite samples were prepared in a similar manner, but in a separate location to avoid contamination. Calcite sample RSB-32 was accidentally first prepared in the same laboratory as the barite samples. No difference in isotopic composition was observed between this sample (32a) and a duplicate (32b) prepared at the other location. This gives a good indication of the cleanliness of my preparation system.

The isotopic analyses were performed at Geochron Laboratories, Cambridge, Massachusetts and at the Department of Geology, Carleton University, Ottawa. Analyses of a control sample revealed no interlaboratory difference (beyond quoted experimental uncertainties). The precision of the Geochron analyses is ± 0.0003 for some samples and ± 0.00008 for others (2 standard deviations for both). At Carleton University analyses were done on a Finnigan-MAT 261 multi-collector mass spectrometer. The estimated precision in the $^{87}Sr/^{86}Sr$ analyses is + 0.00003 (2 standard deviations). The measured $^{87}Sr/^{86}Sr$ ratios for the Eimer and Amend Standard and NBS 987 were 0.70802 ± 0.00002 and 0.71023 ± 0.00003 respectively. All analyses were normalized to $^{88}Sr/^{86}Sr$ = 8.37521.

The carbonate samples were first dissolved in 3N HCl and strontium was then isolated by conventional cation exchange techniques. Barite was first fused with $LiBO_2$ in a graphite crucible, then taken up in dilute HCl.

Results and interpretation

Analytical results are tabulated in Table C.1 and plotted in Figure 4.8. The paths with arrows in Figure 4.8 indicate the change in

strontium ratios along the paragenetic sequence at each mineral occurrence. Strontium concentrations in the carbonates (obtained by atomic absorption techniques) ranged from 60 ppm to 160 ppm. Rubidium concentrations were below the detectable limit in all cases; consequently, corrections for in situ Rb-decay were not made. In the worst case, this correction (over a 300 Ma time span) would approximate the measurement uncertainty.

Observed $^{87}Sr/^{86}Sr$ ratios of the host dolomite (0.70825 to 0.70851) and host limestone (0.70775 to 0.70845) for all deposits are in the range of expected values for Misssissippian sea water (Burke et al., 1982). (The single anhydrite sample has a somewhat higher ratio (0.7090)). The mineralized calcite at Gays River, one of the mineralized calcite samples at Pembroke and the barite at Brookfield all have strontium isotope ratios (0.71127 to 0.7120) substantially higher than that of the host carbonate. This result is similar to that seen in the major Mississippi Valley districts by Kessen et al. (1981)(see Figure 4.7). Post-ore calcite at Gays River indicates a return to lower strontium ratios after the main mineralizing event. Strontium ratios in barite at Gays River, Southvale, Smithfield, Middle Stewiacke, Hilden and Walton are intermediate between the host rock and highly anomalous values. The highest strontium ratios were found in barite within Meguma Group slates at Lake Fletcher.

One or more sources of relatively radiogenic strontium are required to explain the ore-stage data; strontium from the host carbonates and overlying sulfates did not dominate the strontium budget. Meguma Group metasediments, though rather high in strontium ratio, are a possible source of the radiogenic strontium in the ore fluid, as are South

Mountain batholith granodiorites. Horton Group rocks, the clastic equivalents of both rock types, cannot be excluded.

The fluids may have entered the basement rocks along fractures as well as moving through the Horton clastic rocks. The $^{87}Sr/^{86}Sr$ ratios (at 300 Ma) for the Meguma Group metasediments (0.7124 - 0.7244) and the granodiorites (0.7104 - 0.7127) (calculated from data in Lambert et al. (1984) and Clarke and Halliday (1980)) indicate that either could have been a source for the calcite and barite with high strontium ratios. The very heterogeneous Horton Group rocks which are direct clastic derivatives of the Meguma metasediments and the granodiorites could also have been a source. Figure 4.9 is a summary plot of the data at Gays River. Also shown are the calculated ranges in $^{87}Sr/^{86}Sr$ ratios (at 300 Ma) for two possible sources: (i) Meguma Group metasediments - the basement rocks at Gays River and (ii) granodiorite - the major rock type of the large South Mountain batholith (data from Lambert et al. (1984), and Clarke and Halliday (1980)).

The barite vein in Meguma slates at Lake Fletcher (0.71229) could not have been formed from the South Mountain granites (t = 374 to 360 Ma, Clarke and Halliday, 1980) because the strontium available at that time would have had an isotopic ratio (0.7076 to 0.7102) that was too low. But, it may have been formed at that time by barium- and strontium-rich fluids originating within the Meguma (0.7113 to 0.7177). This type of deposit could then have been the source for the later Carboniferous mineralization, but the low solubility of barite may preclude this possibility. Precipitation from fluids penetrating down into the Meguma (and picking up slightly more radiogenic strontium there) along fractures from the overlying Carboniferous basin at 300 Ma is also a

possibility. The range of strontium ratios available in the Meguma metasedimentary rocks is too large to rule out either possibility.

There does appear to be a genetic link between the mineral occurrences around the Minas Sub-basin. The ore minerals of the larger and/or higher grade deposits such as Gays River Zn-Pb deposits, have a relatively high $^{87}Sr/^{86}Sr$ ratio (0.712), suggesting a massive influx of mineralizing fluid considerably different from Carboniferous seawater recorded in the host carbonates ($^{87}Sr/^{86}Sr = 0.708$). Smaller, lower-grade deposits have strontium isotopic compositions that are probably mixtures of mineralizing fluids with locally derived fluids. A possible source for the much more radiogenic strontium is in the continental clastics of the Horton Group.

TABLE 4.1 Sulfur isotopic compositions of sulfates and sulfides.

Sample Number	Location	Composition	Weight (mg)	$\delta^{34}S$ ‰
P5	4.Pembroke	Galena	207	-5.0
RSB-46	4.Pembroke	Galena	207	-2.2
RSB-29a	5.Smithfield	Barite	520	15.1
RSB-119	5.Smithfield	Galena	215	4.8
RSB-121	5.Smithfield	Sphalerite	-	6.8
RSB-125	5.Smithfield	Galena	365	4.2
RSB-35	7.Brookfield	Barite	610	12.7
RSB-38	7.Brookfield	Barite	470	11.2
RSB-62	13. Lake Fletcher	Barite	380	14.8

TABLE 4.2a Hydrogen and oxygen isotopic compositions of fluid inclusions.

Sample Number	Location	Composition	$\delta^{18}O$‰	δD‰
AGR-24b	1.Gays River	Galena	-3.2	-41
RGR-110	1.Gays River	Sphalerite	too small	-58
P5	4.Pembroke	Galena	+4.2	-51
RSB-125	5.Smithfield	Galena	+5.9	-70
RSB-29	5.Smithfield	Barite	-9.5	-56
RSB-36	7.Brookfield	Barite	-10.7	-44
RSB-38	7.Brookfield	Barite	-10.7	-69
EC-789	10.Walton	Barite	-15.8	-86
RSB-69	10.Walton	Barite	too small	-72
RSB-62	13.Lake Fletcher	Barite	-11.0	-27

TABLE 4.2b Measured hydrogen and calculated oxygen isotopic compositions of mineralizing fluids.

Sample Number	Location	Comp.	Th(^{o}C)	$\delta^{18}O$‰ (calcite)	$\delta^{18}O$‰ (water)	δD‰ (water)
AGR-07	1.Gays River	Calcite	169	13.78	+2.9	-41
AGR-91	1.Gays River	Calcite	170	13.93	+3.2	-38
RSB-46	4. Pembroke	Calcite	195	19.34	$\sim$10	-48
RSB-30	5. Smithfield	Calcite	158	20.2	$\sim$8.6	-46

Figure 4.1 Spatial distribution of mineralized and unmineralized calcite at Gays River. An oxygen and carbon isotopic "index" relative to ore-stage calcite from within the mine is indicated, as explained in the text (e.g. small wedges indicate a small deviation from ore-stage calcite values). ⊗ or ⊙ = ore-stage calcite.

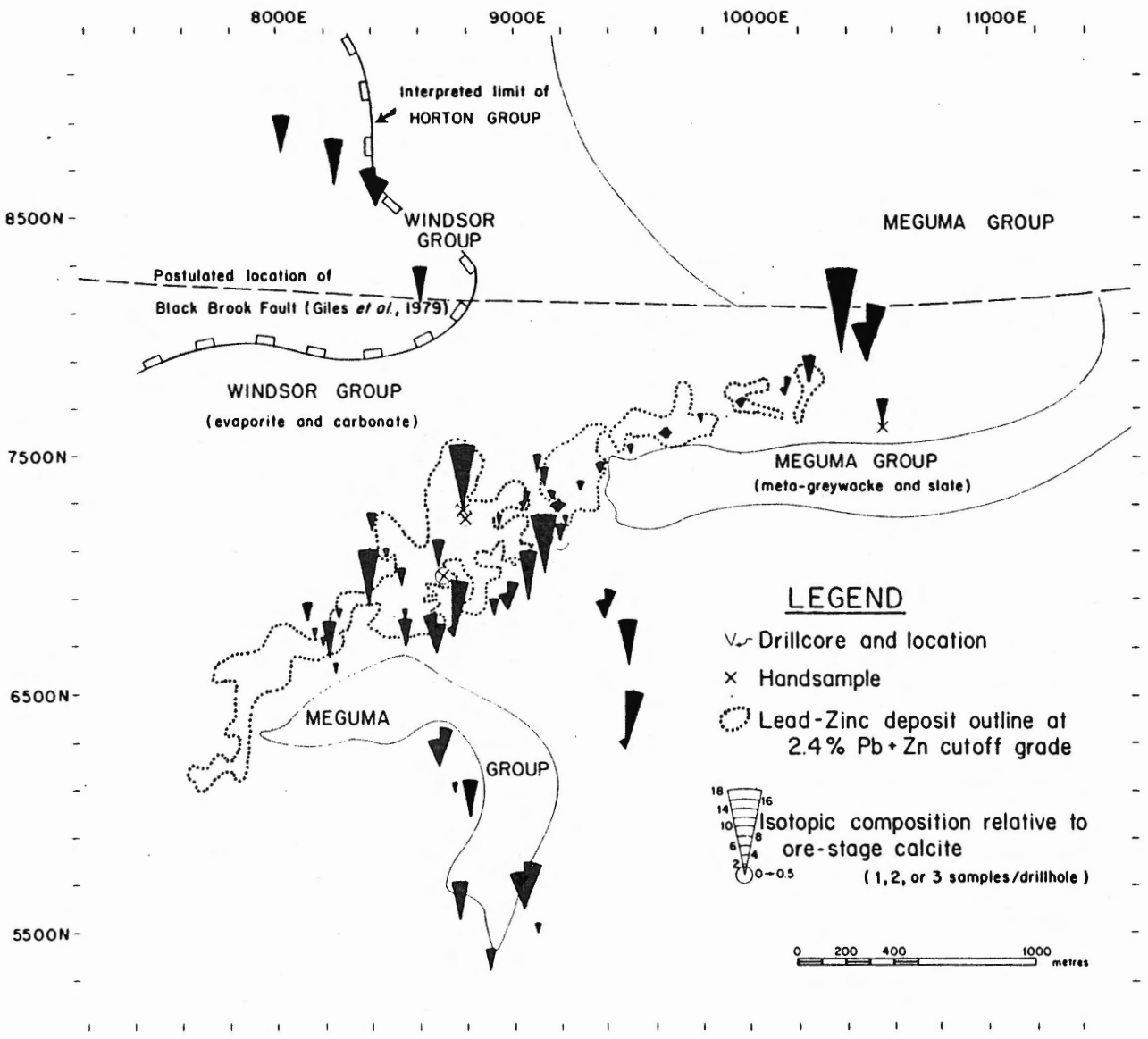
8000E
9000E
10000E
11000E
8500N
7500N
6500N
5500N
Interpreted limit of
HORTON GROUP
WINDSOR
GROUP
MEGUMA GROUP
Postulated location of
Black Brook Fault (Giles et al., 1979)
WINDSOR GROUP
(evaporite and carbonate)
MEGUMA GROUP
(meta-greywacke and slate)
MEGUMA
GROUP
LEGEND
Drillcore and location
Handsample
Lead-Zinc deposit outline at
2.4% Pb + Zn cutoff grade
18
16
14
10
8
6
4
2
0-0.5
Isotopic composition relative to
ore-stage calcite
(1, 2, or 3 samples/drillhole)
0
200
400
1000
metres

Figure 4.1

Figure 4.2 Oxygen and carbon isotopic compositions of host rock and calcite near the Gays River deposit. Outlined fields are from Akande and Zentilli (1984), except for the host rock carbonate field, which was determined in the present study for the larger 2 km radius area. Star, C.L.= average value for Carboniferous limestone (Keith and Weber, 1964). ■ = mineralized calcite, □ = unmineralized calcite, X = post-ore calcite. Ore-stage calcite is mineralized calcite (calcite clearly associated with sphalerite and galena) that Akande (1982) positively identified as having precipitated at the same time as the sulfides. Post-ore calcite is unmineralized calcite that is very clear and is the last calcite to fill vugs, etc.

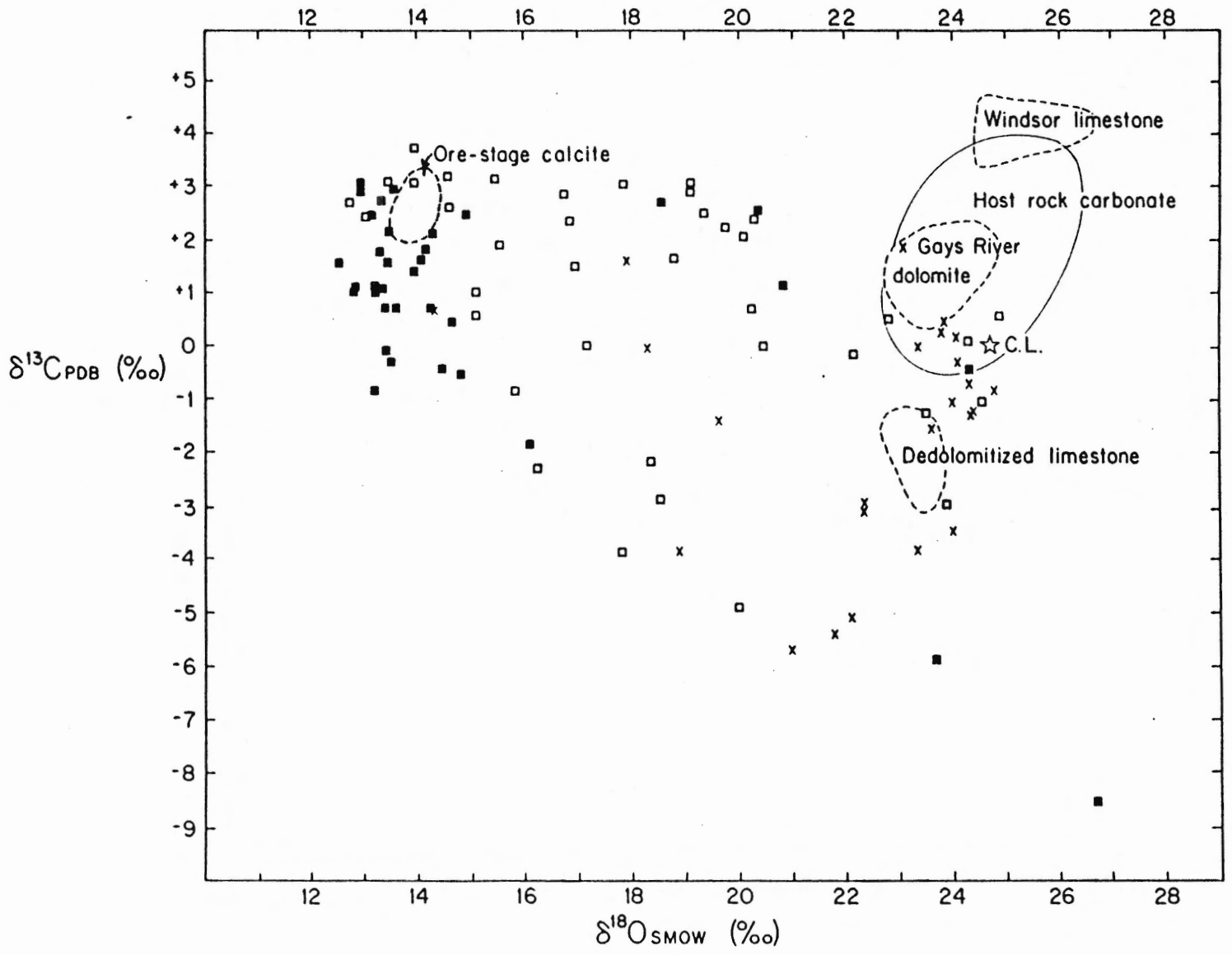
Windsor limestone
Ore-stage calcite
Host rock carbonate
Gays River dolomite
C.L.
Dedolomitized limestone
δ13CPDB (‰)
δ18OSMOW (‰)
12
14
16
18
20
22
24
26
28
+5
+4
+3
+2
+1
0
-1
-2
-3
-4
-5
-6
-7
-8
-9

Figure 4.2

Figure 4.3 Oxygen and carbon isotopic compositions of calcite at Gays River as a function of temperature. ● = ore-stage calcite, O = all other calcite. (a) The $\delta^{18}O$ values of calcite as a function of temperature. Calcite samples for which temperature data is not available are represented by the histogram on the left. Isodelta curves shown are for the various values of $\delta^{18}O_{H2O}$ given in [ ] (calculated according to O'Neil et al., 1969). Each curve gives the isotopic composition of pure water in equilibrium with calcite formed at the temperatures shown. (b) The $\delta^{13}C$ values of calcite as a function of temperature. Histogram as in (a). Quantities in [ ] on the isodelta curves are the values of aqueous $\delta^{13}C_{H2CO3(apparent)}$ (calculated according to Ohmoto and Rye, 1979), in equilibrium with calcites of the indicated compositions at the temperatures shown.

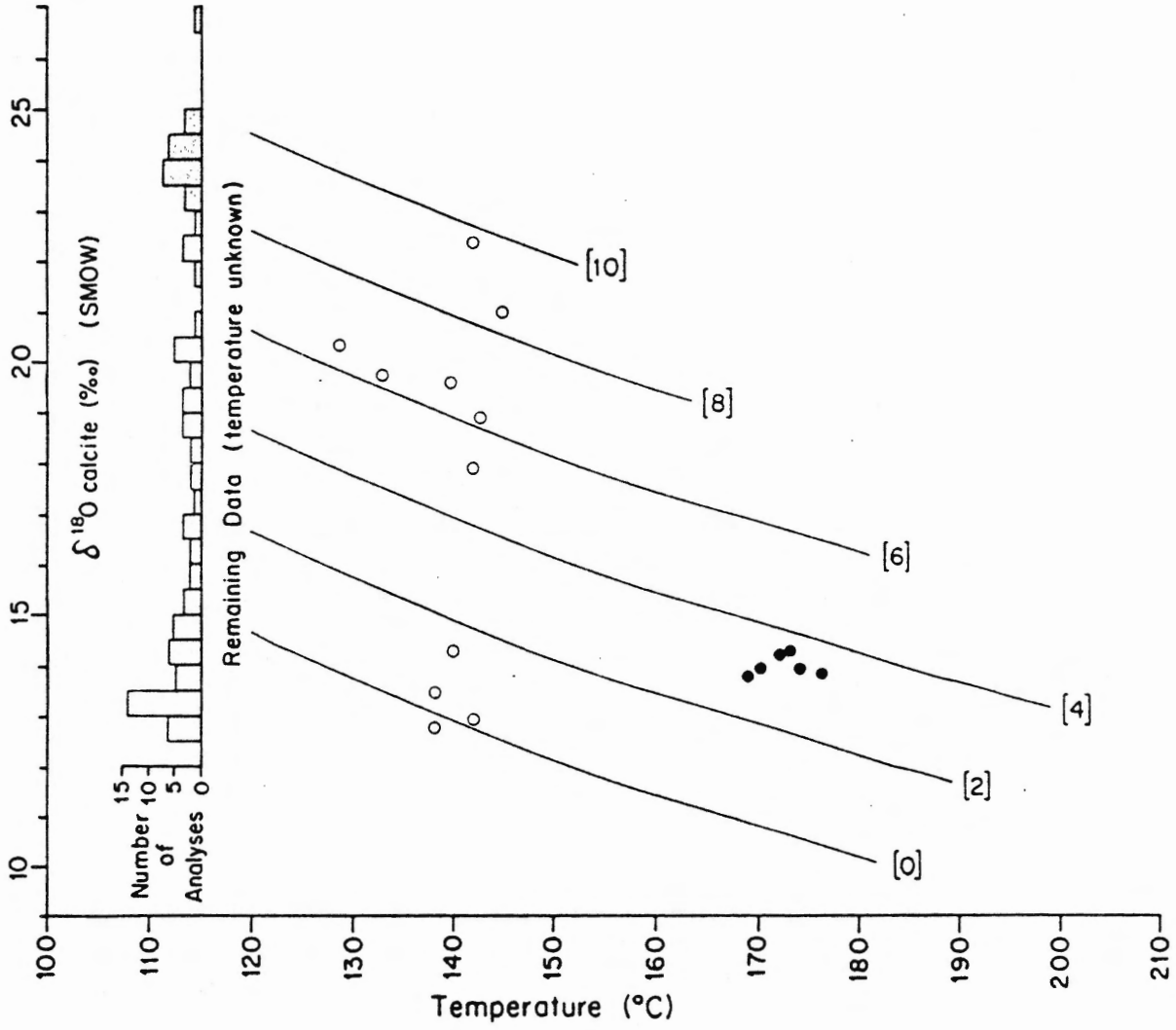
$\delta^{18}O$ calcite (‰) (SMOW)
Number of Analyses
15
10
5
0
Remaining Data (temperature unknown)
[10]
[8]
[6]
[4]
[2]
[0]
Temperature (°C)
100
110
120
130
140
150
160
170
180
190
200
210
10
15
20
25

Figure 4.3a

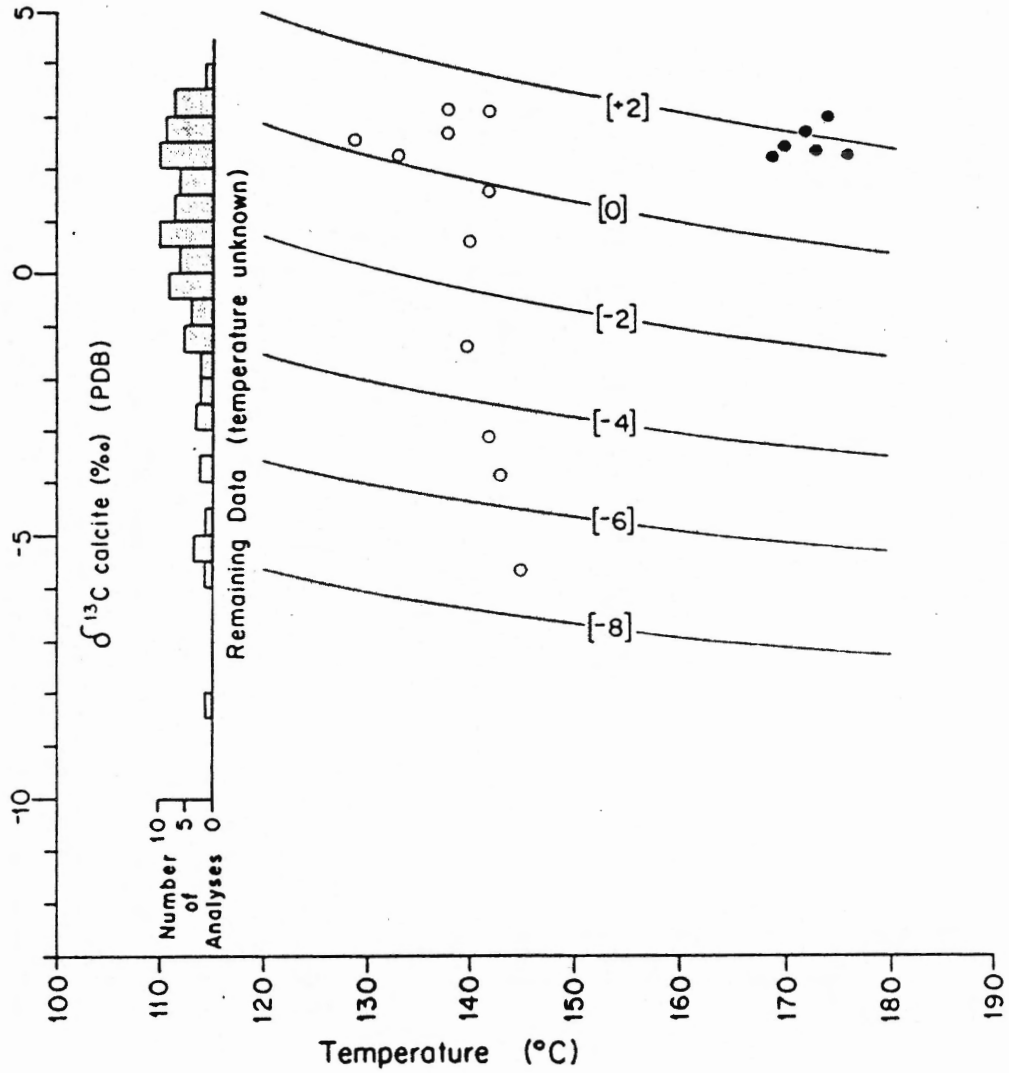
5
0
-5
-10
δ13C calcite (‰) (PDB)
Number of Analyses
10
5
0
Remaining Data (temperature unknown)
[+2]
[0]
[-2]
[-4]
[-6]
[-8]
100
110
120
130
140
150
160
170
180
190
Temperature (°C)

Figure 4.3b

Figure 4.4 Oxygen and carbon isotopic compositions of calcite and carbonates at the deposits: 1=Gays River, 2=Southvale, 3=Selco survey, 4=Pembroke, 5=Smithfield, 6=Middle Stewiacke, 7=Brookfield, 8=Hilden, 9=Black Rock, 10=Walton, 11=Nine Mile River, 12=Upper Brookside. ■ = mineralized calcite, □ = unmineralized calcite, X = post-ore calcite, △ = limestone, ▨ = limestone breccia, O = dolomite.

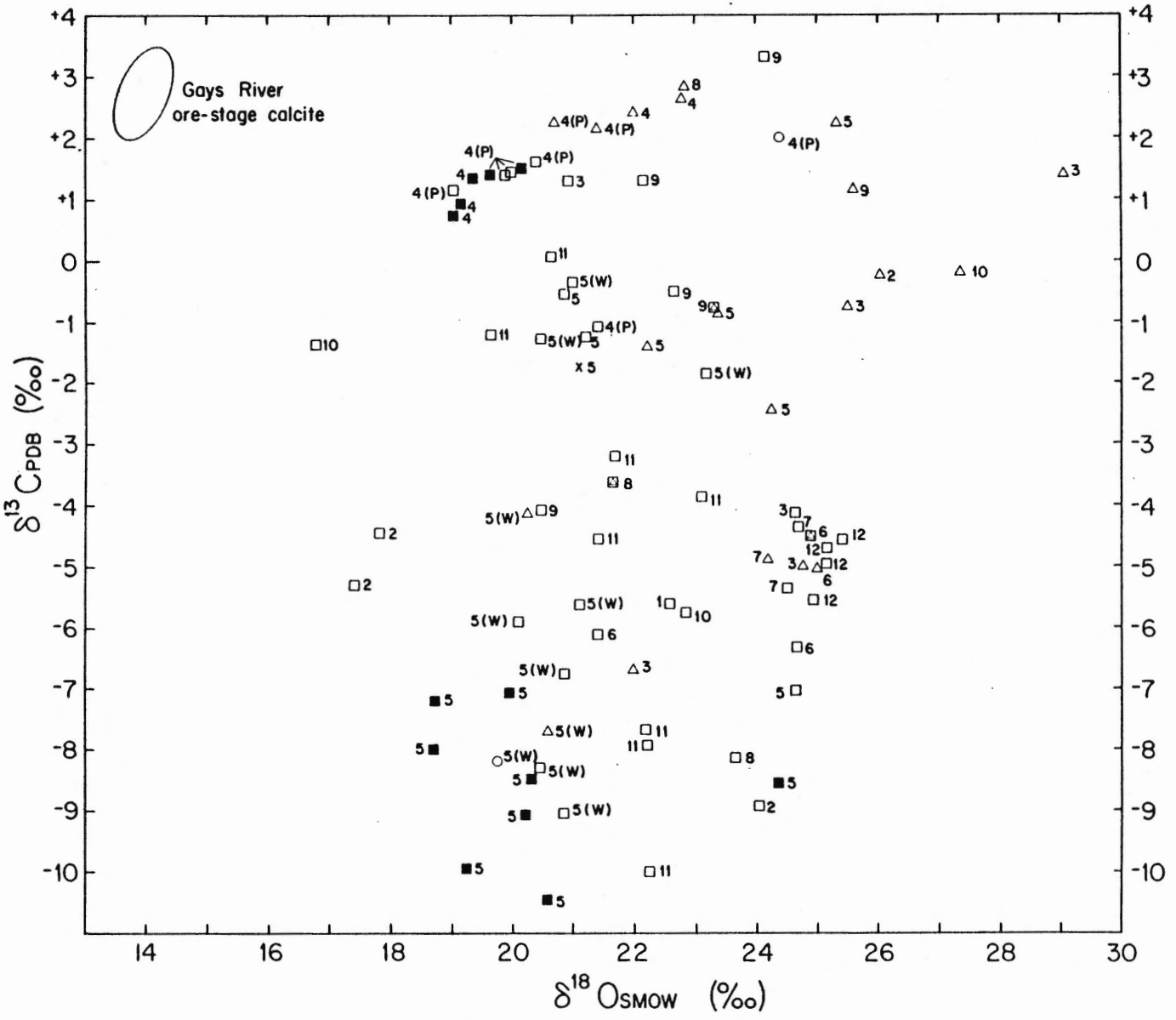
Gays River
ore-stage calcite
δ13CPDB (‰)
δ18OSMOW (‰)
+4
+3
+2
+1
0
-1
-2
-3
-4
-5
-6
-7
-8
-9
-10
14
16
18
20
22
24
26
28
30

Figure 4.4

Figure 4.5 Hydrogen and oxygen isotopic compositions of fluid inclusion fluids at the deposits studied. Numbers indicate deposits as in caption for Figure 4.4. Shown are the ranges of δD and $\delta^{18}O$ for juvenile water, metamorphic waters, oil field brines (formation waters), standard mean ocean water (SMOW) and the meteoric water line (from Taylor, 1979). δD and $\delta^{18}O$ values of ore-forming fluids of the MVT lead-zinc deposits of southwest Wisconsin are from McLimans (1977) in Ohmoto (1986). ■ = ore-stage calcite, ▼ = galena, ▲ = sphalerite, ● = barite.

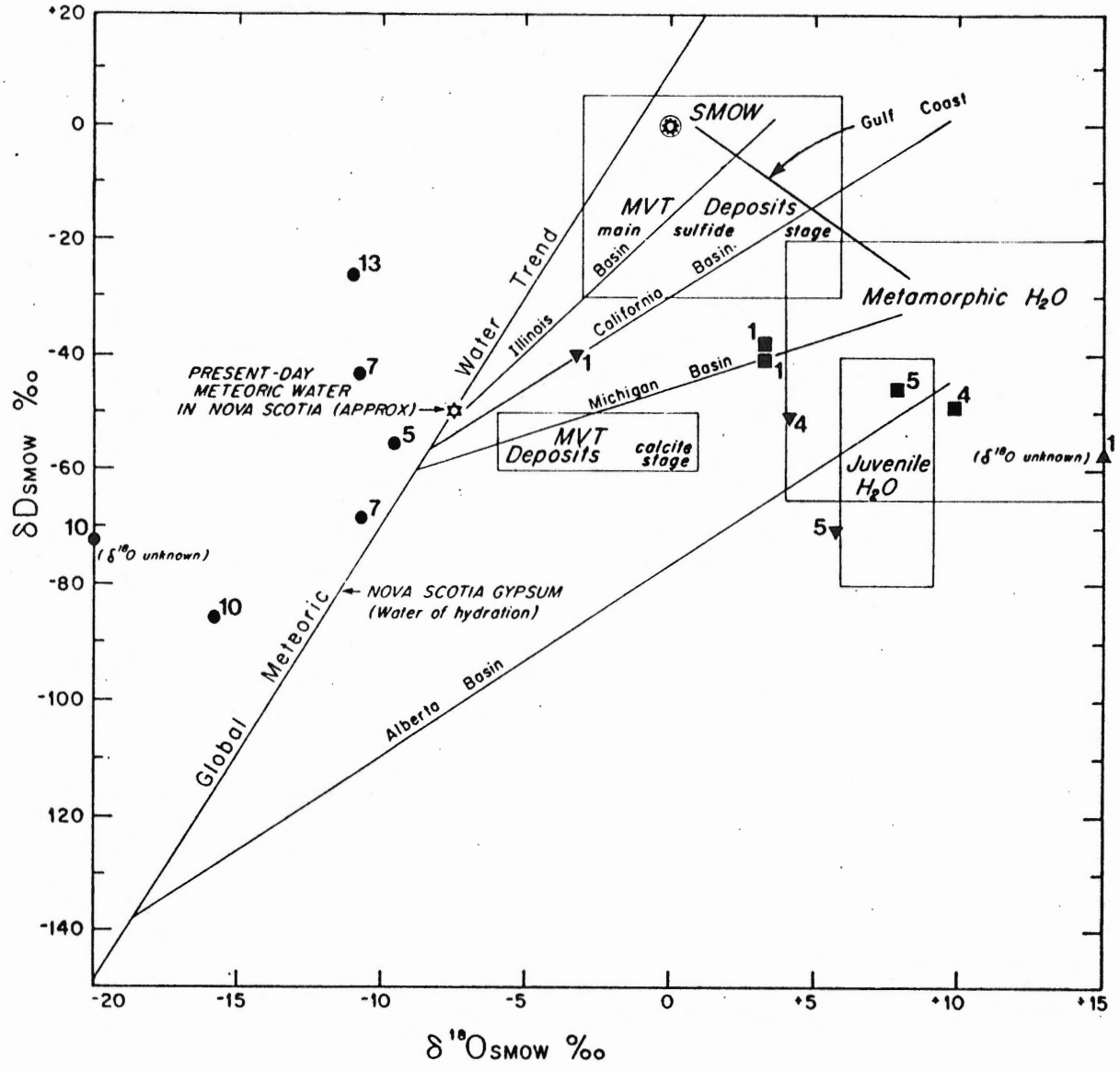
+20
0
-20
-40
-60
-80
-100
120
-140
δDSMOW ‰
-20
-15
-10
-5
0
+5
+10
+15
δ18OSMOW ‰
SMOW
Gulf Coast
MVT Deposits
main sulfide stage
Basin
Basin
Metamorphic H2O
Water Trend
Illinois
California
Michigan Basin
PRESENT-DAY METEORIC WATER IN NOVA SCOTIA (APPROX)
MVT Deposits calcite stage
Juvenile H2O
(δ18O unknown)
(δ18O unknown)
Global Meteoric
NOVA SCOTIA GYPSUM (Water of hydration)
Alberta Basin
13
7
5
7
10
1
1
1
4
5
5
4
1

Figure 4.5

Figure 4.6 Oxygen fugacity - pH diagram for ore-forming fluids at Gays River. T=200°C, $\delta^{34}S_{\Sigma S}$ = 14 o/oo, I=1.0, -•-•- = stability boundary for calcite at ΣC=0.1 moles per kg H_2O, ——— = Fe-S-O mineral boundaries at ΣS=0.001 moles per kg H_2O, ---- = Fe-S-O boundaries at ΣS=0.0001 moles per kg H_2O, —— = $\delta^{34}S_{H2S}$ contours (adapted from Ohmoto, 1972; Olson, 1984).

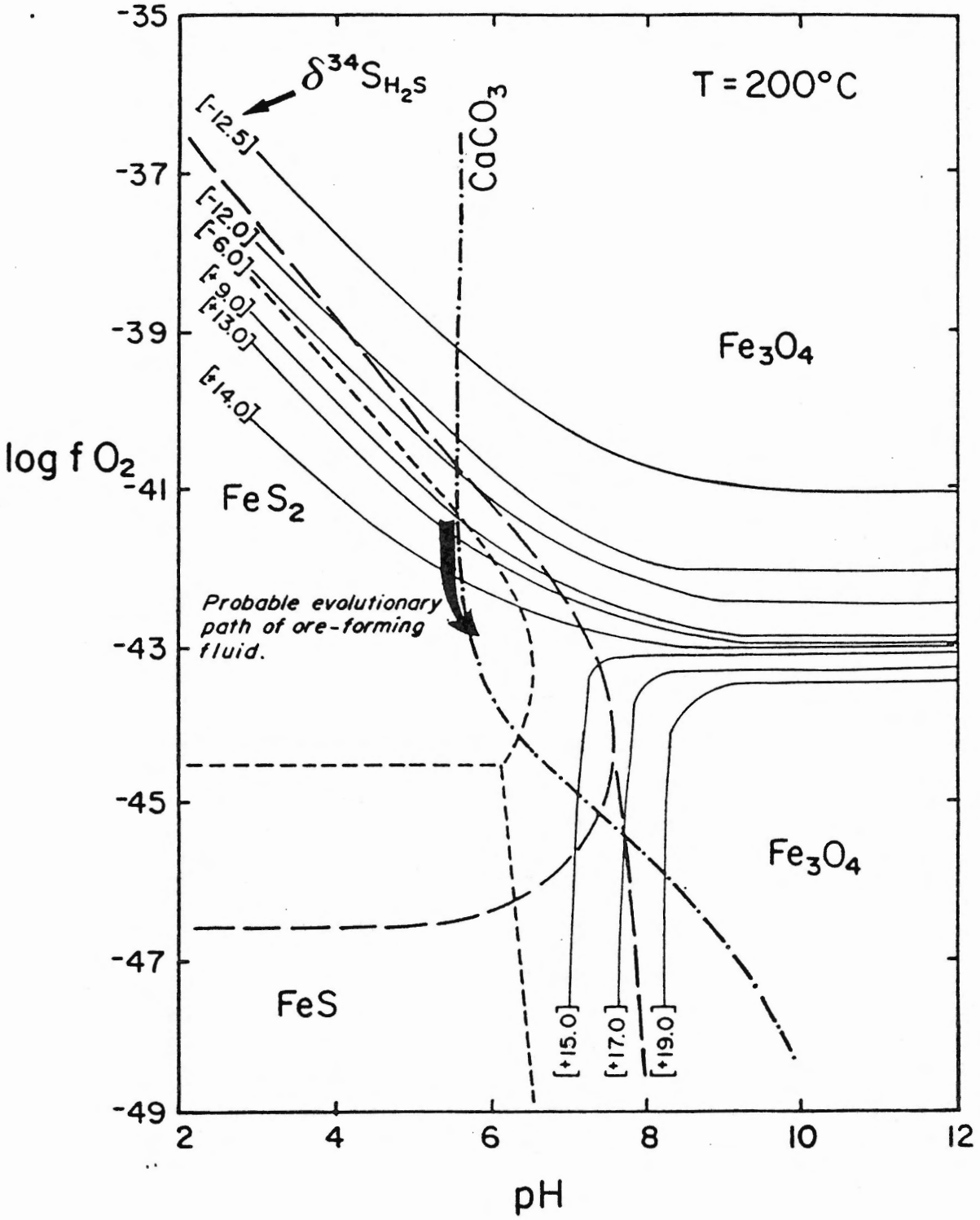
-35
-37
-39
-41
-43
-45
-47
-49
log f O2
2
4
6
8
10
12
pH
δ34SH2S
T = 200°C
CaCO3
[-12.5]
[-12.0]
[-6.0]
[+9.0]
[+13.0]
[+14.0]
[+15.0]
[+17.0]
[+19.0]
Fe3O4
FeS2
FeS
Fe3O4
Probable evolutionary path of ore-forming fluid.

Figure 4.6

Figure 4.7 Strontium isotopic compositions at Mississippi Valley type deposits. The locations of the deposits are shown on Figure 1.4. ■ = mineralized calcite, ⊡ = unmineralized calcite, ▽ = limestone, ▼ = dolomite, ▲ = celestite, ◇ = barite, ● = fluorite. In areas of minor mineralization the $^{87}Sr/^{86}Sr$ ratios fall quite close to the host rock ratios (N.W. Ohio). In the other areas, where there is major economic mineralization, mineral $^{87}Sr/^{86}Sr$ ratios are substantially different from those of the host rocks (adapted from Kessen et al., 1981).

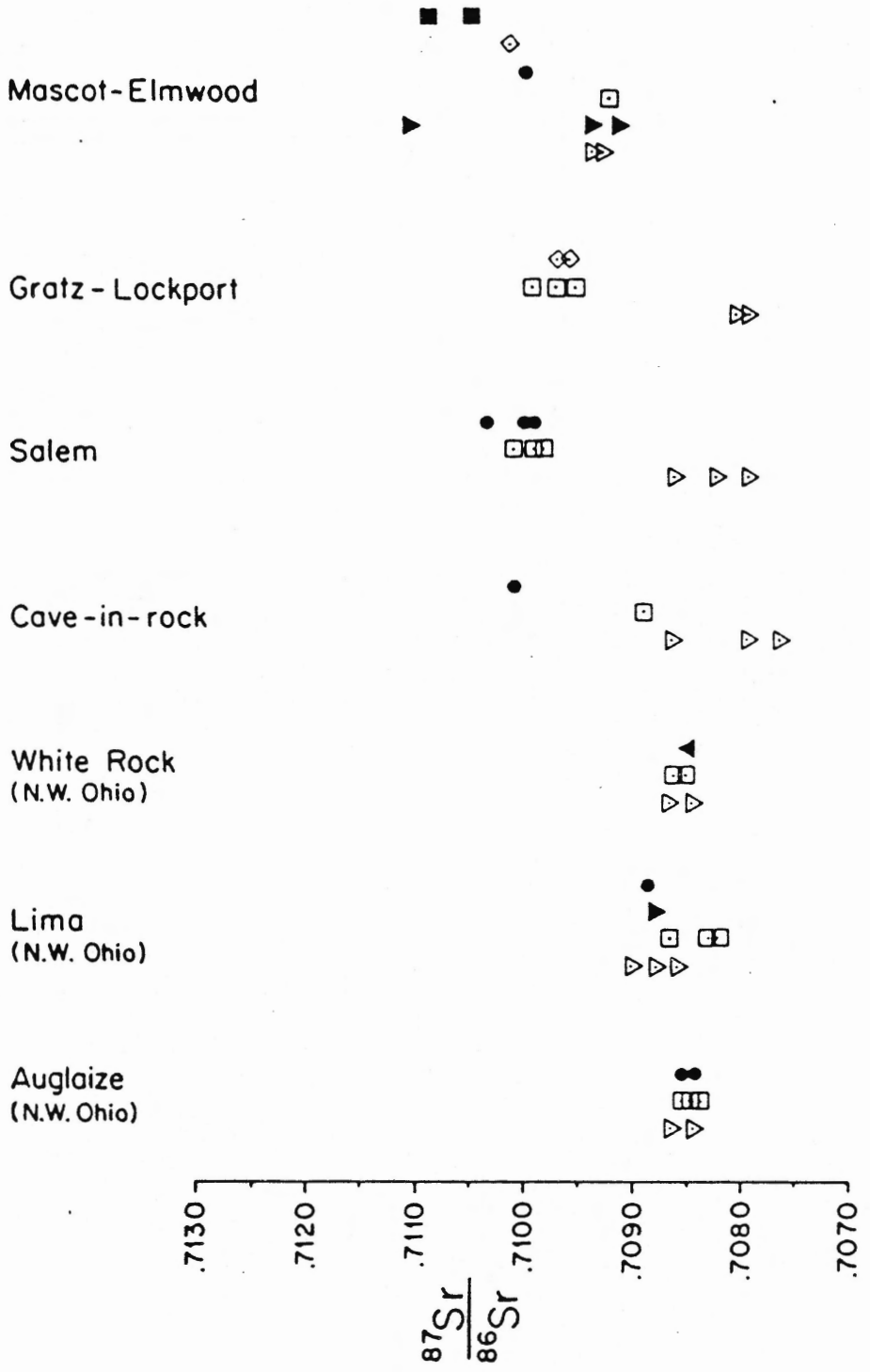
Mascot-Elmwood
Gratz-Lockport
Salem
Cave-in-rock
White Rock
(N.W. Ohio)
Lima
(N.W. Ohio)
Auglaize
(N.W. Ohio)
.7130
.7120
.7110
.7100
.7090
.7080
.7070
$\frac{87Sr}{86Sr}$

Figure 4.7

Figure 4.8 Strontium isotopic compositions at the mineral deposits studied. Shown are $^{87}Sr/^{86}Sr$ ratios of barite, calcite and host rock carbonate. ▽ = host limestone (Visean), ▼ = host dolomite (Visean), + = gypsum (Visean), X = anhydrite (Visean), ● = fluorite, ■ = mineralized vein or vug-filling calcite, ⊡ = post-ore and/or unmineralized calcite, ◇ = barite, △ = post-ore dedolomitized limestone. Analytical errors fall within the symbols. Average Mississippian seawater and range of analyses from Burke et al. (1982). Lines with arrows show probable paragenetic sequence at each deposit.

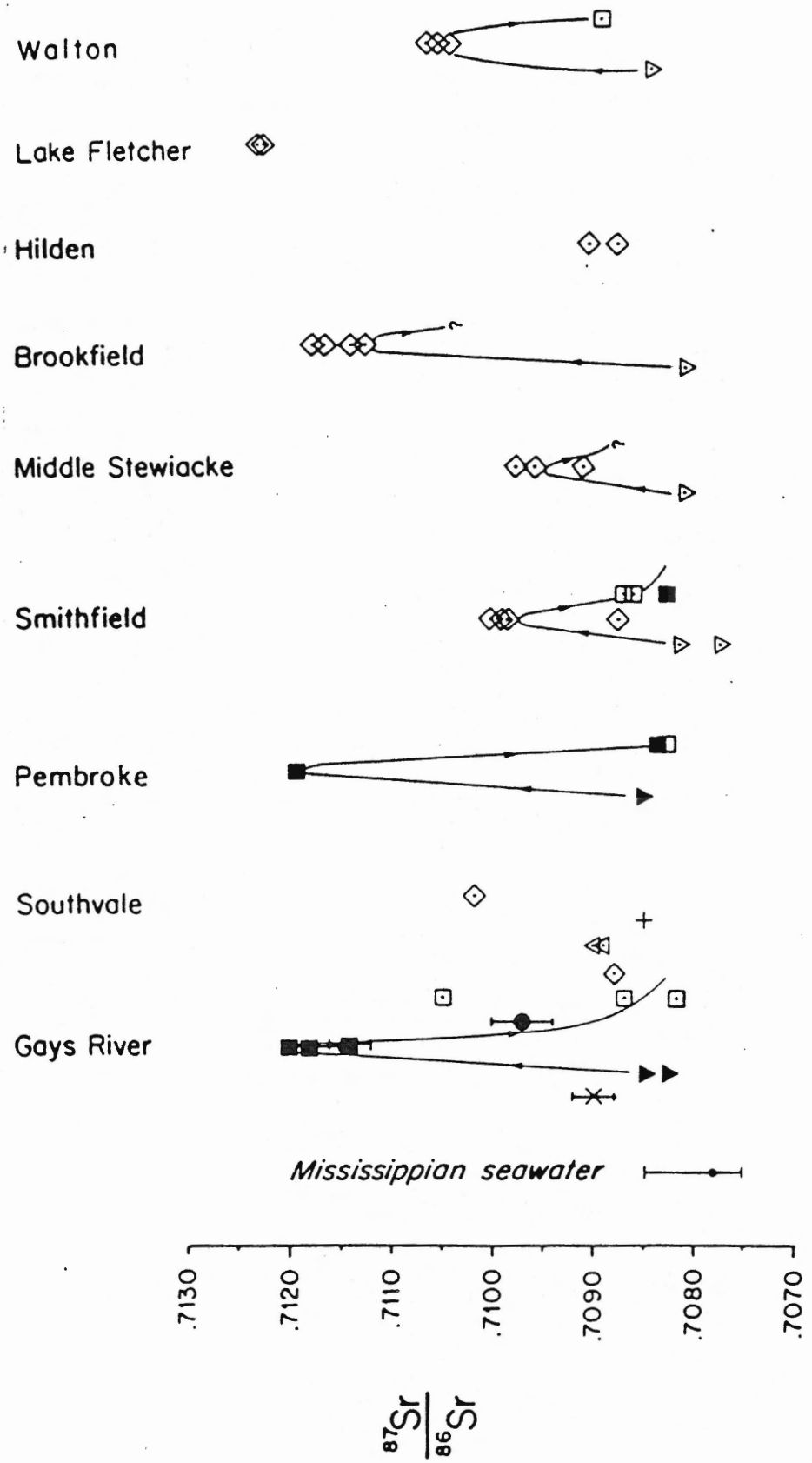
Walton
Lake Fletcher
Hilden
Brookfield
Middle Stewiacke
Smithfield
Pembroke
Southvale
Gays River
Mississippian seawater
.7130
.7120
.7110
.7100
.7090
.7080
.7070
$^{87}Sr/^{86}Sr$

Figure 4.8

Figure 4.9 Strontium isotopic compositions of the mineralization at Gays River. Minerals are arranged in the paragenetic sequence. Error bars represent the 2σ uncertainties. In some cases uncertainties are smaller than the plotted symbol. Also shown are the calculated ranges in $^{87}Sr/^{86}Sr$ ratio (R) at t=300 Ma for (i) Meguma Group metasediments and (ii) South Mountain batholith granodiorites.

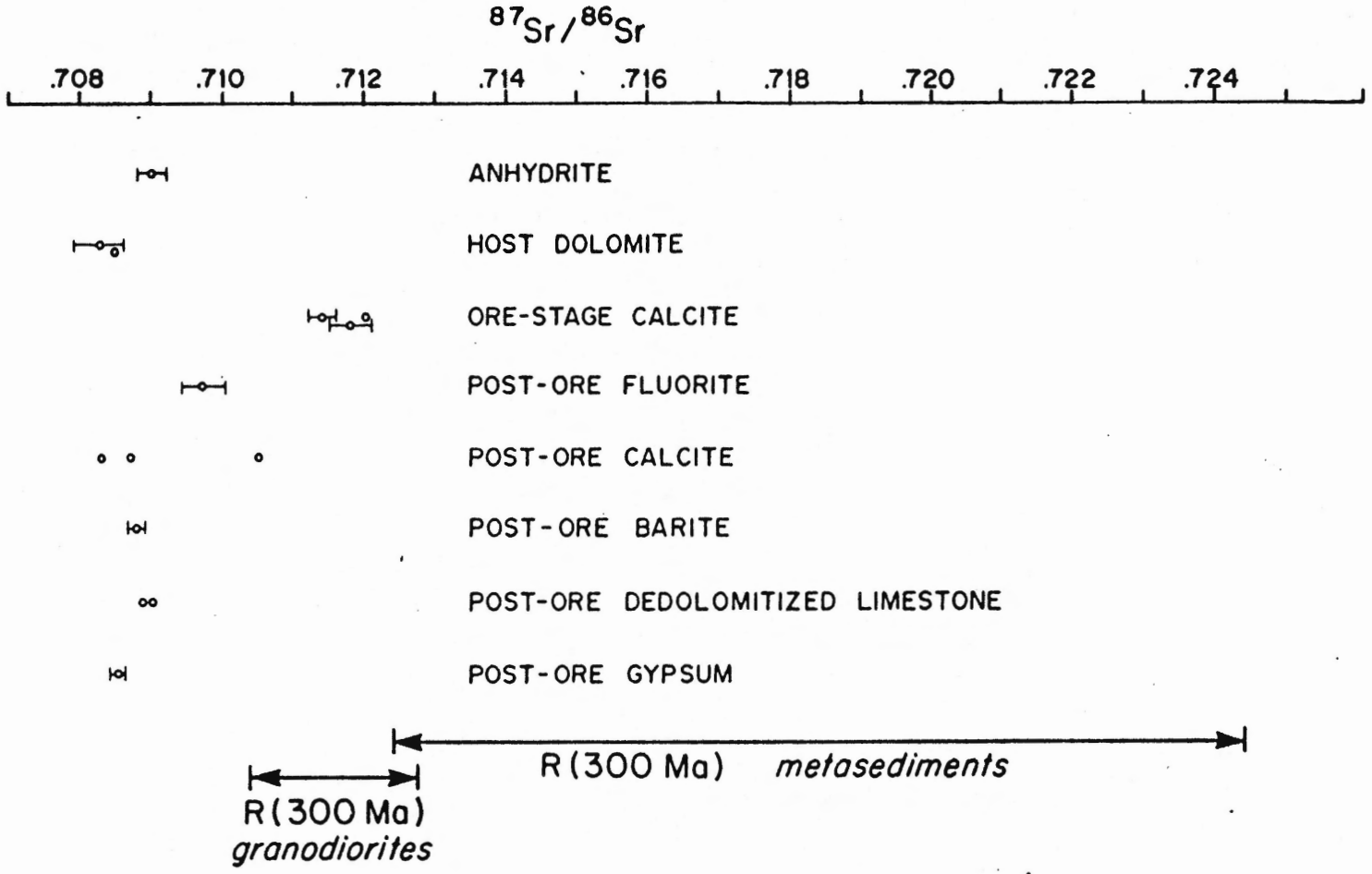
$^{87}Sr/^{86}Sr$
.708
.710
.712
.714
.716
.718
.720
.722
.724
ANHYDRITE
HOST DOLOMITE
ORE-STAGE CALCITE
POST-ORE FLUORITE
POST-ORE CALCITE
POST-ORE BARITE
POST-ORE DEDOLOMITIZED LIMESTONE
POST-ORE GYPSUM
R (300 Ma) metasediments
R (300 Ma)
granodiorites

Figure 4.9

CHAPTER 5

AGE DETERMINATIONS

The age of mineralization is a key parameter needed to constrain the choice of a genetic model for the deposits. The following thermochronometers were chosen for age determinations because they are sensitive to temperatures in the 140° to 250°C range or higher. This is the minimum mineralization temperature range of the mineral deposits studied, determined from fluid inclusions in ore minerals. A pressure correction applied to these fluid inclusion homogenization temperatures would shift this temperature range up by 90°C at most.

5.1 Fission track dating

Development of a fission track dating facility at Dalhousie University was a major part of my thesis work, therefore much of this section involves a detailed explanation of the preparation, counting and calibration techniques.

The fission track dating technique for cooling age determination of minerals was established by the pioneering work of Fleischer, Price and Walker (1965; 1975), Naeser (1967), Wagner (1968) and Aumento (1969). Fission tracks are damage zones in crystals caused by the spontaneous fission of uranium-238 (or the induced fission of uranium-235 or other elements) and are retained in minerals at temperatures below a closure or annealing temperature range (70°-120°C for apatite; 170°-200°C for zircon; $\sim$ 225°C for sphene). Exactly which temperature is the closure temperature depends on the cooling rate. Above these temperatures

tracks anneal and disappear. The density of spontaneous tracks (Ps) is dependent on both the amount of radioactive uranium-238 in the mineral (which can be measured) and the time elapsed since the mineral cooled through its closure temperature. Tracks are revealed by chemical etching techniques and counted at a magnification between 400 and 1250 times.

The range of ages of samples that can be dated with the fission track technique is 8000 to 2.7×10^9 years (Naeser, 1976). The technique has been used for a range of applications from archeology, to the dating of low temperature ore deposits (Naeser and Cunningham, 1984), and for determining the timing and rate of uplift of large, structurally coherent crustal blocks (Zeitler, 1983). The study of fission track dates of apatites from the Swiss alps by Wagner et al. (1977) led to useful conclusions regarding the tectonic history of the region. Recent work by Gleadow et al. (1983, 1986) has shown that the length distribution of confined tracks can reveal the temperature-time path of the cooling/uplift event - information that is not determinable by considering the fission track dates alone.

Fission track annealing is actually a complex time-temperature dependent process that is most readily observed by its effect in reducing the lengths of tracks (and therefore reducing the track density). Laboratory experiments have been done to determine the annealing characteristics of apatite (Naeser and Faul, 1969; Wagner and Reimer, 1972), sphene (Naeser and Faul, 1969) and zircon (Nishida and Takashima, 1975). But, there is still a debate on the relationship of the degree of track fading to temperature and time, especially over geologically significant time periods. Measurement of lengths of

confined tracks in minerals offers the best means of investigating the details of fission track annealing. Work is continuing in this field in thermally well-constrained geological sites such as boreholes (Gleadow et al., 1986).

Laboratory techniques

A fission track dating laboratory was set up at Dalhousie University through my efforts and those of a number of others. Randy Parrish (Geological Survey of Canada) conducted a workshop here, firmly establishing our laboratory techniques which are a modified version of Naeser's (1976). Apatite and zircon are first separated from the 70-120 mesh fraction (210 to 125 μm) of crushed and sieved rock samples. Heavy liquids (tetrabromethane, ρ=2.9 g/cm^3 and metylene iodide, ρ=3.2 g/cm^3), magnetic separation and hand-picking methods were used. Igneous rocks readily give quite concentrated separates, but sedimentary rocks require significant hand-picking.

The external detector method is used for both apatite and zircon. Apatite grains are mounted in Araldite epoxy made up of 4 or 5 parts resin to 1 part hardener and then left to set overnight. Zircon grains are embedded in teflon by sandwiching the teflon and grains between glass slides on a hot plate at 300°C. Grain mounts are polished using the Polimet Polisher (Buehler Ltd.), which is part of the microprobe laboratory. Polishing starts at 600 grit (about 30 μm) paper, then 15 μm wheel, 9 μm diamond paste, and 1 μm diamond paste. We are now switching to 15 μm diamond paste due to shattering of the grains caused by the wheel. Etching of apatite grains is done at 25°C for 40 seconds in 7% HNO3. The zircons are etched in a eutectic melt of 8.0 grams NaOH

- 11.5 grams KOH at 200°C for $\sim$ 40 hours (Gleadow et al., 1976). Track density in zircons is periodically checked at 400X magnification followed by further etching, until it reaches a plateau. We use low uranium mica (Brazilian ruby clear #5 1/2) as a detector. An irregular piece of freshly cleaved mica is attached to the etched grain mount with scotch tape (Naeser, 1976) to serve as a detector of the fission tracks induced in the reactor. A stack of unknowns with interspersed Fish Canyon Standards (provided by Naeser) and four SRM uranium dosimeter glasses (purchased from the National Bureau of Standards) are put into an irradiation capsule and sent to the McMaster University nuclear reactor (site 9D for about 555 seconds).

Upon return of the capsule and after "cooling down" for one or two weeks, the mica detectors from the glass dosimeters are etched in 48% HF for 30 to 45 minutes, then washed repeatedly in distilled water and heated slightly on a hot plate to drive off the HF. The mica is then counted at 400X magnification to establish the neutron flux gradient that existed across the capsule in the reactor. (About 200 grid fields are counted on each one.) The mica detectors from the standards and unknowns are etched in 48% HF for 12 to 15 minutes (washed and heated), and then "registered" to their respective grain mounts on glass slides. (Grain mounts are attached with wax; mica with scotch tape). Counting is done repeatedly from grain to mica at a magnification of 1000X. An Olympus microscope fitted with an eyepiece graticule and a 100X dry objective is used to do the counting. Spontaneous tracks are counted in the grain, induced tracks in the mica detector. (The density of induced tracks (ρi) is dependent on the amount of uranium in the sample and the total neutron flux in the reactor.) Less than 50 grains per sample are

usually counted, taking care to count the exact mirror image area on the mica detector, to the area counted on the grain. Only those polished surfaces approximately parallel to the C-axis of the grain are counted. This is especially important for zircon which shows strongly anisotropic etching rates.

Each pair of track density measurements (ρs and ρi) from each grain, because they ideally originate from the same amount of uranium, should give roughly identical ratios subject to the variation allowed by a Poissonian distribution. However, there are many sources of error that can cause variation beyond that predicted by Poissonian statistics. Therefore the grain and detector counts are subjected to a chi-square test to determine if the data distribution is similar enough to a Poissonian distribution to justify a conventional (Poissonian) analysis (Green, 1981). Galbraith (1981) showed that conventional analysis gives the best estimate of $\rho s/\rho i$ and $\sigma(\rho s/\rho i)$ as long as the observed track counts are acceptable under a chi-square criterion. The chi-square statistic calculated from the data must be less than the 95 percentile value of chi-square for a Poissonian data set. If the data gives a chi-square value that is not acceptable at the 95% level, a mean track density ratio of the $\rho s/\rho i$'s from the grains is calculated and a standard error of the mean is assigned to that quantity (Green, 1981).

For each age standard in the package, an estimate of the zeta parameter for the glass dosimeter is calculated using the interpolated track densities from the glass dosimeters (ρd) as well as ρs and ρi from the age standard.

$$\text{Zeta} = \frac{\exp\left(\lambda_D * T_{std}\right) - 1}{\lambda_D * \left(\rho_s/\rho_i\right)_{std} * g * \rho_d} \qquad (9)$$

(Hurford and Green, 1983)

where ρ_d = interpolated glass dosimeter track density at the location of the age standard.

λ_D = total decay constant of uranium-238

= 1.55125×10^{-19}/yr

Tstd = Fish Canyon tuff standard age

= 27.8 ± 0.2 Ma

(Hurford and Hammerschmidt, 1985)

g = geometry factor

= 0.5 for external detector method

(Gleadow and Lovering, 1977)

Error in zeta is calculated by compounding the individual errors in the quantities making up zeta, by using standard error analysis techniques (see Appendix C).

The zeta parameter method removes the previous requirement of having to accurately know the total thermal neutron flux in the reactor as well as other poorly known parameters. It puts the method on an equal footing with the $^{40}Ar/^{39}Ar$ and other geochronological methods that use age standards. Furthermore, unlike the J parameter used in argon dating, the zeta parameter is not neutron flux dependent. Therefore zeta parameters from one irradiated capsule as well as previous and future capsules from a laboratory, should all fit a normal distribution. Large unexplained errors beyond that in the error statistics exist in each zeta value determined (Hurford and Green, 1983). Thus, an averaged

zeta over many age standards and capsule runs is a much better estimate of the true value of zeta for the particular dosimeter glass used.

When a reliable mean zeta parameter has been established, then the ages of the unknowns can be calculated:

$$T_{unk} = \frac{1}{\lambda_D} * Ln\left[1 + \lambda_D * \overline{Zeta} * \left(\rho_s/\rho_i\right)_{unk} * g * \rho_D\right] \quad (10)$$

where ρ_d = interpolated glass dosimeter track density at the location of the unknown

λ_D, g as in zeta formula

The statistics, error calculations, zeta and unknown age calculations are all done by an interactive computer program written in Fortran and set up on the Dalhousie mainframe Cyber computer (Appendix C).

Samples of coarse clastic Horton Group sediments were collected from Esso minerals drillcore BP-6 and BP-7 in the eastern Rawdon Hills. Three apatite separates were dated in order to determine the uplift history of the Rawdon Hills structural block. Samples were also collected from Horton Group clastics and Meguma Group metaclastics that were intimately associated with the mineralization at a number of Pb-Zn and Ba deposits at the margins of the Minas Sub-basin. Five apatite and eight zircon separates were dated in order to determine the date of mineralization by the $\sim$200^{o}C fluids.

Results and interpretation

Zeta calibration baselines have been established for the dosimeter glasses SRM 963a (0.823 ppm U) for apatite and SRM 962a (37.4 ppm U) for

zircon (Tables 5.1a and 5.1b). The current best estimates of zeta from 20 Fish Canyon apatite age standards representing four separate irradiations, is (110.2 ± 5.0) x 10^{-2} yr-cm^2/track and from 4 Fish Canyon zircon age standards is (3.607 ± .113) x 10^{-2} yr-cm^2/track.

The three apatite samples from the Rawdon Hills (location 19, Figure 1.2), were recalculated from data in Mahony (1986) using the current best estimate of zeta. They give a range of ages from 147 ± 22(2σ) to 188 ± 28(2σ) (Table 5.2). A Mann-Whitney U-test was done on the actual ratios ($\rho s/\rho i$) calculated for each grain counted. The U-test is a non-parametric test that makes no assumptions about data distribution (Mann and Whitney, 1947; Bruning and Kintz, 1968; Mendenhall, 1975), which is different from the more commonly used T-test which requires the assumption of a normal distribution. Only two samples could be tested against each other at one time, so three tests had to be made. The Mann-Whitney U-test revealed significant differences between samples CH-67 and CH-71 and between samples CH-67 and CH-75 at the 5% level. The samples CH-71 and CH-75 were very close to being different at the 5% significance level. Mahony (1986) assumed that samples CH-71 and CH-75 could be combined to give an average age and depth. The difference in stratigraphic elevation between this average and sample CH-67 was used to calculate an "uplift rate" for the Rawdon Hills. The very low number calculated (9 m/Ma) indicates that the difference in age was probably due to the samples being located in the apatite partial annealing zone prior to uplift (temperatures were 80° to 120°C). Therefore, uplift and cooling through the 100°C isotherm probably occurred at t<170 Ma, and about 2 or 3 km of sediment were eroded from the Rawdon Hills (above the Horton/Windsor disconformity).

The 5 apatite samples from the mineral deposits give an age range from 165 ± 52(2σ) Ma to 253 ± 80(2σ) Ma (Table 5.2). The younger ages occur in the southeastern part of the area and older ages in the northwest. No U-tests were done, but the differences among some of the ages are significant (at 2σ).

The zircon fission track data from the deposits give a range of ages from 215 ± 60(2σ) Ma to 334 ± 82(2σ) Ma (Table 5.2). Large errors are quoted because few age standards have been counted (only four from one reactor run) and thus the mean zeta calibration parameter for our laboratory is probably more poorly known than the calculated error in this quantity would indicate. Relative to fission track ages in apatite, the younger zircon ages occur in the northwest and older ages occur to the southeast of the study area. The Mann-Whitney U-test was applied to the Gays River (RGR) and the Smithfield (RSB-21, 22a, 22b) data sets. There was no difference among the Gays River samples at the 5% significance level. This is obvious from the histogram of (ρ_s/ρ_i) ratios from the grains (Figure 5.1). The sum of the ratios forms what appears to be a very nice Poisson distribution for which the calculated age is 313 ± 44(2σ) Ma. Neither was there a difference among the Smithfield samples at the 5% significance level. However, there was a difference between RSB-21 and RSB-22b at the 7% level. A histogram of the data (Figure 5.2) shows that a sum of the ratios from all the grains counted gives a distribution for which the age is 250 ± 34(2σ) Ma.

The range of fission track ages in apatite is very close to that obtained for South Mountain granites 100 km to the southwest (Grist, 1986) indicating that apatite fission track ages throughout this part of Nova Scotia were reset by what we interpret as tectonism including

uplift and erosion during Early Mesozoic rifting, rather than the mineralizing event. Fission track dating of zircon, which has a higher closure temperature (170° to 220°C) than apatite (80° to 120°C), indicates that at the location of the mineral deposits zircons were probably not reset by the latest thermal event recorded in the apatite data. Instead, the zircon ages are probably still indicating the time of mineralization by hot ($\sim$ 200°C) brines at $\sim$ 300 Ma. The slightly younger age at Smithfield and at some of the other deposits may be indicating a partial annealing of tracks in zircon during the Mesozoic rifting event. These deposits may have been more deeply buried than Gays River at that time. Fission track length measurements would have to be done to resolve this question.

One zircon sample (PE-154, Table 5.2) from the South Mountain batholith near St Margarets Bay (Grist, 1986) indicates that the granite in this area was strongly affected by the thermal event at $\sim$ 180 Ma, seen in the apatite data throughout Nova Scotia.

5.2 Rubidium-strontium dating of clays

Rubidium-strontium dating of glauconite or 2M-illite has been shown to result in well-defined isochron ages which are characteristically much younger than the stratigraphic age. Stein and Kish (1985) and Posey et al. (1983) used glauconite from strata of marine origin to determine an isochron as well as model ages. (Model ages can be determined for individual analyses, but require an assumption about the initial $^{87}Sr/^{86}Sr$ ratio). These authors suggested that their data indicate isotopic homogenization of strontium by warm fluids possibly

related to the MVT mineralization of the Viburnum Trend (Figure 1.4). Isotopic homogenization by deep burial or loss of radiogenic strontium during glauconite diagenesis are alternative explanations that are often used in other locations. Grant et al. (1984) obtained Rb-Sr and conventional K-Ar dates from a suite of glauconites. The dates from the two methods are concordant with each other at 3 sites and also agree with the results of Stein and Kish (1985) at the site along the Viburnum trend.

Dating of clays is more complicated because of the presence of both detrital and authigenic clays. If the clay separation technique results in samples containing significant quantities of authigenic 2M-illite (checked by X-ray diffraction), then an isochron would represent a significant strontium isotopic homogenization event in the sediments (Clauer, 1982).

Sample selection, preparation and analytical techniques

Samples of 2 to 4 kg of gray Horton sandstone were selected at regular stratigraphic intervals at location 12 (Figure 1.2). (As much of the weathered material as physically possible was removed from the outcrop before sampling). The site is remote from any large mineral occurrences. Sampling could be done from a large cliff section directly stratigraphically below(?) a highly brecciated and calcite-cemented horizon. The samples covered approximately 10 metres (stratigraphically) of the Horton section. The area is structurally complex with steeply dipping (75 NE) Windsor strata occurring just north of the sampling site, but flat-lying overturned(?) strata at the sampling site itself.

No glauconite could be found in the Horton strata (the assumed aquifer for the mineralizing fluids) probably because of its non-marine origin. Sample preparation procedure for clays was modified from Halliday (1978). The samples were crushed to -18 mesh (<1mm) and dry sieved in a sieve shaker for 20 minutes. About 100 to 600 grams of the -230 mesh (<63μ) fraction of each sample was stirred into one or two litres of distilled water in beakers. After 48 hours the water was siphoned off and samples let dry until sticky/wet. Then using weighing paper (which adhered to the surface), the upper $\simeq$ 1 mm of clays was "skimmed" off. Semi-oriented smears of the samples were run on the X-ray diffractometer for a qualitative determination of the relative amount of illite in each. At this point, about half of the original samples were rejected. Data on the remaining samples are tabulated in Table 5.3.

Analyses of the clays were carried out at the Department of Geology, Carleton University, Ottawa. The clay samples were dissolved in hydrofluoric and perchloric acids. The strontium isotopic composition was measured on the Finnigan-Mat 261 multi-collector mass spectrometer to a precision of $\pm$ 0.004%. Rubidium and strontium concentrations in clays were determined by X-ray fluorescence techniques (to a precision of $\simeq \pm$0.5%), and Rb/Sr ratios were calculated (to a precision of 1.5%).

Results and interpretation

The clay samples separated from Horton rocks (Table 5.3) all contained illite, albite and quartz, but some had substantial amounts of muscovite and chlorite. Five of the six Horton samples define an isochron (Figure 5.3) with a mean square of weighted deviates (MSWD) of

1.0. The MSWD is a measure of the degree to which points fit a line, within experimental error. (A value of 1.0 indicates that they do fit quite well.) The indicated age is 300 ± 6 Ma with an initial ratio of 0.7096 ± 0.0002 (2σ errors quoted). Sample RSB-101, which has the highest Rb/Sr ratio, plots a significant amount off the isochron. The reason for this is unclear, but is probably due to detrital components.

Although other explanations are possible, I interpret the 300 ± 6 Ma isochron age to represent the effects of an anomalous temperature fluid-flow event at 300 Ma that occurred throughout the Horton Group rocks of the Minas Sub-basin. This is the time of what has been called the Hercynian Maritime disturbance (Poole, 1967). The isochron represents the first good age determination of an event which affected Horton clastic rocks in the Pennsylvanian and which may be related to the mineralization in the Minas Sub-basin.

Calcite cementing the nearby brecciated material has $^{87}Sr/^{86}Sr$ ratios of 0.70918 and 0.70867 (Table 5.3), values which are close to the initial ratio of the isochron (0.7096). The breccia therefore was probably a conduit for the homogenizing fluids in this part of the Horton. These data also indicate that the Horton clastic rock at this location could not have been the sole source or conduit for the mineralizing fluids at 300 Ma (see Section 4.5). However, the Horton Group is very heterogeneous, and other parts of the Horton strata may have homogenized at a higher initial $^{87}Sr/^{86}Sr$ ratio.

5.3 Potassium-argon dating

The potassium-argon technique is a well-established dating method which is commonly used to track the cooling history of igneous bodies or to date thermal events. The $^{40}Ar/^{39}Ar$ stepheating technique was a major improvement over the conventional K-Ar method; now, rather than just one age, a series of steps defining an age spectrum is obtained. The $^{40}Ar/^{39}Ar$ method requires irradiation in a nuclear reactor to convert ^{39}K to ^{39}Ar. Measurement of the ratio $^{40}Ar/^{39}Ar$ (in a mass spectrometer) gives the apparent age of the gas evolved in each heating step. Calibration is achieved by analysis of a known age standard that was also included in the capsule sent for irradiation. The thermal history of the sample is usually reflected by all or part of the age spectrum.

The dating of base metal mineralization is a difficult problem because temperatures of mineralization are often not high enough to reset the "argon clock" in the host rocks. Clays, which are alteration products of the mineralization event, are the most likely minerals to have been reset. Halliday (1978) attempted to date clay concentrates from orebodies by the $^{40}Ar/^{39}Ar$ method and found that major losses of ^{40}Ar occurred in the nuclear reactor. Therefore clays can only be dated by the conventional (total gas age) K-Ar method.

Sample preparation and analytical techniques

One sample of muscovite was separated (by Akande, 1982), from altered Meguma wallrock closely associated with ore at the Gays River deposit. It was dated by $^{40}Ar/^{39}Ar$ techniques at the argon dating laboratory here at Dalhousie, using a modified MS-10 mass spectrometer.

I separated clay concentrates from altered wallrock at the Gays River, Brookfield and Smithfield deposits using the separation tecnique of Halliday (1978). The X-ray diffraction technique was used to select those samples with significant amounts of illite. The potassium concentrations in the samples were determined using atomic absorption. Results of the argon analyses of the clay samples are still pending.

No unaltered K-feldspar adequate for dating could be found in the Horton sedimentary rocks and none is known in the Meguma metasedimentary rocks.

Results and interpretation

The $^{40}Ar/^{39}Ar$ spectrum of the wallrock muscovite sample is partially disturbed. It reveals a very good plateau age of $\sim$ 610 Ma in the "retentive" part of the spectrum (Figure 5.4). This is overprinted in the less retentive part of the spectrum by one or more younger thermal events. A partial resetting of the muscovite at 330 Ma or younger is indicated. A more detailed spectrum needs to be produced for this sample and other samples before a definitive statement can be made.

5.4 Lead-lead dating of galena

Lead isotopic data can be used to constrain the sources of the lead and in some cases, the age of the mineralizing event.

Analyses were carried out on 7 galena samples from Gays River, Smithfield, Pembroke and Eastville (Figure 5.5). The Eastville deposit contains disseminated Pb-Zn mineralization located mainly in highly fractured Meguma basement within a few kilometres of the erosional edge of the Carboniferous sediments near the Pembroke Pb deposit (Binney,

1979; MacInnis, 1986). Complete U-Th-Pb-Pb isotope data were obtained for one whole rock Horton siltstone sample from DDH# SB-1, directly beneath the Windsor evaporites in the centre of the Shubenacadie Basin (Figure 1.2). Analyses were carried out by Geospec Consultants Ltd of Edmonton and were done on a cooperative basis with R. Thorpe of the Geological Survey of Canada (GSC). The Goldenville and Pennsylvanian lead data are from R. Thorpe as well. Also plotted (Figure 5.5) are data from Gays River, Pembroke and Walton done by M. Zentilli in cooperation with B. Doe of the U. S. Geological Survey.

Results and interpretation

Gays River galena, both from vein and stratiform ores is characterized by a very uniform isotopic composition (Akande, 1982). Observed $^{206}Pb/^{204}Pb$, $^{207}Pb/^{204}Pb$ and $^{208}Pb/^{204}Pb$ ratios range from 18.040 to 18.063, 15.594 to 15.622 and 38.129 to 38.189 respectively. The $^{207}Pb/^{204}Pb$ - $^{206}Pb/^{204}Pb$ data plot directly on Doe and Zartman's (1979) orogene curve at an apparent age of 540 Ma but above Zartman and Doe's (1981) version II orogen curve (Figure 5.5). (On a $^{208}Pb/^{204}Pb$ - $^{206}Pb/^{204}Pb$ plot the data fall just above both these curves). Akande and Zentilli (1984) interpreted the lead data according to the two-stage model of Stacey and Kramers (1975) which suggests a model age of about 460 Ma. The lead is the least radiogenic of any MVT deposits, including Pine Point (e.g. Figure 2.5, Doe and Zartman, 1979). The Gays River ore fluids were interpreted to have sampled lead preserved in the Cambro-Ordovician metasedimentary basement rocks which represent a sufficiently wide range of source rocks that through the processes of erosion, sedimentation and subsequent metamorphism, mixing was efficient

enough to produce a lead which has an appropriately 'average' composition.

The one complete U-Th-Pb Horton whole rock analysis gave $^{206}Pb/^{204}Pb$ = 19.345, $^{207}Pb/^{204}Pb$ = 15.671, $^{208}Pb/^{204}Pb$ = 39.720, $^{238}U/^{204}Pb$ = 27.49, $^{235}U/^{204}Pb$ = 0.1994, $^{232}Th/^{204}Pb$ = 70.49 (concentrations; U = 4.32 ppm, Th = 10.7 ppm, Pb = 10.3 ppm). The Horton clastic rocks (which were deposited 360 to 348 Ma ago) are probably direct clastic derivatives of the Meguma Group and the granites in this part of Nova Scotia, and received Meguma lead through weathering. Back-calculated to 300 Ma, the Horton whole rock lead isotopic composition agrees closely with that of Gays River galena. At 350 to 360 Ma it falls near the main field for Meguma gold deposits (R. Thorpe, written comm., 1986). These back-calculated isotopic compositions are marked with X's on Figure 5.5.

Galena from some of the other deposits studied (including Pembroke, Smithfield and Walton) have isotopic compositions close to those of Gays River. The two galenas from Smithfield are quite different from each other and further work would be needed to resolve this apparent discrepancy. The Walton galena plots along the same trend as the other data but with a much higher $^{207}Pb/^{204}Pb$ ratio than the other samples. This data point is probably erroneous because other lead isotopic data from Walton plot much closer to the Pembroke data (R. Thorpe, written comm., 1985). Therefore, the lead isotopic composition of galena from deposits studied is relatively homogeneous, suggesting that the fluids sampled the same homogenized source(s). The whole rock data indicate that the Horton clastic rocks could have been that source at 300 Ma.

The Eastville syngenetic(?) deposit in the Meguma near Pembroke may possibly represent a source in the Meguma with an isotopic composition

quite different from that of the gold deposits (e.g. Goldenville). However, my data suggest that the Eastville deposit could also have formed at the same time as the deposits studied, that is, in the Pennsylvanian.

TABLE 5.1a Apatite fission track standards.

Sample number	No. of grains	Ns	Ni	Chi-square	Ns/Ni (convent. analysis)	Mean $\rho s/\rho i$	ZETA for glass stand.SRM-963a (X 10^{-2}) ± 1σ
BCFCN2	60	329	1208	14.5	.272 ± .017		80.0 ± 5.9
BCFCN4	54	279	1122	15.1	.249 ± .017		105.4 ± 8.4
BCFCP1	12	66	273	13.2	.242 ± .033		98.7 ± 14.2
BAFCN2	60	386	1301	25.7	.297 ± .017		73.5 ± 5.1
BAFCN4	64	359	1411	34.4	.254 ± .015		103.0 ± 7.5
CHFCN2	41	203	854	25.1	.238 ± .019		116.3 ± 10.5
CHFCN3	17	85	425	11.6	.200 ± .024		119.3 ± 14.9
CHFCN6	31	122	756	11.3	.161 ± .016		149.1 ± 15.7
CAFCN2	46	229	1054	29.2	.217 ± .016		127.3 ± 10.9
CAFCN3	28	113	636	13.0	.178 ± .018		134.3 ± 14.7
CAFCN6	32	104	702	14.3	.148 ± .016		162.4 ± 18.2
DAFCN4	37	194	733	27.8	.265 ± .021		122.1 ± 11.4
DAFCN7	50	274	962	32.7	.285 ± .020		116.5 ± 9.4
DAFCN8	50	339	877	32.1	.387 ± .025		84.1 ± 6.4
DCFCN6	25	131	469	13.9	.279 ± .028		114.0 ± 12.2
DCFDN7	51	287	908	22.2	.316 ± .021		105.0 ± 8.4
DCFCN8	53	314	890	35.1	.353 ± .023		92.1 ± 7.1
EAFCN7	50	309	953	60.4	.324 ± .021		92.7 ± 6.8
EAFCN8	50	291	1000	35.0	.291 ± .019		102.7 ± 7.6
EAFCN4	50	213	779	33.4	.273 ± .021		105.9 ± 8.9

TABLE 5.1b Zircon fission track standards.

Sample number	No. of grains	Ns	Ni	Chi-square	Ns/Ni (convent. analysis)	Mean $\rho s/\rho i$	ZETA for glass stand.SRM-962a (X 10^2) ± 1σ
FCFCZ1	10	871	1176	21.9		.764 ± .055	3.646 ± .289
FCFCZ2	9	740	1033	8.7	.716 ± .035		3.782 ± .220
FCFCZ3	6	625	876	2.3	.713 ± .037		3.722 ± .228
FCFCZ5	8	1027	1305	22.07		.825 ± .065	3.277 ± .278

TABLE 5.2 Fission track age dates.

Location	Sample No.	No.of grains	Ns	Ni	Chi-square	Ns/Ni (convent. analysis)	Mean ρs/ρi	Age(Ma) ± 1σ
ZETA = (110.2 ± 5.0) X 10^2						Apatite		
1. Gays River	RGR-162	15	793	431	9.6	1.84±.11		189 ± 15
1. Gays River	RGR-165	9	457	270	25.4		1.62+.24	165 ± 26
2. Southvale	RSB-48	9	393	230	8.2	1.71±.14		171 ± 17
5. Smithfield	RSB-22	11	890	457	40.5		2.45+.37	253 ± 40
8. Hilden	RSB-26	13	1114	476	7.1	2.34±.13		237 ± 18
19. DDH# BP-6(186.0 m)	CH-67	20	1319	1089	3.9	1.21±.05		147 ± 11
19. DDH# BP-7(34.0 m)	CH-71	10	592	449	2.6	1.32±.08		169 ± 15
19. DDH# BP-7(147.0 m)	CH-75	17	1647	1088	11.1	1.51±.06		188 ± 14
ZETA = (3.607 ± .113) X 10^2						Zircon		
1. Gays River	RGR-161	3	353	47	3.6	7.51±1.17		271 ± 44
1. Gays River	RGR-162	14	2410	280	9.0	8.61±.54		323 ± 25
1. Gays River	RGR-165	9	568	72	9.8	7.89±.99		295 ± 39
2. Southvale	RSB-48	5	514	65	2.1	7.91±1.04		299 ± 42
5. Smithfield	RSB-21	6	1188	201	5.0	5.91±.45		220 ± 19
5. Smithfield	RSB-22a	11	1277	186	13.9	6.87±.54		247 ± 22
5. Smithfield	RSB-22b	4	746	84	1.4	8.88±1.02		334 ± 41
7. Brookfield	RSB-5 and 24	5	382	67	1.7	5.70±.76		215 ± 30
South Mtn.	PE-154	5	755	155	3.6	4.87±.43		181 ± 18

TABLE 5.3 Rubidium-strontium isotopic compositions of clay samples.

Location	Sample number	Description	Comp. analysed	87Rb/86Sr (±1.5%)	87Sr/86Sr (±0.004%)
12A Upper Brookside	RSB-98	Unweathered upper Horton sandstone with hematite	chlorite muscovite illite	1.05	0.71407
	RSB-101	Horton sandstone 1.5m "below" Windsor. Weathered outcrop	muscovite illite chlorite	8.13 (omitted from isochron)	0.74636
	RSB-102	Horton sandstone 3.0m "below" Windsor. Weathered outcrop	illite muscovite chlorite	failed	failed
	RSB-103	Horton sandstone 4.5m "below" Windsor. Unweathered	illite muscovite chlorite	5.89	0.73506
	RSB-104	Horton sandstone 6.0m "below" Windsor. Some weathering	muscovite illite chlorite	4.93	0.73048
	RSB-105	Horton sandstone 8.0m "below" Windsor. Some weathering	illite muscovite chlorite	6.21	0.73631
	RSB-106	Horton sandstone 10 m "below" Windsor. Some weathering	illite muscovite chlorite	3.19	0.72293
	RSB 100a	1st calcite in breccia Horton/Windsor contact	calcite		0.70867 ±.00005
	RSB 100b	Later brown calcite	calcite		0.70918 ±.00007

Figure 5.1 Histograms of zircon fission track ratios from Gays River. Plotted are the ratios ($\rho s/\rho i$) from all the grains counted. A. sample RGR-161, B. sample RGR-162, C. sample RGR-165, D. summation of the ratios from the three samples.

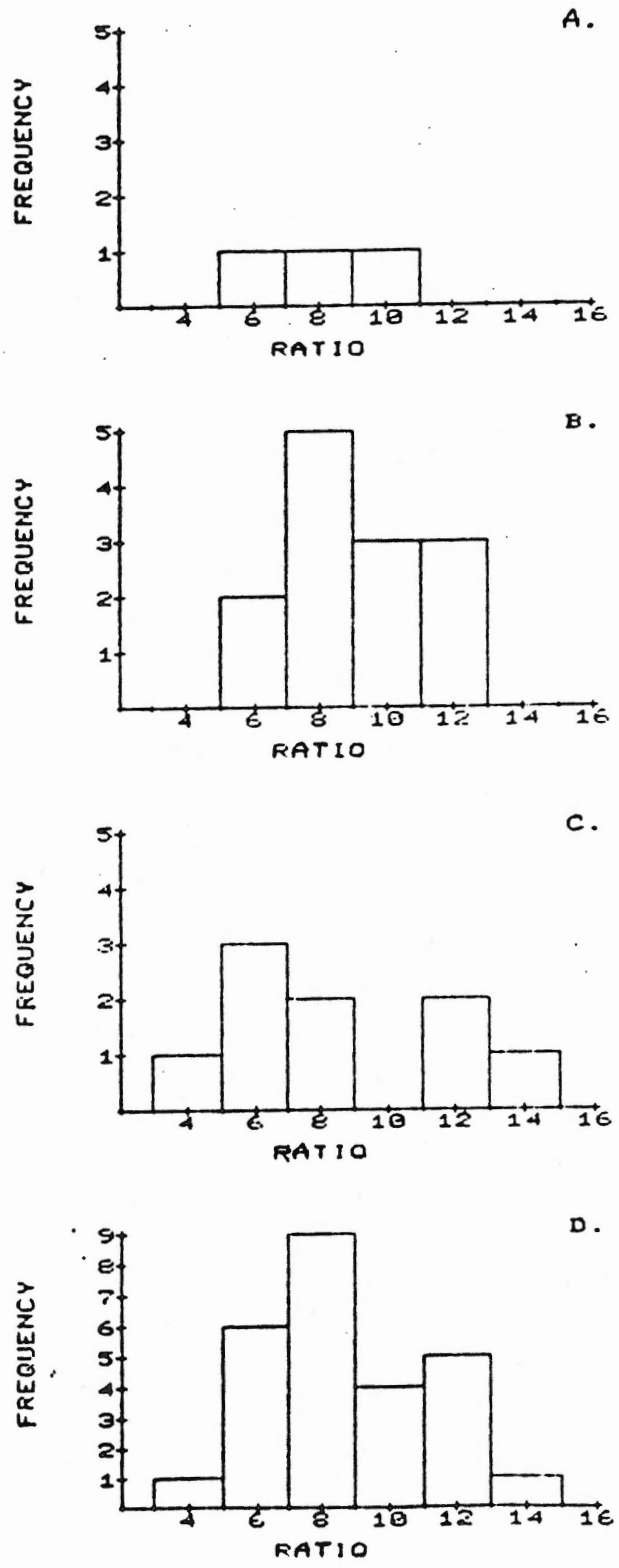
A.
FREQUENCY
1
2
3
4
5
4
6
8
10
12
14
16
RATIO
B.
FREQUENCY
1
2
3
4
5
4
6
8
10
12
14
16
RATIO
C.
FREQUENCY
1
2
3
4
5
4
6
8
10
12
14
16
RATIO
D.
FREQUENCY
1
2
3
4
5
6
7
8
9
4
6
8
10
12
14
16
RATIO

Figure 5.1

Figure 5.2 Histograms of zircon fission track ratios from Smithfield. Plotted are the ratios ($\rho s/\rho i$) from all the grains counted. A. sample RSB-21, B. sample RSB-22a, C. sample RSB-22b, D. summation of the ratios from the three samples.

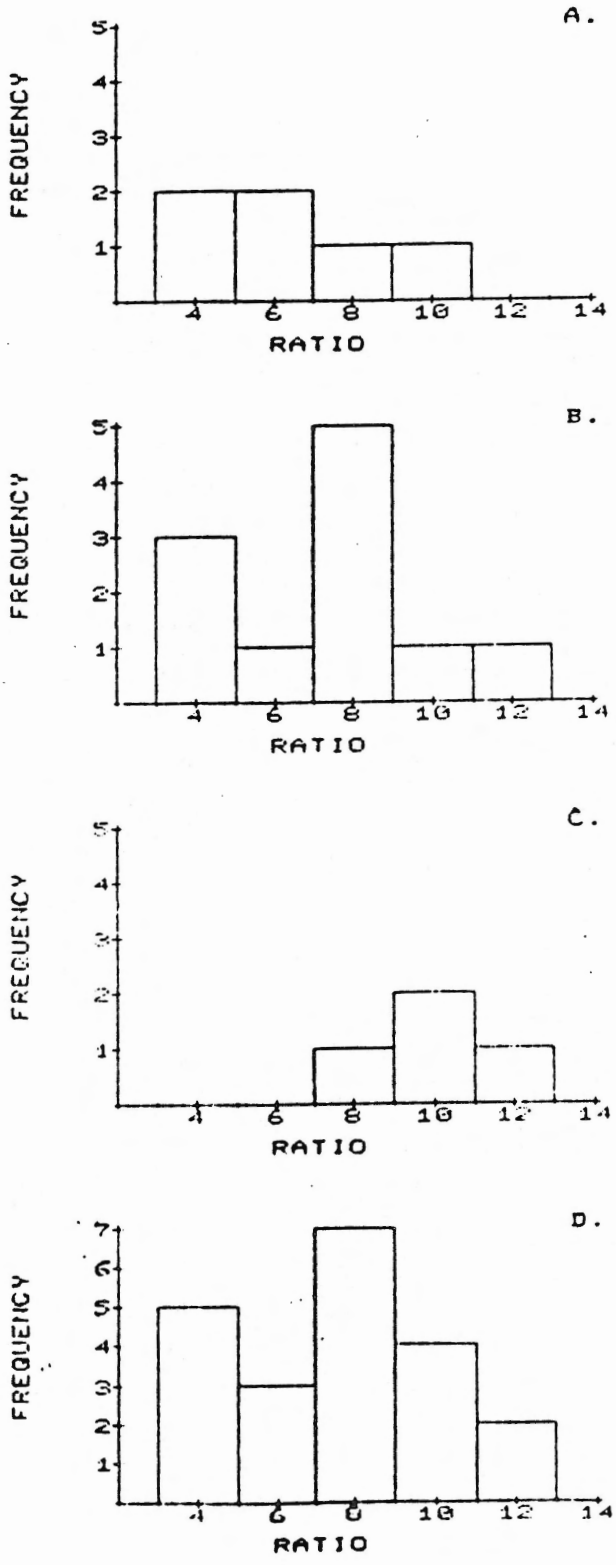
A.
FREQUENCY
RATIO
B.
FREQUENCY
RATIO
C.
FREQUENCY
RATIO
D.
FREQUENCY
RATIO

Figure 5.2

Figure 5.3 Rubidium-strontium isochron. Isochron formed from Rb/Sr and $^{87}Sr/^{86}Sr$ analyses of five clay separates from Horton sandstone collected over a 10 metre stratigraphic interval. Sampling site was 7 km northeast of Truro, Nova Scotia (location 12, Figure 1.2).

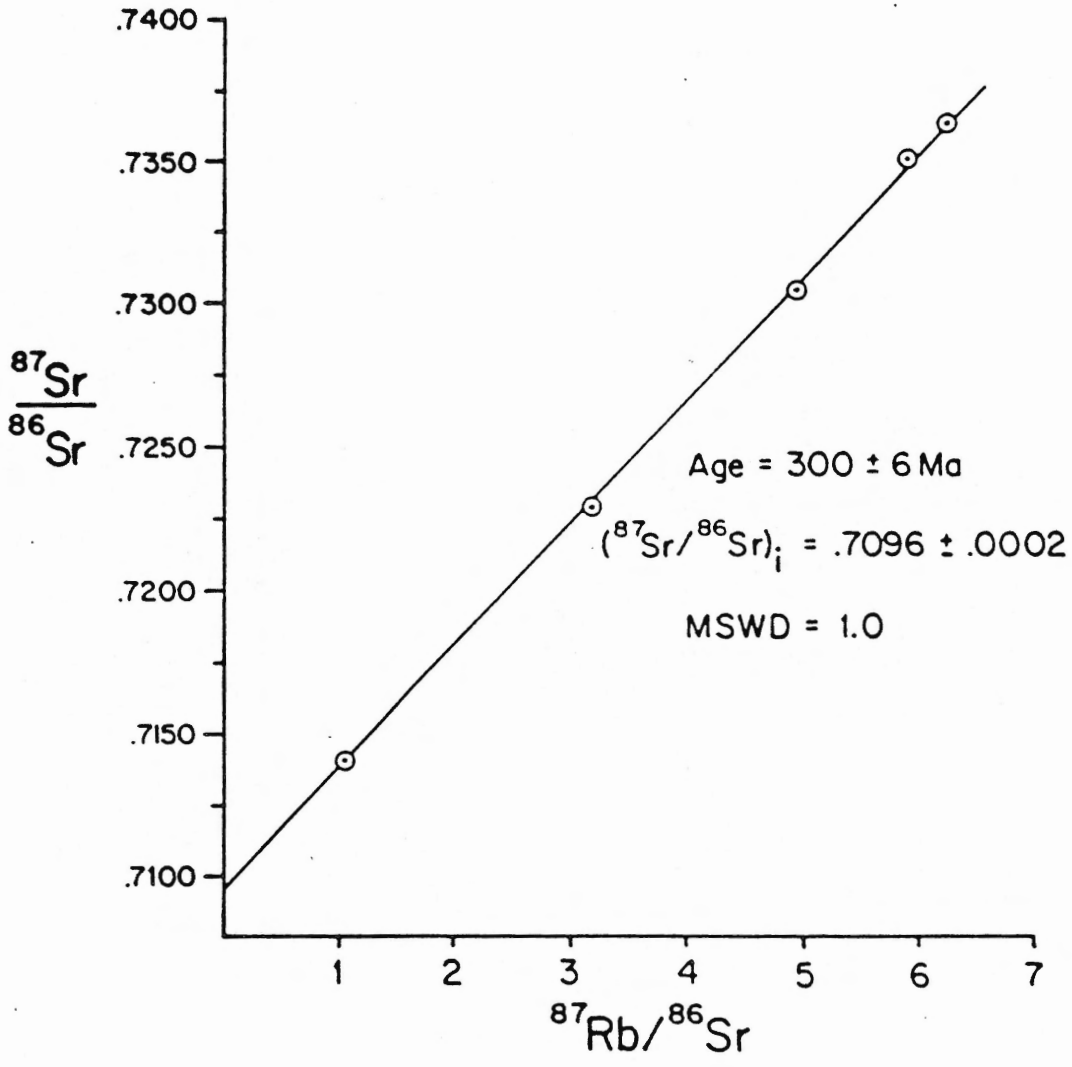
.7400
.7350
.7300
.7250
.7200
.7150
.7100
$^{87}Sr/^{86}Sr$
Age = 300 ± 6 Ma
$(^{87}Sr/^{86}Sr)_i$ = .7096 ± .0002
MSWD = 1.0
1
2
3
4
5
6
7
$^{87}Rb/^{86}Sr$

Figure 5.3

Figure 5.4 $^{40}Ar/^{39}Ar$ age spectrum from Gays River muscovite. Width of each age step indicates percentage of argon gas (of total gas released) analyzed in each step. The "thickness" of the step indicates the range of experimental error ($\pm 1\sigma$) in the apparent age.

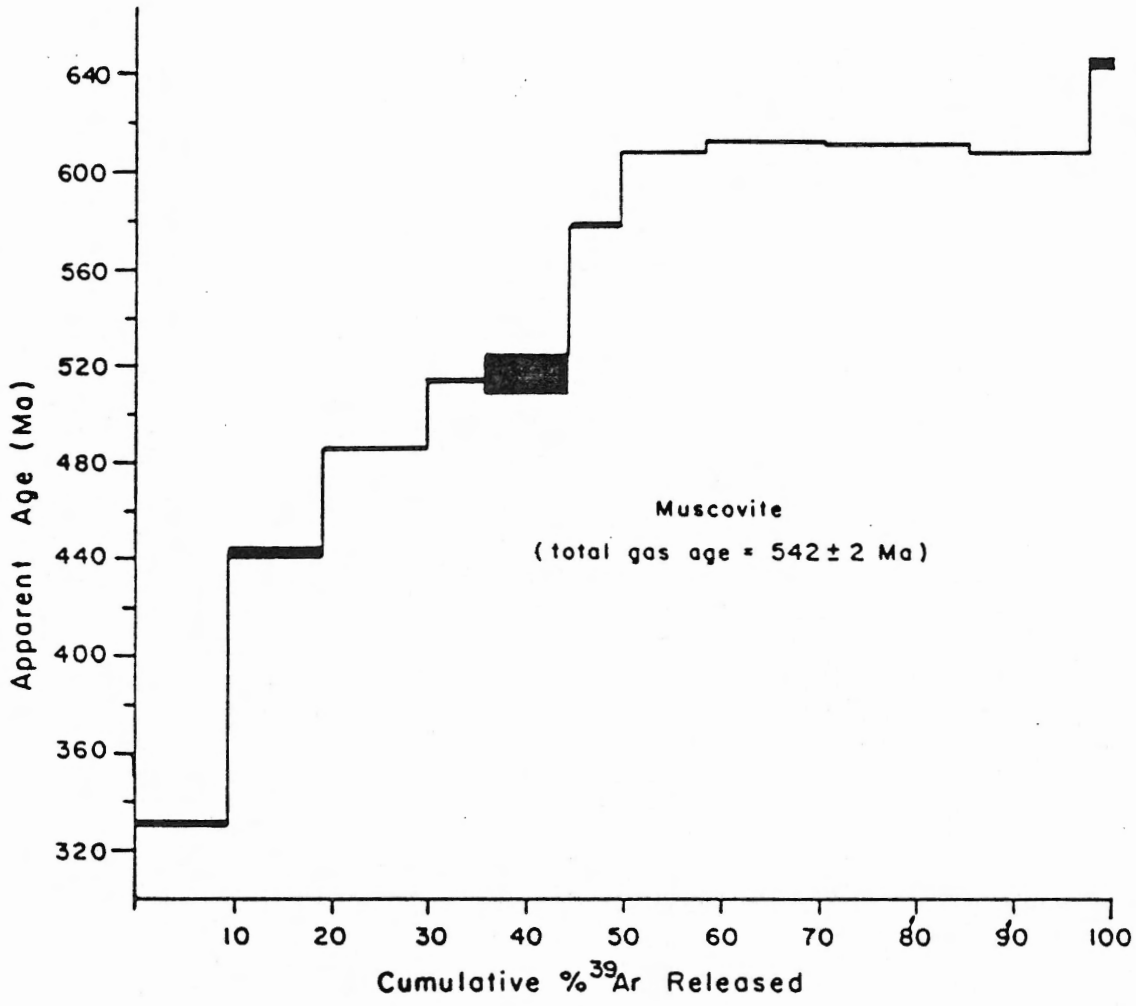
640
600
560
520
480
440
400
360
320
Apparent Age (Ma)
Muscovite
(total gas age = 542 ± 2 Ma)
10
20
30
40
50
60
70
80
90
100
Cumulative %39Ar Released

Figure 5.4

Figure 5.5 Lead isotopic data from some of the deposits. The model curves shown are the orogene and upper crust curves of Zartman and Doe (1981), and the two-stage model curve of Stacey and Kramers (1975). Numbers indicate the deposits: 1=Gays River, 4=Pembroke, 5=Smithfield, 10=Walton. X's mark the back-calculated isotopic compositions of whole rock Horton lead at the dates indicated (in Ma)(R. Thorpe, written comm., 1985).

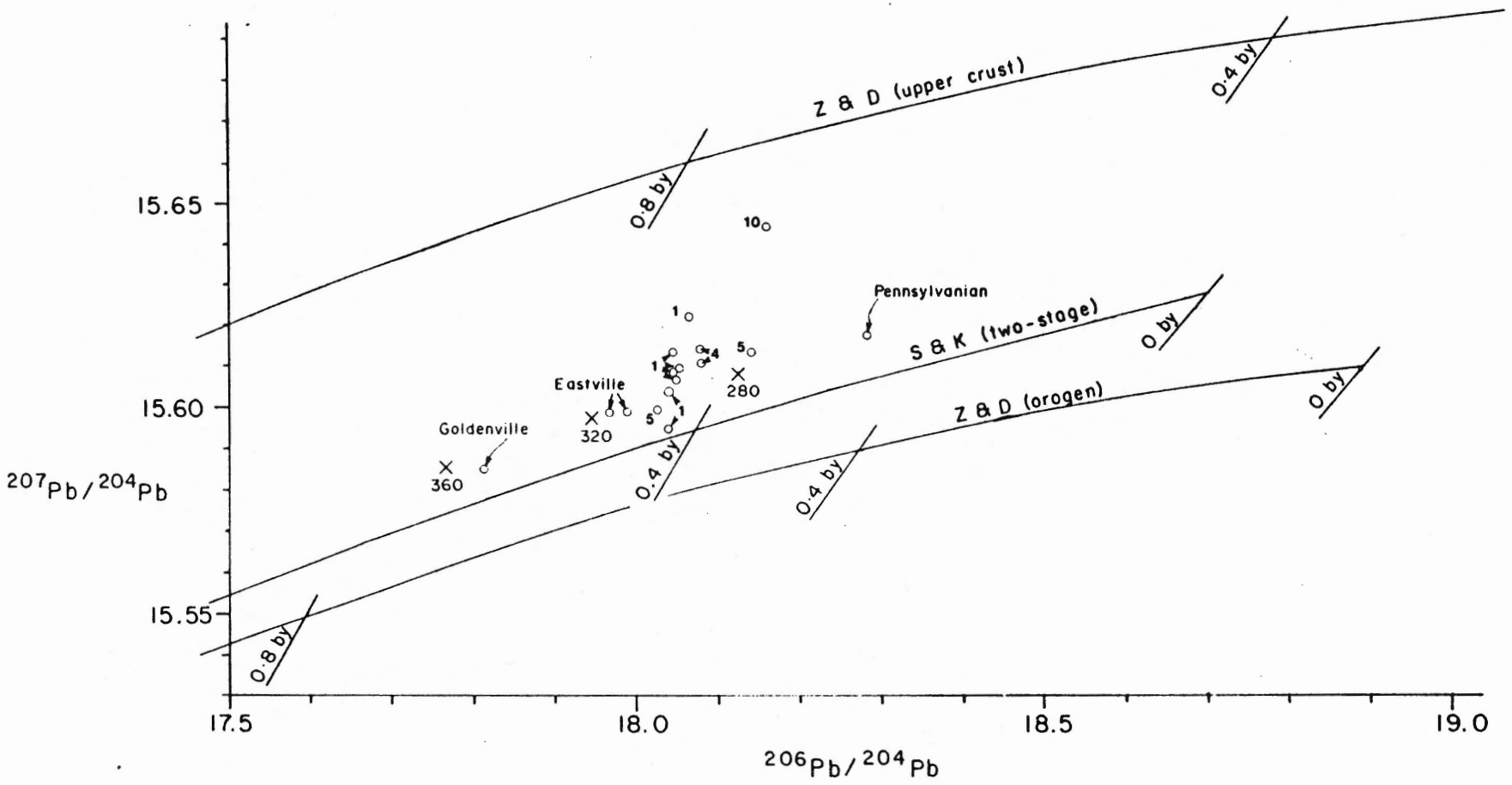
Z & D (upper crust)
0.4 by
0.8 by
10
Pennsylvanian
1
S & K (two-stage)
0 by
Eastville
280
320
Goldenville
360
Z & D (orogen)
0.4 by
0.4 by
0.8 by
15.65
15.60
15.55
17.5
18.0
18.5
19.0
207Pb/204Pb
206Pb/204Pb

Figure 5.5

CHAPTER 6

A QUANTITATIVE FLUID-FLOW MODEL

6.1 Tectonic history of the Fundy/Magdalen Basin

Basin subsidence

The maps of Howie and Barss (1975) show clearly the development of a narrow, trough-like basin in the southern Magdalen Basin under the eastern end of Prince Edward Island (Figure 6.1). This is the postulated source of the mineralizing fluids, and represents the "deep end" of my 2-dimensional model. I have plotted a sediment accumulation curve for that part of the Magdalen Basin (Figure 6.2) using data on the thickness of strata from the isopach maps of Howie and Barss (1975). I assigned "absolute" ages to the boundaries between units, referred to the Harland et al. (1982) geologic time scale. The sedimentation curve shows that there were two episodes of rapid subsidence (assumed to be equal to accumulation), separated by a time when subsidence was relatively slower. Because the thicknesses used are of compacted strata, the sedimentation rates calculated and used in the mathematical model were minimum rates. Therefore, the degree of overpressuring that resulted is also a minimum.

Hercynian Deformation

Keppie (1982) suggested that the Minas Geofracture (Figure 1.2), (here coinciding with the Glooscap Fault System of King et al. (1975)), often referred to as the Cobequid-Chedabucto Fault System (Webb, 1969)(Figure 1.1), underwent about 165 km of dextral movement between Early Westphalian and Late Triassic. This deformation, which Keppie

(1982) refers to as Hercynian, may have taken place during 3 major pulses, during Late Tournaisian, Westphalian B-C and during Late Permian. The best documented major event is the Westphalian deformation, marked by the sub-Pictou Group unconformity which cuts across rocks ranging in age from early Paleozoic to Westphalian B. According to the time scale of Harland et al. (1982), this deformation would have peaked at about 300 Ma. Structures developed during this time are generally upright folds with and without development of cleavage. Recumbent folds and south-vergent thrust faults have been documented by Giles et al. (1979), just north of the Gays River deposit. My data lead me to suggest that the mineralizing episode at Gays River and similar deposits took place during this major deformational pulse.

Permian and Younger Events

Deformation associated with the opening of the Bay of Fundy in the Triassic is inferred to be associated with sinistral movements in the order of 75 km across the Minas Geofracture (Keppie, 1982). Hacquebard (1986), on the basis of rank of coal considerations at Mabou Mines, in the Mabou Sub-basin (Figure 1.1), concludes that major faulting took place in that area in the post-Permian, probably Early Triassic. Taking into account both the earlier dextral movement of 165 km and this later sinistral movement of 75 km, the Gays River and other nearby deposits are at present positioned about 90 km west of where they were at 300 Ma (Figure 6.1). Removing this strike slip displacement would place the deposits approximately in line with the Stellarton Sub-basin and the southern part of the Magdallen Basin.

6.2 Conceptual model

Compaction-driven episodic expulsion of fluids under an evaporite seal is the mechanism that I postulate was responsible for the transfer of hot overpressured brines from deep in the Fundy/Magdalen basin, to the basin margins. My conceptual model for the process is illustrated in Figure 6.3. The specific area modelled spans from the southern part of the Magdalen Basin in eastern Prince Edward Island, south to the Gays River deposit (Figure 6.1). Mineral deposits such as Gays River, that formed along the margins of the Minas Sub-basin have preserved fluid inclusions and isotopic evidence of these hot mineralizing brines.

The fluid pressure, temperature and velocities can be modelled mathematically using numerical iteration techniques (Sharp and Domenico, 1976; Sharp, 1976, 1978; Garven, 1982; Cathles and Smith, 1983; Garven and Freeze, 1984a, 1984b; Bethke, 1985). Sharp (1978) used a 1-dimensional model of energy and momentum transport in the Ouachita basin to show that overpressured brines originating deep in the basin could have been responsible for the lead-zinc mineralization in the northern Arkansas - southeastern Missouri area. He stated that discrete pulses of hot brines would be needed. This is supported by Cathles and Smith (1983) who showed that fluid migration rates 1000 times greater than could be produced by steady subsidence, sedimentation and compaction are needed in order to produce the mineralization temperatures measured in the mineral deposits at the basin margins.

Bethke (1985) developed a rigorous 2-dimensional numerical model of compaction-driven groundwater flow and heat transfer in sedimentary basins. He showed that in basins where no overpressured fluids

developed, heat transfer is conduction dominated and the geothermal gradient is not disturbed at the basin margins where a significant amount of fluid from steady-state basin dewatering is expelled. Assumptions of permeability did not significantly affect fluid velocities over the dewatering history of the basin. Bethke (1985) concluded that gravity-driven fluid-flow or sudden dewatering of overpressures in basins could be mechanisms for the formation of lead-zinc deposits by hot brines at basin margins.

In any compacting sedimentary sequence containing significant thicknesses of muds, shales or evaporites, high pore pressures (often approaching the gravitational load) are a natural consequence of the failure of dewatering to keep up with the increase in lithostatic pressure. The high fluid pressures would be even more pronounced if dehydration reactions (e.g. gypsum or clay dewatering) were occurring under an impermeable layer. The sedimentary package in the Fundy/Magdalen basin contains about 500 metres of laterally extensive evaporites (including gypsum/anhydrite and salt) stratigraphically above 2 to 4 km of Horton clastic rocks (Howie and Barss, 1975). In my conceptual model (Figure 6.3) the evaporites form an effective seal and probably also generated some of the excess fluid and fluid pressure due to gypsum dewatering in the 50° to 100°C temperature range (Hill, 1937; MacDonald, 1953; Fyfe et al., 1978). It has been shown (Bragg, 1937; Bundy, 1956; Allen, 1971) that the gypsum to anhydrite + water reaction releases 48.5% water, and the volume relationships involve a 10% volume increase (Heard and Ruby, 1966). This would occur at only 1.5 to 2 km depth (given "normal" geothermal gradients), but if the migration of the fluids is inhibited (e.g. upwards by an impervious seal and laterally by

sediments with "normal" permeabilities), then the high pressures generated may be sustained throughout the sedimentation of the basin. Other temperature-controlled mechanisms such as montmorillonite-illite transformation, aquathermal pressuring (Magara, 1975a, 1975b; Gretener, 1981) and petroleum and gas generation may also have contributed to fluid pressures. Finally, I cannot rule out the effects of localized tectonic loading during the complex shear events in the Cobequid-Chedabucto Fault System. However, our model does not require these additional sources of overpressure; rapid sedimentation alone would be a sufficient agent.

The amount of fluid available can be estimated by considering the decrease in porosity of the siltstones of the Horton Group as well as the fluid generated by dewatering of the Windsor Group gypsum. A decrease in porosity of 0.5 to 0.37 (using formulae in Bethke, 1984a) is likely to occur as the Horton strata is buried to a depth of 6 km. In the 100 km square area of the southern Magdalen Basin (Figure 6.1), the 3 km of Horton strata would generate about 4000 km^3 of fluids. In the same area, the more than 200 metres of gypsum would dewater to about 50% of its original volume at 50°C (Fyfe et al., 1978), thereby generating another 1000 km^3 of fluid. If a 10 ppm concentration of metals is assumed for this brine (a reasonable assumption as discussed by Anderson and Macqueen, 1982), then $\simeq$ 100 km^3 of fluid would be needed to form a deposit of the size of Gays River (e.g. Anderson and Macqueen, 1982). Some focussing of the fluid would have to occur to achieve this.

Rapid fluid escape is likely to occur as pore fluid pressures approach lithostatic pressures. The λ parameter, which is the ratio of fluid pressure to overburden pressure, is about 0.45 in a normal

(hydrostatic) pressured basin. In nature, there are some cases of overpressured situations in which λ approaches 0.90 (Gretener, 1982) but generally it can be assumed that fluids will escape when λ reaches 0.75 (J. Buruss, oral comm., 1986). Palciauscas and Domenico (1980) stated that for sedimentary rocks containing pore fluids, dilatancy and fracture development has been observed when the ratio of the fluid to confining pressure is equal to about 0.80. I assume that a rapid escape of fluids under the evaporite seal occurs when λ reaches 0.80. Once this hydrofracturing event occurs, the fluid velocities are no longer controlled by sediment permeabilities but instead by the mechanical parameters of the rock controlling fracture formation, such as cohesive strength of the rock. It is only through fracture permeability that the very rapid fluid velocities required to bring hot fluids to the basin margin would be possible.

The stress regime determines the orientation of the fractures and the subsequent movement of the overpressured fluids. In an "unstressed" regime with no horizontal forces and fluids in a hydrostatic state, rocks are in a state of incipient normal faulting, with the minimum horizontal effective stress (σ_h - pore pressure) at about 1/3 of the effective overburden stress (σ_v - pore pressure) (Gretener, 1969, 1981). An increase in pore pressure can easily change the effective stress ratio and cause near-vertical fractures to form perpendicular to the minimum effective stress, which then relieve the overpressures. A further buildup of pressure will then cause the fractures to propagate and the fluids will eventually escape from the system, unless a horizontal bedding plane exists which acts as a barrier (Weertman, 1980). A free-slipping evaporite layer would be especially effective.

In fact, modelling (Weertman, 1980) predicts that upwardly impeded fractures may tend to propagate downwards, in our case perhaps into the basement.

In a regime of horizontal tectonic forces and overpressured pore fluids, the effective minimum horizontal stress (σ_h - pore pressure) could become greater than the effective overburden stress (σ_v - pore pressure). Horizontal fractures will form. As pore-fluid pressure approaches lithostatic pressures, the horizontal fractures will allow rapid fluid expulsion from under the evaporite seal. These overpressured fluids could also have had a significant influence on the tectonics (e.g. Hubert and Rubey, 1959) of the entire Maritime region of Canada in the Carboniferous.

The postulated source of the hot fluids is the southern part of the Magdalen Basin, with fluids moving through the Stellarton Sub-basin and into the Minas Sub-basin (Figures 1.1 and 6.1). Other basins or the basement may have been sources for these fluids, but the main Magdalen basin is the only known basin of great depth in the region that could have generated fluids with temperatures >200^{o}C, given the likely geothermal gradients in the area (see below).

6.3 Mathematical model

The primary objective of the mathematical model is to determine whether excess fluid pressure (approaching lithostatic pressure) could have been created, given the known sedimentation rates and using an average range of permeability values for the rock types found in the basin. The model provides a quantitative analysis of the fluid-flow process by incorporating known or calculated parameters and theoretical

relationships into a partial differential equation with initial conditions and boundary conditions. This equation was solved iteratively by a finite element numerical technique, using the TWODEPEP computer program from International Mathematical and Statistical Libraries, Inc. The model is capable of generating pore-fluid pressure and fluid velocity distribution, throughout the accumulation of basin sediment.

The equation used is derived from physical conservation principles (Sharp, 1976; Sharp and Domenico, 1976) and adapted for the 2-dimensional case.

(1) The excess pore fluid pressure (head) is given by the general differential equation for compaction of a porous medium subject to a forcing function (which is the addition of sediment at the top of the package).

$$\frac{\partial U}{\partial t} = \frac{K_z}{S_s}\frac{\partial^2 U}{\partial Z^2} + \frac{K_x}{S_s}\frac{\partial^2 U}{\partial X^2} + \frac{\rho_s - \rho_w}{\rho_w}\frac{\partial L}{\partial t} \quad (11)$$

where U is the excess pore fluid pressure, S_s is the specific storage of the porous medium, Kx and Kz are the hydraulic conductivities in the horizontal and vertical directions, dL/dt is the sediment accumulation rate and ρs & ρw are the sediment and water densities.

(2) Darcy's Law for conservation of momentum (assuming laminar flow) gives the fluid velocities as functions of hydraulic conductivities (Kx and Kz) and the gradient of the excess pore fluid pressure (U);

$$V_z = -K_z \frac{\partial U}{\partial Z} \quad , \quad V_x = -K_x \frac{\partial U}{\partial X} \qquad (12)$$

The partial differential equation (11) was solved by an iterative numerical technique, subject to the initial excess pore pressure distribution and boundary conditions shown in Figure 6.4. Figure 6.5 is an example of the initial finite element mesh input to the TWODEPEP program. The program then first increases the number of elements to the number desired, by a density code that I specified. The resulting final triangulation (Figure 6.6) illustrates the problem of getting a uniform increase in density of finite elements in the areas of rapid changes in hydraulic conductivities. The TWODEPEP program seems to be deficient in this regard. The problem of non-uniform triangulation resulted in difficulties in achieving a "well-behaved" solution. Increasing the number of time steps within each time period did not resolve the problem. For each time period (Table 6.1) the model was updated for the new sediment thickness and loading rate. The initial excess pore pressure distribution for each time period was taken as the final distribution from the previous step.

The parameters used in the model are tabulated in Table 6.1. The sedimentation rates (Figure 6.2) and total thickness of sediment for the southern Magdalen Basin were derived from isopach maps of Howie and Barss (1975). Average values for sedimentation rates in each interval were used. Although sediment thicknesses are for compacted sediment, this does not seriously affect the model, and gives minimum sedimentation rates. Because the sediment density used is also for compacted sediments, the product of the two (used in equation 11) should be quite close to the true value. A constant porosity of 0.30 was

assumed. The hydraulic conductivity structure of the basin used in the model is shown in Figure 6.4. Average values for hydraulic conductivity were taken from Garven and Freeze (1984b, Table 2)(Figure 6.7), and ratios of horizontal to vertical conductivities from Bethke (1985) were used; Kx/Kz = 2.5 for sandstone and 10.0 for shales. A value of specific storage for flysch sediments in the Ouachita basin (Sharp, 1978) was used in the model.

The geothermal gradient in the basin was calculated as a function of the time since the thermal event associated with the formation of the Magdalen Basin (assumed to be at 365 Ma). Cathles and Smith (1983) argued that the model for cooling of crust at mid-ocean ridges can be applied to conductive cooling of continental crust.

$$A = 11.5 \Big/ \sqrt{t} \qquad (13)$$

where A is basal heat flow in HFU(cal/cm^2-sec x 10^{-6}) and t is time in millions of years since the thermal event.

The geothermal gradient was calculated from:

$$dT/dZ = A/K_T \qquad (14)$$

where K_T is thermal conductivity ($cal/cm\text{-}s\text{-}^{\circ}C$ x 10^{-3}) of the sediments. The geothermal gradient existing during each time interval modelled is used to calculate the temperatures of the pore fluids (Table 6.1). Bethke (1985) showed that in a compacting sedimentary basin, little perturbation of the geothermal gradients can be expected due to steady-state basin dewatering. This is also substantiated by the sensitivity analyses of Sharp and Domenico (1976) which showed that for values of K/S_s and dL/dt such as those used in my model, the geothermal

gradient is essentially steady-state.

Results and interpretation

My results show that depending on hydraulic conductivities used, excess pore fluid pressures built up rapidly under the evaporite seal during periods of rapid sediment loading. During the rapid accumulation of the Windsor Group (348-336 Ma), hydraulic conductivities equal to or less than those listed in Table 6.1 resulted in $\lambda > 0.80$ directly under the seal (Figure 6.8). The conductivities used for each rock type are in the high end of the ranges given in Garven and Freeze (1984b, Table 2)(Figure 6.7). A hydrofracturing event with rapid movement of $\sim 185^{\circ}C$ fluids may have occurred, although the depositional thickness for the Windsor Group may be overestimated due to thickening by evaporite flow.

The Canso-Riversdale period (336 - 305 Ma) was a time of slow sedimentation rates, yet a steady increase in pore fluid pressures occurred. Hydraulic conductivities input to the model were decreased during this time period, thereby representing the effects of diagenesis. At the end of this time period, a huge reservoir of overpressured fluids at $\sim 230^{\circ}C$ may have existed under the evaporite seal (at about 4 km depth). A sudden pulse of sediment or tectonic loading could have set off a rapid dewatering event.

The Cumberland-Pictou period (305 - 280 Ma) was a time (at least initially) of rapid sedimentation (in the Magdalen Basin) and tectonic movement. Hydraulic conductivities at least 10 times lower than in the Windsor period (Table 6.1) are required to produce $\lambda > 0.80$ under the evaporite seal. These conductivities are in the mid-range of values (Figure 6.7) for the Horton and Windsor rock types. The fluid pressures

generated by the model are especially sensitive to the vertical hydraulic conductivity of the evaporite. Figure 6.9 is a plot of excess pore fluid pressures and steady-state fluid dewatering velocities generated by the mathematical model at 299 Ma. One limitation of my mathematical model obvious here (Figure 6.9) is that the sedimentation rate used must be constant across the entire section. In reality, total sediment thickness at the basin margin should be $\simeq$ 3.5 km at 299 Ma rather than 5.2 km. Fluid focussing in the area of the "faulted terrane" at the basin margin results in some high velocities, but this does not represent rapid transport of hot fluids from deep in the basin. Perturbation of the geothermal gradient at the basin margin due to steady-state dewatering is therefore unlikely. By 299 Ma, a massive hydrofracturing event of $\simeq$ 250°C fluids is likely to have occurred, which resulted in substantial perturbation of the geothermal gradient and formed the mineral deposits.

TABLE 6.1 VALUES OF HYDRAULIC, THERMAL AND LITHOSTATIC PARAMETERS USED IN THE MATHEMATICAL MODEL.

Parameter	Value		Reference
Porosity	ϕ=0.30		
Density of fluid	ρ_f=1100 kg/m^3		Sharp(1978)
Density of solids	ρ_r=2650 kg/m^3		Sharp & Domenico (1976)
Density of sediments	ρ_s=2160 kg/m^3		calculated
Thermal conductivity of basin rocks	K_T=3.40x10^{-3}cal/cm-s-^{o}C		calculated from Sharp & Domenico (1976)
Specific storage	S_S=.006 m^{-1}		Sharp(1978)
Hydraulic conductivity (m/yr)	K_x	K_z	Garven and Freeze (1984b, Table 2)
342 to 336 Ma	K_1 = 1.5	0.6	
	K_3 = 0.03	0.00001	see Fig. 8
	K_5 = 3.0	1.2	
305 to 299 Ma	K_1 = 0.15	0.06	
	K_3 = 0.003	0.000001	
	K_5 = 3.0	1.2	
342 to 299 Ma	K_6 = 0.3	0.06	
	K_7 = 10.0	10.0	

K_2 and K_4 were given intermediate values. They were necessary in order to derive a well-behaved mathematical solution.

Geothermal gradient	G =66^{o}C/km for 342-336 Ma =56^{o}C/km for 336-320 Ma =47^{o}C/km for 320-305 Ma =43^{o}C/km for 305-299 Ma	Cathles & Smith (1983)
Total sediments and accumulation rate	L =5 km for 342-336 Ma dL/dt =2.5x10^{-4} m/yr for 342-336 Ma	
	L =6 km for 336-320 Ma L =7 km for 320-305 Ma dL/dt =.59x10^{-4} m/yr for 336-305 Ma	Howie & Barss (1975)
	L =8 km for 305-299 Ma dL/dt =2.5x10^{-4} m/yr for 305-299 Ma	

Figure 6.1 Isopach map of the Fundy/Magdalen Basin. Present-day total thickness of Carboniferous (and some Permian) sediments, as well as some of the main structural elements (from GSC Map 1400 A, Wade et al., 1977) are shown. X's mark the location of some of the main Pb-Zn deposits on the southern platform of the basin. G.R.= Gays River, W.= Walton, S.= Smithfield, P.= Pembroke. I.S. is the location of the Rb-Sr isochron. The pore fluid pressure history of the southern Magdalen Basin (southeastern P.E.I.) was modelled mathematically. Net displacement across the Cobequid-Chedabucto Fault System since Westphalian B (305-300 Ma) is shown. Section A - A' is illustrated in Figure 6.3.

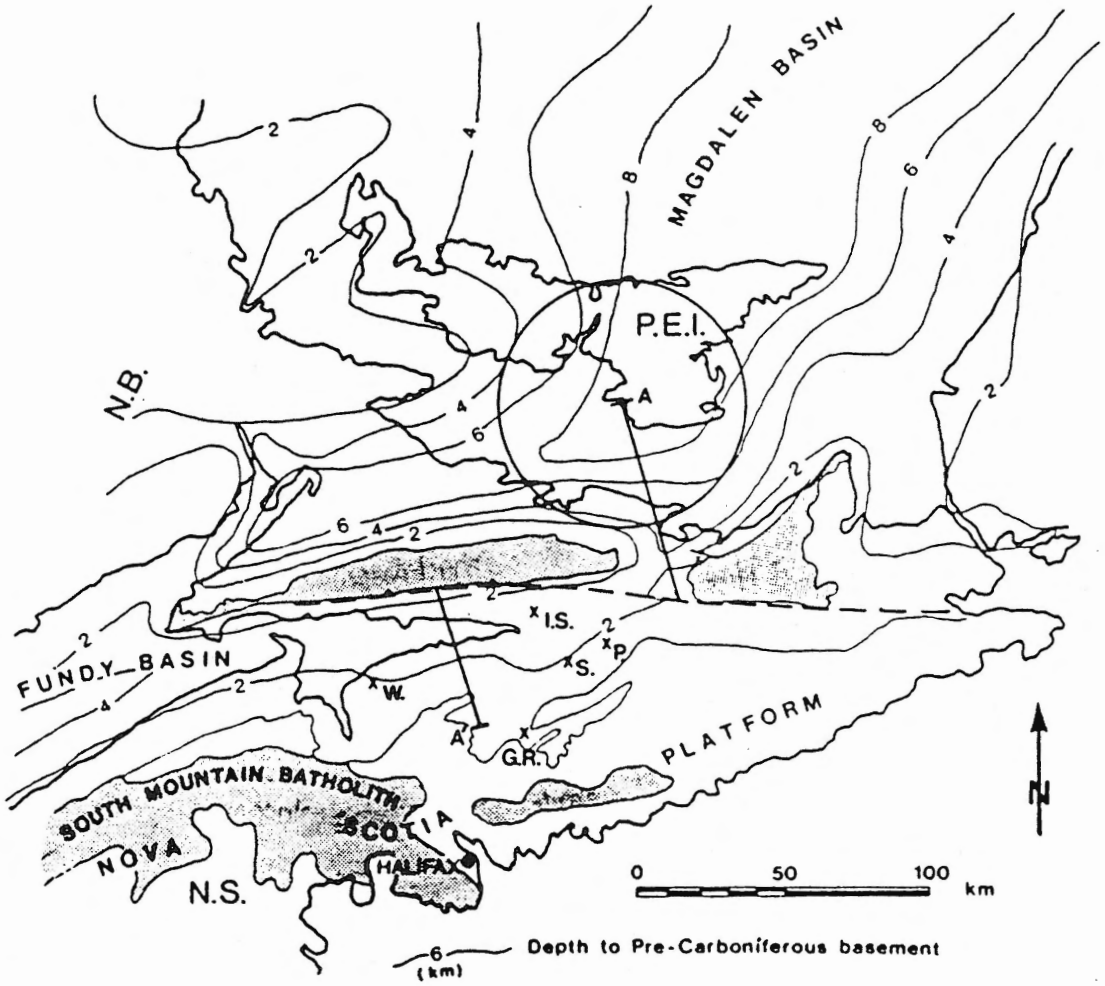
MAGDALEN BASIN
P.E.I.
N.B.
A
A'
FUNDY BASIN
I.S.
S.
P
W.
G.R.
PLATFORM
SOUTH MOUNTAIN BATHOLITH
NOVA SCOTIA
HALIFAX
N.S.
N
0
50
100
km
6 (km)
Depth to Pre-Carboniferous basement

Figure 6.1

Figure 6.2 Sediment accumulation curve for the southern Magdalen Basin (data from Howie and Barss, 1975)(see Figure 2.1). Although for all but one time period sedimentation rates are assumed to be constant between the data points, any combination of rates (including erosion in some cases) could be used to reproduce the known data. Sedimentation of the Cumberland Group (Cum in the Figure) was postulated to have been slightly more rapid than average for the Cumberland-Pictou time period. Sedimentation rates were used in the mathematical model of pore-fluid pressures. Deposition of the Pictou Group was followed by a period of erosion.

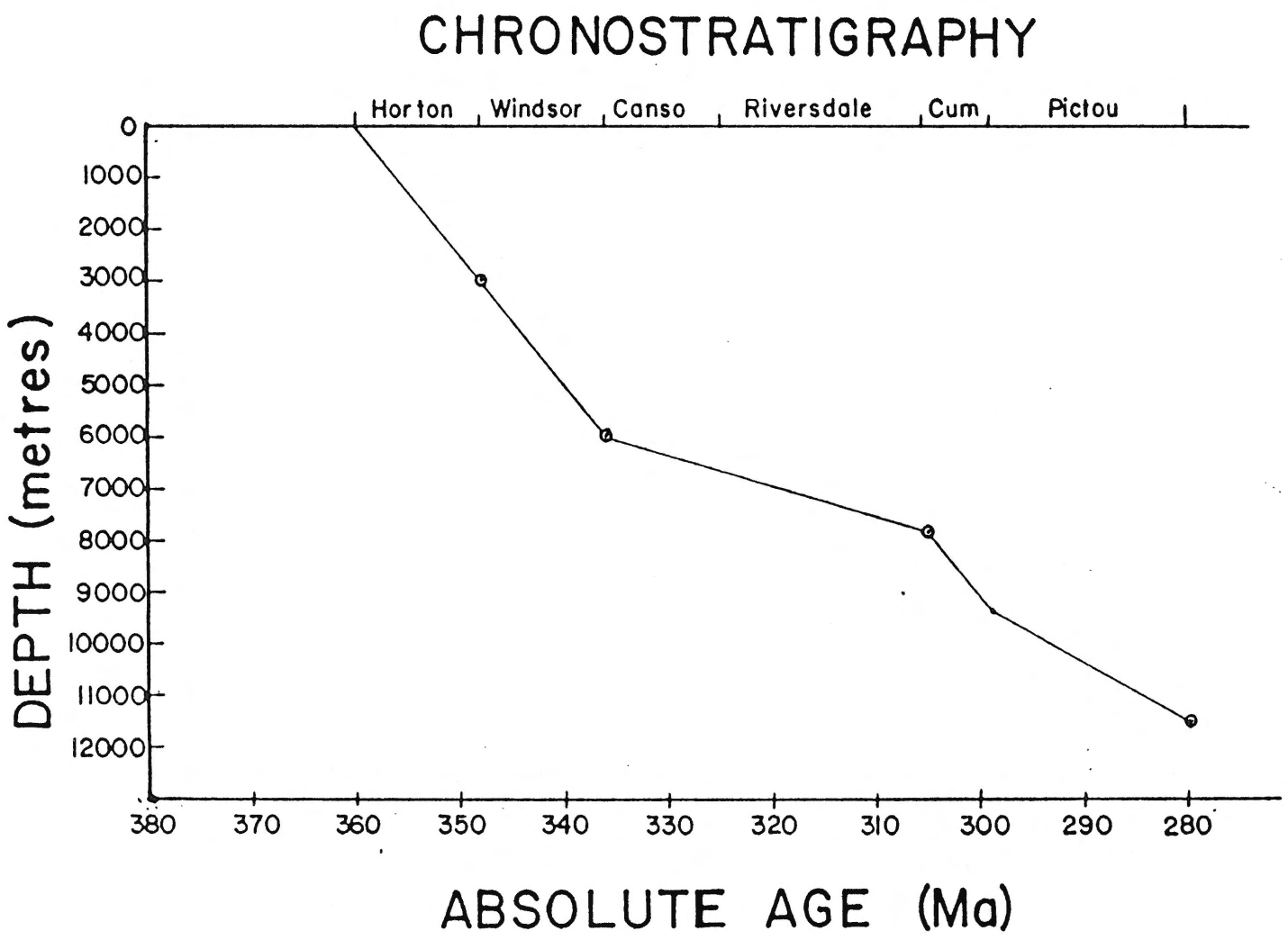
CHRONOSTRATIGRAPHY
Horton
Windsor
Canso
Riversdale
Cum
Pictou
DEPTH (metres)
0
1000
2000
3000
4000
5000
6000
7000
8000
9000
10000
11000
12000
380
370
360
350
340
330
320
310
300
290
280
ABSOLUTE AGE (Ma)

Figure 6.2

Figure 6.3 The conceptual model (section A - A' in Figure 6.1). Overpressured fluids escape from deep in the southern part of the Magdalen Basin by a hydrofracturing mechanism. These hot, rapidly moving brines cause extensive brecciation and dissolution near the top of the aquifer - the Pembroke Breccia - under the evaporite seal. Deposits of Pb-Zn and Ba are formed at the margins of the basin by the hot mineralizing brines.

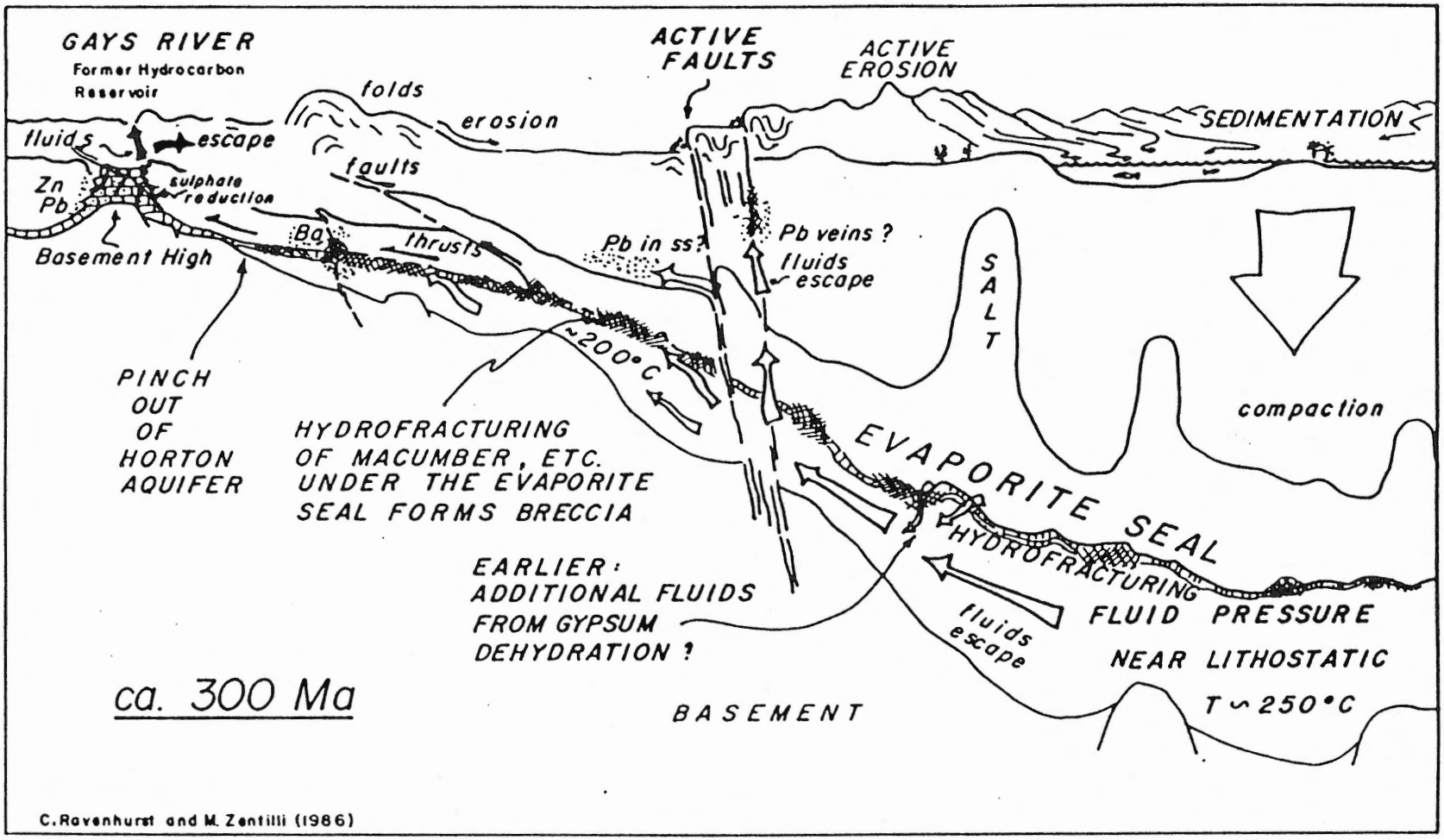
GAYS RIVER
Former Hydrocarbon Reservoir
fluids
escape
Zn
Pb
sulphate reduction
Basement High
folds
erosion
faults
Ba
thrusts
ACTIVE FAULTS
ACTIVE EROSION
SEDIMENTATION
Pb in ss?
Pb veins ?
fluids escape
SALT
~200°C
compaction
PINCH OUT OF HORTON AQUIFER
HYDROFRACTURING OF MACUMBER, ETC. UNDER THE EVAPORITE SEAL FORMS BRECCIA
EVAPORITE SEAL
HYDROFRACTURING
FLUID PRESSURE NEAR LITHOSTATIC
T ~ 250°C
fluids escape
EARLIER: ADDITIONAL FLUIDS FROM GYPSUM DEHYDRATION ?
ca. 300 Ma
BASEMENT
C. Ravenhurst and M. Zentilli (1986)

Figure 6.3

Figure 6.4 Parameters for the mathematical model. Basin geometry, hydraulic conductivity distribution, boundary conditions and initial conditions input to the mathematical model. Depth of basin shown and initial conditions are for the time of Windsor Group deposition (342-336 Ma). U = excess pore fluid pressure, dL/dt = sediment loading rate, Vx = fluid velocity in the x-direction, $\vec{n}$ = unit vector normal to the boundary.

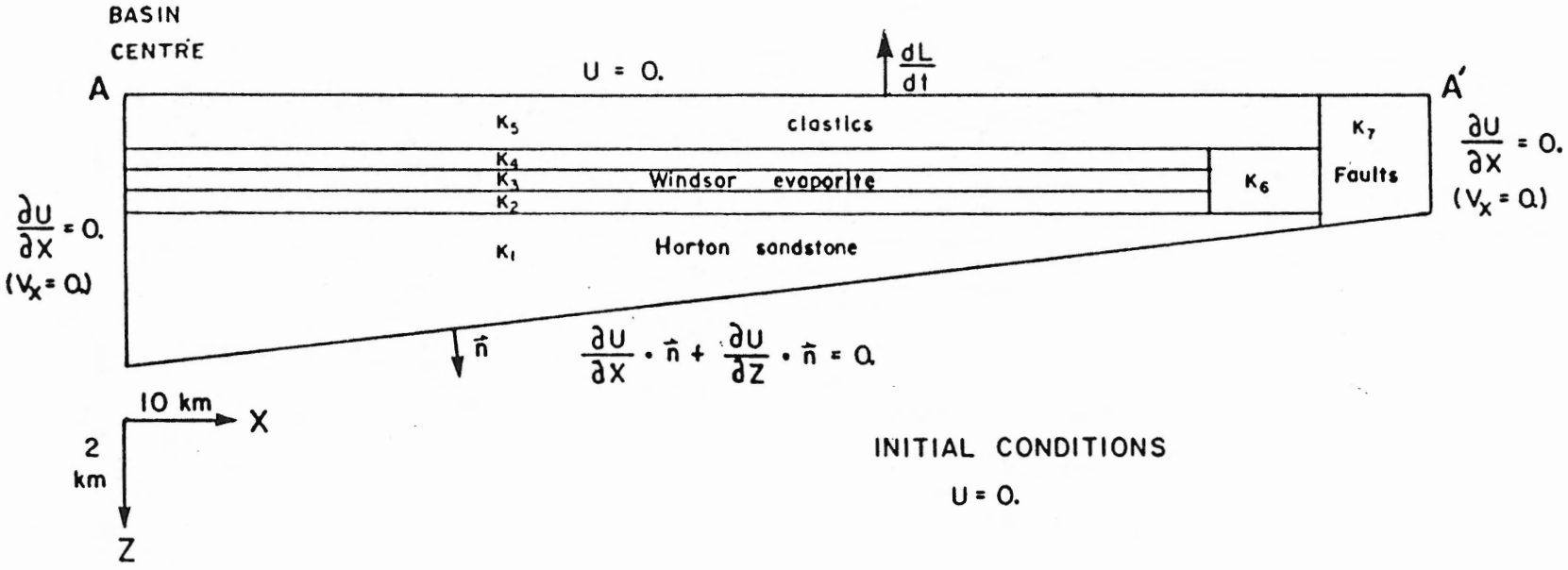
BASIN
CENTRE
A
U = 0.
dL/dt
A'
K5
clastics
K7
Faults
K4
K3
Windsor evaporite
K6
K2
K1
Horton sandstone
∂U/∂X = 0.
(Vx = 0.)
∂U/∂X = 0.
(Vx = 0.)
n̂
∂U/∂X · n̂ + ∂U/∂Z · n̂ = 0.
10 km
X
2
km
Z
INITIAL CONDITIONS
U = 0.

Figure 6.4

Figure 6.5 Initial triangulation. This illustrates the initial finite element mesh input to the TWODEPEP program during the Canso-Riversdale time period.

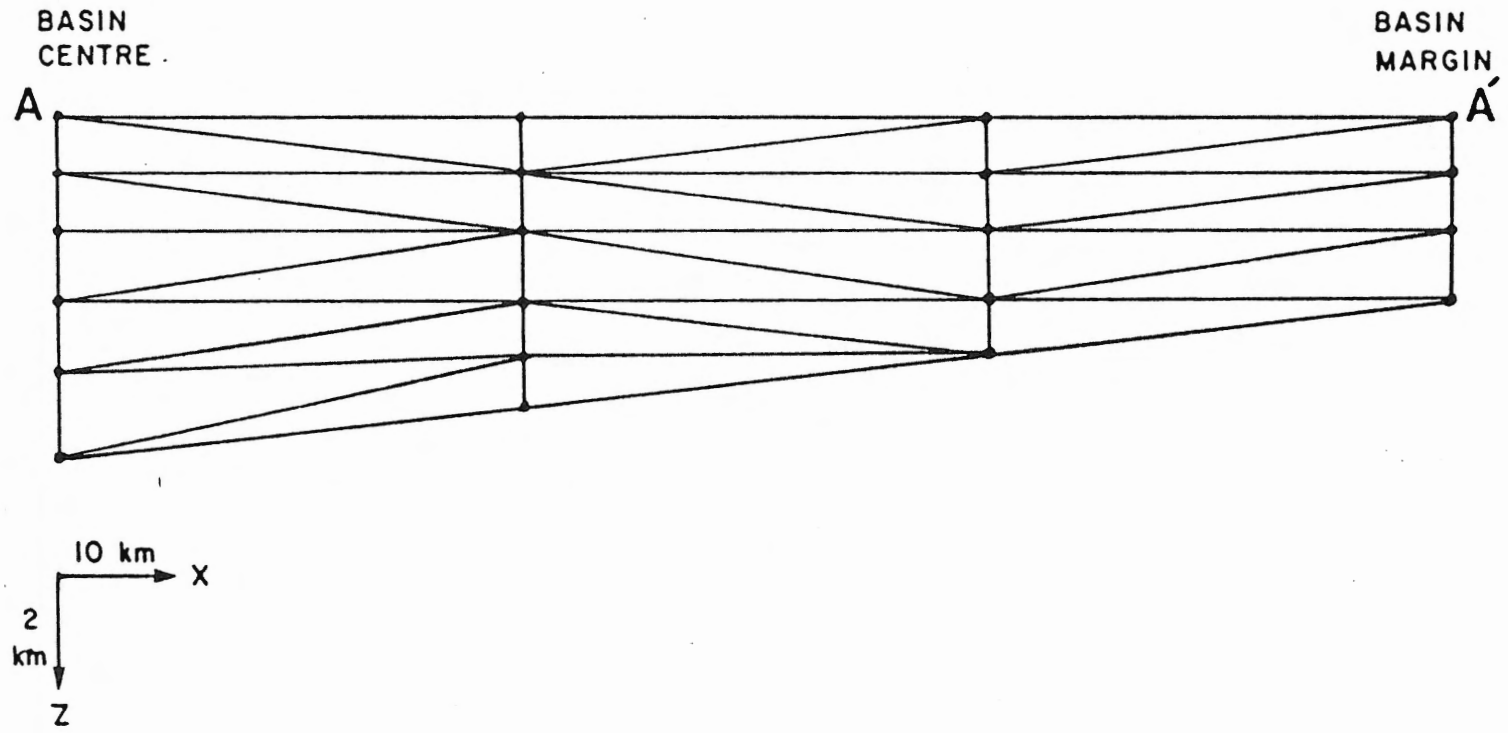

Figure 6.5

Figure 6.6 Final triangulation. This illustrates the final finite element mesh (for the Canso-Riversdale time period) generated by the TWODEPEP program in accordance with my specified mesh density formula.

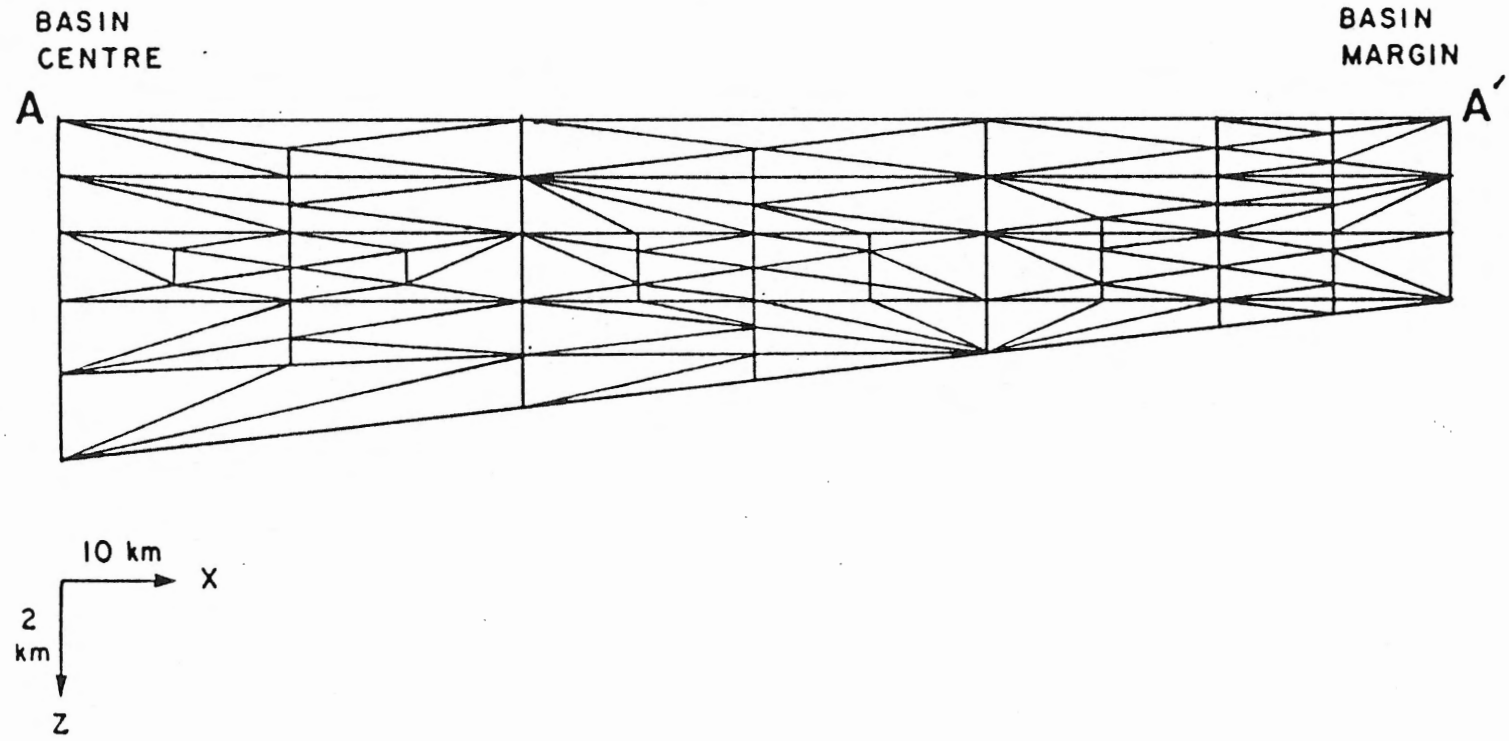

Figure 6.6

Figure 6.7 Hydraulic conductivities of various rock types (from Garven and Freeze, 1982b, Table 2).

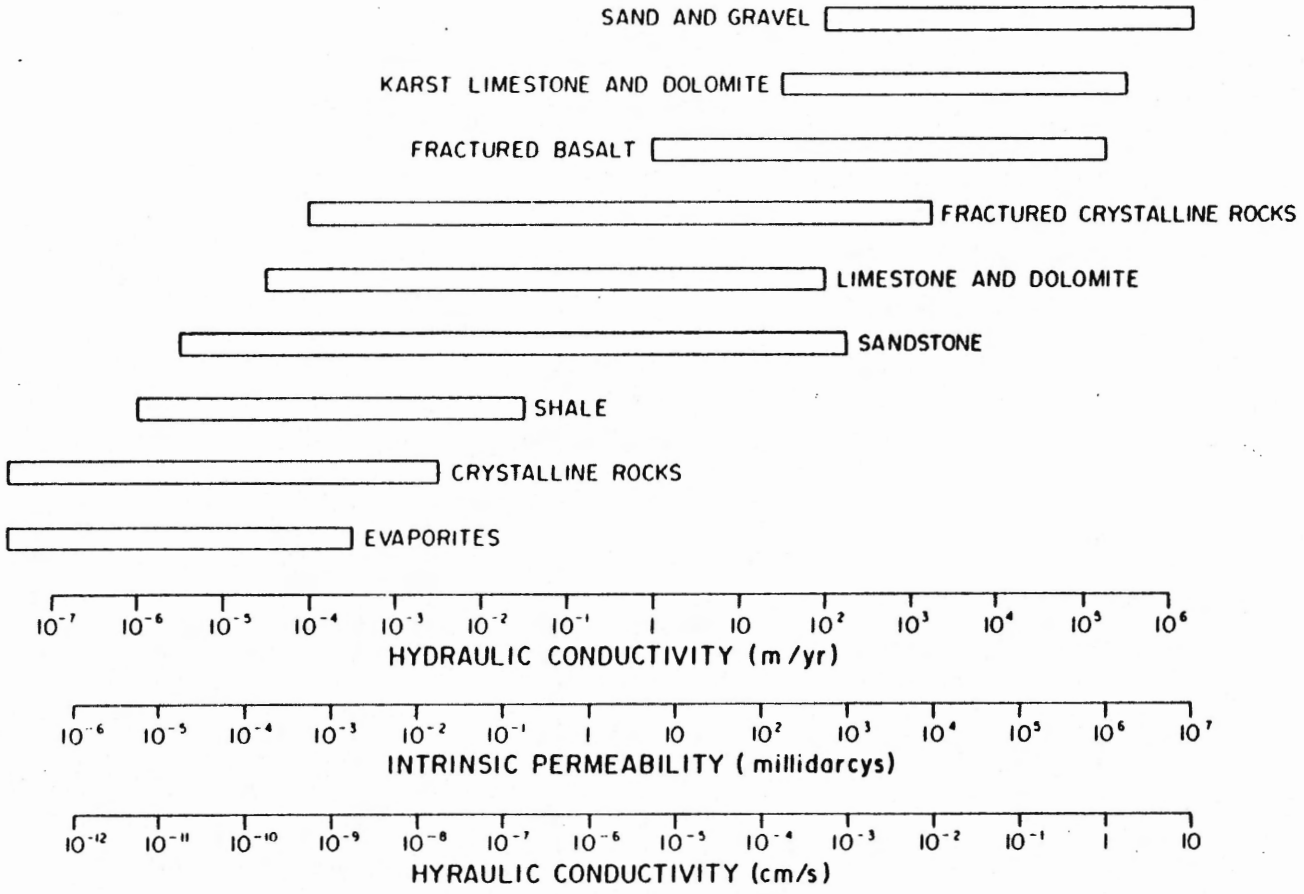
SAND AND GRAVEL
KARST LIMESTONE AND DOLOMITE
FRACTURED BASALT
FRACTURED CRYSTALLINE ROCKS
LIMESTONE AND DOLOMITE
SANDSTONE
SHALE
CRYSTALLINE ROCKS
EVAPORITES
10^{-7} 10^{-6} 10^{-5} 10^{-4} 10^{-3} 10^{-2} 10^{-1} 1 10 10^{2} 10^{3} 10^{4} 10^{5} 10^{6}
HYDRAULIC CONDUCTIVITY (m/yr)
10^{-6} 10^{-5} 10^{-4} 10^{-3} 10^{-2} 10^{-1} 1 10 10^{2} 10^{3} 10^{4} 10^{5} 10^{6} 10^{7}
INTRINSIC PERMEABILITY (millidarcys)
10^{-12} 10^{-11} 10^{-10} 10^{-9} 10^{-8} 10^{-7} 10^{-6} 10^{-5} 10^{-4} 10^{-3} 10^{-2} 10^{-1} 1 10
HYRAULIC CONDUCTIVITY (cm/s)

Figure 6.7

Figure 6.8 Pore fluid pressure and overburden pressure as a function of depth. Mathematical model results at two different times in the southern Magdalen basin. For a given hydraulic conductivity distribution and sediment loading rate, the excess pore fluid pressures shown are mathematically generated under the evaporite seal.

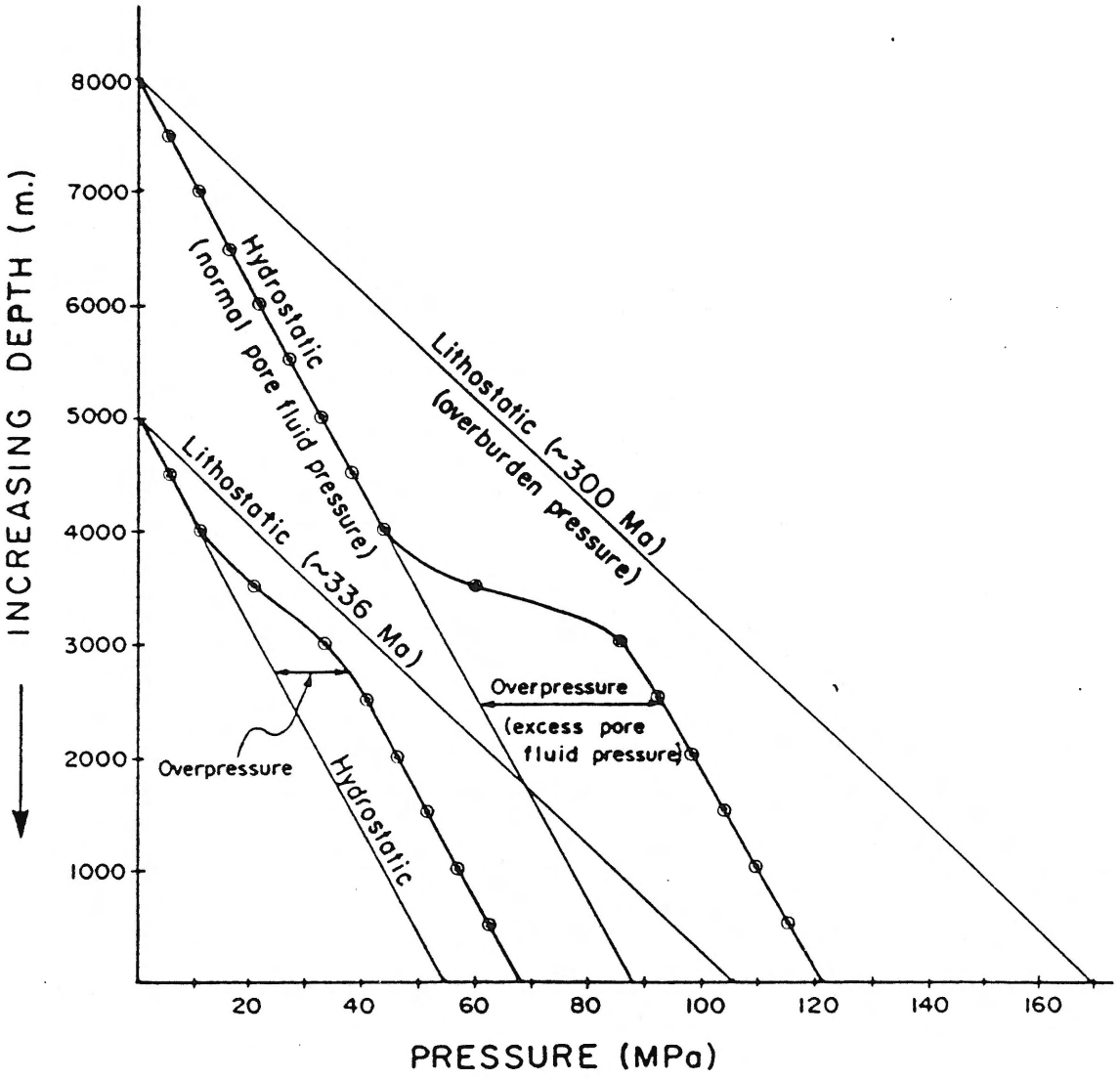
INCREASING DEPTH (m.)
8000
7000
6000
5000
4000
3000
2000
1000
Hydrostatic
(normal pore fluid pressure)
Lithostatic (~300 Ma)
(overburden pressure)
Lithostatic (~336 Ma)
Overpressure
(excess pore
fluid pressure)
Overpressure
Hydrostatic
20
40
60
80
100
120
140
160
PRESSURE (MPa)

Figure 6.8

Figure 6.9 Excess hydraulic head and fluid velocities generated by the mathematical model. Excess hydraulic head (excess pore fluid pressure) and steady-state (dewatering) fluid velocities shown are for the end of Cumberland Group deposition (305-300 Ma). Excess pore fluid pressures with depth near the centre of the basin are plotted in Figure 6.8. The data was generated by the TWODEPEP finite element program.

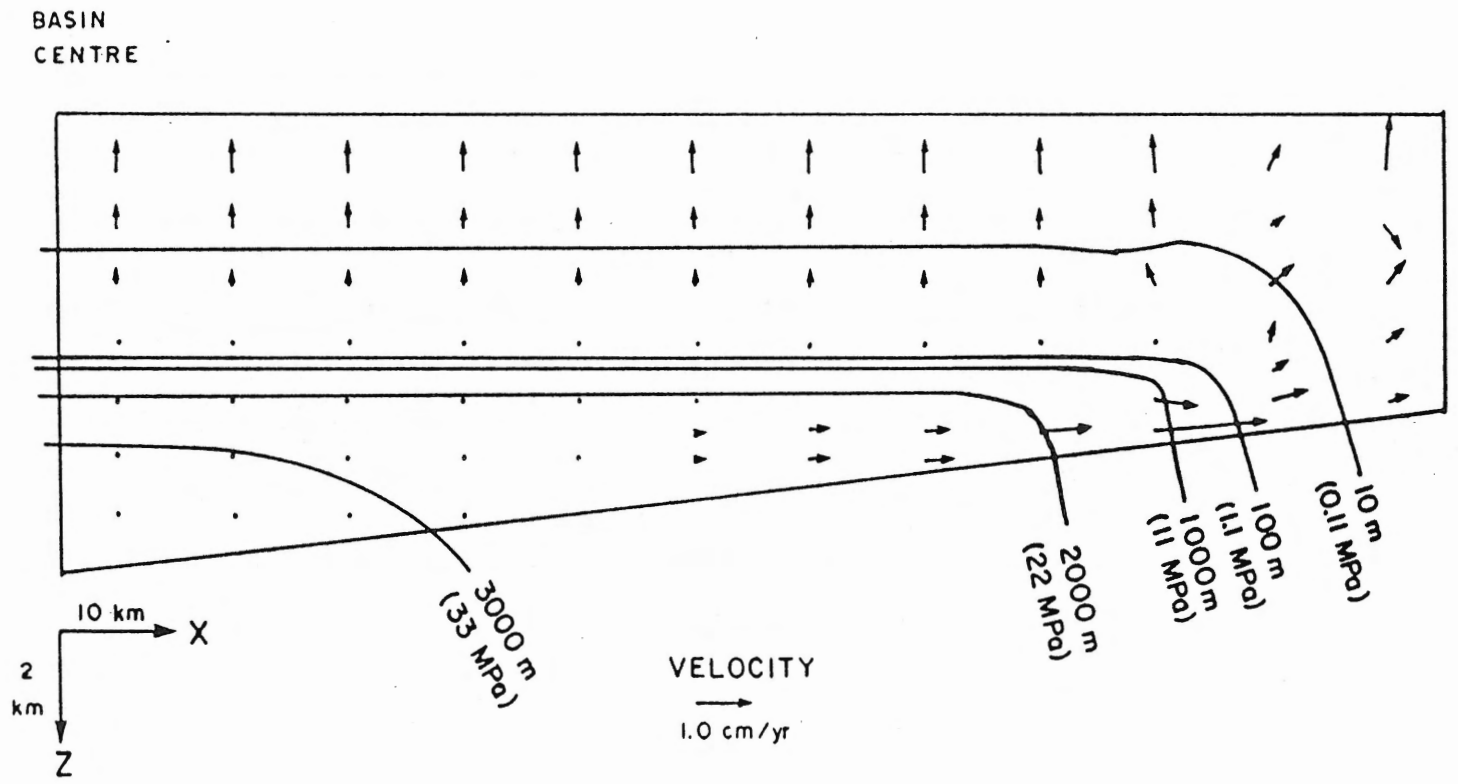
BASIN
CENTRE
10 km
X
2
km
Z
3000 m
(33 MPa)
2000 m
(22 MPa)
1000 m
(11 MPa)
100 m
(1.1 MPa)
10 m
(0.11 MPa)
VELOCITY
1.0 cm/yr

Figure 6.9

CHAPTER 7

DISCUSSION AND CONCLUSIONS

Fluids move in sedimentary basins, both during basin formation and long afterwards, in response to hydrostatic gradients established by compaction, thermal gradients, topographic relief, deformation and other factors. Whether these fluids are petroleum-bearing or metal-bearing is determined by the origin of the fluids, the composition of the sediments, and possibly the timing of the fluid movement. Petroleum moves from source beds to physical traps. Metals move from source beds to chemical traps (Anderson and Macqueen, 1982). The model presented in this thesis addresses the problems of fluid source and temperature, source of the metals and the likely path of the mineralizing fluid from source to depositional site. It brings together the tectonic and sedimentation history of the Fundy/Magdalen basin system with the timing of diagenetic fluid movement and the formation of Pb-Zn and Ba mineral occurrences.

The deposits were formed in structural highs or near faults and the fluids moved through the Pembroke breccia or other aquifers to arrive at the depositional sites. That these sites may have been hydrocarbon traps, together with the necessity of channelling or focussing of the fluids, can both be used as exploration guides.

The interpretation offered here for the Pembroke breccia is controversial, but no all-encompassing origin has been proposed in the literature. A modern analogy for the environment of formation of some of the Pembroke breccia may be the overpressured conditions described for the 1956 blow-out of the Alborz #5 well in Central Iran, recently

discussed by Gretener (1982). Alborz #5 was drilled on a large structure (12 by 50 km), near the holy city of Qum in Central Iran. The well penetrated 2296 m of Tertiary clastics followed by 381 m of evaporites (Mostofi and Gansser, 1957, in Gretener (1982) The hole was then drilled a short distance into what was described as "fractured limestone". At that point the mud column of a density of 2.07 g/cm^3 was blown out of the hole and over the next 82 days the well produced, under partial control, large quantities of gas and an estimated five million barrels of oil. The temperature of the flowing oil at the surface was 115°C. After 82 days the well bridged itself (Gretener, 1982). I suggest that the Pembroke Breccia may be an equivalent of the "fractured limestone" encountered under the evaporite seal at Alborz # 5. As Gretener (1982) suggested, under a perfect seal "the fluid pressure may completely support the overburden - the rock is fully de-stressed. Vertical dilation will occur and permit the development of a network of unoriented, open fractures".

In my model, I have not used a "perfect seal", but instead used reasonable hydraulic conductivity values for evaporites (Garven and Freeze, 1984b). Average thicknesses of formations were calculated for the southern part of the Magdalen Basin from isopach maps of Howie and Barss (1975), and the sedimentation rates were estimated using the absolute time scale of Harland et al. (1982). Using these data, I established that the pore fluid pressure under the Windsor evaporite in the Magdalen Basin was probably anomalously high during most of the basin evolution, and that a significant overpressure could have developed at least once by 300 Ma. This overpressure would clearly have been sufficient to hydrofracture the rocks. The λ parameter (the ratio

of fluid pressure to the total overburden pressure) would have been at a maximum at the highest topographic point within the overpressured reservoir, but would at no time exceed a value of '1', because fracturing would occur. Once the fracturing started, the least work configuration for the breccia aquifer would be a flat, thin layer of fluid (Pollard, 1973; Pollard et al., 1983) moving along the topographically highest zone under the seal. Rushing fluids would be capable of transporting pebbles from the underlying Horton in suspension. This would probably explain the presence of exotic pebbles in an otherwise carbonate-dominated breccia.

The anomalous temperatures at the mineral deposits (140° to 250°C) as shown by fluid inclusions and the level of organic maturation, necessitates a very rapid transfer of the fluids from the deep basin to its margins. Uncertainty in the depth of the overburden at the deposits, means that these temperatures could be even higher due to a pressure correction to the homogenization temperatures. A maximum correction of 90°C due to 3.6 km of overburden is a possibility (Akande, 1982). Because this pressure correction of 25°C/km is different from the estimated geothermal gradient at the time of mineralization ($\sim$40°C/km, Table 6.1), the amount of overburden at the time of mineralization could determine the feasibility of other models of formation. Thus, a major uncertainty still remaining in the model is the pressure-temperature conditions existing at the time of mineralization at all the deposits studied.

The Minas Geofracture/Cobequid-Chedabucto Fault System appears at present to be a barrier or possibly a rapid escape route for the mineralizing fluids, but much of the movement along this fault zone

occurred after 300 Ma. The evaporite was probably unbroken across the Minas Geofracture, or may have resealed itself, at the time of rapid fluid expulsion from the Magdalen Basin. However, a search for mineral deposits in organic-rich strata along the Geofracture zone may prove fruitful. Near some of the mineral deposits, the pinchout of Horton clastics between the evaporite and the basement may have resulted in downward penetration of the fluids into basement faults, further complicating the hydraulic system.

Hydrogen and oxygen isotopic data suggest that the mineralizing fluid at the deposits was a basinal brine, possibly mixed with some metamorphic and igneous fluids. Carboniferous seawater was probably not directly involved in the mineralizing process. The lead isotope data suggest that the source of the metals was the direct clastic derivatives of the basement rocks accumulated in the adjacent sedimentary basin. Strontium isotope data for calcite indicate that at least part of the strontium (and presumably therefore part of the calcium) in the mineralizing fluids originated from a source more radiogenic than Carboniferous carbonates or evaporites. The clastic sediments of the adjacent sedimentary basin are a likely source of this radiogenic component. The $\delta^{13}C_{\Sigma C}$ value deduced for the mineralizing fluid ($\sim$ +2 o/oo) suggests that carbonates were the main source of carbon during the mineralizing event. Organic carbon became more important as mineralization progressed. Sulfate was probably derived from Mississippian evaporites which are extensive in the Shubenacadie basin and stratigraphically overlie the deposits. The hot mineralizing fluids must therefore have originated at >5 km depth and interacted with clastic, carbonate and evaporite sedimentary sequences on their way to

the depositional site.

Conditions necessary for the fluid transport of significant concentrations of Pb and Zn have been discussed by Helgeson (1969), Barnes (1979), Sverjensky (1981b) and by Anderson and Macqueen (1982). If metals were carried as chloride complexes at concentrations >10 ppm, the pH of the fluid was either low (how low depends on temperature) and H_2S was carried in solution, or the fluids were oxidized and carried SO_4 in solution. Evidence cited above suggests that $\delta^{34}S$ of the H_2S from which the sulfide minerals precipitated at Gays River was very similar to that of the stratigraphically overlying sulfate, the assumed sulfur source. If H_2S and metals were carried together, or if the metal-bearing fluids encountered a large H_2S reservoir at the depositional site, Anderson and Garven (1987) and Anderson (1983) showed that hydrogen ions (acid) would be generated leading to extensive dissolution of the carbonate host rocks and probably solution collapse brecciation of host rocks and/or sulfides. At Gays River and Pembroke there is little evidence of these features.

I suggest that some of the ore fluids carried barium in solution (probably as chloride), which was precipitated at the Horton/Windsor contact due to mixing there with the sulfate-rich water from the evaporites (e.g. Leach, 1980). As the mineralizing fluids moved on, I suggest that they had pH >5 and carried sulfate in solution. Upon arrival of the fluids at the Pb-Zn depositional sites, complete reduction of sulfate occurred by reaction with a reduced carbon species, possibly petroleum or methane (see Olson, 1984; Barton, 1967) and sulfides were precipitated. Only weak acid is generated in these reactions. This model is attractive because the geology of the Gays

River carbonate mound and the Pembroke fossiliferous limestone both suggest classic hydrocarbon traps. Pyrobitumen occurs throughout the Gays River deposit (Akande, 1982). Work by Powell and Macqueen (1984) on the Pine Point deposit indicates that bitumen in proximity to the sulfide orebodies participated in the thermochemical reduction of sulfate. Sulfur isotopic compositions of sulfides at the K-57 orebody show a range from 13.1 to 23.5 o/oo (Kyle, 1983), possibly a result of precipitation of sulfides while the sulfate ($\delta^{34}S$ = 19 o/oo) was being reduced. The mechanism of nonbiogenic reduction is still not understood (Trudinger et al., 1985) but a reaction that may have been slow at the 100°C temperatures of Pine Point may have resulted in relatively instantaneous total sulfate reduction at the 200°C plus temperatures at Gays River.

At Gays River, precipitation of ore-stage sulfides at 200°C under reduced sulfur conditions was followed at $\sim$ 170° to 130°C by deposition of ore-stage and postore calcite in an oxidized carbon environment. Organic carbon (with relatively low $\delta^{13}C$ values) became quantitatively important during deposition of postore calcite. Carbon and oxygen isotopic analyses of mineralized and unmineralized calcite samples within a 2 km radius of the Gays River mine, indicate that isotopic analyses of vein and vug-filling calcite has application as an exploration guide to highly mineralized zones.

A number of different dating techniques support a mineralization age of 300 Ma. The rubidium-strontium isotope data, although limited, suggest a hydrothermal event at 300 Ma that homogenized strontium at a scale of tens of metres in the Horton strata. Further Rb-Sr dating in other upper Horton strata are needed. At the deposits, fission track

dating of zircon indicates that mineralization occurred at 313 ± 44(2σ) Ma at Gays River and at 250 ± 34(2σ) Ma at Smithfield. The slightly younger age at Smithfield (although errors are quite large) and the suggestion of younger ages at some of the other deposits, could indicate longer-lasting hydrothermal events there, or a partial resetting due to deeper burial during the 180 to 200 Ma thermal and uplift event that completely reset the fission track ages in apatite. Further fission track dating work will lower the errors in these data and may also clarify the reason for the apparent age differences between the deposits. $^{40}Ar/^{39}Ar$ dating of one muscovite sample from altered wallrock at Gays River suggests a thermal (mineralization) event there at about 330 Ma. A repeat analysis to obtain a more detailed age spectrum is needed. One set of whole rock lead isotope data on a Horton siltstone indicates that the Horton derived its lead from the Meguma and probably had the right isotopic composition at 300 Ma to form the galena at the deposits. Again, more whole rock lead data of Upper Horton strata on a regional scale are needed.

Some of the main uncertainties remaining in my compaction-driven fluid fluid flow model are the structural and depositional histories of the Fundy/Magdalen Basin and the spatial configuration of the Basin at the time of mineralization. The funnelling of all the mineralizing fluids through the Stellarton Sub-basin as proposed in my model is rather tenuous. A deep basinal source south of the Cobequid-Chedabucto Fault System (Figures 1.1 and 6.1) would make a much more reasonable model. A deep source of fluids in the granite/metasedimentary basement is also still a possibility; these fluids would also have been trapped by the evaporite seal and would have been isotopically altered and

enriched in Pb and Zn by interaction with the Horton Group clastic rocks.

The gravity-driven model of Garven and Freeze (1984a, 1984b) applied to this region, could also explain many of the data if the tectonic setting involved uplift of part of the basin at the time of mineralization. (Meteoric fluid could be significantly altered and heated by deep circulation, thereby attaining the the isotopic signature of the mineralizing fluids). The high temperatures of the mineralizing fluids and the possibility that the Pembroke breccia was formed by a hydrofracturing event involving rapid fluid movement, argue against this model. The early diagenetic convection model of Russell (1976) is difficult to envisage in a sedimentary package with significant thicknesses of evaporites. Jowett's (1986) horizontal convection model for the Rotliegende brines underneath a seal requires further consideration. However, this model requires a significant horizontal variation in the geothermal gradient in order to drive the convection cells.

A tectonic event in pre-Late Westphalian B-Early C (300 Ma by the time scale of Harland et al., 1982) is well documented (Keppie, 1982), and may have been the push that set off the hydrothermal fluid flow. Further tectonic activity took place in the Triassic-Jurassic, as confirmed by my fission track dating of apatites. Block faulting contributed to the dislocation of the Carboniferous basin, and erosion must have removed at least 2 km of overlying sediments. By the mid-Cretaceous, the Gays River reef and enclosed lead zinc deposit was exposed to karstification, and partial destruction (Davies et al., 1984), which nearly obliterated the high grade zones. Other deposits

similarly located in structural highs were probably eroded at this same time.

APPENDIX A

VITRINITE REFLECTANCE DATA AND HISTOGRAMS

Tabulated here are the vitrinite reflectance measurements, histograms, edited histograms and calculated means and standard deviations of the non-rotated measurements (Ro non-rotated). Ro max is calculated from Ro non-rotated and tabulated in Table 3.2. Data was collected and compiled by Mike Avery of the Atlantic Geoscience Centre (AGC) as part of a cooperative venture. A report on some of these data written by Avery (1986) is available at AGC.

FILE >> C0014C DESCRIPTION FOLLOWS :
DEPTH RGR-21', RAVENHURST/86, MPA, DEC-13-86

COL>	0	1	2	3	4	5	6	7	8	9
ROW		.75	.83	*1.04	*1.05	*1.05	*1.06	*1.10	*1.13	*1.14
1	*1.21	*1.22	*1.26	*1.30	*1.30	*1.36	*1.36	*1.39	*1.39	*1.40
2	*1.42	*1.54	*1.54	*1.55	*1.58	1.85	1.88	1.94	1.98	2.15
3	2.25	2.28	2.34	2.35	2.39	2.49	2.79	2.89	3.04	

	MEAN	STAND.DEV.	PTS	MIN	MAX	SUM
TOTAL >	1.65	.60	38	.75	3.04	62.59
*EDIT >	1.29	.18	22	1.04	1.58	28.39

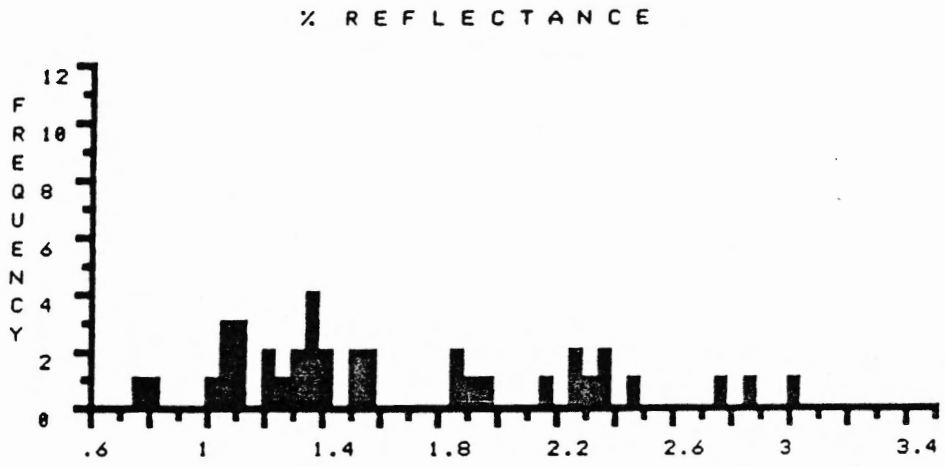

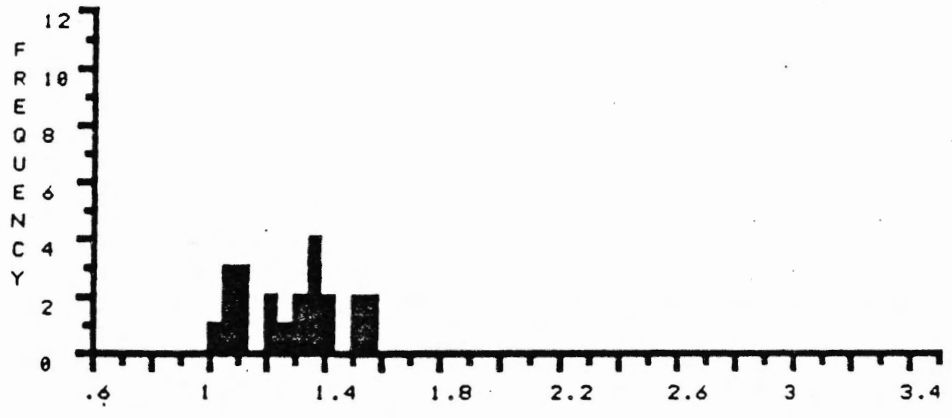

FILE >> C0015A DESCRIPTION FOLLOWS :
DEPTH RGR-69', RAVENHURST/86, MPA, JAN-19-87

COL>	0	1	2	3	4	5	6	7	8	9
ROW		*.81	*.89	*.90	*.98	*1.04	*1.07	*1.09	*1.10	*1.10
1	*1.17	*1.23	1.43	1.74						

	MEAN	STAND.DEV.	PTS	MIN	MAX	SUM
TOTAL >	1.12	.25	13	.81	1.74	14.55
*EDIT >	1.03	.13	11	.81	1.23	11.38

% R E F L E C T A N C E

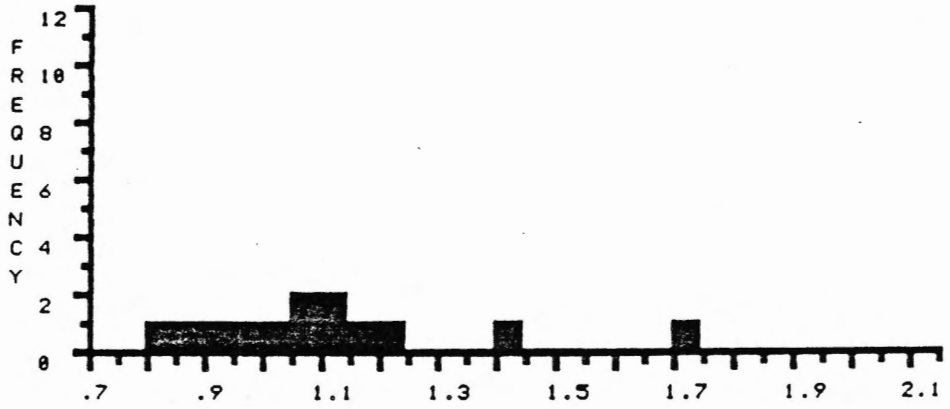

% R E F L E C T A N C E * * EDITED * *

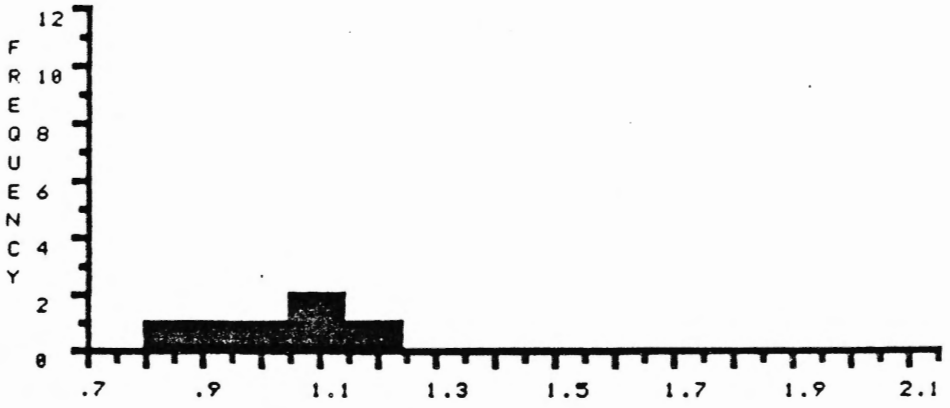

FILE >> C00158 DESCRIPTION FOLLOWS :
DEPTH RGR-111', RAVENHURST/86, MPA, JAN-19-87

COL>	0	1	2	3	4	5	6	7	8	9
ROW		.83	*.90	*.92	*.92	*.93	*.94	*.94	*.95	*.95
1	*.95	*.96	*.96	*1.00	*1.00	*1.00	*1.01	*1.03	*1.03	*1.03
2	*1.03	*1.04	*1.05	*1.05	*1.05	*1.06	*1.07	*1.08	*1.08	*1.08
3	*1.09	*1.09	*1.09	*1.09	*1.10	*1.11	*1.12	*1.12	*1.12	*1.13
4	*1.13	*1.13	*1.13	*1.14	*1.14	*1.15	*1.15	*1.16	*1.16	*1.17
5	*1.17	*1.17	*1.17	*1.17	*1.18	*1.19	*1.20	*1.20	*1.20	*1.21
6	*1.21	*1.22	*1.22	*1.24	*1.25	*1.26	*1.27	*1.27	*1.27	*1.28
7	*1.29	*1.29	*1.29	*1.29	*1.30	*1.31	*1.31	*1.32	*1.32	*1.36
8	*1.36	*1.37	*1.37	*1.38	*1.39	1.47				

	MEAN	STAND.DEV.	PTS	MIN	MAX	SUM
TOTAL >	1.14	.14	85	.83	1.47	97.13
*EDIT >	1.14	.13	83	.90	1.39	94.83

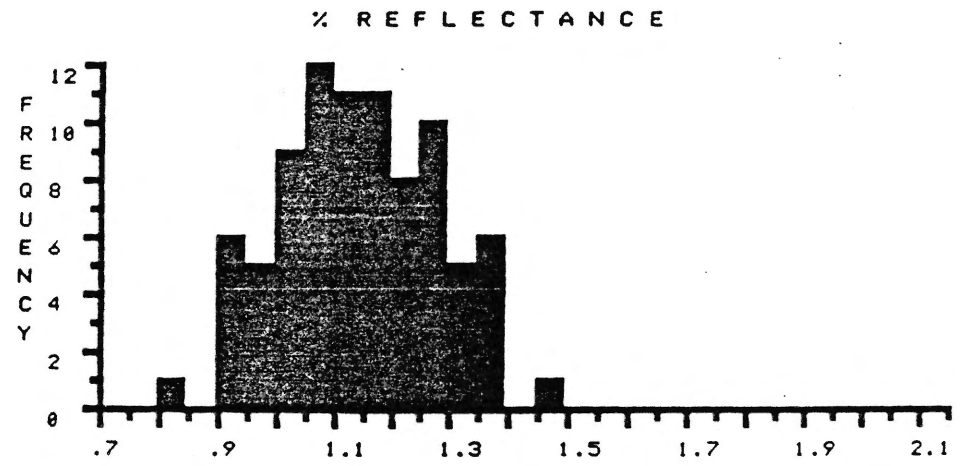

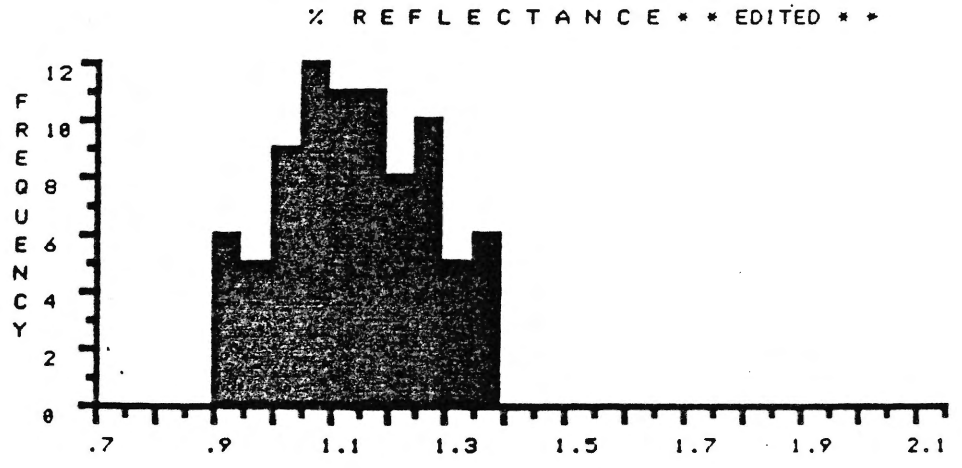

FILE >> C0015C DESCRIPTION FOLLOWS :
DEPTH RGR-126', RAVENHURST/86, MPA, JAN-19-87

COL>	0	1	2	3	4	5	6	7	8	9
ROW		*1.35	1.70	1.77	1.78	1.83	1.87	1.88	1.91	1.91
1	1.91	1.92	1.95	1.98	1.99	2.01	2.06	2.07	2.07	2.14
2	2.18	2.21	2.22	2.23	2.25	2.25	2.27	2.29	2.31	2.31
3	2.33	2.37	2.42	2.47	2.49	2.60				

	MEAN	STAND.DEV.	PTS	MIN	MAX	SUM
TOTAL >	2.09	.26	35	1.35	2.60	73.3
*EDIT >	1.35		1	1.35	1.35	1.35

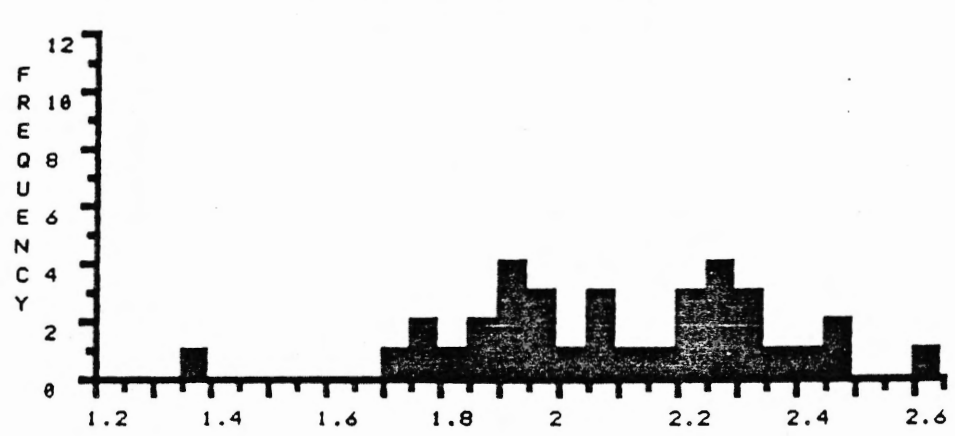

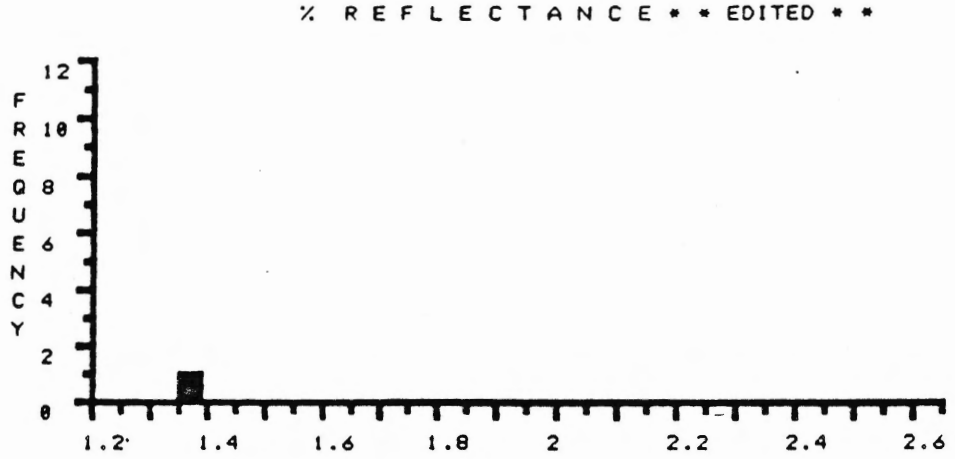

FILE >> C0016A DESCRIPTION FOLLOWS :
DEPTH RGR-140', RAVENHURST/86, MPA, JAN-19-87

COL>	0	1	2	3	4	5	6	7	8	9
ROW		1.05	1.05	1.10	1.10	1.11	1.11	1.12	1.12	1.14
1	1.14	1.15	1.15	1.15	1.17	1.17	1.18	1.19	1.19	1.19
2	1.20	1.21	1.21	1.22	1.23	1.23	1.23	1.24	1.24	1.26
3	1.27	1.27	1.27	1.28	1.29	1.30	1.30	1.30	1.31	1.32
4	1.34	1.35	1.40							

	MEAN	STAND.DEV.	PTS	MIN	MAX	SUM
TOTAL >	1.21	.08	42	1.05	1.40	50.85

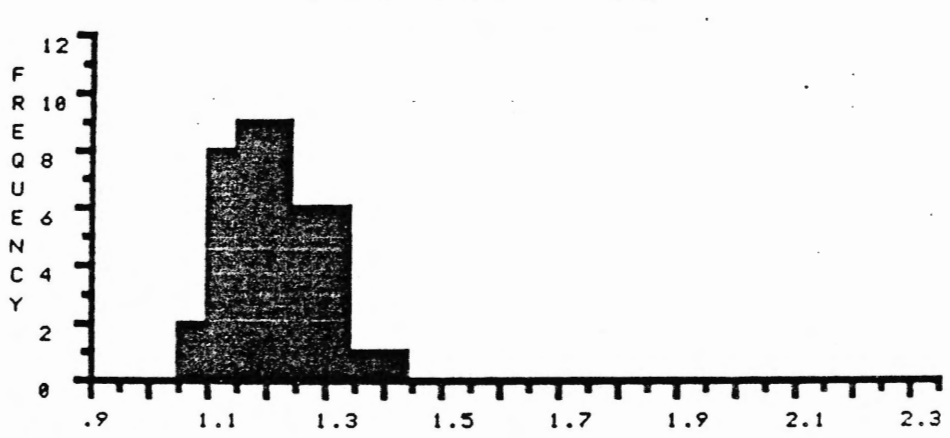

FILE >> C00178 DESCRIPTION FOLLOWS :
DEPTH RSB-122', RAVENHURST/86, MPA, JAN-20-87

COL>	0	1	2	3	4	5	6	7	8	9
ROW		1.40	1.81	1.98	1.99	2.07	2.08	2.26	2.30	2.33
1	2.41	2.45	2.45	2.47	2.48	2.54	2.55	2.58	2.58	2.60
2	2.61	2.64	2.65	2.66	2.69	2.73	2.75	2.75	2.77	2.79
3	2.81	2.82	2.89	2.91	2.92	2.93	2.98	2.98	2.99	3.01
4	3.02	3.03	3.04	3.08	3.08	3.09	3.10	3.15	3.16	3.19
5	3.23	3.28	3.31	3.35	3.36	3.42	3.45	3.47	3.50	3.51
6	3.54	3.55	3.55	3.55	3.56	3.60	3.60	3.62	3.63	3.64
7	3.65	3.66	3.67	3.67	3.72	3.73	3.75	3.80	3.83	3.86
8	3.88	3.94	3.95	3.96	3.96	4.00	4.02	4.02	4.02	4.03
9	4.04	4.04	4.06	4.11	4.11	4.12	4.12	4.16	4.16	4.60

	MEAN	STAND.DEV.	PTS	MIN	MAX	SUM
TOTAL >	3.22	.65	99	1.40	4.60	318.91

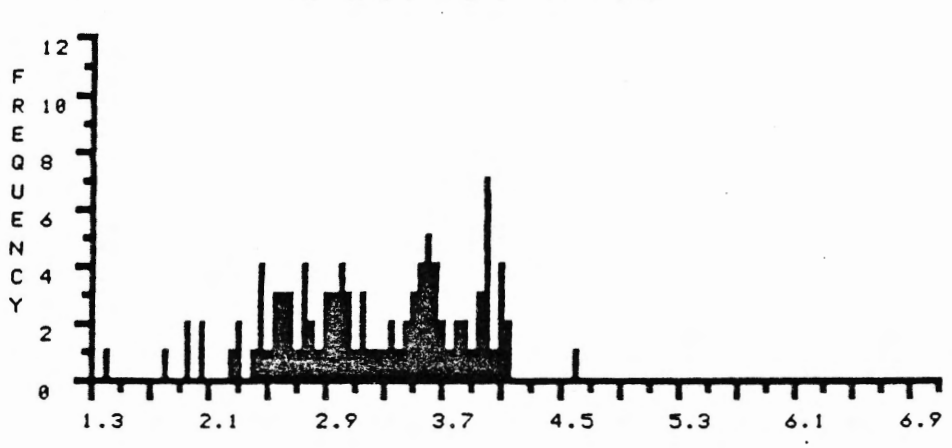

FILE >> CR0178 DESCRIPTION FOLLOWS :
INT. >RSB-122. RAVENHURST/86. MPA. JAN-20-87

COL>	1	2	3	4	5	6	7	8	9	0
RND										
ROW	2.93	4.08	2.14	2.79	2.07	3.09	3.22	2.61	2.15	3.12
1	2.02	2.54	2.63	1.83	3.75	3.54	2.77	3.67	4.17	3.54
2	4.02	2.42	3.43	4.19	3.51	3.74	3.77	2.73	4.21	2.66
3	2.57	3.70	3.68	1.75	3.32	2.47	2.33	3.15	3.03	2.89
4	2.20	2.21	2.96	3.68	3.81	2.33	2.35	2.69	2.21	3.88
MAX										
ROW	4.19	4.20	3.82	3.15	3.99	3.36	3.40	4.15	3.13	3.28
1	3.90	4.26	4.22	3.95	4.00	3.59	3.99	4.03	4.29	4.28
2	4.11	4.08	3.80	4.20	4.09	3.95	3.97	4.21	4.24	4.25
3	4.21	3.76	4.02	4.33	3.71	4.07	3.57	3.15	3.70	3.52
4	3.76	3.92	3.71	3.90	3.81	4.39	3.85	4.23	3.42	4.01
MIN										
ROW	2.21	3.43	2.12	2.52	2.01	3.01	2.89	2.16	2.08	2.71
1	1.85	2.12	1.60	1.76	3.36	2.82	2.19	3.40	3.61	3.30
2	3.86	2.38	2.50	1.73	3.38	2.57	2.56	1.92	1.70	2.32
3	1.96	3.35	1.80	1.75	2.34	1.86	1.87	2.96	2.60	2.17
4	1.85	1.63	2.79	3.55	2.88	1.54	2.13	2.16	1.85	3.27

STATISTICS BASED ON 50 POINTS.

	MEAN	STAND.DEV.	MIN	MAX	SUM
RND >	3.01	.70	1.75	4.21	150.55
MAX >	3.90	.33	3.13	4.39	195.12
MIN >	2.45	.63	1.54	3.86	122.38

U-TYPES FREQUENCY (PERCENT)

	15	16	17	18	19	20	21	22	23	24	25	26	27	28	29	30	31	32	33	34	35	36	37	38
RND >			2	2		4	4	6	6	4	4	8	6	2	4	4	4	2	2	2	6	6	8	4
MAX >																	6	2	2	4	6		10	8
MIN >	2	4	8	12	4	4	14	2	6		8	2	4	6	2	2		2	8	4	2	2		2

	39	40	41	42	43
RND >		4	4	2	
MAX >	16	14	6	22	4
MIN >					

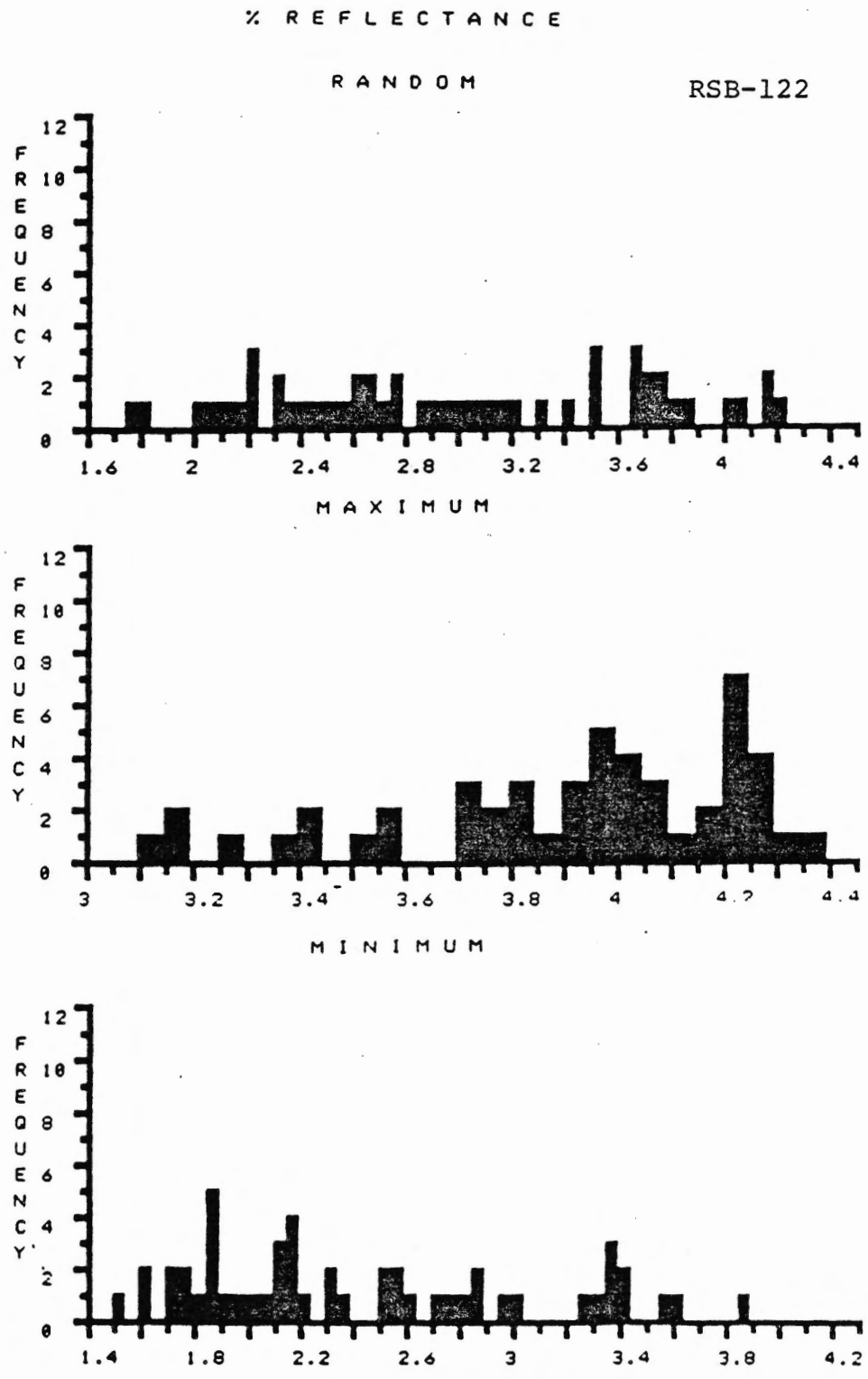
% REFLECTANCE
RANDOM
RSB-122
FREQUENCY
12
10
8
6
4
2
0
1.6
2
2.4
2.8
3.2
3.6
4
4.4
MAXIMUM
FREQUENCY
12
10
8
6
4
2
0
3
3.2
3.4
3.6
3.8
4
4.2
4.4
MINIMUM
FREQUENCY
12
10
8
6
4
2
0
1.4
1.8
2.2
2.6
3
3.4
3.8
4.2

FILE >> C0016C DESCRIPTION FOLLOWS :
DEPTH RSB-53', RAVENHURST/86, MPA, JAN-19-87

COL>	0	1	2	3	4	5	6	7	8	9
ROW		*.56	*.56	*.56	*.57	*.58	*.58	*.59	*.60	*.60
1	*.60	*.60	*.61	*.62	*.62	*.62	*.62	*.62	*.63	*.63
2	*.63	*.64	*.64	*.65	*.66	*.70	*.75	*.77	*.78	1.02
3	1.37	1.38	2.10							

	MEAN	STAND.DEV.	PTS	MIN	MAX	SUM
TOTAL >	.73	.32	32	.56	2.10	23.46
*EDIT >	.63	.06	28	.56	.78	17.59

% R E F L E C T A N C E

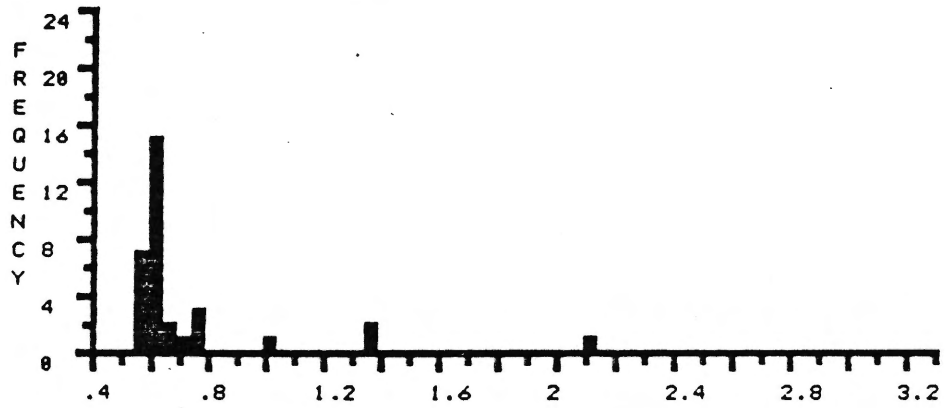

% R E F L E C T A N C E * * EDITED * *

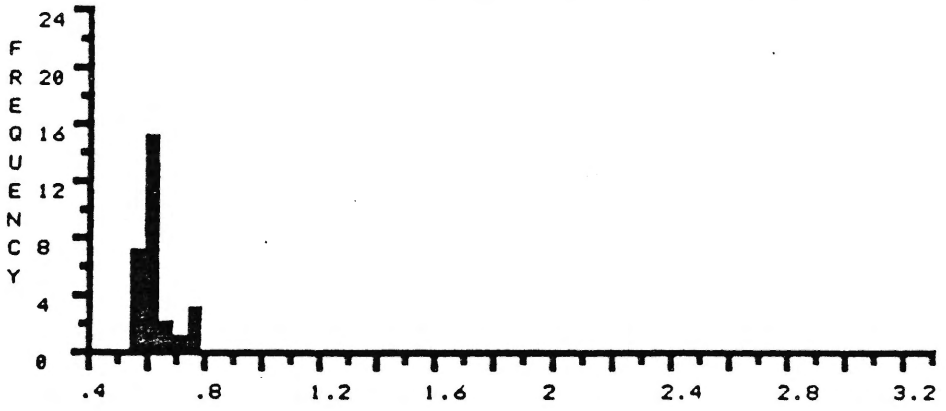

FILE >> C00168 DESCRIPTION FOLLOWS :
DEPTH RSB-25', RAVENHURST/86, MPA, JAN-19-87

COL>	0	1	2	3	4	5	6	7	8	9
ROW		*1.82	3.17	3.49						

	MEAN	STAND.DEV.	PTS	MIN	MAX	SUM
TOTAL >	2.83	.89	3	1.82	3.49	8.48
*EDIT >	1.82		1	1.82	1.82	1.82

% R E F L E C T A N C E

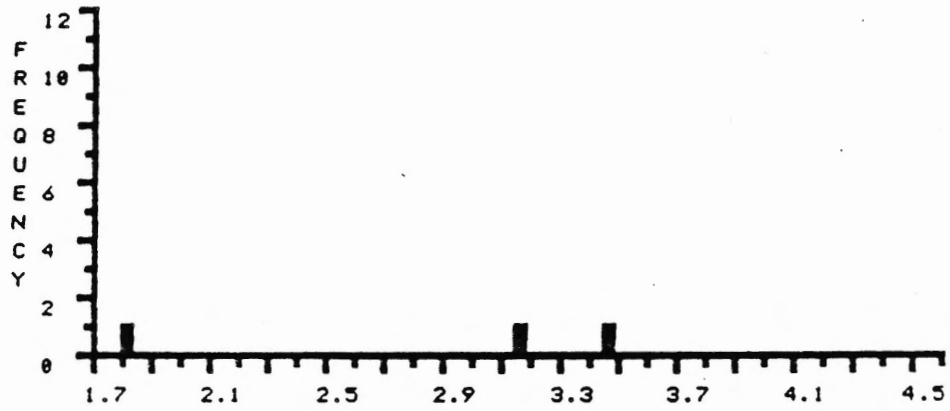

% R E F L E C T A N C E * * EDITED * *

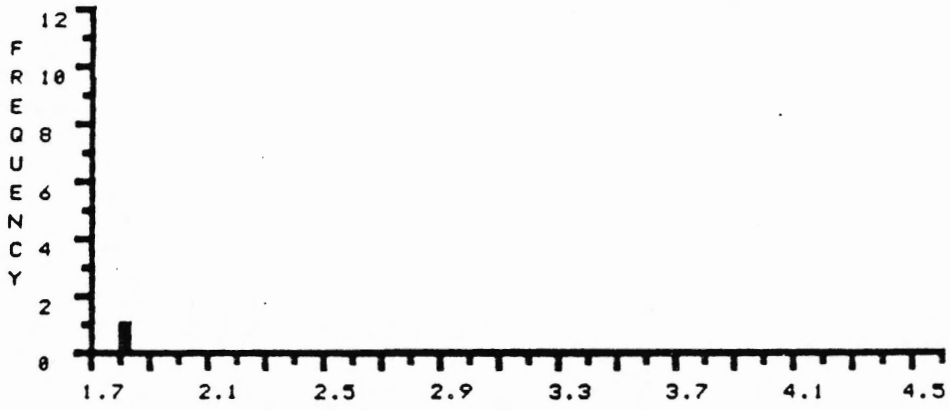

FILE >> C0017A DESCRIPTION FOLLOWS :
DEPTH RSB-117', RAVENHURST/86, MPA, JAN-20-87

COL>	0	1	2	3	4	5	6	7	8	9
ROW		.74	.75	.75	.76	.76	.76	.77	.77	.77
1	.77	.77	.78	.78	.78	.79	.79	.79	.80	.80
2	.80	.80	.80	.80	.80	.81	.81	.81	.82	.82
3	.82	.82	.83	.83	.83	.84	.84	.84	.84	.84
4	.84	.84	.85	.85	.86	.86	.86	.86	.88	.88

	MEAN	STAND.DEV.	PTS	MIN	MAX	SUM
TOTAL >	.81	.04	49	.74	.88	39.66

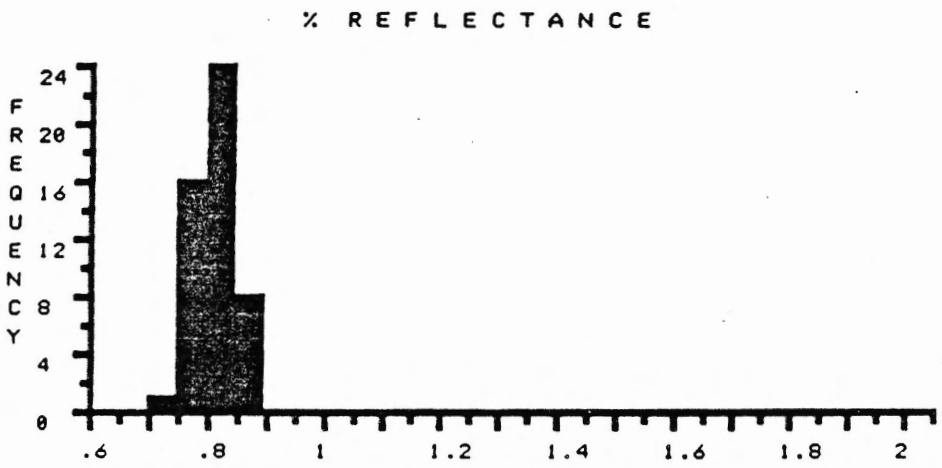

FILE >> C0017C DESCRIPTION FOLLOWS :
DEPTH RSB-124', RAVENHURST/86, MPA, JAN-20-87

COL>	0	1	2	3	4	5	6	7	8	9
ROW		*.32	*.32	*.33	*.33	*.35	*.35	*.36	*.36	*.37
1	*.37	*.37	*.38	*.38	*.39	*.39	*.39	*.39	*.39	*.39
2	*.40	*.40	*.41	*.41	*.41	*.42	*.42	*.43	*.44	*.51
3	*.54	.91								

	MEAN	STAND.DEV.	PTS	MIN	MAX	SUM
TOTAL >	.41	.10	31	.32	.91	12.63
*EDIT >	.39	.05	30	.32	.54	11.72

% REFLECTANCE

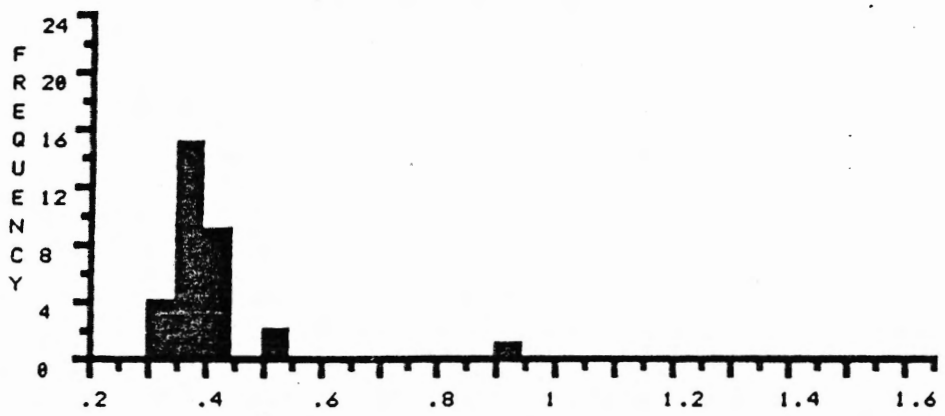

% REFLECTANCE * * EDITED * *

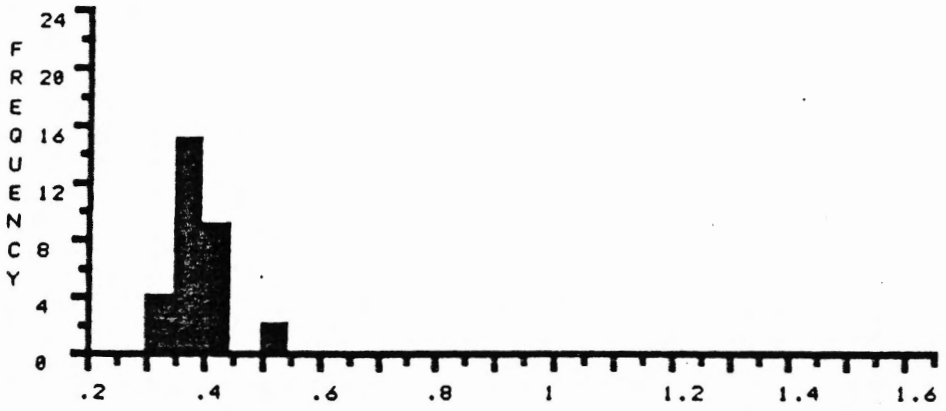

FILE >> C0010B DESCRIPTION FOLLOWS :
DEPTH RSB-87', RAVENHURST/85, MIKE AVERY, DEC-10-85

COL>	0	1	2	3	4	5	6	7	8	9
ROW		.8	.81	.82	.83	.86	.87	.88	.88	.89
1	.89	.9	.91	.91	.92	.93	.93	.93	.93	.93
2	.93	.94	.94	.95	.95	.98	.99	.99	.99	.99
3	1	1	1.01	1.02	1.02	1.02	1.02	1.02	1.04	1.05
4	1.05	1.05	1.05	1.06	1.07	1.08	1.09	1.1	1.13	1.13
5	1.13	1.16	1.17	1.19						

	SUM	NUMBER	MIN	MAX	MEAN	STAND.DEV.
TOTAL >	52.13	53	.8	1.19	.98	.1

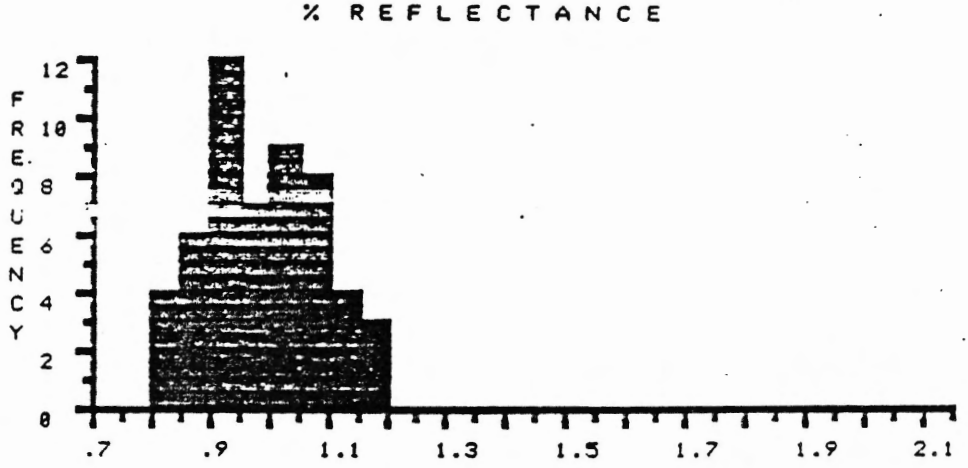

FILE >> C0012A DESCRIPTION FOLLOWS :
DEPTH RSB-89', RAVENHURST/85, MIKE AVERY, DEC-13-85

COL>	0	1	2	3	4	5	6	7	8	9
ROW		*.71	*.75	*.76	*.76	*.8	*.8	*.82	*.82	*.82
1	*.83	*.84	*.84	*.84	*.88	*.91	*.91	*.92	*.93	*.93
2	*.93	*.94	*.95	*.95	*.95	*.95	*.96	*.96	*.96	*.97
3	*.97	*.98	*.98	*.99	*1	*1.01	*1.01	*1.02	*1.03	*1.03
4	*1.03	*1.03	*1.04	*1.06	*1.06	*1.07	*1.07	*1.08	*1.08	*1.09
5	*1.09	*1.11	*1.11	*1.11	*1.13	*1.14	*1.15	*1.16	*1.18	*1.18
6	*1.2	*1.21	1.29	1.3	1.45					

	SUM	NUMBER	MIN	MAX	MEAN	STAND.DEV.
TOTAL >	63.83	64	.71	1.45	1	.14
*EDIT >	59.79	61	.71	1.21	.98	.12

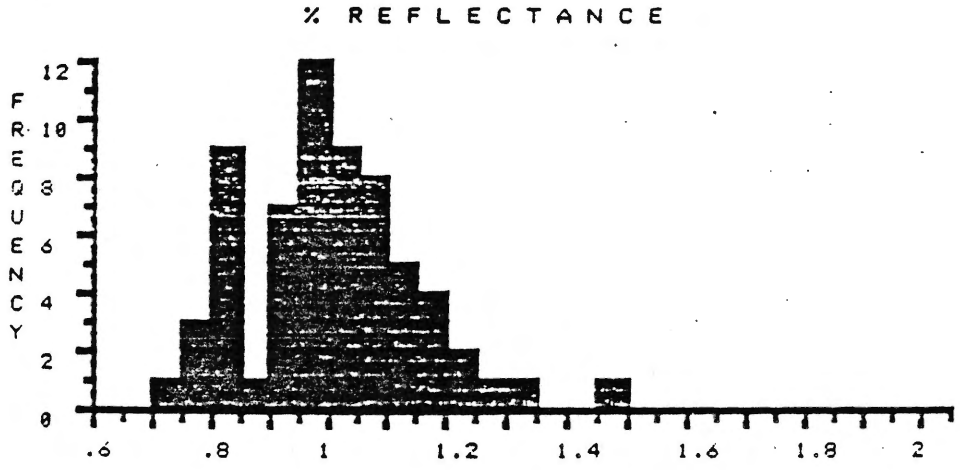

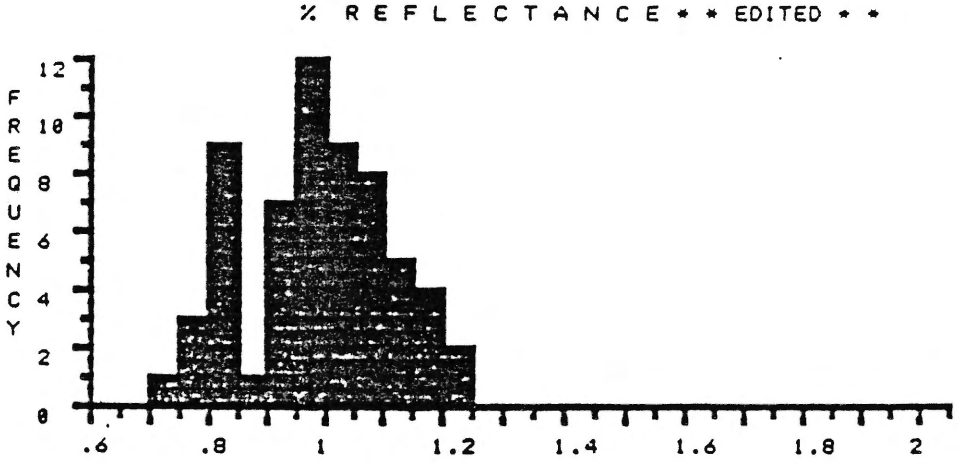

FILE >> C0010C DESCRIPTION FOLLOWS :
DEPTH RSB-90', RAVENHURST/85, MIKE AVERY, DEC-10-85

COL>	0	1	2	3	4	5	6	7	8	9
ROW		.7	.74	.75	.78	.79	.8	.8	.8	.8
1	.81	.81	.81	.81	.83	.83	.84	.84	.84	.84
2	.85	.85	.85	.85	.85	.85	.86	.86	.86	.87
3	.88	.88	.9	.9	.9	.91	.91	.91	.91	.92
4	.92	.92	.93	.93	.93	.93	.93	.93	.94	.94
5	.94	.94	.94	.95	.95	.95	.95	.95	.96	.96
6	.96	.97	.97	.97	.97	.97	.98	.98	.98	.98
7	.98	.98	.99	.99	.99	.99	.99	1	1	1.01
8	1.01	1.02	1.02	1.02	1.03	1.03	1.04			

	SUM	NUMBER	MIN	MAX	MEAN	STAND.DEV.
TOTAL >	78.4	86	.7	1.04	.91	.08

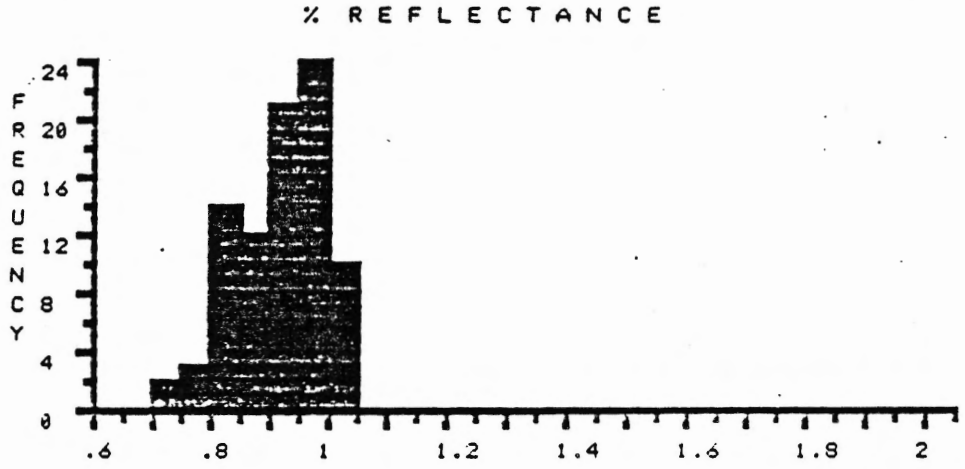

FILE >> C0012B DESCRIPTION FOLLOWS :
DEPTH RS8-91', RAVENHURST/85, MIKE AVERY, DEC-13-85

COL>	0	1	2	3	4	5	6	7	8	9
ROW		.66	.7	.7	.7	.73	.74	.74	.75	.75
1	.75	.76	.77	.77	.77	.77	.78	.78	.78	.78
2	.79	.79	.79	.79	.79	.8	.8	.8	.81	.81
3	.81	.81	.81	.81	.82	.82	.82	.82	.83	.83
4	.83	.84	.86	.86	.87	.87	.87	.88	.88	.88
5	.88	.89	.89	.89	.89	.9	.9	.9	.91	.91
6	.92	.93	.93	.93	.93	.93	.93	.93	.94	.95
7	.95	.95	.95	.96	.97	.97	.97	.97	.98	.98
8	.98	.98	.99	1	1	1.01	1.01	1.01	1.03	

	SUM	NUMBER	MIN	MAX	MEAN	STAND.DEV.
TOTAL >	76.14	88	.66	1.03	.87	.09

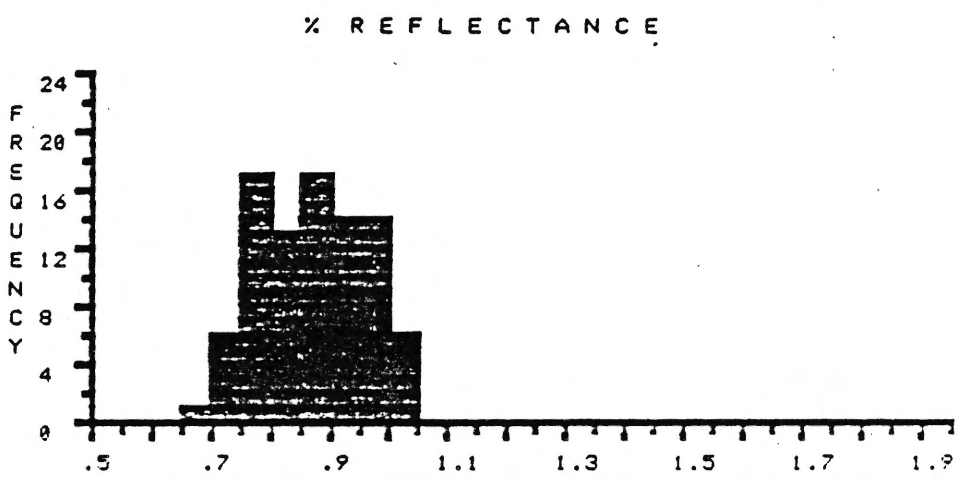

FILE >> C0012C DESCRIPTION FOLLOWS :
DEPTH HH2-1', RAVENHURST/85, MIKE AVERY, DEC-16-85

COL>	0	1	2	3	4	5	6	7	8	9
ROW		.35	.37	.8	*.89	*.9	*.9	*.93	*.93	*.95
1	*.95	*.96	*.98	*.98	*.99	*1	*1	*1	*1	*1.01
2	*1.02	*1.02	*1.03	*1.03	*1.03	*1.04	*1.05	*1.06	*1.09	*1.13
3	*1.13	*1.14	*1.15	*1.16	*1.16	*1.18	*1.18	*1.19	*1.19	*1.19
4	*1.21	*1.21	*1.22	*1.25	1.3	1.31	1.32	1.33	1.39	1.45
5	1.51									

	SUM	NUMBER	MIN	MAX	MEAN	STAND.DEV.
TOTAL >	53.56	50	.35	1.51	1.07	.21
*EDIT >	42.43	40	.89	1.25	1.06	.1

% R E F L E C T A N C E

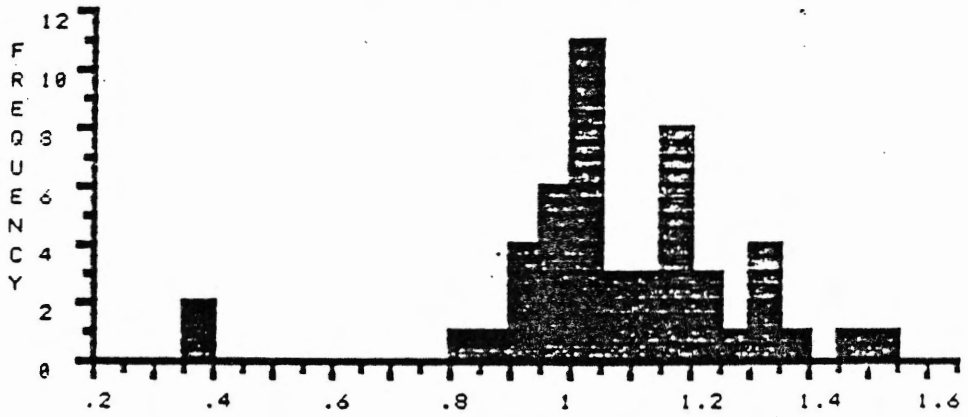

% R E F L E C T A N C E * * EDITED * *

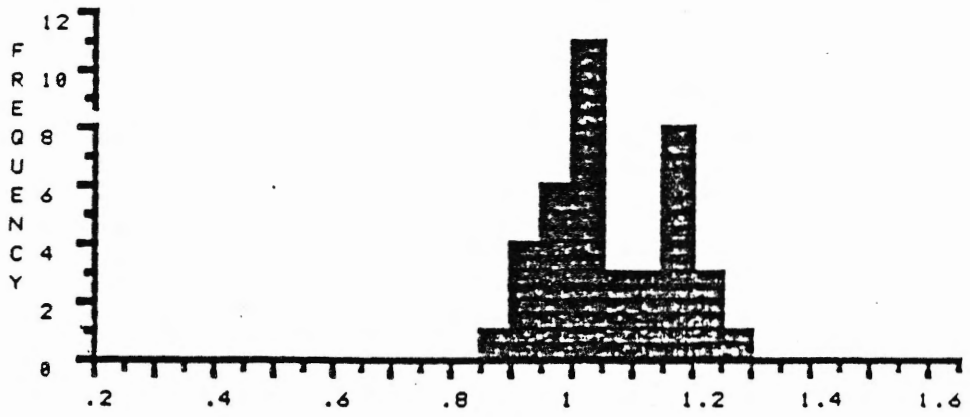

FILE >> C0010A DESCRIPTION FOLLOWS :
DEPTH BP6-820', RAVENHURST/85, MIKE AVERY, DEC-10-85

COL>	0	1	2	3	4	5	6	7	8	9
ROW		.84	.89	.92	.94	.94	.95	.95	.97	.99
1	1	1.1	1.12	1.13	1.13	1.14	1.14	1.15	1.17	1.17
2	1.17	1.18	1.19	1.2	1.23	1.24	1.24	1.26	1.27	1.27
3	1.28	1.3	1.3	1.31	1.31	1.31	1.32	1.33	1.34	1.37
4	1.38	1.38	1.39	1.39	1.39	1.4	1.41	1.42	1.44	1.45
5	1.45	1.51	1.51	1.52	1.54	1.56	1.57			

	SUM	NUMBER	MIN	MAX	MEAN	STAND.DEV.
TOTAL >	69.79	56	.84	1.57	1.25	.19

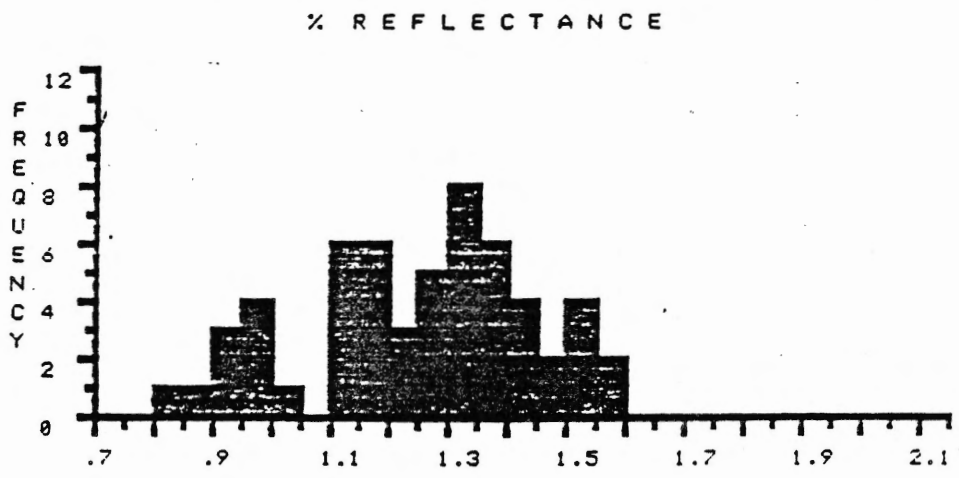

FILE >> C0011C DESCRIPTION FOLLOWS :
DEPTH BP6-797', RAVENHURST/85, MIKE AVERY, DEC-10-85

COL>	0	1	2	3	4	5	6	7	8	9
ROW		*.81	*.85	*.87	*.89	*.89	*.93	*.93	*.94	*.94
1	*.95	*.98	*.98	*1.02	*1.02	*1.03	*1.04	*1.05	*1.07	*1.08
2	*1.08	*1.08	*1.08	*1.11	*1.12	*1.13	*1.14	*1.14	*1.15	*1.16
3	*1.17	*1.17	*1.18	*1.21	*1.21	*1.21	*1.21	*1.24	*1.25	*1.25
4	*1.25	*1.27	*1.27	*1.27	*1.27	*1.27	*1.27	*1.28	*1.28	*1.29
5	*1.3	*1.3	*1.3	*1.31	*1.31	*1.31	*1.32	*1.33	*1.34	*1.34
6	*1.34	*1.34	*1.35	*1.35	*1.35	*1.36	*1.37	*1.37	*1.39	*1.39
7	*1.4	*1.41	*1.41	*1.42	*1.43	*1.44	*1.48	*1.48	*1.51	*1.54
8	1.6	1.63	1.69	1.82						

	SUM	NUMBER	MIN	MAX	MEAN	STAND.DEV.
TOTAL >	102.31	83	.81	1.82	1.23	.2
*EDIT >	95.57	79	.81	1.54	1.21	.17

% R E F L E C T A N C E

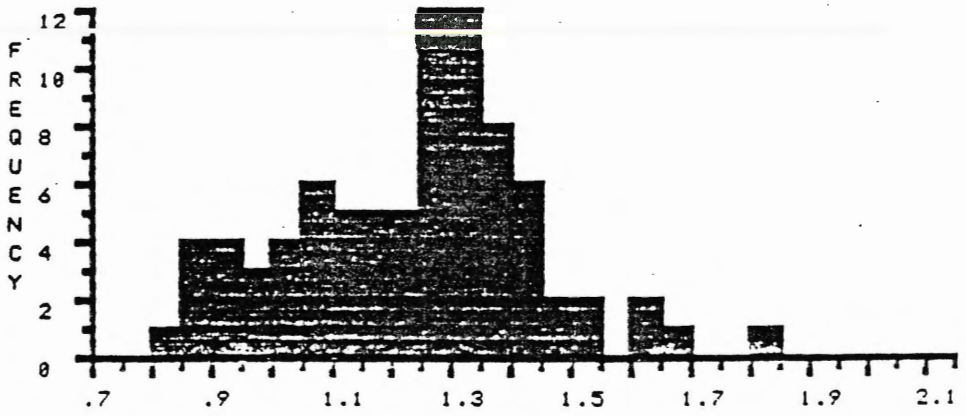

% R E F L E C T A N C E * * EDITED * *

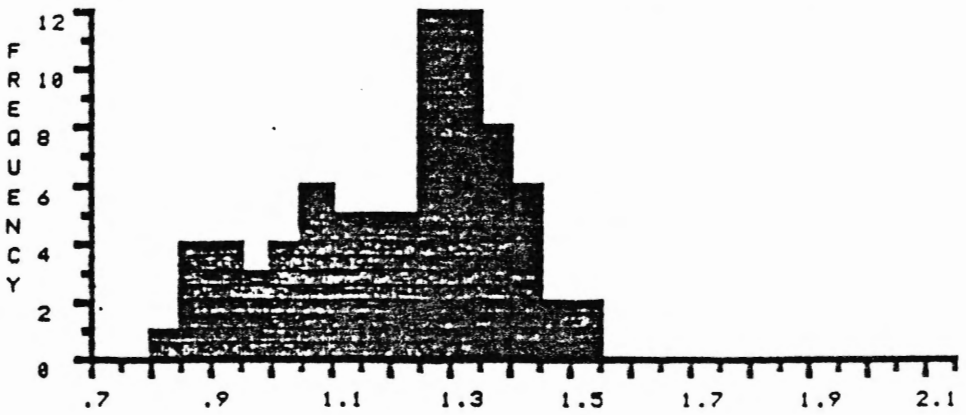

FILE >> C0011B DESCRIPTION FOLLOWS :
DEPTH BP6-624', RAVENHURST/85, MIKE AVERY, DEC-10-85

COL>	0	1	2	3	4	5	6	7	8	9
ROW		.81	*.87	*.88	*.89	*.9	*.9	*.9	*.9	*.91
1	*.91	*.93	*.93	*.94	*.96	*.97	*.97	*.97	*.98	*.98
2	*1	*1.02	*1.02	*1.03	*1.04	*1.04	*1.05	*1.05	*1.05	*1.06
3	*1.06	*1.06	*1.07	*1.07	*1.08	*1.08	*1.09	*1.1	*1.1	*1.1
4	*1.1	*1.1	*1.11	*1.11	*1.11	*1.12	*1.12	*1.12	*1.12	*1.13
5	*1.13	*1.13	*1.13	*1.14	*1.14	*1.14	*1.14	*1.14	*1.14	*1.15
6	*1.15	*1.15	*1.15	*1.15	*1.15	*1.16	*1.16	*1.16	*1.16	*1.16
7	*1.17	*1.17	*1.17	*1.17	*1.17	*1.18	*1.18	*1.18	*1.18	*1.18
8	*1.18	*1.19	*1.2	*1.2	*1.2	*1.2	*1.2	*1.2	*1.2	*1.2
9	*1.2	*1.21	*1.22	*1.22	*1.24	*1.24	*1.28	1.52	1.55	

	SUM	NUMBER	MIN	MAX	MEAN	STAND.DEV.
TOTAL >	108.14	98	.81	1.55	1.1	.12
*EDIT >	104.26	95	.87	1.28	1.1	.1

% REFLECTANCE

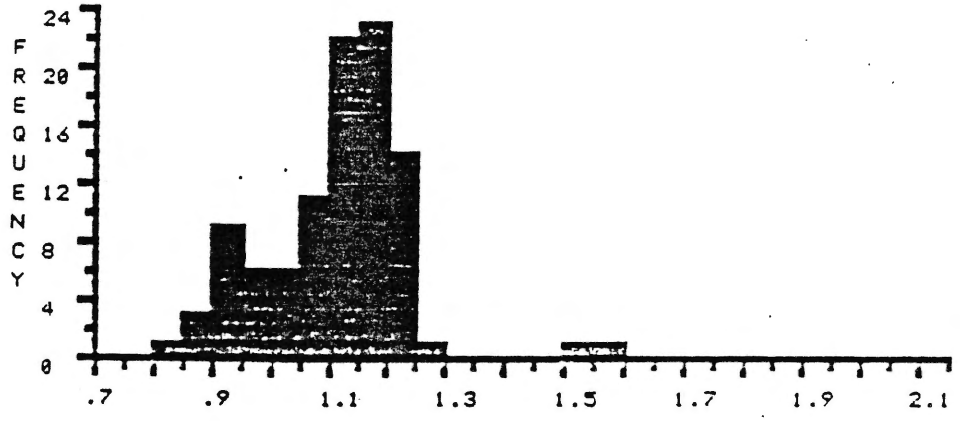

% REFLECTANCE * * EDITED * *

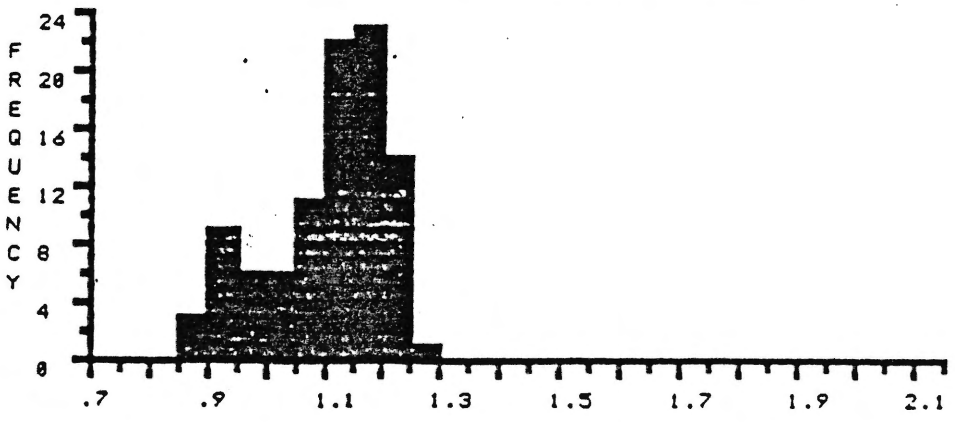

FILE >> C0011A DESCRIPTION FOLLOWS :
DEPTH BP6-500', RAVENHURST/85, MIKE AVERY, DEC-10-85

COL>	0	1	2	3	4	5	6	7	8	9
ROW		.85	.92	.97	.97	1	1.01	1.03	1.03	1.09
1	1.09	1.11	1.11	1.11	1.11	1.13	1.13	1.14	1.15	1.16
2	1.16	1.17	1.2	1.21	1.21	1.21	1.23	1.23	1.24	1.24
3	1.25	1.26	1.26	1.26	1.26	1.26	1.27	1.28	1.28	1.28
4	1.28	1.28	1.3	1.3	1.3	1.31	1.31	1.31	1.32	1.32
5	1.32	1.33	1.34	1.34	1.35	1.35	1.36	1.36	1.37	1.37
6	1.39	1.41	1.43	1.55						

	SUM	NUMBER	MIN	MAX	MEAN	STAND.DEV.
TOTAL >	77.17	63	.85	1.55	1.23	.13

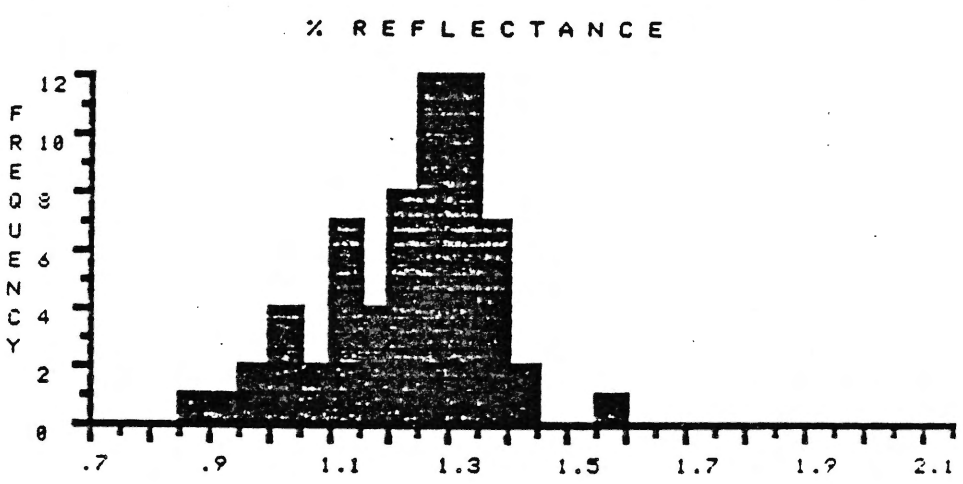

FILE >> C0013A DESCRIPTION FOLLOWS :
DEPTH SB1-2914', RAVENHURST/86, MPA, DEC-13-86

COL>	0	1	2	3	4	5	6	7	8	9
ROW		1.62	1.65	1.66	1.66	1.68	1.74	1.78	1.82	1.83
1	1.84	1.85	1.86	1.86	1.92	1.95	1.99	2.01	2.02	2.03
2	2.06	2.08	2.08	2.09	2.09	2.10	2.10	2.12	2.13	2.15
3	2.15	2.22	2.24	2.26	2.27	2.29	2.31	2.32	2.32	2.33
4	2.39	2.39	2.40	2.40	2.44	2.44	2.45	2.46	2.47	2.47
5	2.47	2.50	2.51	2.52	2.52	2.54	2.55	2.55	2.56	2.57
6	2.59	2.62	2.63	2.63	2.64	2.64	2.66	2.67	2.68	2.69
7	2.71	2.72	2.72	2.73	2.74	2.74	2.75	2.76	2.78	2.78
8	2.79	2.79	2.80	2.80	2.82	2.82	2.85	2.86	2.87	2.87
9	2.87	2.89	2.91	2.91	2.91	2.93	2.95	2.99	3.07	3.08

	MEAN	STAND.DEV.	PTS	MIN	MAX	SUM
TOTAL >	2.42	.38	99	1.62	3.08	239.74

% R E F L E C T A N C E

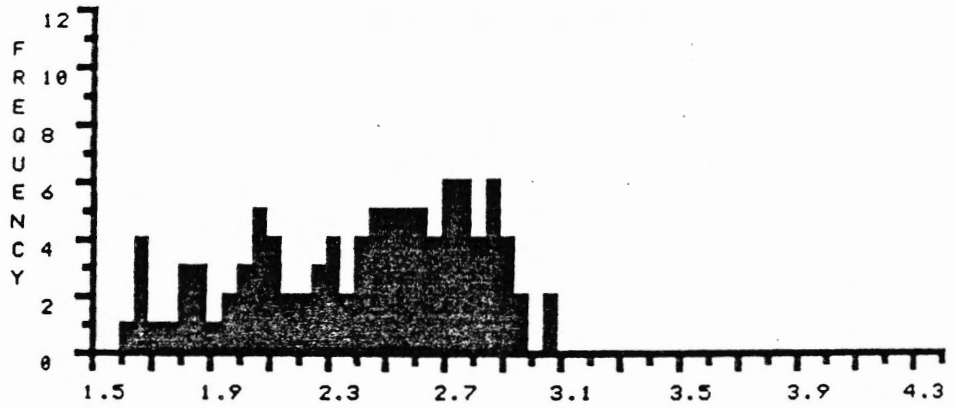

FILE >> C00138 DESCRIPTION FOLLOWS :
DEPTH SB1-2917', RAVENHURST/86, MPA, DEC-13-86

COL>	0	1	2	3	4	5	6	7	8	9
ROW		1.92	1.99	1.99	2.01	2.02	2.04	2.08	2.08	2.12
1	2.17	2.19	2.20	2.22	2.28	2.29	2.32	2.33	2.34	2.34
2	2.35	2.35	2.36	2.36	2.40	2.40	2.40	2.40	2.40	2.42
3	2.43	2.44	2.44	2.45	2.45	2.45	2.46	2.46	2.48	2.49
4	2.51	2.53	2.54	2.54	2.56	2.57	2.57	2.58	2.58	2.59
5	2.59	2.59	2.60	2.62	2.63	2.63	2.64	2.64	2.66	2.68
6	2.68	2.68	2.69	2.70	2.73	2.77	2.77	2.77	2.79	2.80
7	2.80	2.81	2.81	2.82	2.82	2.83	2.83	2.84	2.85	2.90
8	2.91	2.91	2.91	2.92	2.95	2.95	2.95	2.95	2.96	2.97
9	2.98	2.98	3.02	3.04	3.04	3.06	3.09	3.09	3.14	3.16

	MEAN	STAND.DEV.	PTS	MIN	MAX	SUM
TOTAL >	2.59	.30	99	1.92	3.14	256.84

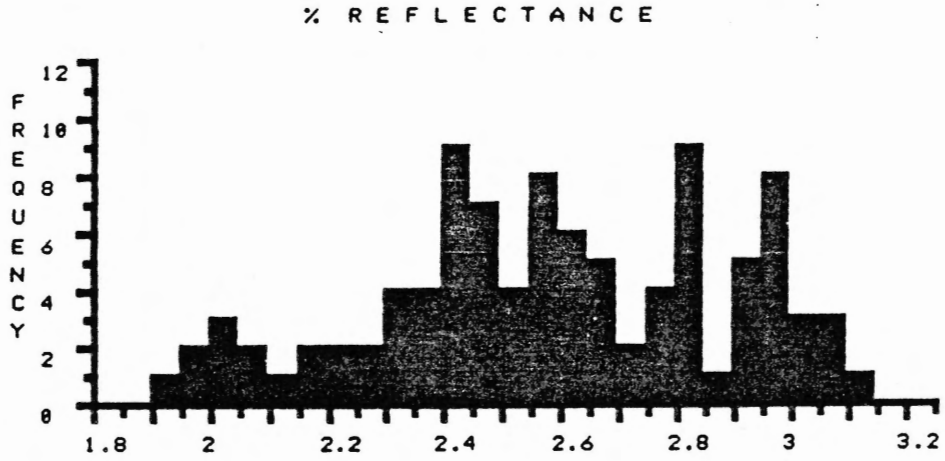

FILE >> C0013C DESCRIPTION FOLLOWS :
DEPTH SB1-2919', RAVENHURST/86, MPA, DEC-13-86

COL>	0	1	2	3	4	5	6	7	8	9
ROW		.85	*1.83	*1.86	*1.93	*1.98	*2.00	*2.00	*2.02	*2.07
1	*2.11	*2.13	*2.13	*2.17	*2.19	*2.19	*2.20	*2.22	*2.24	*2.25
2	*2.25	*2.26	*2.27	*2.31	*2.32	*2.32	*2.32	*2.33	*2.34	*2.39
3	*2.39	*2.40	*2.42	*2.43	*2.43	*2.44	*2.44	*2.45	*2.46	*2.46
4	*2.47	*2.47	*2.48	*2.49	*2.49	*2.50	*2.51	*2.51	*2.51	*2.53
5	*2.54	*2.54	*2.55	*2.55	*2.55	*2.56	*2.56	*2.57	*2.57	*2.58
6	*2.58	*2.58	*2.59	*2.60	*2.60	*2.60	*2.62	*2.62	*2.63	*2.64
7	*2.64	*2.65	*2.65	*2.65	*2.66	*2.68	*2.70	*2.70	*2.71	*2.71
8	*2.77	*2.77	*2.81	*2.82	*2.82	*2.87	*2.88	*2.88	*2.89	*2.91
9	*2.92	*2.94	*3.03	*3.03	*3.04	*3.10	*3.12	*3.13	*3.24	*3.40

	MEAN	STAND.DEV.	PTS	MIN	MAX	SUM
TOTAL >	2.51	.35	99	.85	3.40	248.51
*EDIT >	2.53	.31	98	1.83	3.40	247.66

% REFLECTANCE

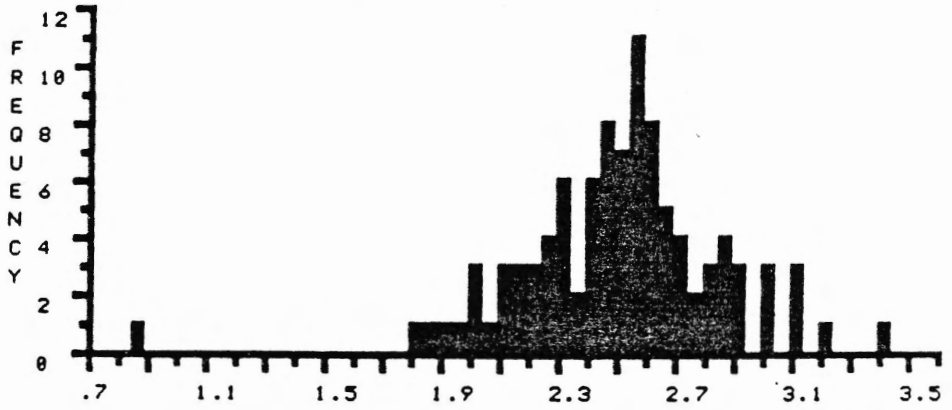

% REFLECTANCE * * EDITED * *

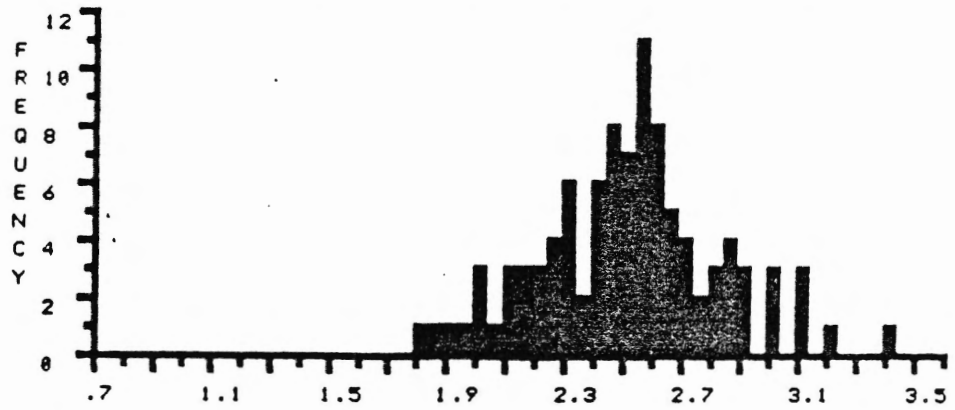

FILE >> C0014A DESCRIPTION FOLLOWS :
DEPTH SB1-2926', RAVENHURST/86, MPA, DEC-13-86

COL>	0	1	2	3	4	5	6	7	8	9
ROW		1.88	1.98	2.15	2.26	2.31	2.33	2.33	2.35	2.36
1	2.56	2.60	2.60	2.67	2.72	2.76	2.77			

	MEAN	STAND.DEV.	PTS	MIN	MAX	SUM
TOTAL >	2.41	.27	16	1.88	2.77	38.63

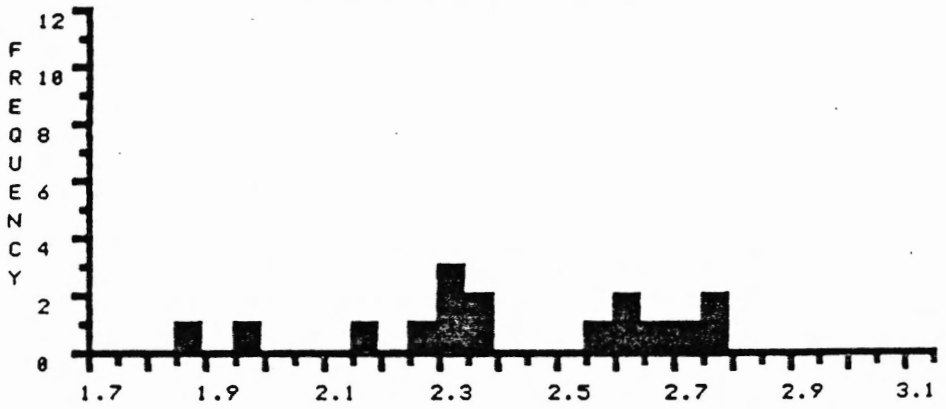

APPENDIX B

OXYGEN AND CARBON ISOTOPIC COMPOSITIONS

Table B.1 illustrates the effects of both grainsize and reaction time on the measured oxygen and carbon isotopic compositions of mixed dolomite/calcite and calcite samples. Some samples of unrestricted grainsize, that appeared to be a mix of calcite and dolomite were reacted with 100% phosphoric acid for two different time lengths at a temperature of 50°C. A short reaction time of 5 minutes was used to obtain a CO_2 gas approaching the calcite isotopic composition. The CO_2 gas evolved during 5 minutes to 2.5 hours after the start of the reaction was thought to approach the dolomite isotopic composition. Some samples were then sieved and analyzed again (twice) after 5 minute and 20 minute reaction times. The results of this study were compared to X-ray diffraction (XRD) determinations of the relative amounts of dolomite and calcite present. The method of Hutchison (1974) was used to determine the % dolomite present in the sample.

The results (Table B1) indicate that there was a significant effect (up to 6.5 o/oo difference) depending on reaction time and grainsize used. A very short reaction time of 5 minutes appears to result in a fractionation of the lighter oxygen and carbon isotopes into the CO_2 gas, even for pure calcite samples. For mixed samples it appears that even for restricted grainsize a small amount of CO_2 gas from the dolomite is being produced during a 20 minute reaction period. However in general, for samples containing significant (>50%) amounts of calcite, there is little contamination (<1 o/oo) from dolomite.

The oxygen and carbon isotopic compositions of clean calcite at the Gays River deposit (Tables B.2 and B.3) were measured using unrestricted grainsize reacted with 100% phosphoric acid for 15 or 20 minutes in the vacuum line at 50°C. Samples that appeared to be a contaminated with host rock dolomite were cleaned by handpicking, crushed, sieved to 45 to 150 um and washed in distilled water (then let air dry), before being reacted with the phosphoric acid for 15 to 20 minutes. These results are also part of Tables B.2 and B.3.

Table B1. Effect of preparation method on measured oxygen and carbon isotopic compositions.

Sample No.	Unrestricted Grainsize						Restricted Grainsize (45-150 μm)				XRD	Description
	0-20 min		0-5 min		5min - 2.5h		0-5 min		0-20 min		%Dolo	
	$\delta^{13}C$	$\delta^{18}O$	$\delta^{13}C$	$\delta^{18}O$	$\delta^{13}C$	$\delta^{18}O$	$\delta^{13}C$	$\delta^{18}O$	$\delta^{13}C$	$\delta^{18}C$		
RGR 15	-.2	24.39					.67	22.64	1.13	23.88		Dolostone
RGR 22b	-.77	18.95					-1.04	17.93			43%	Dolo. w calcite v.
RGR 29	.47	16.39	.06	14.18	.87	20.18			.36	15.12	46%	Unmin. dolostone
RGR 43	2.15	18.02	1.83	16.36	2.58	23.1			2.26	17.38	66%	Dolo. w v.f. calcite
RGR 75	2.23	19.76	2.14	19.74	2.43	20.4					0%	V.f. calcite
RGR 105	-.01	23.36					-1.11	19.13	-.18	22.07		Dolostone
RGR 112							- .16	18.03	-.07	18.27		V.f. calcite
RGR 120							- .15	17.31	-.01	17.15		Small calcite veinlet in dolostone
RGR 125							1.06	20.67	1.17	20.85		Min. calcite v. in dolo.

TABLE B.2 Oxygen and carbon isotopic composition of calcite at the Gays River deposit.

Sample Number	Coord.	Composition	Description	Mineral $\delta^{18}O$‰	Mineral $\delta^{13}C$‰
RGR-03	8774.2 N 8014.8 E	Unmin. calcite	V. calcite in dolo.	14.14	-5.15
RGR-07a	8647.8 N 8240.8 E	Unmin. calcite	V. calcite in dolo.	20.00	-4.88
RGR-16a	8558.3 N 8405.1 E	Unmin. calcite	Vf. calcite in dolo.	18.33	-2.17
RGR-17	8558.3 N 8405.1 E	Unmin. calcite	V. calcite in b.b.	16.23	-2.28
RGR-22a	8142.5 N 8608.8 E	Unmin. calcite	V. calcite in dolo.	18.56	-2.88
RGR-27	7428.8 N 9094.5 E	Min. calcite	V. calcite in b.b.	13.39	-0.11
RGR-30	7324.9 N 9156.2 E	P.O. calcite	V. calcite in b.b.	23.62	-1.53
RGR-31	7324.9 N 9156.2 E	P.O. calcite	V. calcite in b.b.	24.37	-1.21
RGR-32	7324.9 N 9156.2 E	Min. calcite	Recryst. dolo.	13.94	+1.38
RGR-33	7324.9 N 9156.2 E	Min. calcite	Recryst. dolo.	14.07	+1.59
RGR-34	7272.7 N 9184.3 E	Min. calcite	V. calcite in b.b.	13.43	+1.57
RGR-35	7272.7 N 9184.3 E	Min. calcite	Recryst. dolo.	14.16	+1.79
RGR-37a	7272.7 N 9184.3 E	Unmin. calcite	Vf. calcite in dolo.	13.03	+2.42
RGR-40	7216.8 N 9218.5 E	Unmin. calcite	Recryst. dolo.	15.46	+3.15
RGR-41	7273.6 N 9047.5 E	Min. calcite	V. calcite in Meguma basement	14.82	-0.54
RGR-42	7273.6 N 9047.5 E	Min. calcite	V. calcite in b.b.	12.81	+1.00
RGR-44	7211.6 N 8939.6 E	Min. calcite	V. calcite in b.b.	12.53	+1.53

RGR-53a	7027.2 N 8683.4 E	Unmin. calcite	Vf. calcite dolo.	18.80	+1.67
RGR-57	6964.2 N 8520.4 E	Min. calcite	V. calcite in b.b.	14.45	-0.45
RGR-68	6815.6 N 8262.1 E	Min. calcite	V. calcite in b.b.	14.29	+2.09
107-2	7277.0 N 8784.0 E	Min. calcite	V. calcite in Meguma basement	23.69	-5.85
RGR-69	7378.1 N 9124.0 E	Min. calcite	Vf. calcite in dolo.	14.64	+0.47
RGR-71	6883.7 N 8395.2 E	Unmin. calcite	V. calcite in dolo.	24.54	-1.02
RGR-75	6688.1 N 8676.0 E	Unmin. calcite	Vf. calcite in dolo.	19.76	+2.23
RGR-76	6688.1 N 8676.0 E	Unmin. calcite	Calcite in b.b.	20.10	+2.05
RGR-77	6745.8 N 8755.9 E	Unmin. calcite	Vf. calcite in dolo.	15.54	+1.88
RGR-78	6745.8 N 8755.9 E	Unmin. calcite	V. calcite in b.b.	23.51	-1.25
RGR-79	6801.8 N 8869.5 E	P.O. calcite	V. calcite in dolo.	24.34	-1.27
RGR-80	6801.8 N 8869.5 E	P.O. calcite	V. calcite in b.b.	24.77	-0.82
RGR-82	6834.8 N 8920.1 E	Unmin. calcite	V. calcite in dolo.	16.73	+2.86
RGR-83	6863.7 N 8975.8 E	Min. calcite	V. calcite in dolo.	14.91	+2.47
RGR-84	6863.7 N 8975.8 E	Min. calcite	Vf. calcite in dolo.	18.55	+2.71
RGR-86	6905.0 N 9059.8 E	P.O. calcite	Vf. calcite in dolo.	22.35	-2.95
RGR-87	7365.3 N 9277.5 E	Min. calcite	Vf. calcite in dolo.	14.24	+0.69
RGR-88	7365.3 N 9277.5 E	Min. calcite	Vf. calcite in dolo.	12.84	+1.12
RGR-89	7440.6 N 9365.2 E	Unmin. calcite	Vf. calcite in b.b.	12.73	+2.71
RGR-90	7440.6 N 9365.2 E	Min. calcite	Vf. calcite in dolo.	13.04	+2.45

RGR-91	7515.7 N 9493.5 E	Unmin. calcite	Vf. calcite in b.b.	14.61	+2.59
RGR-92	7577.2 N 9639.0 E	Min. calcite	Vf. calcite in b.b.	13.32	+2.72
RGR-93	7577.2 N 9639.0 E	Min. calcite	V. calcite in in b.b.	12.96	+3.11
RGR-94	7577.2 N 9639.0 E	Min. calcite	Vf. calcite in dolo.	13.14	+2.46
RGR-96	7648.8 N 9793.2 E	P.O. calcite	V. calcite in Meguma basement	22.08	-5.11
RGR-97	7648.8 N 9793.2 E	Min. calcite	Vf. calcite in dolo.	13.29	+1.77
RGR-98	7708.2 N 9954.0 E	Min. calcite	V. calcite in b.b.	13.40	+0.72
RGR-99	7708.2 N 9954.0 E	Min. calcite	Vf. calcite in dolo.	13.45	+2.16
RGR-100	7756.2 N 10135.4 E	Min. calcite	V. calcite in b.b.	13.33	+1.07
RGR-101	7756.2 N 10135.4 E	Unmin. calcite	Recryst. dolo.	15.11	+0.57
RGR-102	7812.9 N 10241.0 E	Min. calcite	V. calcite in b.b.	16.11	-1.86
RGR-103	7910.0 N 10484.0 E	Unmin. calcite	V. calcite in dolo.	17.80	-3.83
RGR-104	7910.0 N 10484.0 E	Unmin. calcite	Calcite in b.b.	23.90	-2.93
RGR-109	7937.0 N 10383.0 E	Min. calcite	V. calcite in dolo.	26.72	-8.48
RGR-112	6777.9 N 9546.3 E	P.O. calcite	Vf. calcite in dolo.	18.27	-0.07
RGR-114	6684.9 N 9588.8 E	P.O. calcite	V. calcite in dolo.	23.36	-0.06
RGR-115	6717.2 N 9453.9 E	P.O. calcite	V. calcite in dolo.	24.07	+0.14
RGR-118	6620.8 N 9482.5 E	Unmin. calcite	V. calcite in dolo.	22.82	+0.52
RGR-119	6824.6 N 9375.2 E	Unmin. calcite	V. calcite in dolo.	15.85	-0.85
RGR-120	6824.6 N 9375.2 E	Unmin. calcite	V. calcite in dolo.	17.15	-0.01

RGR-122	6322.1 N 8615.7 E	P.O. calcite	V. calcite in dolo.	24.01	-3.43
RGR-123	6322.1 N 8615.7 E	P.O. calcite	V. calcite in b.b.	21.77	-5.39
RGR-124	6202.0 N 8682.5 E	Unmin. calcite	V. calcite in dolo.	19.37	+2.50
RGR-125	6202.0 N 8682.5 E	Min. calcite	V. calcite in dolo.	20.85	+1.17
RGR-129	6085.8 N 8749.2 E	Unmin. calcite	Vf. calcite in dolo.	15.11	+1.02
RGR-131	5979.8 N 8811.0 E	Unmin. calcite	V. calcite in dolo.	20.23	+0.70
RGR-133	5592.5 N 9039.8 E	Unmin. calcite	V. calcite in b.b.	22.17	-0.13
RGR-134	5592.5 N 9039.8 E	Unmin. calcite	V. calcite in b.b.	20.48	+0.00
RGR-135	5500.0 N 9095.0 E	P.O. calcite	Vf. calcite in b.b.	23.33	-3.79
RGR-136	5500.0 N 9095.0 E	Unmin. calcite	V. calcite in b.b.	13.46	+3.08
RGR-137	5346.0 N 8894.0 E	Unmin. calcite	V. calcite in b.b.	16.97	+1.49
RGR-138	5553.0 N 8772.0 E	Unmin. calcite	V. calcite in dolo.	20.29	+2.38
RGR-139	5553.0 N 8772.0 E	Unmin. calcite	V. calcite in dolo.	16.84	+2.35
RGR-140	5237.9 N 8970.2 E	P.O. calcite	Vf. calcite in dolo.	23.08	+1.84
RGR-141	5237.9 N 8970.2 E	P.O. calcite	V. calcite in b.b.	23.85	+0.47
RGR-142	6647.9 N 8219.2 E	Min. calcite	Vf. calcite in dolo.	20.37	+2.53
RGR-143	6594.4 N 8249.3 E	Unmin. calcite	Vf. calcite in dolo.	13.94	+3.75
RGR-144	6698.2 N 8188.2 E	Min. calcite	Vf. calcite in dolo.	- 12.93	+2.88
RGR-146	6749.3 N 8156.3 E	Min. calcite	Vf. calcite in b.b.	13.62	+0.71
RGR-147	6798.4 N 8126.4 E	Min. calcite	V. calcite in dolo.	13.21	-0.85

RGR-148	6988.3 N 8359.2 E	P.O. calcite	V. calcite in b.b.	23.98	-1.07
RGR-150	6694.4 N 8536.3 E	Unmin. calcite	V. calcite in b.b.	19.10	+3.12
RGR-151	6818.9 N 8540.3 E	Min. calcite	V. calcite in b.b.	13.19	+1.1
RGR-152	7177.1 N 8399.7 E	Min. calcite	V. calcite in dolo.	13.50	-0.3
RGR-155	7072.8 N 8457.4 E	Min. calcite	V. calcite in dolo.	13.19	+0.99
RGR-156	7025.4 N 9131.4 E	Unmin. calcite	Vf. calcite in dolo.	24.28	+0.08
RGR-157	7025.4 N 9131.4 E	Min. calcite	Petroliferous vug-fill calcite in dolo.	24.32	-0.47
RGR-158	7025.4 N 9131.4 E	P.O. calcite	Petroliferous vug-fill calcite in dolo.	23.82	+0.23
RGR-159	7138.9 N 9198.9 E	Unmin. calcite	Vf. calcite in dolo.	13.93	+3.04
RGR-160	7138.9 N 9198.9 E	Unmin. calcite	Vf. calcite in dolo.	17.83	+3.05
RGR-168	6282.0 N 9464.0 E	Unmin. calcite	Vf. calcite in host carbonate	14.54	+3.21
RGR-169	6282.0 N 9464.0 E	Unmin. calcite	Vf. calcite in dolo.	24.89	+0.56
RSB-16a	7630.0 N 10560.0 E	Unmin. calcite	Vf. calcite in dolo.	19.08	+2.90

Unmin. = Unmineralized
Min. = Mineralized
Recryst. = Recrystallized
V. = Vein
Vf. = Vug-filling
O.S. = Ore-stage
P.O. = Postore
dolo. = dolomite host
b.b. = basal breccia

TABLE B.3 Oxygen and carbon isotopic compositions of calcite and carbonate at the other deposits.

Sample Number	Location	Composition	Description	Mineral $\delta^{18}O$‰	Mineral $\delta^{13}C$‰
RSB-113	1.near G.R. N-4992090 E-473120	Unmin. calcite	V. calcite	22.61	-5.58
RSB-47b	2.Southvale	Calcite	Gray lmst. host rock	26.04	-0.24
RSB-48	2.Southvale	Unmin. calcite	V. calcite in b.b.	17.78	-4.46
RSB-72	2.Southvale	Unmin. calcite	V. calcite in silty Macumber	17.38	-5.29
RSB-73	2.Southvale	Unmin. calcite	V. calcite in Macumber	24.05	-8.93
SV-01	3.Selco survey	Unmin. calcite	V. calcite in Macumber lmst.	20.95	+1.36
SV-04	3.Selco survey	Unmin. calcite	V. calcite in Green Oaks fm.	24.81	-4.71
SV-09	3.Selco survey	Calcite	Fossil. gray lmst.	25.48	-0.74
SV-10	3.Selco survey	Calcite	Fossil. gray lmst.	24.76	-5.01
RSB-70	3.Selco survey	Calcite	Lmst. breccia	21.99	-6.71
RSB-46	4.Pembroke	Min. calcite	V. calcite in fossil. lmst.	19.34	+1.32
RSB-71	4.Pembroke	Min. calcite	V. calcite in fossil. lmst.	19.05	+0.76
P-9H	4.Pembroke	Calcite	Fossil. gray lmst.	21.70 22.28	+2.24 +2.42
P-14HM	4.Pembroke	Calcite	Altered fossil. lmst	22.70 22.90	+2.65 +2.66
(P) Data from Ponsford (1983) plotted as well.					
RSB-29b	5. Smithfield	Calcite	Lmst. w. organics	23.39	-0.85
RSB-30a	5. Smithfield	Min. calcite	V. calcite in lmst.	20.18	-9.07

RSB-30b	5. Smithfield	Min. calcite	Petroliferous Vf. calcite	19.25	-9.94
RSB-31a	5. Smithfield	Unmin. calcite	V. calcite in lmst.	20.83	-0.52
RSB-31b	5. Smithfield	Calcite	Lmst. host rock	25.31	2.23
RSB-32	5. Smithfield	Postore calcite	Pink v.calcite	21.09	-1.73
RSB-33a	5. Smithfield	Unmin. calcite	Petroliferous v. calcite	21.18	-1.24
RSB-33b	5. Smithfield	Calcite	Lmst. rock	24.25	-2.45
RSB-34a	5. Smithfield	Unmin. calcite	V. Calcite	24,65	-7.04
RSB-34b	5. Smithfield	Calcite	Lmst. host rock	22.21	-1.41
RSB-118	5. Smithfield	Min. calcite	V. calcite in lmst.	18.67	-7.98
RSB-120a	5. Smithfield	Min. calcite	Dark gray early calcite	24.39	-8.55
RSB-120b	5. Smithfield	Min. calcite	V. calcite in lmst.	20.57	-10.47
RSB-121	5. Smithfield	Min. calcite	Vf. calcite	19.93	-7.12
RSB-123	5. Smithfield	Min. calcite	V. calcite in lmst.	18.78	-7.22
RSB-125	5. Smithfield	Min. calcite	V. calcite in lmst.	20.28	-8.5
(W) Data from Walker (1978) plotted as well.					
RSB-51	6. Mid. Stewiacke	Calcite	Lmst. host rock	25.0	-5.04
RSB-52	6. Mid. Stewiacke	Calcite	Lmst. breccia	24.92	-4.47
RSB-54	6. Mid. Stewiacke	Calcite w. barite	V.& Vf.calcite in host lmst.	21.39	-6.12
RSB-55	6. Mid. Stewiacke	Unmin. calcite	Green vf. calcite	24.64	-6.32
RSB-40	7. Brookfield	Calcite	Macumber lmst. near quarry	24.20	-4.91

RSB-41	7. Brookfield	Unmin. calcite	V. calcite in lmst.	24.50	-5.35
RSB-42	7. Brookfield	Unmin. calcite	V. calcite in lmst.	24.71	-4.35
RSB-64	8.Hilden	Calcite	Lmst. breccia	21.62	-3.64
RSB-65	8.Hilden	Calcite	Petroliferous Macumber lmst.	22.80	+2.73
RSB-66	8.Hilden	Calcite w. barite	V. calcite	23.67	-8.17
RSB-56	9.Black Rock	Calcite	Macumber lmst.	25.59	+1.16
RSB-57	9.Black Rock	Unmin. calcite	V. calcite in lmst.	22.13	+1.28
RSB-58	9.Black Rock	Calcite	Lmst. breccia	23.35	-0.80
RSB-59	9.Black Rock	Unmin. calcite	V. calcite in lmst.	22.63	-0.50
RSB-60	9.Black Rock	Unmin. calcite	V. calcite 2nd generation	20.48	-4.12
RSB-61	9.Black Rock	Unmin. calcite	Massive v. calcite	24.15	+3.28
EC-788	10.Walton	Unmin. calcite	Crystalline calcite	22.86	-5.78
EC-785	10.Walton	Calcite	Macumber lmst. host rock	27.32	-0.20
RSB-127	10.Walton	Unmin. calcite	Calcite w. quartz	16.79	-1.37
RSB-110	11.Nine Mile R.	Unmin. calcite	V. calcite in b.b.	21.41	-4.53
RSB-111	11.Nine Mile R.	Unmin. calcite	V. calcite in b.b.	21.71	-3.18
RSB-112	11.Nine Mile R.	Unmin. calcite	V. calcite in Meguma	19.62	-1.20
RSB-114	11.Nine Mile R.	Unmin. calcite	V. calcite in Meguma	23.12	-3.87
RSB-115a	11.Nine Mile R.	Calcite w. barite	Early v. calcite in lmst.	22.25	-10.02
RSB-115b	11.Nine Mile R.	Calcite w. barite	V. calcite in lmst.	22.21	-7.93

RSB-116	11.Nine Mile R.	Unmin. calcite	V. calcite in Horton SS.	22.18	-7.93
RSB-124	11.Nine Mile R.	Calcite w. barite	V. calcite in lmst.	20.64	+0.06
RSB-100a	12. Up. Brookside	Unmin. calcite	1st calcite in brecciated Horton	25.41	-4.56
RSB-100b	12. Up. Mile R.	Unmin. calcite	Brown calcite w. chlorite	24.93	-5.51
RSB-100c	12. Nine Mile R.	Unmin. calcite	Last calcite	25.20	-4.74
RSB-100d	12. Nine Mile R.	Unmin. calcite	Carbonoceous calcite in brown calcite	25.11	-4.98

Unmin. = Unmineralized V. = Vein
Min. = Mineralized Vf. = Vug-filling
b.b. = basal breccia

APPENDIX C

STRONTIUM ISOTOPIC COMPOSITION

Table C.1 is a compilation of all strontium isotopic data obtained on the deposits studied. Most of the analyses were done at Carleton University, Ottawa, but some (of lower precision) were done by Geochron Laboratories. One sample was analysed in both laboratories (AGR-139). All the Gays River samples were collected by Samuel Akande (1982). Most of the Pembroke samples were collected by Mark Ponsford. The EC samples from Walton are part of the Economic Geology collection at Dalhousie.

TABLE C.1 Results of strontium isotopic analyses.

Location	Sample number	Composition	Description	87Sr/86Sr
1.Gays River	AGR-137	Preore dolomite	Recrystallized micrite host rock	0.70825
1.Gays River	AGR-139	Preore dolomite	Recrystallized micrite host rock	0.70847
1.Gays River	SPA-105-1	Ore-stage calcite	Vein calcite intergrown with sphalerite	0.71200
1.Gays River	AGR-119-2	Postore calcite	Vug-filling calcite overgrowths on galena	0.7083
1.Gays River	AGR-201-2	Postore calcite	Vug-filling calcite in fracture-related cavity	0.71050
1.Gays River	NE-105-1	Postore calcite	Scalenohedral calcite in vugs	0.70868
1.Gays River	AGR-131	Postore calcite	Recrystallized secondary limestone (dedolomite)	0.70890
1.Gays River	AGR-133a	Postore calcite	Recrystallized limestone breccia	0.70895
1.Gays River	AGR-139 (Geochron)	Preore dolomite	Recrystallized micrite	0.7082 +.0003
1.Gays River	DW4-360	Preore anhydrite	Stratigraphically higher evaporite	0.7090 +.0002
1.Gays River	AGR-07	Ore-stage calcite	Vein calcite	0.7118 +.0003
1.Gays River	AGR-91	Ore-stage calcite	Vein calcite	0.7114 +.0002
1.Gays River	AGRF-1	Postore fluorite		0.7097 +.0003
1.Gays River	AGRB-1	Postore barite		0.7088 +.0001
1.Gays River	DW4-405	Postore gypsum	Vug-filling	0.7085 +.0001
2. Southvale	RSB-47	Barite	White barite in basal Windsor carbonate	0.71018
4. Pembroke	FHd	Preore dolomite	Skeletal grainstone host rock	0.70851
4. Pembroke	P13-VN	Mineralized calcite	Vein calcite with galena	0.71193

4. Pembroke	RSB-46	Mineralized calcite	Vein calcite with galena	0.70837
4. Pembroke	P9-VN	Unmineral. calcite	Vein calcite	0.70833
5. Smithfield	RSB-31	Preore calcite	Carbonaceous limestone host rock	0.70775
5. Smithfield	RSB-34b	Preore calcite	Limestone host from quarry 800 m west	0.70816
5. Smithfield	RSB-27	Barite	Pink crystalline barite	0.70978
5. Smithfield	RSB-28a	Barite	Reddish crystalline barite	0.70875
5. Smithfield	RSB-28b	Barite	White crystalline barite	0.70990
5. Smithfield	RSB-29a	Barite	White crystalline barite	0.71002
5. Smithfield	RSB-30	Mineralized calcite	Vein calcite	0.70828
5. Smithfield	RSB-32	Postore calcite	Vein calcite a) prep with barites b) prep with calcites	 0.70867 0.70864
6.Middle Stewiacke	RSB-51	Preore calcite	Limestone host rock	0.70812
6. Stewiacke	RSB-49	Barite	Red vein barite	0.70958
6. Stewiacke	RSB-50	Barite	Pink to white vein barite	0.70977
6. Stewiacke	RSB-54	Barite	Vein barite which cuts calcite veins	0.70912
7. Brookfield	RSB-40	Preore calcite	Porous crystalline Windsor limestone	0.70808
7. Brookfield	RSB-35	Barite	Pink massive barite from quarry centre	0.71175
7. Brookfield	RSB-36	Barite	Red massive barite from quarry centre	0.71171
7. Brookfield	RSB-37	Barite	Pink massive barite from SW quarry wall	0.71145
7. Brookfield	RSB-38	Barite	White massive barite from SW quarry wall	0.71144
7.	RSB-39	Barite	Pink massive barite	0.71127

Brookfield			from quarry centre	
8.Hilden	RSB-67	Barite	Pink vein barite	0.70877
8.Hilden	RSB-68	Barite	Pink massive barite assoc with siderite	0.70904
10.Walton	RSB-69	Barite	Cryst. barite with sulfides	0.71055
10.Walton 650'level	EC-788	Umineral. calcite	Crystalline calcite	0.70894
10.Walton 850'level	EC-785	Pre-ore lmst.	Dark, laminated Macumber lmst.	0.70845
10.Walton 850'level	EC-761	Barite	Massive, white fine-grained	0.71058
10.Walton 850'level	EC-752	Barite	Laminated, pink-white	0.71049
10.Walton 850'level	EC-789	Barite	Crystalline pink-white	0.71064 0.71065
13.Lake Fletcher	RSB-62	Barite	White vein barite in Meguma slate	0.71230
13.Lake Fletcher	RSB-63	Barite	White vein barite in Meguma slate	0.71228

APPENDIX D

COMPUTER PROGRAM

FOR FISSION TRACK AGE CALCULATIONS

```
      PROGRAM FTCALC(OFT,INPUT,TAPE1=OFT)
      REAL NTS,NTI,NNS,NNI
      REAL NS(200),NI(200)
      CHARACTER CHAR(4),C,M,Q,A,Z
      C='C'
      M='M'
      Q='Q'
      A='A'
      Z='Z'
C     PROGRAM TO CALCULATE THE CHI-SQUARE STATISTIC FOR FT DATA
C     AND THEN CALCULATE RATIO PS/PI, AND ZETA OR AGE.
C
C     N IS NUMBER OF GRAINS COUNTED
C     NS(I) IS NUMBER OF SPONTANEOUS TRACKS IN ITH GRAIN.
C     NI(I) IS NUMBER OF INDUCED TRACKS IN ITH IMAGE.
C     FNS IS FITTED NS VALUE FOR ITH GRAIN.
C     FNI IS FITTED NI VALUE FOR ITH GRAIN.
C     NTS IS TOTAL NUMBER OF SPONTANEOUS TRACKS.
C     NTI IS TOTAL NUMBER OF INDUCED TRACKS.
      N=0
      NTS=0.0
      NTI=0.0
      PRINT *,'THE GRAIN COUNTS AND MICA COUNTS ENTERED ARE:'
2     READ(1,*,END=10) NNS,NNI
      N=N+1
      WRITE(*,5) NNS,NNI
      NS(N)=NNS
      NI(N)=NNI
      NTS=NTS+NNS
      NTI=NTI+NNI
      GO TO 2
10    WRITE(*,15) N
5     FORMAT(F4.0,2X,F4.0)
15    FORMAT('THE TOTAL NUMBER OF GRAINS COUNTED = ',I3)
      RNTS=NTS/(NTS+NTI)
      RNTI=NTI/(NTS+NTI)
      WRITE(*,25) NTS
      WRITE(*,26) NTI
25    FORMAT('TOTAL NUMBER OF GRAIN COUNTS = ',F5.0)
26    FORMAT('TOTAL NUMBER OF MICA COUNTS = ',F5.0)
C     NOW CALCULATE THE CHI-SQUARE STATISTIC
      CHSQ=0.0
      DO 20 I=1,N
      FNS=RNTS*(NS(I)+NI(I))
```

```
      FNI=RNTI*(NS(I)+NI(I))
      CHSQ=CHSQ+((NS(I)-FNS)**2)/FNS+((NI(I)-FNI)**2)/FNI
20    CONTINUE
      WRITE(*,35) CHSQ
35    FORMAT('THE VALUE OF THE CHI-SQUARE STATISTIC IS  ',F6.2)
      NDF=N-1
      WRITE(*,45) NDF
45    FORMAT('THE NUMBER OF DEGREES OF FREEDOM - N-1 = ',I4)
      PRINT *,'NOW ENTER EITHER "C" FOR CONVENTIONAL ANALYSIS,'
      PRINT *,' IF CHI-SQUARE IS ACCEPTABLE AT THE 5% LEVEL,'
      PRINT *,' OR "M" FOR MEAN PS/PI IF CHI-SQUARE IS NOT ACCEPTABLE.'
      READ(*,55) CHAR
55    FORMAT (4A1)
30    I=1
31       IF(CHAR(I) .EQ. C) GO TO 40
         IF(CHAR(I) .EQ. M) GO TO 50
         IF(I .EQ. 4) GO TO 33
         I=I+1
      GO TO 31
33    PRINT *,'NEITHER "C" NOR "M" WERE ENTERED,'
      PRINT *,'ENTER ONE OF THESE, OR "Q" TO EXIT PROGRAM.'
      READ(*,55) CHAR
      I=1
32       IF(CHAR(I) .EQ. Q) GO TO 100
         IF(I .EQ. 4) GO TO 30
         I=I+1
      GO TO 32
C   CONVENTIONAL ANALYSIS
40    RATIO=NTS/NTI
      QRT=1/NTS+1/NTI
      SERROR=RATIO*SQRT(QRT)
      WRITE(*,65) RATIO
      WRITE(*,75) SERROR
65    FORMAT('NS/NI BY CONVENTIONAL ANALYSIS =',F8.3)
75    FORMAT('THE STANDARD ERROR IS ',F8.3)
      GO TO 100
C   MEAN PS/PI RATIO AND STANDARD ERROR OF THIS MEAN
50    SUM=0.0
      SSUM=0.0
      RN=N
      DO 60 I=1,N
      RATIO=NS(I)/NI(I)
      SUM=RATIO + SUM
60    SSUM=SSUM + RATIO**2
      RATIO=SUM/RN
      QRT=RN*SSUM-SUM**2
      SDEV=SQRT(QRT/(RN*(RN-1)))
      SERROR=SDEV/SQRT(RN)
      WRITE(*,85) RATIO
      WRITE(*,95) SERROR
85    FORMAT('MEAN PS/PI =',F8.3)
95    FORMAT('THE STANDARD ERROR OF THIS MEAN =',F8.3)
100   PRINT *,'     '
```

```
      PRINT *,'     '
      PRINT *,'NOW CALCULATE ZETA OR AGE OF THE UNKNOWN'
      PRINT *,'     '
      PRINT *,'ENTER "Z" FOR ZETA CALCULATION OR "A" FOR AGE'
      READ(*,55) CHAR
C   TDC IS TOTAL DECAY CONSTANT OF U238.
C   UUR IS U235/U238 ISOTOPIC ABUNDANCE RATIO.
C   G IS GEOMETRY FACTOR
C   TSTD IS AGE OF FISH CANYON STANDARD.
C   ETSTD IS ERROR IN THIS AGE
      TDC=1.55125E-10
      UUR=7.2527E-3
      G=0.5
      TSTD=27.8
      ETSTD=0.2
      WRITE(*,135) TSTD
135   FORMAT('THE F.C. AGE FROM HURFORD & HAMMERSCHMIDT, 1985 =',F6.2)
      WRITE(*,136) ETSTD
136   FORMAT('ERROR GIVEN FOR THIS AGE IS =',F4.2)
101   I=1
102      IF(CHAR(I) .EQ. A) GO TO 110
         IF(CHAR(I) .EQ. Z) GO TO 120
         IF(I .EQ. 4) GO TO 105
         I=I+1
      GO TO 102
105   PRINT *,'NEITHER "Z" NOR "A" WERE ENTERED,'
      PRINT *,'ENTER ONE OF THESE, OR "Q" TO EXIT PROGRAM.'
      READ(*,55) CHAR
      I=1
106      IF(CHAR(I) .EQ. Q) GO TO 200
         IF(I .EQ. 4) GO TO 101
         I=I+1
      GO TO 106
C  ZETA CALCULATION
120   PRINT *,'WHAT IS THE INTERPOLATED TRACK DENSITY AND '
      PRINT *,'STANDARD ERROR IN THE DOSIMETER GLASS, '
      PRINT *,'AT THE POSITION OF THE FC STANDARD'
      PRINT *,'EG.  2.32E+4 .09E+4 '
      READ(*,*) PD,EPD
      ZETA=(EXP(TDC*TSTD)-1.0)/(TDC*RATIO*G*PD)
      PRINT *,'     '
      WRITE(*,125) ZETA
125   FORMAT('          ZETA = ',F9.7)
      FIRST=(1.0-EXP(-TDC*TSTD))/TDC
      SDEV=ZETA*SQRT((ETSTD/FIRST)**2+(SERROR/RATIO)**2+(EPD/PD)**2)
      PRINT *,'     '
      PRINT *,'ERROR IN ZETA IS CALCULATED FROM THE SQUARE ROOT'
      PRINT *,'OF THE SUM OF THE SQUARES OF [PARTIAL DERIVATIVE * THE'
      WRITE(*,126) SDEV
126   FORMAT('ERROR] OF EACH QUANTITY MAKING UP ZETA = ',F9.7)
      GO TO 200
C  CALCULATE THE AGE OF THE UNKNOWN
110   PRINT *,'WHAT IS THE CURRENT BEST ESTIMATE OF ZETA?'
```

```
      READ(*,*) ZETA
      PRINT *,'WHAT IS ITS STANDARD ERROR?'
      READ(*,*) SDEV
      PRINT *,'WHAT IS INTERPOLATED TRACK DENSITY AND STANDARD ERROR,'
      PRINT *,'IN THE DOSIMETER GLASS AT THE POSITION OF THE SAMPLE?'
      PRINT *,'(EG.)  2.32E+4  .09E+4'
      READ(*,*) PD,EPD
      BRACK=1.0+TDC*ZETA*RATIO*G*PD
      AGE=(1.0/TDC)*ALOG(BRACK)
      ARG=(RATIO*PD*SDEV)**2+(ZETA*PD*SERROR)**2+(ZETA*RATIO*EPD)**2
      CC=(1.0-EXP(-AGE*TDC))/(AGE*TDC)
      EAGE=CC*(G/BRACK)*SQRT(ARG)
      WRITE(*,145) AGE
      WRITE(*,146) EAGE
145   FORMAT('           AGE IN MA = ',F6.2)
146   FORMAT('THE ERROR IN THE AGE = ',F6.2)
200   STOP
      END
```

```
      PROGRAM COUNTS(TAPE2,INPUT,TAPE1=INPUT)
      PRINT *,'     '
      PRINT *,'PROGRAM TO ENTER FISSION TRACK DATA. '
      PRINT *,'_____________________________________ '
      PRINT *,'     '
      PRINT *,'     '
      PRINT *,'ENTER GRAIN TRACK COUNTS (PS) FIRST, '
      PRINT *,'THEN PRESS THE SPACE BAR AND '
      PRINT *,'ENTER MICA TRACK COUNTS (PI) '
      PRINT *,'     '
      PRINT *,'AFTER EACH PAIR OF DATA IS ENTERED, PRESS <RETURN>. '
      PRINT *,'     '
      PRINT *,'WHEN FINISHED ENTERING DATA, PRESS <RETURN> '
      PRINT *,'INSTEAD OF ENTERING VALUES. '
      PRINT *,'     '
      PRINT *,'PLEASE ENTER DATA NOW. '
300   READ(1,*,END=100) PS,PI
      WRITE(2,*) PS,PI
      GO TO 300
100   PRINT *,'FINISHED INPUTTING DATA. '
      STOP
      END
```

```
      PROGRAM STGLAS(OFT,INPUT,TAPE1=OFT)
C    PROGRAM TO CALCULATE THE MEAN AND STANDARD DEVIATION OF COUNTS
C     FROM THE MICA COVERING THE NBS STANDARD GLASS 963A DOSIMETERS.
C    THEN CALCULATE THE TRACK DENSITY ASSUMING OUR STANDARD GRID
C     WAS USED AND COUNTING WAS DONE AT 400X MAGNIFICATION.
      DIMENSION DOS(1000)
      PRINT *,'ENTER THE NUMBER OF DATA POINTS IN THE FILE'
      READ(*,*) N
      READ(1,*) (DOS(I),I=1,N)
10    WRITE(*,15) N
15    FORMAT('THE NUMBER OF FIELDS COUNTED =',I5)
C    NOW CALCULATE MEAN AND STANDARD DEVIATION
      SUM=0.0
      SSUM=0.0
      RN=N
      DO 20 I=1,N
      SUM=SUM+DOS(I)
      SSUM=SSUM+DOS(I)**2
20    CONTINUE
      WRITE(*,16) SUM
16    FORMAT('THE TOTAL NUMBER OF TRACKS COUNTED =',F6.0)
      XMEAN=SUM/RN
      QRT=RN*SSUM-SUM**2
      SDEV=SQRT(QRT/(RN*(RN-1.0)))
      SERROR=SDEV/SQRT(RN)
      AREA=1.59E-4
      TDEN=XMEAN/AREA
      EAREA=0.04E-4
      ETDEN=TDEN*SQRT((SERROR/XMEAN)**2+(EAREA/AREA)**2)
      WRITE(*,25) XMEAN
      WRITE(*,30) SDEV
      WRITE(*,35) SERROR
      PRINT *,'     '
      PRINT *,'TO CALCULATE THE TRACK DENSITY:'
      WRITE(*,40) AREA
      WRITE(*,45) EAREA
      PRINT *,'     '
      WRITE(*,50) TDEN
      WRITE(*,55) ETDEN
25    FORMAT('MEAN =',F6.3)
30    FORMAT('STANDARD DEVIATION =',F6.3)
35    FORMAT('STANDARD ERROR OF THE MEAN =',F6.3)
40    FORMAT('USED GRID AREA (IN CM**2) AT 400X OF ',E10.3)
45    FORMAT('ESTIMATED AREA MEASUREMENT ERROR AS ',E10.3)
50    FORMAT('TRACK DENSITY IN TRACKS/CM**2 =',E12.5)
55    FORMAT('ERROR IN TRACK DENSITY        =',E12.5)
      STOP
      END
```

Procedure file used to run above programs.

```
.PROC,FTSTATS*I
,OFT[FILE NAME OF OBSERVED DATA]=(*F)
.
.HELP,,NOLIST.
   THE OBSERVED FISSION TRACK DATA WAS ENTERED USING THE
  "FTDATA" PROCEDURE.  "OFT" IS THE NAME OF THE FILE
  PRODUCED BY THAT PROCEDURE.
.
.ENDHELP
$GET,OFT/NA.
$IF,FILE(OFT,.NOT.AS),THEN.
$   NOTE.// DATA FILE NAMED DOES NOT EXIST.  PLEASE CHECK THAT NAME IS C
$   REVERT,NOLIST.
$ENDIF,THEN.
$GET,CFTCALC/UN=DUGB480.
 CFTCALC,OFT.
$REVERT,NOLIST.
.PROC,STGLASS*I
,OFT[FILE NAME OF OBSERVED DOSIMETER DATA]=(*F)
.
$GET,OFT/NA.
$IF,FILE(OFT,.NOT.AS),THEN.
$   NOTE.// ERROR ---   DATA FILE NAMED DOES NOT EXIST.
$   REVERT,NOLIST.
$ENDIF,THEN.
$GET,CSTGLAS/UN=DUGB480.
 CSTGLAS,OFT.
$REVERT,NOLIST.
.PROC,FTDATA*I
,OFT[ENTER NEW NAME FOR THIS DATA FILE]=(*F)
.
$GET,COUNTC/UN=DUGB480.
 COUNTC,OFT.
$IF,FILE(OFT,AS),THEN.
$   SAVE,OFT.
$ELSE,THEN.
$   NOTE.// ERROR ---   DATA FILE WAS NOT CREATED...PLEASE START OVER.
$ENDIF,THEN.
$REVERT,NOLIST.
```

REFERENCES

Akande, S. O., 1982, Genesis of the lead and zinc mineralization at Gays River, Nova Scotia, Canada: A geologic, fluid inclusion and stable isotopic study: Unpublished Ph.D. thesis, Dalhousie University, 349p.

Akande, S. O. and Zentilli, M., 1983, Genesis of the lead-zinc mineralization at Gays River, Nova Scotia, Canada; in Kisvarsanyi, G., Grant, S.K., Pratt, W.P., and Koenig, J.W., eds., Internat. conf. on Mississippi Valley type lead-zinc deposits, proceedings volume: Rolla, Missouri, University of Missouri-Rolla, p.546-557.

Akande, S.O. and Zentilli, M., 1984, Geologic, fluid inclusion and stable isotope studies of the Gays River lead-zinc deposit, Nova Scotia, Canada: Econ. Geol., v.79, p.1187-1211.

Allen, D.G., 1971, The origin of sheet fractures in the Galore Creek copper deposits, British Columbia: Can. J. Earth Sci., v.8, p.704-711.

Anderson, G.M., 1978, Basinal brines and Mississippi Valley type ore deposits: Episodes, no.2, p.15-19.

Anderson, G.M., 1983, Some geochemical aspects of sulfide precipitation in carbonate rocks, in Kisvarsanyi, G., Grant, S.K., Pratt, W.P., and Koenig, J.W., eds., Internat. Conf. on Mississippi Valley type lead-zinc deposits: Rolla, Missouri, p.61-76.

Anderson, G.M. and Garven, G., 1987, Sulfate-sulfide-carbonate associations in Mississippi Valley-type lead-zinc deposits: Econ. Geol., v.82, p.482-488.

Anderson, G.M. and Macqueen, R.W., 1982, Ore deposits models - 6. Mississippi Valley-type lead-zinc deposits: Geoscience Canada, v.9, p.108-117.

Aumento, F., 1969, The mid-Atlantic ridge near 45 N. Fission track and manganese chronology: Canadian J. Earth Sci., v.6, p.1431-1440.

Avery, M.P., 1986, Vitrinite reflectance (Ro) on coaly samples from the Rawdon Hills area, Nova Scotia: Canada Geological Survey/Eastern Petroleum Geology, report no. EPGS-DOM.1-86MPA.

Barton, P.B., 1967, Possible role of organic matter in the precipitation of the Mississippi Valley ores: Econ. Geol., Monograph 3, p.371-377.

Barnes, H.L., 1979, Solubilities of ore minerals, in

Barnes, H.L., ed., Geochemistry of hydrothermal ore deposits: New York, Wiley, p.404-460.

Beales, F.W., Jackson, F.C., Jowett, E.C., Pearce, G.W., and Wu, Y., 1980, Paleomagnetism applied to the study of timing in stratigraphy with special reference to ore and petroleum problems, in Strangway, D.W., ed., The continental crust and its mineral deposits: Geol. Assoc. Canada, Spec. Paper 20, p.

Bell, W.A., 1929, Horton-Windsor district, Nova Scotia: Canada Geol. Survey Memoir, v.155, 268p.

Belt, E.S., 1964, Revision of Nova Scotia Middle Carboniferous units: Am. J. Sci., v.262, p.653-673.

Belt, E.S., 1968, Post-Acadian rifts and related facies, Eastern Canada, in Zen, E. et al., eds., Studies of Appalachian geology: Northern and Maritime: Interscience, New York, p.95-113.

Bethke, C.M., 1985, A numerical model of compaction-driven groudwater flow and heat transfer and its application to the paleohydrology of intracratonic sedimentary basins: J. of Geophys. Research, v.90, p.6817-6828.

Binney, W.P., 1979, Report on 1979 diamond drilling, Gold Brook - Project 224 for St. Joseph Explorations Ltd.: Confidential report.

Bird, J.M. and Dewey, J.F., 1970, Litosphere plate-continental margin tectonics and the evolution of the Appalachian orogen: Geol. Soc. Am. Bull., v.81, p.1031-1060.

Blanchard, M.-C., Jamieson, R.A., and More, E.B., 1984, Late Devonian - Early Carboniferous volcanism in Western Cape Breton Island, Nova Scotia: Canadian J. Earth Sci., v.21, p.762-774.

Boehner, R.C., 1986, Salt and potash resources of Nova Scotia: Nova Scotia Dept. Mines and Energy, Bull. 5, 346p.

Boyle, R.W., 1972, The geology, geochemistry, and origin of the barite, manganese, and lead-zinc-copper-silver deposits of the Walton-Cheverie area, Nova Scotia: Canada Geol. Survey Bull., v.166, 181p.

Boyle, R.W., Wanless, R.K., and Stevens, R.D., 1976, Sulfur isotope investigation of the barite, manganese, and lead-zinc-copper-silver deposits of the Walton-Cheverie area, Nova Scotia, Canada; Econ. Geol., v.71, p.749-762.

Boyce, A.J., Anderton, R., and Russell, M.J., 1983,

Rapid subsidence and early Carboniferous base-metal mineralization in Ireland: Trans. Instn. Min. Metall. v.92, p.B55-B66.

Bradley, D.C., 1982, Subsidence in Late Paleozoic basins in the northern Appalachians: Tectonics, v.1, p.107-123.

Bragg, W.L., 1937, The Atomic Structure of Minerals: Cornell University Press, Ithaca, N.Y.

Bruning, J.L. and Kintz, B.L., 1968, Computational handbook of statistics: Scott, Foresman and Company, Atlanta, 269p.

Bundy, W.M., 1956, Petrology of gypsum-anhydrite deposits of southwestern Indiana: J. Sedimentary Petrol., v.26, p.240-252.

Burke, W.H., Denison, R.E., Heatherington, E.A., Koepick, R.B., Nelson, H.F., and Otto, J.B., 1982, Variation of seawater 87Sr/86Sr throughout Phanerozoic time: Geology, v.10, p.516-519.

Bustin, R.M., Barnes, M.A. and Barnes, W.C., 1985, Diagenesis 10. Quantification and modelling of organic diagenesis: Geoscience Canada, v.12, p.4-21.

Carothers, W.W. and Kharaka, Y.K., 1980, Stable carbon isotopes of HCO3- in oil field waters - implications for the origin of CO2: Geochim. Cosmochim. Acta, v.44, p.323-332.

Cathles, L.M. and Smith, A.T., 1983, Thermal constraints of the formation of Mississippi Valley-type lead-zinc deposits and their implications for episodic basin dewatering and deposit genesis: Econ. Geol., v.78, p.983-1002.

Charef, A. and Sheppard, S.M.F., 1984, Carbon and oxygen isotope analysis of calcite or dolomite associated with organic matter, Isotope Geoscience, v.2, p.325-333.

Chiba, H. and Sakai, H., 1985, Oxygen isotope exchange rate between dissolved sulfate and water at hydrothermal temperatures: Geochim. Cosmochim. Acta, v.49, p.993-1000.

Clarke, D.B. and Halliday, A.N., 1980, Strontium isotope geology of the South Mountain batholith, Nova Scotia: Geochim. Cosmochim. Acta, v.44, p.1045-1058.

Clauer, N., 1982, The rubidium-strontium method applied to sediments - certitudes and uncertainties, in Odin, G.S. (ed.), Numerical Dating in Stratigraphy: Wiley, New York, p.245-276.

Claypool, G.E., Holser, W.T., Kaplan, I.R., Sakai, H., and Zak, I., 1980, The age curves of sulfur and oxygen isotopes in

marine sulfate and their mutual interpretation: Chemical Geology, v.28, p.199-260.

Clifton, H.E., 1967, Solution-collapse and cavity filling in the Windsor Group, Nova Scotia, Canada: Geol. Survey Am. Bull., v.78, p.819-832.

Cox, K.G., Bell, J.D. and Pankhurst, R.J., 1979, The Interpretation of Igneous Rocks: George Allen and Unwin, London, 450p.

Crawford, M.L., 1981, Phase equilibria in aqueous fluid inclusions, in Hollister, L.S. and Crawford, M.L., eds., Short course in fluid inclusions; applications to petrology: G.A.C./M.A.C. Calgary '81, p. 75-100.

Crowell, J.C., 1974, Origin of late Cenozoic basins in southern California, in Dickinson, W.R., ed., Tectonics and Sedimentation, Soc. Econ. Paleont. Mineral., Spec. Publ. 22, p.190-204.

Davies, E.H., Akande, S.O., and Zentilli, M., 1983, Early Cretaceous deposits in the Gays River lead-zinc mine, Nova Scotia, Canada: Canada Geol. Survey, Current Research, Part A, Paper 84-1A, p. 353-358.

Deines, P., 1980, The isotopic composition of reduced carbon, in, Fritz, P. and Fontes, J.Ch., eds., Handbook of Environmental Isotope Geochemistry, v.1, p.329-406.

Dembicki, H.Jr., Horsfield, B. and Ho, T.T.Y., 1983, Source rock evaluation by pyrolysis-gas chromatography: Am. Assoc. Petrol. Geology Bull., v.67, p.1094-1103.

Diessel, F.K., 1982, University of Newcastle Research Report: Australia.

Doe, B.R. and Zartman, R.E., 1979, Plumbotectonics, the Phanerozoic, in Barnes, H.L., ed., Geochemistry of hydrothermal ore deposits, 2nd edition: New York, Wiley, p. 22-70.

Eisbacher, G.H., 1969, Displacement and stress field along part of the Cobequid Fault, Nova Scotia: Canadian J. Earth Sci., v.6, p.1095-1104.

Eisbacher, G.H., 1970, Deformation mechanics of mylonitic rocks and fractured granites in the Cobequid Mountains, Nova Scotia Canada: Geol. Soc. of Am. Bull., v.81, p.2009-2020. 2020.

Engel, A.E., Clayton, R.N. and Epstein, S., 1958,

Variations in the isotopic composition of oxygen and carbon in Leadville limestone in its hydrothermal and metamorphic phases: J. Geol., v.66, p.374-393.

Falvey, D.A. and Deighton, I., 1982, Recent advances in burial and thermal geohistory analysis, Australian Petrol. Expl. Assoc. J., v.22, p.65-81.

Faure, G., 1977, Principles of isotope geology: New York, Wiley, 464p.

Felderhof, G.W., 1978, Barite, celestite and fluorite in Nova Scotia: Nova Scotia Dept. of Mines and Energy, Bull. 4, 463 p.

Fleischer, R.L., Price, P.B. and Walker, R.M., 1965, Effects of temperature, pressure and ionization on the formation and stability of fission tracks in minerals and glasses: J. Geophys. Research, v.70, p.1497-1502.

Fleischer, R.L., Price, P.B., and Walker, R.M., 1975, Nuclear tracks in solids; principles and application: Berkeley, University of California Press, 605 p.

Fralick, P.W. and Schenk, P.E., 1981, Mollasse deposition and basin evolution in a wrench tectonic setting: The late Paleozoic, eastern Cumberland basin, Maritime Canada: in Miall, A.D. (ed.), Sedimentation and Tectonics in Alluvial Basins, Geol. Assoc. of Canada, Spec. Paper 23, p.77-97.

Friedman, I. and O'Neil, J.R., 1977, Compilation of stable isotope fractionation factors of geochemical interest, in Fleischer, M., ed., Data of Geochemistry, 6th edition: U.S. Geol. Survey Prof. Paper 440-KK.

Fritz, P., 1969, The oxygen and carbon isotopic composition of carbonates from the Pine Point lead-zinc ore deposits: Econ. Geol., v.64, p.733-742.

Fritz, P., 1976, Oxygen and carbon isotopes in ore deposits in sedimentary rocks, in Wolf, K.H., ed., Handbook of strata-bound and stratiform ore deposits: New York, Elsevier, v.2, p.191-217.

Fyfe, W.S., Price,N.J., Thompson, A.B., 1978, Fluids in the Earth's Crust: Elsevier, New York, 383 p.

Galbraith, R.F., 1981, On statistical models for fission track counts: Mathematical Geol., v.13, p.471-488.

Garven, G., 1982, The role of groundwater flow in the genesis of stratabound ore deposits; a quantitative analysis: Unpublished Ph.D. thesis, University of British Columbia, 304p.

Garven, G. and Freeze, R.A. 1984a. Theoretical analysis of the role of groundwater flow in the genesis of stratabound ore deposits. 1. Mathematical and numerical model: Am. J. Sci., v.284, p.1085-1124.

Garven, G. and Freeze, R.A. 1984b. Theoretical analysis of the role of groundwater flow in the genesis of stratabound ore deposits. 2. Quantitative results: Am. J. Sci., v.284, p.1125-1174.

Geldsetzer, H.H.J., 1978, The Windsor Group in Atlantic Canada; an update: Canada Geol. Survey, Current Research, Part C, Paper 78-1C, p. 43-48.

Giles, P., 1981, Major transgressive-regressive cycles in Middle to Late Visean rocks of Nova Scotia: Nova Scotia Department of Mines and Energy, Paper 81-2, 27 p.

Giles, P. and Boehner, R.C., 1979, Windsor Group stratigraphy in the Shubenacadie and Musquodoboit basins, central Nova Scotia: Nova Scotia Dept. Mines and Energy, Open-File Rept.410.

Giles, P., Boehner, R.C., and Ryan, R.J., 1979, Carbonate banks of the Gays River formation in central Nova Scotia: Nova Scotia Dept. Mines and Energy, Paper 79-7, 57 p.

Gize, A.P. and Barnes, H.L., 1982, The organic geochemistry of the Gays River, Nova Scotia, deposit: 11th Internat. Congress on Sedimentology, Abs., p.19.

Gleadow, A.J.W. and Lovering, J.F., 1977, Geometry factor for external detectors in fission track dating: Nuclear Track Detection, v.1, p.99-106.

Gleadow, A.J.W., Duddy, I.R. and Lovering, J.F., 1983, Fission track analysis: A new tool for the evaluation of thermal histories and hydrocarbon potential: Australian Petrol. Explor. Assoc. J., v.23, p.93-102.

Gleadow, A.J.W., Hurford, A.J. and Quaife, R.D., 1976, Fission track dating of zircon; improved etching techniques: Earth Planet. Sci. Letters, v.33, p.273-276.

Gleadow, A.J.W., Duddy, I.R., Green, P.F. and Hegarty, K.A., 1986, Fission track lengths in the apatite annealing zone and the interpretation of mixed ages: Earth Planet. Sci. Letters, v.78, p.245-254.

Grant, N.K. and Bliss, M.C., 1983, Strontium isotope and rare earth element variations in non-sulphide minerals from the Elmwood-Gordonsville mines, central Tennessee, in, Kisvarsanyi, G., Grant, S.K., Pratt, W.P. and Koenig, J.W., eds., Internat. Conf. on Mississippi Valley

type lead-zinc deposits: Rolla, Missouri, p.206-210.

Grant, N.K., Laskowski, T.E. and Foland, K.A., 1984, Rb-Sr and K-Ar ages of paleozoic glauconites from Ohio, Indiana and Missouri, U.S.A.: Isotope Geoscience, v.2, p.217-239.

Green, P., 1981, A new look at statistics in fission track dating: Nuclear Tracks, v.5, p.77-86.

Gretener, P.E., 1969, Fluid pressure in porous media - its importance in geology; a review: Canadian Soc. Petrol. Geologists Bull., v.17, p.255-295.

Gretener, P.E. 1981. Pore pressure: Fundamentals, general ramifications, and implications for structural geology (revised). Am. Assoc. of Petrol. Geologists, Education Course Note Series, no.4, 131 p.

Gretener, P.E., 1982, Another look at Alborz No. 5 in central Iran: Bull. Verinigung Schwiez Petrol. Geologen und Ingenieure, v.48, p.1-8.

Grist, A.M. 1986. Low temperature geochronology of the South Mountain batholith, Nova Scotia using 40Ar/39Ar and fission track techniques: Unpublished B.Sc. thesis, Dalhousie University, 102 p.

Hacquebard, P.A., Barss, M.S., and Donaldson, J.R., 1960, Distribution and stratigraphic significance of small spore genera in the Upper Carboniferous of the Maritime Provinces of Canada: 4th Internat. Congress of Stratigraphy and Carboniferous Geology, Heerlen, 1958, Compte Rendu, v.1, p.237-245.

Hacquebard, P.A., 1972, The Carboniferous of eastern Canada, in Septieme Congres International de Stratigraphie et de Geologie du Carbonifere, republished in Ross, C.A. and Ross, J.R.P., 1984, eds., Benchmark Papers in Geology, v.77, p. 45-66.

Hacquebard, P.A., 1974, A composite coalification curve for the Maritime region and its value for petroleum exploration: Canada Geol. Survey, Paper 74-1, p.12-23.

Hacquebard, P.A., 1984, Composition, origin and geology of coal: Course notes, Dalhousie University, 150p.

Hacquebard, P.A. 1986. The Gulf of St. Lawrence Carboniferous Basin; the largest coalfield of eastern Canada. Canadian Mining and Metallurgical Bull., v.79, p.67-78.

Hacquebard, P.A. and Donaldson, J.R., 1970, Coal metamorphism and hydrocarbon potential in Upper Paleozoic of the Atlantic

provinces, Canada: Canadian J. Earth Sci., v. 7, p. 1139-1163.

Hall, W.E. and Friedman, I., 1963, Composition of fluid inclusions, Cave-in-rock fluorite district, Illinois, and upper Mississippi valley zinc-lead district: Econ. Geol., v. 58, p. 886-911.

Hall, W.E. and Friedman, I., 1969, Oxygen and carbon isotopic composition of ore and host rock of selected Mississippi Valley deposits: U.S. Geol. Survey, Prof. Paper 650-C, p.C140-C148.

Hallam, A., 1977. Secular changes in marine inundation of USSR and North America through the Panerozoic: Nature, v.269, p.769-772.

Halliday, A.N., 1978, 40Ar/39Ar stepheating studies of clay concentrates from Irish orebodies: Geochim. Cosmochim Acta, v.42, p.1851-1858.

Halliday, A.N. and Mitchell, J.G., 1983, K-Ar ages of clay concentrates from Irish orebodies and their bearing on the timing of mineralization: Trans. Royal Soc. Edinburgh; Earth Sciences, v.74, p.1-14.

Halliday, A.N. and Mitchell, J.G., 1984, K-Ar ages of clay-size concentrates from the mineralization of the Pedroches Batholith, Spain, and evidence for Mesozoic hydrothermal activity associated with the breakup of Pangea: Earth Planet. Sci. Letters, v.68, p.229-239.

Hanor, J.S., 1979, The sedimentary genesis of hydrothermal fluids, in Barnes, H.L., ed., Geochemistry of hydrothermal ore deposits, 2nd edition: New York, Wiley, p. 137-172.

Hanor, J.S., 1980, Dissolved methane in sedimentary brines: Potential effect on PVT properties of fluid inclusions: Econ. Geol., v.75, p.603-617.

Harland, W.B., Cox, A., Llewellyn, P.G., Pickton, C.A.G., Smith, A.G., and Walters, R., 1982, A geologic time scale: Cambridge, Cambridge Univ. Press, 131 p.

Harrison, T.M. and Be', K., 1983, $^{40}Ar/^{39}Ar$ age spectrum analysis of detrital microclines from the southern San Joaquin Basin, California; an approach to determining the thermal evolution of sedimentary basins: Earth Planet. Sci. Letters, v. 64, p. 244-256.

Heard, H. and Ruby, W.W., 1966, Tectonic implication of gypsum dehydration: Geol. Soc. Am. Bull., v.77, p.741-760.

Helgeson, H.C., 1969, Thermodynamics of hydrothermal systems at elevated temperatures and pressures: Am. J. Sci., v.267,

p.729-804.

Hill, A.E., 1937, The transition temperature of gypsum to anhydrite: Am. Chem. Soc., v.59, p.2242-2244.

Howie, R.D. and Barss, M.S., 1975, Upper Paleozoic rocks of the Atlantic provinces, Gulf of St. Lawrence, and adjacent continental shelf: Canada Geol. Survey Paper 74-30, p.35-50.

Hsu, K.J., 1972, Origin of saline giants; a critical review after the discovery of the Mediterranean evaporite: Earth Sci. Reviews, v.8, p.371-396.

Hubbert, M.K. and Rubey, W.W., 1959, Role of fluid pressure in mechanics of overthrust faulting. I. Mechanics of fluid-filled porous solids and its application to overthrust faulting: Geol. Soc. of Am. Bull., v.70, p.115-166.

Hurford, A.J. and Green, P.F., 1983, The zeta age calibration of fission-track dating: Isotope Geoscience, v.1, p.285-317.

Hurford, A.J. and Hammerschmidt, K, 1985, 40Ar/39Ar and K/Ar dating of the Bishop and Fish Canyon Tuffs: Calibration ages for fission-track dating standards: Chemical Geology, v.58, p.23-32.

Hutchison, C.S., 1974, Laboratory Handbook of Petrographic Techniques: Wiley, London, p.214-218.

Jackson, S.A. and Beales, F.W., 1967, An aspect of sedimentary basin evaluation; the concentration of Mississippi Valley type ores during late stages of diagenesis: Canadian Soc. Petrol. Geologists Bull., v. 15, p. 383-433.

Jowett, C.E., 1986, Genesis of Kupferschiefer Cu-Ag deposits by convective flow of Rotliegende brines during Triassic rifting: Econ. Geol., v.81, p.1823-1837.

Keith, M.L., and Weber, J.N., 1964, Carbon and oxygen isotopic composition of selected limestones and fossils: Geochim. Cosmochim. Acta, v.28, p.1787-1816.

Kelley, D.G., 1967, Baddeck and Whycocomagh Map-areas with emphasis on Mississippian stratigraphy of central Cape Breton Island, Nova Scotia, Canada Geol. Survey Memoir, v.351, p.6-59.

Kendall, A.C., 1984, Evaporites, in Walker, R.G. (ed.), Facies Models, 2nd edition, Geoscience Canada, reprint series 1, p.259-296.

Keppie, J.D., 1982, The Minas geofracture: Geol. Assoc. Canada,

Spec. Paper 24, p.263-280.

Kesler, S.E., Ruiz, J., and Jones, L.M., 1983, Strontium-isotopic geochemistry of fluorite mineralization (Coahuila, Mexico): Isotope Geoscience, v.1, p.65-75.

Kessen, K.M., Woodruff, M.S., and Grant, N.K., 1981, Gangue mineral 87Sr/86Sr ratios and the origin of Mississippi Valley-type mineralization: Econ. Geol., v. 76, p. 913-920.

King, L.H., Hyndman, R.D., and Keen, C.E., 1975: Geological development of the continental margin of Atlantic Canada: Geoscience Canada, v.2, p.26-35.

Kharaka, Y.K. and Carothers, W.M., 1986, Oxygen and hydrogen isotope geochemistry of deep basin brines, in Fritz, P. and Fontes, J.Ch., eds., Handbook of environmental isotope geochemistry: Elsevier, Amsterdam, v.2, p.305-360.

Krebs, W. and Macqueen, R., 1984, Sequence of diagenetic and mineralization events, Pine Point lead-zinc property, N.W.T.: Canadian Soc. Petrol. Geologists Bull., v.32, p.434-464.

Kubilius, W.P., 1983, Sulfur isotopic evidence for country rock contamination of granitoids in southwestern Nova Scotia: Unpublished M.S. thesis, Pennsylvania State University, 103 p.

Kyle, J.R., 1981, Geology of the Pine Point lead-zinc district, in, Wolf, K.H., ed., Handbook of strata-bound and stratiform ore deposits: Elsevier, Amsterdam, v.9, p.643-741.

Kyle, R.J., 1983, Temporal and spatial aspects of mineralization in the K57 orebody, Pine Point district, Northwest Territories, Canada, in Kisvarsanyi, G., Grant, S.K., Pratt, W.P., Koenig, J.W., eds., Internat. Conf. on Mississippi Valley type lead-zinc deposits: Rolla, Missouri, p.338-346.

Lambert, R.St.J., Chamberlain, V.E. and Muecke, G.K., 1984, Rb-Sr age and geochemistry of the Halifax formation, Meguma Group, Nova Scotia: Geol.Assoc.Canada-Mineralog.Assoc.Canada, Program with Absracts, v.9, p.81.

Lange, S., Chaudhuri, S., and Clauer, N., 1983, Strontium isotopic evidence for the origin of barites and sulfides from the Mississippi Valley-type ore deposits in southeast Missouri: Econ. Geol., v.78, p. 1255-1261.

Leach, D.L., 1980, Nature of mineralizing fluids in the barite deposits of central and southeast Missouri: Econ. Geol., v. 75, p. 1168-1180.

Leach, D.L. and Rowan, E.L., 1986, Genetic link between

Ouachita foldbelt tectonism and the Mississippi Valley-type lead-zinc deposits of the Ozarks: Geology, v.14, p.931-935.

Lloyd, R.M., 1968, Oxygen isotope behaviour in the sulfate-water system: J. Geophys. Research, v.73, p.6099-7110.

Longstaffe, F.J., 1983, Diagenesis 4. Stable isotope studies of diagenesis in clastic rocks: Geoscience Canada, v.10, p.43-58.

Lopatin, N.V., 1971, Temperature and geologic time as factors in coalification: Academiia Nauk SSSR Izvestiia Seriia Geologicheskaia, No.3, p.95-106. (In Russian.) English translation by N.H. Bostick, 1972, Illinois State Geol. Survey.

Lydon, J.W., 1978, Observations on some lead-zinc deposits of Nova Scotia: Canada Geol. Survey Paper 78-1A, p.293-298.

MacEachern, S.B. and Hannon, P., 1974a, The Gays River discovery-a Mississippi Valley-type lead-zinc deposit in Nova Scotia: Canadian Mining and Metallurgical Bull., v.67, p.61-66.

MacEachern, S.B. and Hannon, P., 1974b, The Gays River discovery: Can. Mining J., v.95, p.77-79.

MacInnis, I.N., 1986, Lithogeochemistry of the Goldenville-Halifax Transition (GHT) of the Meguma Group in the manganiferous zinc-lead deposit at Eastville, Nova Scotia: Unpublished B.Sc. thesis, Dalhousie University, 138 p.

Mackenzie, A.S., Beaumont, C., Boutillier, R., and Rullkoten, J., 1983, Aromatization and isomerization of hydrocarbons and the thermal evolution of the Nova Scotia continental margin, in International colloquium - thermal phenomena in sedimentary basins: Bordeaux, France, ADERA, session 3.5, 4 p.

MacLeod, J., 1975, Diagenesis and sulfide mineralization at Gays River, Nova Scotia: Unpublished B.Sc. thesis, Dalhousie University, 132p.

MacLeod, J.L., 1984, Diagenesis and its effects on base metal mineralization within a Mississippian carbonate complex, Gays River, Nova Scotia, Canada: 9th Internat. Congress, Strat. and Geol. of the Carboniferous, 1979, Compte Rendu, v.3, p.193-204.

Magara, K., 1975a, Reevaluation of montmorillonite dehydration as cause of abnormal pressure and hydrocarbon migration: Am. Assoc. Petrol. Geologists Bull., v.59, p.292-302.

Magara, K., 1975b, Importance of aquathermal pressuring effect in Gulf Coast: Am. Assoc. Petrol. Geologists Bull.,

v.59, p.2037-2045.

Mahony, H., 1986, Sedimentology and tectonic activities in Rawdon Hills, Nova Scotia: Unpub. B.Sc. thesis, Dalhousie University, 90p.

Mann, H.B. and Whitney, D.R. 1947, On a test of whether one of two random variables is larger than the other: Annals Math. Statist., v.18, p.50-60.

Mann, P., Hempton, M.R., Bradley, D.C., and Burke, K., 1983, Development of pull-apart basins: J. Geology, v.91, p. 529-554.

Matsubaya, O. and Sakai, H., 1973, Oxygen and hydrogen isotopic study on the water of crystallization of gypsum from the Kuroko-type mineralization: Geochem. J., v.7, p.153-165.

McDonald, G.J., 1953, Anhydrite-gypsum equilibrium relations: Am. J. Sci., v.251, p.884-898.

McKenzie, D.P., 1978, Some remarks on the development of sedimentary basins, Earth Planet. Sci. Letters, v.40, p.25-32.

McLaughlin, R.J. and Nilson, T.H., 1982, Neogene non-marine sedimentation and tectonics in small pull-apart basins of the San Andreas fault system, Sonoma County, California: Sedimentology, v.29, p.865-876.

McLimans, R.K., 1977, Geologic, fluid inclusion and stable isotope studies of the Upper Mississippi Valley zinc-lead district, southwest Wisconsin: Unpub. Ph.D. thesis, The Pennsylvania State University, 175p.

Medford, G.A., Maxwell, R.J., and Armstrong, R.L., 1983, 87Sr/86Sr ratio measurements on sulfides, carbonates, and fluid inclusions from Pine Point, NWT, Canada; an 87Sr/86Sr ratio increase accompanying the mineralizing process: Econ. Geol., v. 78, p. 1375-1378.

Mendenhall, W., 1975, Introduction to Probability and Statistics, 4th edition: Duxbury Press, North Scltuate, MA., 460p.

Mostofi, B. and Gansser, A., 1957, The story behind the 5 Alborz: Oil and Gas J., v.55, p.78-84.

Naeser, C.W., 1967, The use of apatite and sphene for fission track age determinations: Geol. Soc. Am. Bull., v.76, p.1523-

Naeser, C.W., 1976, Fission track dating; theory and

and laboratory procedures: U.S. Geol. Survey, Open-file report 76-190.

Naeser, C.W., 1979, Thermal history of sedimentary basins; fission-track dating of subsurface rocks: Soc. Econ. Paleont. Mineral., Spec. Publ. 26, p. 109-112.

Naeser, C.W. and Cunningham, C.G., 1984, Age and paleothermal anomaly of the Eagle Mine ore body, Gilman district, Colorado: A fission-track study: Geol. Soc. Am., Abstr. with Programs, v.16, p.607.

Naeser, C.W. and Faul, H., 1969, Fission track annealing in apatite and sphene: J. Geophys. Research, v.74, p.705-710.

Nishida, T., and Takashima, Y., 1975, Annealing of fission tracks in zircons: Earth Planet. Sci. Letters, v.27, p.257-264.

North, F.K., 1985, Petroleum Geology: Allen and Unwin, Boston, 607p.

Northrop, D.A. and Clayton, R.N., 1966, Oxygen isotope fractionation in systems containing dolomite: J. Geol., v.74, p.174-196.

Ohmoto, H., 1972, Systematics of sulfur and carbon isotopes in hydrothermal ore deposits: Econ. Geol., v.67, p.551-578.

Ohmoto, H., 1986, Stable isotope geochemistry of ore deposits, in Valley, J.W., Taylor, H.P.Jr. and O'Neil, J.R., eds., Stable isotopes in high temperature geological processes: Mineral. Soc. Am., Reviews in Mineralogy, v.16, p.491-560.

Ohmoto H., and Rye, R.O., 1979, Isotopes of sulfur and carbon, in Barnes, H.L., ed., Geochemistry of hydrothermal ore deposits, 2nd edition: New York, Wiley, p. 509-567.

Oliver, J., 1986, Fluids expelled from orogenic belts: Their role in hydrocarbon migration and other geologic phenomena: Geology, v.14, p.99-102.

Olson, R.A., 1984, Genesis of paleokarst and strata-bound zinc-lead sulfide deposits in a Proterozoic dolostone, northern Baffin Island, Canada: Econ. Geol., v.79, p.1056-1103.

O'Neil, J.R., 1986, Theoretical and experimental aspects of isotopic fractionation, in Valley, J.W., Taylor, H.P.Jr., and O'Neil, J.R., eds., Stable isotopes in high temperature geological processes: Mineral. Soc. Am., Reviews in Mineralogy, v.16, p.1-40 and 561-569.

O'Neil, J.R., Clayton, R.N. and Mayeda, T.K., 1969, Oxygen isotope fractionation in divalent metal carbonates: J. Chem. Physics, v.51, p.5547-5558.

O'Neil, J.R. and Kharaka, Y.K., 1976, Hydrogen and oxygen isotope exchange reactions between clay minerals and water: Geochim. Cosmochim. Acta, v.40, p.241-246.

Pagel, M. and Poty, B., 1983, The evolution of composition, temperature and pressure of sedimentary fluids over time; a fluid inclusion reconstruction, in Internat. colloquium - thermal phenomena in sedimentary basins: Bordeaux, France, ADERA.

Palciauskas, V.V. and Domenico, P.A., 1980, Microfracture development in compacting sediments: Relation to hydrocarbon maturation kinetics: Am. Assoc. Petrol. Geologists Bull., v.64, p.927-937.

Parrish, R.R., 1983, Cenozoic thermal evolution and tectonics of the Coast Mountains of British Columbia. 1. Fission track dating, apparent uplift rates, and patterns of uplift: Tectonics, v.2, p.601-631.

Pinckney, D.M., and Rye, R.O., 1972, Variation of $^{18}O/^{16}O$, $^{13}C/^{12}C$, texture and mineralogy in altered limestone in the Hill mine, Cave-in-District, Illinois: Econ. Geol., v. 67, p. 1-18.

Pollard, D.D., 1973, Derivation and evaluation of a mechanical model for sheet intrusions: Tectonophysics, v.19, p.233-269.

Pollard, D.D., Delaney, P.T., Duffield, W.A., Endo, E.T. and Okamura, A.T. 1983. Surface deformation in volcanic rift zones. Tectonophysics, v.94, p.541-584.

Ponsford, M.A.P., 1983, Geologic, fluid inclusion and stable isotope study of a carbonate-hosted lead deposit at Pembroke (Glenbervie), Colchester County, Nova Scotia: Unpublished B.Sc. thesis, Dalhousie University, 65 p.

Poole, W.H., 1967, Tectonic evolution of Appalachian region of Canada: Geol. Assoc. Canada, Spec. Paper 4, p. 9-51.

Posey, H.H., Stein, H.J., Fullager, P.D., and Kish, S.A., 1983, Rb-Sr isotopic analysis of the Upper Cambrian glauconites, southern Missouri; implications for movement of Mississippi Valley-type ore fluids in the Ozark region, in Kisvarsanyi, G., Grant, G., Pratt, S.K., and Koenig, J.W., eds., Internat. conf. on Mississippi Valley type lead-zinc deposits, proceedings volume: Rolla, Missouri, University of Missouri-Rolla, p. 166-173.

Potter, II, R.W., Clynne, M.A., and Brown, D.L., 1978, Freezing point depression of aqueous sodium chloride solutions: Econ. Geol., v.73, p.284-285.

Powell, T.G. and Macqueen, R.W., 1984, Precipitation of sulfide ores and organic matter/sulfate reactions at Pine Point, Canada: Science, v.224, p.63-66.

Reynolds, P.H., Zentilli, M., and Muecke, G.K., 1981, K-Ar and 40Ar/39Ar geochronology of granitoid rocks from southern Nova Scotia; its bearing on the geological evolution of the Meguma Zone of the Appalachians: Canadian J. Earth Sci., v. 18, p.386-394.

Robinson, B.W., 1975, Carbon and oxygen isotopic equilibrium in hydrothermal calcites: Geochem. J., v.9, p.43-46.

Rodgers, J., 1970, Tectonics of the Appalachians, Interscience, New York, 271 p.

Roedder, E., 1976, Fluid-inclusion evidence on the genesis of ores in sedimentary and volcanic rocks, in Wolf, K.H., ed., Handbook of stratabound and stratiform ore deposits, geochemical studies: New York, Elsevier.

Roedder, E., 1979, Fluid inclusions as samples of ore fluids, in Barnes, H.L., ed., Geochemistry of hydrothermal ore deposits, 2nd edition: New York, Wiley, p. 684-737.

Roedder, E., 1984, Fluid Inclusions: Mineral. Soc. Am., Reviews in Mineralogy, v.12, 644p.

Russell, M.J., 1976, Incipient plate separation and possible related mineralization in lands bordering the north Atlantic, in Strong, D.F., ed., Metallogeny and plate tectonics: Geol. Assoc. Canada, Spec. Paper 14, p.339-349.

Russell, M.J., 1978, Downward-excavating hydrothermal cells and hydrothermal ore deposits; importance of an underlying thick Caledonian prism: Inst. Mining Metall. Trans., v. 87, Sec. B, p. B168-B171.

Rye, R.O., 1974, A comparison of sphalerite-galena sulfur isotope temperatures with filling temperatures of fluid inclusions: Econ. Geol., v. 69, p. 26-32.

Rye, R.O. and Ohmoto, H., 1974, Sulfur and carbon isotopes and ore genesis: A reveiw: Econ. Geol., v.69, p. 826-843.

Sangster, D.F., 1983, Mississippi Valley-type deposits; a geological melange, in Kisvarsanyi, G., Grant, S.K., Pratt, W.P., and Koenig, J.W., eds., Internat. conf. on Mississippi Valley type lead-zinc deposits, proceedings volume: Rolla,

Missouri, University of Missouri-Rolla, p. 7-19.

Schenk, P.E., 1967, The Macumber Formation of the Maritime Provinces, Canada - A Mississippian analogue to Recent strandline carbonates of the Persian Gulf: J. of Sedimentary Petrology, v.37, p.365-376.

Schenk, P.E., 1969, Carbonate-sulfate-redbed facies and cyclic sedimentation of the Windsorian Stage (Middle Carboniferous), Maritime Provinces: Canadian J. Earth Sci., v. 6, p. 1037-1066.

Schenk, P.E., 1984, Carbonate-sulfate relations in the Windsor Group - central Nova Scotia, Canada: 9th Internat. Congress of Carboniferous Stratigraphy and Geology 1979, Compte Rendu, v.3, p.143-162.

Schenk, P.E. and Hatt, B.L., 1984, Depositional environment of the Gays River reef, Nova Scotia, Canada: 9th Internat. Congress of Carboniferous Stratigraphy and Geology 1979, Compte Rendu, v.3, p.117-129.

Schreiber, B.C., Friedman, G.M., Decima, A., and Schreiber, E., 1976, Depositional environments of Upper Miocene (Messinian) evaporite deposits of the Sicilian basin: Sedimentology, v.23, p.729-760.

Sharp, J.M., 1976, Momentum and energy balance equations for compacting sediments; Mathematical Geology, v.8, p.305-322.

Sharp, J.M., Jr., 1978, Energy and momentum transport model of the Ouachita Basin and its possible impact on the formation of economic mineral deposits: Econ. Geol., v. 73, p. 1057-1068.

Sharp, J.M. and Domenico, P.A., 1976, Energy transport in thick sequences of compacting sediments; Geol. Soc. Am. Bull., v.87, p.390-400.

Shearman, D.J., 1971, Marine evaporites: the calcium sulfate facies: Am. Assoc. of Petrol. Geologists Bull., Seminar, University of Calgary, 65p.

Shelton, K.L., 1981, Carbon and oxygen isotopes as an exploration tool and ore guide for skarn-type ore deposits: an example from the Gaspe peninsula, Quebec (abs.): Geol. Soc. Am., Abstracts with Programs, v.13, p.552.

Shelton, K.L., 1983, Composition and origin of ore-forming fluids in a carbonate-hosted porphyry copper and skarn deposit: a fluid inclusion and stable isotope study of Mines Gaspe, Quebec: Econ. Geol., v.78, p.387-421.

Sheppard, S.M.F., 1976, Identification of the origin of

ore-forming solutions by the use of stable isotopes, in Volcanic Processes in Ore Genesis: Geol. Soc. London, Spec. Publ. 7.

Sheppard, S.M.F., 1983, Stable isotope studies of sedimentary basins and associated Pb-Zn deposits, in Internat. colloquium - Thermal phenomena in sedimentary basins: Bordeaux, France, Institut Francais du Petrole.

Sheppard, S.M.F., 1986, Characterization and isotopic variations in natural waters, in Valley, J.W., Taylor, H.P.Jr. and O'Neil, J.R., eds., Stable isotopes in high temperature geological processes: Mineral. Soc. Am., Reviews in Mineralogy, v.16, p.165-184.

Sheridan, R.E. and Drake, C.L., 1968, Seaward extension of the Canadian Appalachians: Canadian J. Earth Sci., v.5, p.337-374.

Smith, L. and Collins, J.A., 1984, Unconformities, sedimentary copper mineralization and thrust faulting in the Horton and Windsor Groups, Cape Breton Island and central Nova Scotia: 9th Internat. Congress of Carboniferous Stratigraphy and Geology 1979, Compte Rendu, v.3, p.105-116.

Stacey, J.S. and Kramers, J.D., 1975, Approximation of terrestrial lead isotopic evolution of two stage model: Earth Planet. Sci. Letters, v. 26, p. 207-221.

Stein, H.J. and Kish, S.A., 1985, The timing of ore formation in southwestern Missouri; rubidium-strontium glauconite dating at the Magmont Mine, Viburnum Trend; Econ. Geol., v.80, p.739-753.

Stevenson, I.M., 1951, Structure and petrology of the barite deposit at Brookfield, Colchester County, Nova Scotia: Unpublished M.Sc. thesis, McGill University, 50 p.

Stevenson, I.M., 1959, Shubenacadie and Kennetcook map areas, Colchester, Hants and Halifax counties, Nova Scotia: Canada Geol. Survey Memoir, v.302.

Sverjensky, D.A., 1981a, Isotopic composition of carbonate host rock as a function of water to rock ratio - an example from the Upper Mississippi zinc-lead district: Econ. Geol., v.76, p.154-172.

Sverjensky, D.A., 1981b, The origin of a Mississippi Valley-type deposit in the Viburnum trend, southeast Missouri: Econ. Geol., v.76, p.1848-1872.

Sverjensky, D.A. and Wasserman, M.D., 1978, Hydrothermal alteration around a MVT deposit in the Viburnum trend,

southeast Missouri: Geol. Soc. Am., Abstract with Programs, v. 10, no. 7, p. 501.

Taylor, H.P., Jr., 1974, The application of oxygen and hydrogen isotope studies to problems of hydrothermal alteration and ore deposition: Econ. Geol., v. 69, p. 843-883.

Taylor, H.P., Jr., 1979, Oxygen and hydrogen isotope relationships in hydrothermal mineral deposits, in Barnes, H.L., ed., Geochemistry of hydrothermal ore deposits: New York, Wiley, p. 236-277.

Thode, H.G. and Monster, J., 1965, Sulfur isotope geochemistry of petroleum, evaporite, and ancient seas: Am. Assoc. Petrol. Geologists, Memoir 4, p.367-377.

Trudinger, P.A., Chambers, L.A., and Smith, J.W., 1985, Low-temperature sulfate reduction: biological versus abiological: Canadian J. Earth Sci., v.22, p.1910-1918.

Truesdell, A.H., 1971, Nonideality of oxygen isotope fugacity in salt solutions at elevated temperatures [abs.]: Geol. Soc. Am., Abstracts with Program, v.3, p.735.

Truesdell, A.H., 1974, Oxygen isotope activities and concentrations in aqueous solutions at elevated temperatures: Consequences for isotope geochemistry: Earth Planet. Sci. Letters, v.23, p.387-396.

Ulrich, M.R. and Bodnar, J.R., 1984, Systematics of stretching of fluid inclusions in barite at 1 atm confining pressure: Geol. Soc. Am., Abstracts with Programs, v.16, p.680.

Utting, J., 1980, Palynology of the Windsor Group (Mississippian) in a borehole at Stewiacke, Shubenacadie Basin, Nova Scotia: Canadian J. Earth Sci., v.17, p.1031-1045.

van de Poll, H.W., 1972, Stratigraphy and economic geology of Carboniferous basins in the Maritime Provinces, Int. Geol. Congr. 24th, Field Excursion A-60 Guidebook, 96p.

Visser, W., 1982, Maximum diagenetic temperature in a petroleum source rock from Venezuela by fluid inclusion geothermometry: Chemical Geology, v. 37, p. 95-101.

Wade, J.A., Grant, A.C., Sanford, B.V., and Barss, M.S., 1977, Basement structure of Eastern Canada and adjacent areas: Canada Geol. Survey Map 1400 A.

Wagner, G.A., 1968, Fission track dating of apatites: Earth Planet. Sci. Letters, v.4, p.411-415.

Wagner, G.A. and Reimer, G.M., 1972, Fission track tectonics: The tectonic interpretation of fission track apatite ages: Earth Planet. Sci. Letters, v.14, p.263-268.

Wagner, G.A., Reimer, G.M. and Jager, E., 1977, Cooling ages derived by apatite fission-track, mica Rb-Sr and K-Ar dating; the uplift and cooling history of the central Alps: Memorie degli Istituti di Geologia e Mineralogia dell'Universita di Padova, v.30.

Walker, S.D., 1978, Geological and mineralogical studies at the Smithfield lead-zinc prospect, Colchester County, Nova Scotia: Unpub. B.Sc. thesis, Dalhousie University, 93 p.

Walters, L.J., Claypool, G.E. and Choquette, P.W., 1972, Reaction rates and $\delta^{18}O$ variation for the carbonate-phosphoric acid preparation method: Geochim. Cosmochim. Acta, v.36, p. 129-140.

Webb, C.A., 1969, Paleozoic wrench faults in the Canadian Appalachians; Am. Assoc. Petrol. Geologists, Memoir 12, p.754-786.

Weeks, L.J., 1948, Londonderry and Bass River map areas, Cochester and Hants counties, Nova Scotia; Canada Geol. Survey Memoir, v.245, 86p.

Weertman, J., 1980, The stopping of a rising, liquid-filled crack in the Earth's crust by a freely slipping joint: J. Geophys. Research, v.85, p.967-976.

Wu, Y. and Beales, F., 1981, A reconnaissance study by paleomagnetic methods of the age of mineralization along the Viburnum trend, southeast Missouri: Econ. Geol, v. 76, p. 1879-1894.

York, D., Hanes, J.A., Kuybida, P., Hall, C.M., Kenyon, W.J., Masliwec, A., Scott, S.D., and Spooner, E.T.C., 1980, The direct dating of ore minerals: EOS, v.61, p.399.

Zartman, R.E. and Doe, B.R., 1981, Plumbotectonics - the model: Tectonophysics, v.75, p.135-162.

Zeitler, P.K., 1983, Uplift and cooling history of the N.W. Himalaya, nothern Pakistan; evidence from fission-track and 40Ar/39Ar cooling ages: Unpub. Ph.D. thesis, Dartmouth College, 297p.

Zentilli, M. and Reynolds, P.H., 1985, 40Ar/39Ar dating of micas from East Kemptville tin deposit, Yarmouth County, Nova Scotia: Canadian J. Earth Sci., v.22, p.1546-1548.

VITA

NAME:	Casey Edward Ravenhurst
BIRTHDATA:	January 10th, 1954 Toronto, Ontario
POST-SECONDARY EDUCATION:	Ph.D. Geology, Sept.1982 to June 1987 Dalhousie University, Halifax, Nova Scotia
	M.S. Geophysics, Sept.1978 to November 1980 Penn State University, University Park, PA.
	B.Sc. Geophysics, Sept.1973 to May 1975 Sept.1976 to May 1978 University of Western Ontario, London, Ont.
HONOURS AND AWARDS:	University of Western Ont. Entrance Scholarship. DUCA (Toronto) Credit Union Scholarship. NSERC Postgraduate Scholarships 1978-80 & 1982-85. Petro-Canada Graduate Research Award 1985-86. Gulf Canada Graduate Fellowship 1985-86 (refused).
RELATED WORK EXPERIENCE:	Senior Geophysicist, Kidd Creek Mines Ltd., 1982. Regional Geophysicist, Molycorp Inc., 1981-82. Geophysical Technician, Texasgulf Inc., 1975-76, and summers 1977 & 78.
PUBLICATIONS:	Ravenhurst, C.E., Zentilli, M., 1987, Model for the evolution of hot (>200 C) overpressured brines under an evaporite seal; The Fundy/Magdalen Carboniferous Basin of Atlantic Canada and its associated Pb-Zn-Ba deposits: Can. Soc. Petrol. Geologists, Mem. 12 (in print).
	Ravenhurst, C.E., Reynolds, P.H., Zentilli, M., and Akande, S.O., 1987, Isotopic constraints on the genesis of Pb-Zn mineralization at Gays River, Nova Scotia, Canada: Econ. Geol. (in print).
	Ravenhurst, C.E., Reynolds, P.H., and Zentilli, M., 1986, Strontium isotopic studies of rock and mineral samples in the Shubenacadie Basin, Nova Scotia: G.S.C. Current Research, v.86-1B, p.547-555.
	Ravenhurst, C.E., Reynolds, P.H., Akande, S.O., and Zentilli, M., 1986, Isotopic constraints on the genesis of the Pb-Zn mineralization at Gays River, Nova Scotia: G.A.C. Program with Abstracts, v.11, p.118.